Institute of Earth and Environmental Science

Spatiotemporal Variations of Key Air Pollutants and Greenhouse Gases in the Himalayan Foothills

A cumulative dissertation for

the degree of Doctor of Natural Sciences

"doctor rerum naturalium"

(Dr. rer. Nat.) in Geoecology

Submitted to

Faculty of Mathematics and Natural Sciences

at the University of Potsdam

by

Khadak Singh Mahata

Potsdam, September 2021

Submission date: 1 October 2019

Date of PhD defense: 28 June 2021

Khadak Singh Mahata: Spatiotemporal variations of key air pollutants and greenhouse gases in the Himalayan foothills

Referees:

Prof. Dr. Mark Lawrence
University of Potsdam, Institute of Earth and Environmental Science
Managing Scientific Director, Institute for Advanced Sustainability Studies (IASS)
Germany

Prof. Dr. Juergen P. Kroop
University of Potsdam, Institute of Earth and Environmental Science
Potsdam Institute for Climate Impact Research (PIK)
Germany

Prof. Nguyen Thi Kim Oanh
Asian Institute of Technology, Department of Energy, Environment and Climate, Scholl of Environment, Resources and Development
Thailand

Published online on the
Publication Server of the University of Potsdam:
https://doi.org/10.25932/publishup-51991
https://nbn-resolving.org/urn:nbn:de:kobv:517-opus4-519910

Abstract

South Asia is a rapidly developing, densely populated and highly polluted region that is facing the impacts of increasing air pollution and climate change, and yet it remains one of the least studied regions of the world scientifically. In recognition of this situation, this thesis focuses on studying (i) the spatial and temporal variation of key greenhouse gases (CO_2 and CH_4) and air pollutants (CO and O_3) and (ii) the vertical distribution of air pollutants (PM, BC) in the foothills of the Himalaya. Five sites were selected in the Kathmandu Valley, the capital region of Nepal, along with two sites outside of the valley in the Makawanpur and Kaski districts, and conducted measurements during the period of 2013-2014 and 2016. These measurements are analyzed in this thesis.

The CO measurements at multiple sites in the Kathmandu Valley showed a clear diurnal cycle: morning and evening levels were high, with an afternoon dip. There are slight differences in the diurnal cycles of CO_2 and CH_4, with the CO_2 and CH_4 mixing ratios increasing after the afternoon dip, until the morning peak the next day. The mixing layer height (MLH) of the nocturnal stable layer is relatively constant (~ 200 m) during the night, after which it transitions to a convective mixing layer during the day and the MLH increases up to 1200 m in the afternoon. Pollutants are thus largely trapped in the valley from the evening until sunrise the following day, and the concentration of pollutants increases due to emissions during the night. During afternoon, the pollutants are diluted due to the circulation by the valley winds after the break-up of the mixing layer. The major emission sources of GHGs and air pollutants in the valley are transport sector, residential cooking, brick kilns, trash burning, and agro-residue burning. Brick industries are influential in the winter and pre-monsoon season. The contribution of regional forest fires and agro-residue burning are seen during the pre-monsoon season. In addition, relatively higher CO values were also observed at the valley outskirts (Bhimdhunga and Naikhandi), which indicates the contribution of regional emission sources. This was also supported by the presence of higher concentrations of O_3 during the pre-monsoon season.

The mixing ratios of CO_2 (419.3 ±6.0 ppm) and CH_4 (2.192 ±0.066 ppm) in the valley were much higher than at background sites, including the Mauna Loa observatory (CO_2: 396.8 ± 2.0 ppm, CH_4:1.831 ± 0.110 ppm) and Waligaun (CO_2: 397.7 ± 3.6 ppm, CH_4: 1.879 ± 0.009 ppm), China, as well as at an urban site Shadnagar (CH_4: 1.92 ± 0.07 ppm) in India.

The daily 8 hour maximum O_3 average in the Kathmandu Valley exceeds the WHO recommended value during more than 80% of the days during the pre-monsoon period, which represents a significant risk for human health and ecosystems in the region. Moreover, in the measurements of the vertical distribution of particulate matter, which were made using an ultralight aircraft, and are the first of their kind in the region, an elevated polluted layer at around ca. 3000 m asl. was detected over the Pokhara Valley. The layer could be associated with the large-scale regional transport of pollution. These contributions towards understanding the distributions of key air pollutants and their main sources will provide helpful information for developing management plans and policies to help reduce the risks for the millions of people living in the region.

Zusammenfassung

Südasien ist eine sich schnell entwickelnde, dicht besiedelte und stark umweltbelastete Region, die mit den Auswirkungen der zunehmenden Luftverschmutzung und des Klimawandels konfrontiert ist, und dennoch bleibt sie wissenschaftlich gesehen eine der am wenigsten untersuchten Regionen der Welt. In Anerkennung dieser Situation liegt der Schwerpunkt dieser Arbeit auf der Untersuchung (i) der räumlichen und zeitlichen Variation der wichtigsten Treibhausgase (CO_2 und CH_4) und Luftschadstoffe (CO und O_3) und (ii) der vertikalen Verteilung der Luftverschmutzung (PM, BC) in den Vorgebirgen des Himalayas. Fünf Standorte wurden im Kathmandu-Tal, der Hauptstadtregion Nepals, sowie zwei Standorte außerhalb des Tals in den Distrikten Makawanpur und Kaski ausgewählt und im Zeitraum 2013-2014 und 2016 wurden Messungen durchgeführt. Diese Messungen werden in dieser Arbeit analysiert.

Die CO-Messungen an mehreren Standorten im Kathmandu-Tal zeigten einen klaren Tagesablauf: Die Werte am Morgen und am Abend waren hoch, mit einem Rückgang am Nachmittag. Es gibt leichte Unterschiede in den Tageszyklen von CO_2 und CH_4, wobei die Mischungsverhältnisse von CO_2 und CH_4 nach dem Nachmittagsdip bis zu den höchsten Werten am nächsten Morgen zunehmen. Die Höhe der nächtlichen stabilen planetaren Grenzschicht ist relativ konstant (~ 200 m), danach geht sie tagsüber in eine konvektive Mischschicht über und die MLH ("Mixing layer height") steigt am Nachmittag auf bis zu 1400 m an. So werden Schadstoffe vom Abend bis zum Sonnenaufgang des folgenden Tages weitgehend im Tal gefangen, und die Schadstoffkonzentration steigt durch nächtliche Emissionen an. Während des Nachmittags werden die Schadstoffe aufgrund der Zirkulation durch die Talwinde nach dem Aufbrechen der Mischschicht verdünnt. Die Hauptemissionsquellen für GHGs und Luftschadstoffe im Tal sind der Verkehrssektor, das Kochen in privaten Haushalten, Ziegeleien, die Müllverbrennung und die Verbrennung von landwirtschaftlichen Reststoffen. Die Ziegelindustrie ist in der Winter- und Vormonsunzeit von großer Bedeutung für die Emissionen von Ruß. Der Beitrag der regionalen Waldbrände und der Verbrennung von landwirtschaftlichen Reststoffen ist besonders wichtig in der Vormonsunzeit. Darüber hinaus wurden auch am Talrand (Bhimdhunga und Naikhandi) relativ hohe CO-Werte beobachtet, was auf den Beitrag der regionalen Emissionsquellen hinweist.

Dies wurde auch durch das Vorhandensein höherer Konzentrationen von O_3 während der Vormonsunzeit unterstützt.

Die Mischungsverhältnisse von CO_2 (419,3 ±6,0 ppmv) und CH_4 (2.192 ±0,066 ppmv) im Tal waren viel höher als an bekannten Hintergrundstandorten, darunter das Observatorium Mauna Loa (CO_2: 396,8 ± 2,0 ppmv, CH_4:1.831 ± 0,110 ppmv) und Waligaun (CO_2: 397,7 ± 3,6 ppmv, CH_4: 1,879 ± 0,009 ppmv), China, sowie an einem städtischen Standort Shadnagar (CH_4: 1,92 ± 0,07 ppmv) in Indien.

Der tägliche 8-stündige maximale O_3-Durchschnitt im Kathmandu-Tal übersteigt den WHO-Empfehlungswert an mehr als 80% der Tage während der Vormonsunzeit, was ein erhebliches Risiko für die menschliche Gesundheit und die Ökosysteme in der Region darstellt. Darüber hinaus wurde bei den Messungen der vertikalen Verteilung der Feinstaubpartikel, die mit einem Ultraleichtflugzeug durchgeführt wurden und die ersten ihrer Art in der Region sind, eine höherliegende verschmutzte Schicht, ca. 3000 m über dem mittleren Meeresspiegel über dem Pokhara-Tal, festgestellt. Die Schicht könnte mit dem großräumigen regionalen Transport von Schadstoffen in Verbindung gebracht werden. Diese Beiträge zum Verständnis der Verteilung der wichtigsten Luftschadstoffe und ihrer Hauptquellen werden hilfreiche Informationen für die Entwicklung von Mitigationsplänen und -strategien liefern, die dazu beitragen, die Risiken für die Millionen von Menschen, die in der Region leben, zu verringern.

Acknowledgement

I would like to acknowledge some notable persons and organizations who helped me in different ways to bring out this thesis.

First of all, I would like to thank my supervisor Prof. Dr. Mark G. Lawrence for providing me an opportunity to work with him as a junior fellow at IASS, Germany and accepting me as a PhD scholar as well as for his guidance to complete the thesis and papers. I am grateful to my mentor Dr. Maheswar Rupakheti at IASS for his timely advice and guidance. I am also grateful to Dr. Arnico K. Panday at ICIMOD, Nepal for his continuous support and guidance.

I am thankful to IASS which provided me the fellowship to complete the doctoral degree as well as funding for the research work. Similarly, I would also like to thank my PhD advisory committee (PAC) members Prof. Peter Builtjes and Prof. Tim Butler for their guidance, and colleagues at IASS Dr.Ashish Singh, Dr. Andrea Mues, Dr. Pankaj Sadavarte, Dr. P. S. Praveen, Dr. Noelia Otero Felipe, Tanja Baines, Iris Schuetze, Cordula Granderath who supported me during my doctoral degree.

I would like to thank ICIMOD for helping in technical and logistic support during the SusKat-ABC campaign in Nepal as a collaborating partner.

I would also like to thank Shyam Newar, Bhogendra Kathayat, Dipesh Rupakheti and Raviram Pokharel who helped me during SusKat-ABC campaign.

Lastly, I would express my deep gratitude to my parents, my brother, Tika Ram Mahata, my friend, Dr. Naresh Neupane and my wife, Bhumika Mahata.

Table of Contents

Abstract i
Zusammenfassung iii
Acknowledgement vi
Table of Contents viii
List of Figures x
List of Tables xii
Abbreviations and Symbols xiv
Chapter 1 1
1.1. Motivation of the study 4
1.2. Set up, site selection and methods 5
1.3. Hypothesis, key research questions and organization of the thesis 6
1.4. Key results of the three studies 10
1.4.1. CH_4 and CO_2 in the region 10
1.4.2. Air pollutants (CO and O_3) at multiple sites in the Kathmandu Valley 11
1.4.3. Vertical distribution of air pollutants 12
1.5. Further contributions 12
Chapter 2 14
Abstract 14
2.1. Introduction 15
2.2. Experiment and Methodology 18
2.2.1. Kathmandu Valley 18
2.2.2. Study sites 20
2.2.2.1. Bode (SusKat-ABC supersite) 20
2.2.2.2. Chanban 20
2.2.3. Instrumentation 21
2.3. Results and discussion 24
2.3.1. Time series of CH_4, CO_2, CO and water vapor mixing ratios 24
2.3.2. Monthly and seasonal variations 28
2.3.3. Diurnal variation 35
2.3.4. Seasonal interrelation of CO_2, CH_4 and CO 40
2.3.5. CO and CO_2 ratio: Potential emission sources 40
2.3.6. Comparison of CH_4 and CO_2 at semi-urban site (Bode) and rural site (Chanban) 44
2.4 Conclusions 47
Chapter 3 50

Abstract 50
3.1 Introduction 51
3.2 Study sites and methods 55
3.3 Results and discussion 60
3.3.1 CO mixing ratio at multiple sites 60
3.3.2 Diurnal and seasonal variations of CO 61
3.3.2.1 Diurnal pattern of CO at multiple sites 61
3.3.2.2 CO diurnal variation across seasons 64
3.3.2.3 Regional influence on CO in the valley 66
3.3.3 O_3 in the Kathmandu Valley and surrounding areas 68
3.3.4 O_3 seasonal and diurnal variation 72
3.3.5 CO emission flux estimate 74
3.4 Conclusions 79
Chapter 4 81
4 An Overview on the Airborne Measurement in Nepal, - Part 1: Vertical Profile of Aerosol Size-Number, Spectral Absorption, and Meteorology 81
Abstract 81
4.1 Introduction 82
4.2 Ultralight measurements in Nepal 84
4.2.1 Details of the airborne measurement unit 84
4.2.2 Site description 86
4.2.3 Test flight patterns over the Pokhara Valley 86
4.2.4 Data processing and quality 87
4.3 Results 88
4.3.1 General meteorology and air quality, aerosol properties in the Pokhara Valley 88
4.3.1.1 Local and synoptic meteorology in the Pokhara Valley 88
4.3.1.2 Overview of the aerosol properties in the Pokhara Valley during the test flight period 90
4.3.2 Vertical profiles of absorbing aerosols, particle number and size distribution, temperature, and dew point 91
4.3.3 Diurnal variation in the vertical profiles 93
4.3.4 Nature of absorbing aerosols in the Pokhara Valley 94
4.3.5 Comparison of the satellite-derived vertical profiles with measurements 96
4.3.6 Role of synoptic circulation in modulating aerosol properties over the Pokhara Valley 97
4.4 Conclusion 99
Chapter 5 101
Discussion and Conclusions 101

5.1 Overview and key messages 101
5.2 Conclusions and future priorities 105
Bibliography 127
Declaration of Authorship 144

List of Figures

2.1. Location of the measurement sites and general setting of a supersite Bode 22
2.2. Time series of hourly average mixing ratios of CH_4, CO_2, CO, and water vapor and temperature and rainfall at Bode. 25
2.3. Monthly variations of the mixing ratios of hourly CH_4, CO_2, CO, and water vapor observed at Bode in the Kathmandu Valley 28
2.4. Relation between mixing ratios of CH_4, CO_2, CO and wind direction observed at Bode in the Kathmandu Valley from March 2013 to February 2014 33
2.5. Satellite detected fire counts in Mar, Apr, May 2013 in the broader region surrounding Nepal and total number of fire counts detected by MODIS during Jan 2013-Feb 2014 .. 34
2.6. Diurnal variations of CH_4, CO_2, CO, and water vapor in different seasons observed at Bode in the Kathmandu Valley 36
2.7. Diurnal variations of hourly mixing ratios of CH_4, CO_2, CO, and mixing layer height (MLH) at Bode in different seasons 39
2.8. Seasonal polar plot of hourly dCO/dCO_2 ratio based upon wind direction and wind speed 43
2.9. Seasonal frequency distribution of hourly dCO/dCO_2 ratio during morning hours and evening hours 44
2.10. Comparison of hourly average mixing rations of CH_4, CO_2, CO, and water vapor observed at Bode and Chanban. 45
2.11. Diurnal variations of hourly average mixing ratios of CH_4, CO_2, CO and water vapor observed at Bode and Chanban 46

3.1. Observation sites in the SusKat-ABC international air pollution campaign during 2013-2014 in the Kathmandu Valley 57
3.2. Hourly average CO mixing ratios observed at a supersite (Bode) and three satellite sites (Bhimdhunga, Naikhandi and Nagarkot) 60
3.3. Diurnal variations of CO mixing ratios during the common observation period (13 February–03 April, 2013) at Bode, Bhimdhunga, Naikhandi and Nagarkot 62
3.4. Comparison of seasonal diurnal variation of hourly average CO mixing ratios at Bode, Bhimdhunga and Naikhandi 64
3.5. Comparison of hourly average CO mixing ratios during normal days and episode days in 2013 at Bode, Bhimdhunga and Naikhandi in the Kathmandu Valley 67

3. 6. Time series of hourly average and daily maximum 8-hr average O3 mixing ratio at Bode, Paknajol, Nagarkot and Pulchowk 69

3.7. Seasonal diurnal pattern of hourly average O_3 mixing ratio during January 2013-January 2014 at Bode, Paknajol, and Nagarkot 73

3. 8. Monthly CO emission flux based on the mean diurnal cycle of CO mixing ratios with all days (CO Flux) and with only morning hours data (CO Flux minimum). 77

4.1. A typical test flight within the Pokhara Valley on 5 May 2016 87

4.2. Daily wind vector data at 850 and 500 mb, plotted using the NCEP NCAR reanalysis (2.5° x 2.5°) data over South Asia from 1-7 May 2016 89

4.3. AOD and other data products from the Level1.5 AERONET direct product in the Pokhara Valley from 1-10 May 2016. 90

4.4. Vertical profiles of aerosol species and meteorological parameters during the 5-7 May 2016 test flights in the Pokhara Valley using the IKARUS microlight aircraft 92

4.5. Aerosol extinction coefficient (at 532 nm) vertical profile and aerosol type classification based on the CALIPSO level 2 retrieval 95

4.6. YSPLIT 3 day back trajectories of air masses arriving at 3 different heights (800 m, 1500 m and 2500 m) from above the ground level in the Pokhara Valley. 96

A.1. Correlation between hourly Picarro and Horriba CO mixing ratios at Bode during 6 March to 7 June 2013 in the Kathmandu Valley. 107

A.2. Seasonal diurnal variation of hourly average wind directions at Bode. 108

A.3. Seasonal diurnal variation of hourly average wind speeds at Bode. 109

A.4. Time series of hourly average ambient temperature, wind speed, pressure, and rainfall observed at Chanban site in Makwanpur district 110

B.1. Testing and assembly of the instrument package inside IKARUS-C42, field station in Pokhara Valley and sketch of the Instrument package 111

B.2. Monthly mean values of key meteorological parameters at the Pokhara regional airport 112

B.3. Frequency of wind speed and direction observed in the Pokhara Valley during May 2016 113

B.4. Daily temperature and relative humidity at 500mb using the NCEP NCAR reanalysis (2.5x 2.5o) data over South Asia from May 1 to 7 2016. 114

B.5. Monthly mean value of AOD 500 nm in Pokhara Valley for 2010-2016 115

B.6. Local Meteorology in the Pokhara Valley from 1-10 May 2016. 116

B.7. AERONET-based aerosol optical depth and radiative properties in the Pokhara Valley from 2010 to 2016. 120

B.8. MODIA AQUA AND TERRA AOD at 550 nm over the IGP and Himalayan region from 1 – 7 May 122

B.9. Locally or nationally recorded active fire for the same period by the National Emergency Operation Centre 123

B.10. Morning test flight (Flight F3) on 6 May 2016 124

B.11. Estimating the AAE value using the power fit and linear fit. 125

List of Tables

2.1. Instruments and sampling at Bode and Chanban sites 21

2.2. Summary of monthly average CH_4 and CO_2 mixing ratios observed at Bode in the Kathmandu Valley during March 2013 to Feb 2014 27

2.3. Summary of CH_4 and CO_2 mixing ratios at Bode across four seasons during March 2013 to Feb 2014 29

2.4. Comparison of monthly average CH_4 and CO_2 mixing ratios at Bode and Chanban sites in Nepal with other urban and background sites in the region 30

2.5. Emission ratio of CO/CO_2 (ppb ppm-1) derived from emission factors 41

2.6 Average of the ratio of dCO to dCO_2, their Geometric mean over a period of 3 hours during morning peak, evening peak and seasonal of the ambient mixing ratios of CO and CO_2 and their lower and upper bound. 44

3.1 Information of the sampling sites of the SusKat-ABC campaign during 2013-2014 in the Kathmandu Valley. 56

3.2. Details of the instruments deployed at different sites during the observation period during January 2013-March 2014 in the Kathmandu Valley. 58

3.3. Summary of the monthly average ozone mixing ratios (ppb) at four sites in the Kathmandu Valley, Nepal; and two sites (Manora Peak and Delhi) in India. 70

3.4. verege CO mixing ratio at different time of the day (daytime and nighttime) and the monthly average (total) at four sites in the Kathmandu Valley 70

T.1 126

Abbreviations and Symbols

AGL	: Above Ground Level
AOD	: Aerosol Optical Depth
ASL	: Above Sea Level
AWS	: Automatic Weather Station
BC	: Black Carbon
CBS	: Central Bureau of Statistics
CO	: Carbon Monoxide
CO_2	: Carbon Dioxide
CH_4	: Methane
GBD	: Global Burden of Disease
GoN	: Government of Nepal
GHG	: Greenhouse Gas
HKH	: Hind Kush Himalaya
IASS	: Institute for Advanced Sustainability Studies
ICIMOD	: International Centre for Integrated Mountain Development
IGP	: Indo-Gangetic Plain
INTEX-B	: Intercontinental Chemical Transport Experiment - Phase B
IPCC	: Intergovernmental Panel on Climate Change
MLH	: Mixing Layer Height
MOPITT	: Measurements of Pollution in the Troposphere
NOx	: Nitrogen dioxides
O_3	: Ozone
OC	: Organic Carbon
PM	: Particulate Matter

REAS	: Regional Emission Inventory in Asia
RCP	: Representative Concentration Pathways
SLCPs	: Short-Lived Climate-forcing Pollutants
SO_2	: Sulphur Dioxide
SusKat-ABC	: Sustainable Atmosphere for the Kathmandu Valley – Atmospheric Brown Clouds
TP	: Tibetan Plateau
VOCs	: Volatile Organic Compounds
WHO	: World Health Organization

Chapter 1

Introduction and Overview

Climate change and air pollution are closely interlinked challenges for human societies and ecosystems (IPCC 2013). Both air pollution and climate change are adversely impacting public health, crops, weather and climate, as well as global ecosystems, which ultimately affects the livelihood of the people, environment, economies and sustainable development of societies. This worsening situation needs effective policies to limit anthropogenic emissions of air pollutants, including short-lived climate-forcing pollutants (SLCPs), as well as greenhouse gases (GHGs). Sources of these anthropogenic emissions are mainly industries, the energy sector, the transport sector, household cooking, biomass burning (including agro-residue burning) and land-use change (deforestation). While the emissions from several of these sectors are going down in developed countries due to effective implementation of environmental protection laws, they are instead mostly increasing in developing and under-developed nations, such as in South Asia, due to either non-existent or ineffective protection measures.

Local emission sources (for example, transport, residential, and industrial activities) are not only responsible for degrading air quality, but they are also playing significant role in the increasing atmospheric mixing ratios of GHGs in South Asia, including in the central Himalayan mountain region. The regional scale air pollution (now called atmospheric brown clouds, ABC) in South Asia has come into the spotlight after the findings of the INDOEX field campaign during 1999, in which it was found that ABCs extend vertically to several kilometers above the ground, with sometimes elevated layers found at an altitude of ca. 3000 m asl. (Ramanathan et al., 2001). Furthermore, air pollution is found to be responsible for over a million pre-mature deaths annually in the southern Asian region. Several studies have examined how such sources and pollutants are major contributors to the ever-deteriorating air quality in the region (Panday and Prinn, 2009; Putero et al., 2014; Sinha et al., 2014; Marinoni et al., 2013). In order to develop effective mitigation strategies, it is important to understand the influence of regional emission sources on the various air pollutants and their horizontal and vertical distributions in the region.

The effects of air pollution on human health have become recognized as being very significant (WHO 2014; UNEP/WMO 2011), with an estimated 8 million premature deaths annually around the world, especially in less-developed regions, with ~ 90% of the premature deaths in low and middle income nations (https://www.who.int/airpollution/en/). The effects are particularly bad in South Asia in comparison to other parts of the World (Forouzanfar, 2015). In Nepal, a small country in the central Himalayas, air pollution (both outdoor and indoor) has become the most significant environmental health risk, responsible for about 45305 premature death in 2016 (WHO 2018). In addition, the damage to ecosystems, including agriculture, is also immense. For example, worldwide reductions in crop yields due to high levels of tropospheric ozone (O_3) were estimated to be $11-18 billion in 2000 (Avnery et al., 2011; UNEP and WMO 2011). Crop damage is also particularly bad in developing regions like South Asia; for example, in India alone the wheat loss mainly due to O_3 was equivalent to $5 billion in 2010 (Burney and Ramanathan, 2014).

Tropospheric O_3 is not only detrimental to human health, ecosystem and crop productivity (Monks et al., 2015; WHO, 2003), but it is also a greenhouse gas. A recent study reported that the levels of O_3 are decreasing in western Europe and North America, while they have been increasing in East Asia during the period of 2000 to 2014 (Chang et al., 2017), and could not be reported on reliably for South Asia because of the lack of monitoring stations, although South Asia is expected to become one of the global hotspots for O_3 pollution by 2030 (IEA 2016; Dentener et al., 2006). In South Asia, O_3 levels are observed to be high during the pre-monsoon season (March-May) (Bhardwaj et al., 2018; Putero et al., 2015; Gouda et al., 2014; Lawrence and Lelieveld, 2010; Pudasainee et al., 2006), because of the high temperature and solar insolation coupled with urban precursors along with an increase in forest fires and agro-residue burning compared to other seasons (Putero et al., 2015; Kumar et al., 2011; Dev Roy et al., 2009). There are several other important pollutants in urban environments, including the main precursors of O_3: nitrogen oxides (NOx), carbon monoxide (CO), methane (CH_4) and volatile organic compounds (VOCs). Among these, CO is a toxic gas and has direct and indirect impacts on health and the environment (Raub et al., 2000; White et al., 1989). It is emitted from incomplete combustion of biomass and fossil fuels. Urban areas normally have a large number of industries and vehicles which emit CO. CO is a useful indicator for monitoring urban air pollution because of having similar combustion sources to particulates and other primary pollutants. Because of its 4-8 weeks tropospheric lifetime, it is also considered to be a good indicator of regional (and/or intercontinental) pollution transport (Yashiro et al., 2009).

CO does not have a direct impact on the climate (it is not a greenhouse gas), but it contributes considerably to O_3 production in urban areas.

Beyond tropospheric O_3, the most important GHGs are CO_2 and CH_4 (Stevenson et al., 2013; Xu et al., 2016; IPCC, 2013; Ramanathan and Carmichael, 2008; IPCC, 2007). CO_2 and CH_4 are relatively non-reactive gases and are thus relatively long-lived and well-mixed in the troposphere. Their mixing ratios have risen by 40% and 150%, respectively, since the beginning of the industrial age to 2011 (IPCC, 2013), contributing significantly to the projected increase in global average temperature exceeding 2 °C by the end of 21st century (IPCC, 2013). In addition to industrial, energy and mobility sector process, land use changes, especially due to rapid urbanization and deforestation to create agricultural lands, are also responsible for the increasing mixing ratios of these species in the atmosphere. Asia is one of the global hotspots for CH_4 emissions, due to livestock farming, cultivation of soils and especially of rice beds, coal extraction, ineffective waste disposal, etc. (EDGAR2FT, 2013). South Asia contributed nearly 40 Tg annually to CH_4 emissions, or about 8 % of total global emissions (500 Tg) in the 2000s (Patra et al., 2013).

Especially the Hindu Kush-Himalayan (HKH) region of South Asia, which is rich in biodiversity and water resources, is highly vulnerable to the impacts of climate change and air pollution, as evident in many ways. However, South Asia in general is a relatively poorly studied region. Developing reliable estimates of emissions and their contribution to pollution levels and global warming is made complicated by the fact that the majority of the people in the region still depend on solid fuels (wood, dung, charcoal, coal) for household cooking and heating (UNEP, 2018), and the GDP of most countries in South Asia is based on agriculture (CBS, 2011; Pandey et al., 2014). Most of the energy required for the economic development is generated from low grade coal thermal plants and low-quality fossil fuels for the transport and industrial sectors. Because of the low per capita income and often corrupt bureaucracy, it is hard to implement effective policies to curb air pollution. Thus, most of the transport sector, agriculture and energy sectors still use inefficient technologies, often without filters for controlling air pollutants, and burn low grade fuels. Better knowledge of the levels and sources of various pollutants and greenhouse gases is needed in order to help policymakers and the broader public aware of the issue of air pollution and climate change, in order to support effective mitigation actions. However, developing this knowledge for this region is significantly hindered by the lack of high-quality observations, including intensive field measurements and longer-term monitoring stations, as well as information on the spatial and

temporal distributions of air pollutants and GHGs and their relationship to the regional meteorological parameters. Establishing this would be useful for policymakers in developing science-informed mitigation plans. As described in the following sections, this thesis contributes s an important contribution to improving the understanding characteristics of key air pollutants and greenhouse gases and their sources in this vulnerable region.

1.1. Motivation of the study

Nepal is situated in the central Himalayas, and its highly populated Kathmandu Valley is located at the foothills of the Himalaya, midway between the Indo-Gangetic Plain (IGP) and Tibetan Plateau (TP), and is highly vulnerable to air pollution and climate change. However, the government of Nepal (GoN) has only limited research results available on air quality and climate change, due to lack of research and resources. Although GoN has recently started setting up air quality monitoring stations in Nepal, including few sites in and around the Kathmandu Valley and other regions such as the Pokhara Valley to the west of Kathmandu, the number of stations is not yet sufficient to provide an adequate picture of the state of air quality throughout the country with complex topography. Thus, further scientific studies of the regional air quality and climate change are necessary to understand major air pollutants and greenhouse gases, their sources (local and regional), their temporal and spatial (both horizontal and vertical) distributions in the atmosphere, their potential impacts on human health and ecosystems, and the implications for socio-economic development, as a basis for designing appropriate mitigation measures.

Associated with the diverse physical topography and landscape of Nepal, numerous valleys and gorges act as pathways for the transport of polluted air masses from the IGP to the TP (Dhungel et al., 2018; Lüthi et al., 2016; Putero et al., 2015; Bonasoni et al., 2010). Furthermore, recent studies have shown that the pollution from the IGP region, along with regional forest fires and agro-residue burning, influence the air pollution in this region, including the high Himalayas and the TP (Bhardwaj et al., 2018; Mahata et al., 2018; Li et al., 2017; Rupakheti et al., 2017; Putero et al., 2015; Sinha et al., 2014; Marinoni et al., 2013; Bonasoni et al., 2010). Many of the transported air pollutants, such as O_3, CO, and also components of particulate matter (PM) such as black carbon (BC) aerosol particles cause heating of the lower atmosphere and surface, which influences the Indian monsoon circulation (Ramanathan et al, 2001; 2005). Similarly, BC and mineral dust deposit on the snow and glaciers, and their light-absorbing components accelerate glacier retreat, which affects billions

of people in the region (Wester, 2019; UNEP, 2018; Li et al., 2017; Li et al., 2016). Improving knowledge of air pollution and climate change, as well as the sources of air pollutants and GHGs in the Himalayan-Tibetan mountain and foothill regions, will require well-placed and high-quality observations of atmospheric constituents, as well as a quantitative, spatiotemporal analysis of air pollutants and GHGs in the region.

1.2. Set up, site selection and methods

The international air pollution measurement campaign "Sustainable Atmosphere for the Kathmandu Valley-Atmospheric Brown Clouds (SusKat-ABC)" was conducted from December 2012 to June 2013 (with some of the measurements being continued for more than a year beyond that). SusKat-ABC campaign was led by the Institute for Advanced Sustainability Studies (IASS), Germany, in collaboration with the International Centre for Integrated Mountain Development (ICIMOD), Nepal. In addition, 18 research groups from 9 countries joined in to make additional measurements during the campaign. Simultaneous measurements of various air pollutants and GHGs were carried out at 6 sites in the Kathmandu Valley and several regional sites in Nepal (Lumbini, Pokhara, Jomsom, Dhunche and the "Pyramid" station at the base camp of Mt. Everest), as well as in India (Nainital, Pantanagar and Mohali) and China (Nam Co station and the Everest station) (Rupakheti et al., 2019, in preparation). More than 40 papers based on the SusKat-ABC campaign have been published or are under review. This thesis is based on three published peer-reviewed papers that focus on the seasonal and diurnal variation of GHGs and air pollutants, the spatial distribution of air pollutants, an emission flux estimation for carbon monoxide, and the vertical distribution of aerosol particles and the extent of their regional transport in the foothills of the Himalaya. The studies included in this thesis were conducted mainly in the Kathmandu Valley and the Pokhara Valley in Nepal, with a main overarching objective of understanding the spatiotemporal distribution of air pollutants and GHGs in the foothills of the central Himalaya.

To understand the spatial and temporal distribution of air pollutants, 5 sites were selected for observations within the Kathmandu Valley. Two sites were on the valley floor (Bode, 1345 m asl. in the suburbs, and Paknajol, 1380 m asl. in the city center), two sites on the mountain rim of the Valley (Bhimdhunga, 1522 m asl. and Nagarkot, 1901 m asl.), and one site near the only river outlet (Naikhandi, 1233 m asl.). Similarly, two regional sites were selected outside of the Kathmandu Valley: Chanban (1896 m asl.) and Pokhara (890 m asl.). The details of the sites and instrumentations are presented in material and methods section of individual papers (i.e., chapter 2, 3 and 4).

The regional site from which the airborne measurements were also based was in the Pokhara Valley, 150 km to the west of the Kathmandu Valley and ~ 90 km away from the southern plains, i.e, from the northern edge of IGP. Each site was equipped with an automatic weather station (AWS) to monitor the following meteorological data: (i) temperature, (ii) relative humidity, (iii) wind speed, (iv) wind direction, (v) solar radiation, (vi) pressure and (vii) precipitation.

The detailed lists of the instruments used at each of the sites and in the airborne observations are in Table 1, Table 2 and Table 1 of Chapter 2, 3 and 4 respectively. The description of all the instruments used in the observations including their working principles and calibrations are described in second section of each of the papers (Chapters 2, 3 and 4).

1.3. Hypothesis, key research questions and organization of the thesis

The SusKat project had an overarching hypothesis that the availability of collective new scientific information on sources, ambient concentrations, atmospheric processes and impacts of air pollution as well as the underlying factors that govern air pollution (i.e., finance, technology, policies and regulations, people's behaviors etc.) can substantially support formulation and implementation of effective air pollution mitigation measures. Guided by this overarching hypothesis, three studies carried out for this thesis focused on the following specific hypothesis and research questions.

- Measurement of key air pollutants (CO, O_3 and PM) and greenhouse gases (CO_2 and CH_4) with sufficient temporal and spatial (horizontal as well as vertical) coverage can be used to develop a basic understanding of their variabilities and the local and regional emission sources, including source-strength, in the central Himalayan region.

Based on this hypothesis, three key research questions are addressed in this thesis:

(i) How do key GHGs (CH_4 and CO_2) and air pollutants (CO, O_3, and PM) vary temporally (diurnally, seasonally etc.) and spatially (horizontally and vertically) at selected locations, and what is the role of meteorology in determining their distributions in the foothills of the Himalaya?

(ii) What are the likely local and regional emission sources and their relative contributions to ambient levels of GHGs and air pollutants in the region?

(iii) How are aerosol particles distributed vertically (measured using an airborne platform) and what is the role of regional emissions and transport in determining the aerosol vertical distribution in the region?

Paper 1 and paper 2 address research questions (i) and (ii) while paper 3 addresses research questions (ii) and (iii).

These papers, mainly based on analyzing the spatio-temporal distribution of air pollutants and key greenhouse gases and vertical distribution of PM in the central Himalayan region, are interlinked to each other mainly through understanding the impact of regional emissions. Papers 1 and 2, based on the measurements in the Kathmandu Valley, not only classify the potential emission sources but also use the observations to partly quantify the influence of regional emission sources. Similarly, the observed elevated pollution layer (as evident in PM and BC measurements) at an altitude of about 3000 m over the Pokhara Valley in paper 3 indicates the significance of emissions from regional pollution sources (especially from forest fires and agro-residue burning), combined with transport of pollution from the IGP and the foothills of the Himalaya to the observation locations near the Himalayan mountains. Although only PM and BC were measured in the pollution layers during aerial sampling and only gaseous species (CO_2, CH_4, CO, O_3) observed and studied in the 1st and 2nd papers, these two studies and other complementary studies (Putero et al. 2015; Bhardwaj et al. 2018, Dhungel et al. 2018) indicate emissions of aerosols and gaseous species from these regional sources are both transported horizontally and vertically over a large region including the Kathmandu Valley (Putero et.al., 2015; Bhawdwaj et al., 2018) and Himalayan mountain region, near Mt. Everest (Putero et al., 2019) and Jomsom Valley to the north of Pokhara Valley (Dhungel et al., 2018).

Following the motivation, background and introduction to the study provided above, the present section also describes key scientific contributions of the three papers included in this thesis. Chapters 2, 3 and 4 present the three papers on which the thesis is based, while the last chapter provides a brief overarching discussion and the key conclusions based on the three main papers, which are published on Atmospheric Chemistry and Physics (ACP), included here.

Chapter 2: Paper 1: **Mahata, K.S.**, Panday, A., Rupakheti, M., Singh, A., Naja, M., Lawrence, M.G. Seasonal and diurnal variability in methane and carbon dioxide in the Kathmandu Valley in the foothills of the central Himalayas, Atmos. Chem. Phys., 17, 12573–12596, 2017.

My contribution: study design along with other coauthors, site selection, setting up the instruments, their operation, calibration and maintenance, data collection, data quality check and quality control, data analysis, and preparation of draft manuscript and finalization by incorporating comments from coauthors and reviewers.

Chapter 3: Paper 2: **Mahata, K.S.**, Rupakheti, M., Panday, A.K., Bhardwaj, P., Naja, M., Singh, A., Mues, A., Cristofanelli, P., Pudasainee, D., Bonasoni, P., Lawrence, M.G. Observation and analysis of spatiotemporal characteristics of surface ozone and carbon monoxide in the Kathmandu Valley, Nepal, Atmos. Chem. Phys., 18:14113-14132, 2018.

My contribution: study design along with other coauthors, site selection, setting up the instruments, their operation, calibration and maintenance, data collection, data quality check and quality control and data analysis and preparation of draft manuscript and finalization manuscript by incorporating comments from coauthors and reviewers.

Chapter 4: Paper 3: An overview of airborne measurement in Nepal, - part 1: Vertical profile of aerosol size, number, spectral absorption and meteorology (Singh, A., **Mahata, K.S.**, Rupakheti, M., Junkermann, W., Panday, A.K., Lawrence, M. G. Atmos. Chem. Phys., 19, 245-258, 2019.

My contribution: data quality check and quality control and data analysis of part of the observation data, and providing input to finalize the draft manuscript.

The data collected and analyzed in this thesis was also important in the following co-authored studies:

1. Bhardwaj, P., Naja, M., Rupakheti, M., Lupascu, A., Mues, A., Panday, A.K., Kumar, R., **Mahata, K. S.**, Lal, S., Chandola, H. C., and Lawrence, M. G.: Variations in surface ozone and carbon monoxide in the Kathmandu Valley and surrounding broader regions during SusKat-ABC field campaign: role of local and regional sources, Atmos. Chem. Phys., 18, 11949-11971, https://doi.org/10.5194/acp-18-11949-2018, 2018.

   My contribution: Setting up the instruments, collecting and analyzing part of the observation data, and providing input towards finalizing the manuscript.

2. Dhungel, S., Kathayat, B., **Mahata, K. S.**, and Panday, A..: Transport of regional pollutants through a remote trans-Himalayan valley in Nepal, Atmos. Chem. Phys., 18, 1203-1216, https://doi.org/10.5194/acp-18-1203-2018, 2018.

My contribution: Site selection and instrument set-up, collecting and partly analyzing the observational data, and providing input towards finalizing the manuscript.

3. Cho, C., Kim, S-W., Rupakheti, M., Park, J-S., Panday, A., Yoon, S-C., Kim, J-H., Kim, H., Jeon, H., Sung, M., Kim, B. M., Hong, S. K., Park, R. J., Rupakheti, D., **Mahata, K. S.**, Praveen, P. S., Lawrence, M. G., and Holben, B.: Wintertime aerosol optical and radiative properties in the Kathmandu Valley during the SusKat-ABC field campaign, Atmos. Chem. Phys., 17, 12617-12632, https://doi.org/10.5194/acp-17-12617-2017, 2017.

   My contribution: Site selection and instrument set-up, collecting and partly analyzing the observational data, and providing input towards finalizing the manuscript.

4. Rupakheti, D., Adhikary, B., Praveen, P. S., Rupakheti, M., Kang, S., **Mahata, K. S.**, Naja, M., Zhang, Q., Panday, A. K., and Lawrence, M. G.: Pre-monsoon air quality over Lumbini, a world heritage site along the Himalayan foothills, Atmos. Chem. Phys., 17, 11041-11063, https://doi.org/10.5194/acp-17-11041-2017, 2017.

   My contribution: Site selection, setting up and calibrating instruments (Thermo Scientific 48i, Thermo Scientific 49i, Aethalometer, Cimel sun-photometer, Automatic weather station), data collection, analyzing the observational data and providing input towards preparing the manuscript.

5. Kiros, F., Shakya, K. M., Rupakheti, M., Maharjan, R., Byanju, R. M., Regmi, R. P., Naja, M., **Mahata, K. S.**, Kathayat, B, Peltier, R. E. Variability of anthropogenic gases: nitrogen oxides, Sulphur dioxide, ozone and ammonia in Kathmandu Valley, Nepal. Aerosol and Air Quality Research, 16: 3088–3101, https://doi: 10.4209/aaqr.2015.07.0445, 2016.

   My contribution: Site selection and involvement in data collection in the first phase of the passive sampling campaign, and input in preparing the manuscript.

6. Sarkar, C., Sinha, V., Kumar, V., Rupakheti, M., Panday, A., **Mahata, K. S.**, Rupakheti, D., Kathayat, B., and Lawrence, M. G. Overview of VOC emissions and chemistry from PTR-TOF-MS measurements during the SusKat-ABC campaign: high acetaldehyde, isoprene and isocyanic acid in wintertime air of the Kathmandu Valley, Atmos. Chem. Phys., 16, 3979-4003, https://doi.org/10.5194/acp-16-3979-2016, 2016.

My contribution: Instrument set-up, maintaining the AWS, AWS data collection and input towards preparing the manuscript.

1.4. Key results of the three studies

This section gives a brief overview of the key questions addressed and results obtained in the three publications in the following chapters. A more general summary of the results, together with an overall conclusions and outlook is then provided in Chapter 5.

1.4.1. CH_4 and CO_2 in the region

Measurements of GHGs are lacking in the central Himalayan region. This study measures three important GHGs, CH_4, CO_2 and water vapor, for the first time in Nepal; at Bode in the Kathmandu Valley and at a rural site Chanban in the Makwanpur district on the other side of the ridge just outside the Kathmandu Valley. Higher mixing ratios of CH_4 and CO_2 were observed at Bode in comparison to Chanban. Similarly, CH_4 and CO_2 mixing ratios were higher at Bode in comparison to global background sites such as the Mauna Loa Observatory, and also urban (Ahmadabad) and sub-urban (Shadnagar) sites in India. This is because of the high local sources and the bowl-shaped topographic features of the Kathmandu Valley. An analysis of the CO/CO_2 ratio shows that two of the major sources in the Kathmandu Valley throughout the year are residential cooking and the transport sector. However, brick kilns become the dominant source in the winter. The bowl-shaped topography of the valley and the mixing layer height (MLH) play important roles in the diurnal patterns of the concentrations of CO, CO_2 and CH_4. At Bode the latter two show strong diurnal patterns of a pronounced morning peak, a dip in the afternoon and gradual build up through the night until the next morning peak. In contrast, at Chanban CH_4 does not show any noticeable diurnal variation. Seasonally, CO_2 mixing ratios are high in the pre-monsoon and low in the monsoon seasons. Regional forest fires and agro-residue burning are associated with the pre-monsoon peak, along with the existing local polluting sources (Mahata et al., 2018; Rupakheti et al., 2017; Putero et al., 2015). Frequent rainfall during the monsoon suppresses the biomass burning activities in the region, and the closure of the brick industries in the valley reduces the emissions of pollutants as well as CO_2 in this season. Hence, this study provides key information on the diurnal and seasonal variations of CO_2 and CH_4 in the region. Furthermore, it sheds light on the possible emission sources, including the contribution of urban local sources, by examining the CO and CO_2 ratios, and by comparing the mixing ratios of these species between semi-urban and rural sites.

1.4.2. Air pollutants (CO and O_3) at multiple sites in the Kathmandu Valley

CO and O_3 observations made for the first time for a longer period at 5 sites in the Kathmandu Valley provide unique datasets which help in characterizing their diurnal and seasonal variations at multiple sites, and attributing the sources responsible for these pollutants. As in the first study (paper 1), this study (paper 2) confirms that the major, contributing sources of air pollution in the valley are the transport sector, residential sector, brick kilns, trash burning and regional forest and agro-residue burning (Mahata et al., 2018; Kim et al., 2015; Putero et al., 2015). The high CO mixing ratios during the morning and evening at most of the sites shows the influence of local polluting sources with favorable meteorological parameters (calm winds). After the break-up of the MLH (late morning to early evening), fresh air coming from outside the valley is mixed with the polluted air due to higher wind speeds, which reduces the pollutant levels to their minimum in the valley (Mahata et al., 2018; Mues et al., 2016; Panday et al., 2009). It might be possible to make use of this information about the time windows of pollutant mixing, etc., in order to help improve air quality via careful management of the timing of the operation of brick industries, trash burning, private vehicles (especially diesel trucks), etc.

A key result of this study is calculating an estimate of the CO emissions flux for the valley, which is estimated to be 2-14 times higher than the available global and regional emission data bases used in models (EDGAR HTAP-2, REAS, INTEX-B). This is consistent with an underestimate of pollutants such as CO and BC noted in model simulations of the region. This large difference points towards the need to update the emission inventories for South Asia.

A further result from this study is the analysis of simultaneous O_3 observation at Paknajol (city center), Bode (sub-urban) and Nagarkot (hill top) for a full year, which is the first of this kind of observations in the Kathmandu Valley, and is also unprecedented for the broader Himalayan region. Our study reported for the first time that the O_3 level exceeds the WHO recommended value by more than 78% of the days at all sites during the pre-monsoon period, which is of significant concern for human health and ecosystems within the valley and the surrounding regions. Further, the higher number of days per year with O_3 exceedances at Nagarkot in comparison to Paknajol and Bode supports the idea of stratospheric intrusions and regional, long-range transport, as well as indicating the regional-scale ozone pollution. These will provide valuable support for policy makers to help understand measures needed to curb the increasing air pollutant levels in the foothills of the Himalayas.

1.4.3. Vertical distribution of air pollutants

Airborne measurements were carried out based out of the Pokhara Valley (~815 m asl, ~150 km due west of Kathmandu, and ~90 km northward from the southern plains) onboard flights with an ultralight aircraft, aimed at quantifying the vertical distribution of aerosol particles in the foothills of the Himalayas and investigate the extent of regional pollutant transport into the Himalayas. A high aerosol concentration is nearly ubiquitously observed below 2000 m asl, decreasing with altitude up to 4500 m asl. An elevated aerosol layer was regularly detected around 3000 m asl. The aerosol number concentration and BC concentration of the elevated layer is similar to the aerosol loading near the surface (<1000 m asl.); however, it is comparable to BC in Kanpur, a major city in the IGP in India, but lower than the BC levels observed in the Kathmandu Valley during the pre-monsoon season (Singh et al., 2019; Mues et al., 2017). A high aerosol extinction co-efficient at 550 nm, along with the observation of polluted dust and smoke in the elevated layer indicates regional transport of the pollutants. Furthermore, long-term measurements (2010-2016) of aerosol optical depth (AOD) show the strong seasonality of AOD (Singh et al., 2019). The maximum AOD observed in the pre-monsoon season could be linked to the transport of dust and aerosol by westerly advection from the IGP to the foothills of the Himalaya and the mountain valleys.

All of the past studies, to the extent known, are based on ground based measurements of the air pollutants. The measurement of vertical profiles of pollutants, which are presented here, is thus quite important, and provides clear evidence of regional transport. Hence, the need for air borne measurements, which are the first of their kind in the central Himalayan region, is considered in this paper, focusing on quantifying the vertical distribution of aerosol particles and regional transport of the pollutants in the foothills of the Himalaya.

1.5. Further contributions

My contribution to other papers as a coauthor not only enhanced my knowledge by participating in various interesting studies led by the collaborating partners, but they also make further use of the observations data that I carefully gathered in the field, and support the results of my main 3 research papers. Three of the peer-reviewed papers, Dhungel et al. (2018), Rupakheti et al. (2017) and Bhardwaj et al. (2018), connect how the regional pollution (from the IGP), especially during the pre-monsoon season, affects air pollutants from the foothills of the Himalayas up to the high Himalayas, including the Kathmandu Valley. It also supports an understanding of why O_3 increases during the pre-monsoon period, and provides information on some regional sources of the air pollutants. The passive sampling study by Kiros et al.

(2016) corroborates the results of our study (real time monitoring) finding high O_3 at a rural site in comparison to the urban city center. Finally, Kim et al. (2017) and Sarkar et al. (2015) clearly show the seasonal contributions of the transport sector, brick kilns and trash burning towards deteriorating Kathmandu's air quality. These results, similar to the results described in the three papers included in this thesis, will provide further solid scientific information as a basis for the future design and monitoring of effective mitigation measures.

Chapter 2

Seasonal and Diurnal Variations of Methane and Carbon Dioxide in the Kathmandu Valley in the Foothills of the Central Himalaya

Abstract

The SusKat-ABC (Sustainable Atmosphere for the Kathmandu Valley- Atmospheric Brown Clouds) international air pollution measurement campaign was carried out during December 2012-June 2013 in the Kathmandu Valley and surrounding regions in Nepal. The Kathmandu Valley is a bowl-shaped basin with a severe air pollution problem. This paper reports measurements of two major greenhouse gases (GHGs), methane (CH_4) and carbon dioxide (CO_2), along with the pollutant CO that began during the campaign and were extended for a year at the SusKat-ABC supersite in Bode, a semi-urban location in the Kathmandu Valley. Simultaneous measurements were also made during 2015 in Bode and a nearby rural site (Chanban), ~25 km (aerial distance) to the southwest of Bode, on the other side of a tall ridge. The ambient mixing ratios of methane (CH_4), carbon dioxide (CO_2), water vapor, and carbon monoxide (CO) were measured with a cavity ring down spectrometer (Picarro G2401, USA), along with meteorological parameters for a year (March 2013 - March 2014). These measurements are the first of their kind in the central Himalayan foothills. At Bode, the annual average mixing ratios of CO_2 and CH_4 were 419.3(±6.0) ppm and 2.192(±0.066) ppm, respectively. These values are higher than the levels observed at background sites such as Mauna Loa, USA (CO_2: 396.8 ± 2.0 ppm, CH_4: 1.831 ± 0.110 ppm) and Waliguan, China (CO_2: 397.7 ± 3.6 ppm, CH_4: 1.879 ± 0.009 ppm) during the same period, and at other urban/semi-urban sites in the region such as Ahmedabad and Shadnagar (India). They varied slightly across the seasons at Bode, with seasonal average CH_4 mixing ratios being 2.157(±0.230) ppm in the pre-monsoon season, 2.199(±0.241) ppm in the monsoon, 2.210(±0.200) ppm in the post-monsoon, and 2.214(± 0.209) ppm in the winter season. The average CO_2 mixing ratios were 426.2(±25.5) ppm in pre-monsoon, 413.5(±24.2) ppm in monsoon, 417.3(±23.1) ppm in post-monsoon, and 421.9(±20.3) ppm in winter season. The maximum seasonal mean mixing ratio of CH_4 in winter was only 0.057 ppm or 2.6% higher than the seasonal minimum during the

pre-monsoon period, while CO_2 was 12.8 ppm or 3.1% higher during the pre-monsoon period (seasonal maximum) than during the monsoon (seasonal minimum). On the other hand, the CO mixing ratio at Bode was 191% higher during the winter than during the monsoon season. The enhancement in CO_2 mixing ratios during the pre-monsoon season is associated with additional CO_2 emissions from forest fire and agro-residue burning in northern South Asia in addition to local emissions in the Kathmandu Valley. Published CO/CO_2 ratios of different emission sources in Nepal and India were compared with the observed CO/CO_2 ratios in this study. This comparison suggested that the major sources in the Kathmandu Valley were residential cooking and vehicle exhaust in all seasons except winter. In winter, the brick kiln emissions were a major source. Simultaneous measurement in Bode and Chanban (15 July-3 Oct 2015) revealed that the mixing ratio of CO_2, CH_4 and CO mixing ratios were 3.8%, 12%, and 64% higher in Bode than Chanban. Kathmandu Valley, thus, has significant emissions from local sources, which can also be attributed to its bowl-shaped geography that is conducive to pollution build-up. At Bode, all three gas species (CO_2, CH_4 and CO) showed strong diurnal patterns in their mixing ratios with a pronounced morning peak (ca. 08:00), a dip in the afternoon, and again gradual increase through the night until the next morning, whereas CH_4 and CO at Chanban did not show any noticeable diurnal variations.

These measurements provide the first insights into diurnal and seasonal variation of key greenhouse gases and air pollutants and their local and regional sources, which are important information for the atmospheric research in the region.

2.1. Introduction

The average atmospheric mixing ratios of two major greenhouse gases (GHGs), CO_2 and CH_4, have increased by about 40% (from 278 to 390.5 ppm) and about 150% (from 722 to 1803 ppb) respectively since pre-industrial times (~1750 AD). This is mostly attributed to anthropogenic emissions (IPCC, 2013). The current global annual rate of increase of the atmospheric CO_2 mixing ratio is 1-3 ppm, with average annual mixing ratios now exceeding a value of 400 ppm at the background reference location in Mauna Loa (WMO, 2016). Between 1750 and 2011, 240(±10) PgC of anthropogenic CO_2 was accumulated in the atmosphere of which two thirds were contributed by fossil fuel combustion and cement production, with the remaining coming from deforestation and land use/land cover changes (IPCC, 2013). CH_4 is the second largest gaseous contributor to anthropogenic radiative forcing after CO_2 (Forster et al., 2007). The major anthropogenic sources of atmospheric CH_4 are rice paddies, ruminants and fossil fuel

use, contributing approximately 60% to the global CH_4 budget (Chen and Prinn, 2006; Schneising et al., 2009). The remaining fraction is contributed by biogenic sources such as wetlands and fermentation of organic matter by microbes in anaerobic conditions (Conrad, 1996).

Increasing atmospheric mixing ratios of CO_2 and CH_4 and other GHGs and short-lived climate-forcing pollutants (SLCPs) such as black carbon (BC) and tropospheric ozone (O_3) have caused the global mean surface temperature to increase by 0.85°C from 1880 to 2012. The surface temperature is expected to increase further by up to 2 degrees at the end of the 21st century in most representative concentration pathways (RCP) emission scenarios (IPCC, 2013). The increase in surface temperature is linked to melting of glaciers and ice sheets, sea level rise, extreme weather events, loss of biodiversity, reduced crop productivity, and economic losses (Fowler and Hennessy, 1995; Guoxin and Shibasaki, 2003).

Seventy percent of global anthropogenic CO_2 is emitted in urban areas (Fragkias et al., 2013). Developing countries may have lower per capita GHG emissions than developed countries, but the large cities in developing countries, with their high population and industrial densities, are major consumers of fossil fuels and thus, emitters of GHGs. South Asia, a highly populated region with rapid growth in urbanization, motorization, and industrialization in recent decades, has an ever increasing fossil fuel demand and its combustion emitted 444 Tg C/year in 2000 (Patra, et al., 2013), or about 5% of the global total CO_2 emissions. Furthermore, a major segment of the population in South Asia has an agrarian economy and uses biofuel for cooking activities, and agro-residue burning is also common practice in the region, which are important major sources of air pollutants and greenhouse gases in the region (CBS, 2011; Pandey et al., 2014; Sinha et al., 2014).

The emission and uptake of CO_2 and CH_4 follow a distinct cycle in South Asia. By using inverse modeling, Patra et al. (2011) found a net CO_2 uptake (0.37 ± 0.20 Pg C yr^{-1}) during 2008 in South Asia and the uptake (sink) is highest during July-September. The remaining months acts as a weak gross sink but a moderate gross source for CO_2 in the region. The observed variation is linked with the growing seasons. Agriculture is a major contributor of methane emission. For instance, in India it contributes to 75% of CH_4 emissions (MoEF, 2007). Ambient CH_4 concentrations are highest during June to September (peaking in September) in South Asia which are also the growing months for rice paddies (Goroshi et al.,

2011). The minimum column averaged CH_4 mixing ratios are in February-March (Prasad et al., 2014).

Climate change has impacted South Asia in several ways, as evident in temperature increase, change in precipitation patterns, higher incidence of extreme weather events (floods, droughts, heat waves, cold waves), melting of snowfields and glaciers in the mountain regions, and impacts on ecosystems and livelihoods (ICIMOD, 2009; MoE, 2011). Countries such as Nepal are vulnerable to impacts of climate change due to inadequate preparedness for adaptation to impacts of climate change (MoE, 2011). Decarbonization of its economy can be an important policy measure in mitigating climate change. Kathmandu Valley is one of the largest metropolitan cities in the foothills of the Hindu Kush-Himalaya which has significant reliance on fossil fuels and biofuels. In 2005, fossil fuel burning accounted for 53% of total energy consumption in the Kathmandu Valley, while biomass and hydroelectricity were 38% and 9%, respectively (Shrestha and Rajbhandari, 2010). Fossil fuel consumed in the Kathmandu Valley accounts for 32% of the country's fossil fuel imports, and the major fossil fuel consumers are residential (53.17%), transport (20.80%), industrial (16.84%), and commercial (9.11%) sectors. Combustion of these fuels in traditional technologies such as Fixed Chimney Bulls Trench Kiln (FCBTK) and low efficiency engines (vehicles, captive power generator sets etc.) emit significant amounts of greenhouse gases and air pollutants. This has contributed to elevated ambient concentrations of particulate matter (PM), including black carbon and organic carbon, and several gaseous species such as ozone, polycyclic aromatic hydrocarbons (PAHs), acetonitrile, benzene and isocyanic acid (Pudasainee et al., 2006; Aryal et al., 2009; Panday and Prinn, 2009; Sharma et al., 2012; World Bank, 2014; Chen et al., 2015; Putero et al., 2015: Sarkar et al., 2016). The ambient levels often exceed national air quality guidelines (Pudasainee et al., 2006; Aryal et al., 2009; Putero et al., 2015) and are comparable or higher than ambient levels observed in other major cities in South Asia.

Past studies in the Kathmandu Valley have focused mainly on a few aerosols species (BC, PM) and short-lived gaseous pollutants such as ozone and carbon monoxide (Pudasainee et al., 2006; Aryal et al., 2009; Panday and Prinn, 2009; Sharma et al., 2012, Putero et al., 2015). To the best of authors' knowledge, no direct measurements of CO_2 and CH_4 are available for the Kathmandu Valley. Recently, emission estimates of CO_2 and CH_4 were derived for the Kathmandu Valley using the International Vehicle Emission (IVE) model (Shrestha et al., 2013). The study estimated 1554 Gg of annual emission of CO_2 from a fleet of vehicles (that consisted of public buses, 3-wheelers, taxis and motor cycles; private cars, trucks and non-road

vehicles were not included in the study) for the year 2010. In addition, the study also estimated 1.261 Gg of CH_4 emitted from 3 wheelers (10.6 %), taxis (17.7 %) and motorcycles (71 %) for 2010

This study presents the first 12 months of measurements of two key GHGs, CH_4 and CO_2 along with other trace gases and meteorological parameters in Bode, a semi-urban site in the eastern part of the Kathmandu Valley. The year-long measurement in Bode is a part of the SusKat-ABC (Sustainable Atmosphere for the Kathmandu Valley – Atmospheric Brown Clouds) international air pollution measurement campaign conducted in and around the Kathmandu Valley from December 2012 to June 2013. Details of the SusKat-ABC campaign are described in Rupakheti et al. 2019 (manuscript in preparation). The present study provides a detailed account of seasonal and diurnal behaviors of CO_2 and CH_4 and their possible sources. To examine the rural-urban differences and estimate the urban enhancement, these gaseous species were also simultaneously measured for about three months (Jul-Oct) in 2015 at Chanban, a rural site about 25 km (aerial distance) outside and southwest of Kathmandu Valley. The seasonality of the trace gases and influence of potential sources in various (wind) directions are further explored by via ratio analysis. This measurement provides unique data from highly polluted but relatively poorly studied region (central Himalayan foothills in South Asia) which could be useful for validation of emissions estimates, model outputs and satellite observations. The study, which provides new insights on potential sources, can also be a good basis for designing mitigation measures for reducing emissions of air pollutants and controlling greenhouse gases in the Kathmandu Valley and the region.

2.2. Experiment and Methodology

2.2.1. Kathmandu Valley

The Kathmandu Valley consists of three administrative districts: Kathmandu, Lalitpur, and Bhaktapur, situated between 27.625° N, 27.75° N and 85.25°E, 85.375°E. It is a nearly circular bowl-shaped valley with a valley floor area of approximately 340 km^2 located at an altitude of 1300 m mean sea level (asl.). The surrounding mountains are close to 2000-2800 in height above sea level with five mountain passes located at about 200-600 m above the valley floor and an outlet for the Bagmati River southwest of the Kathmandu Valley. Lack of decentralization in in Nepal has resulted in the concentration of economic activities, health and education facilities, the service sector, as well as most of the central governmental offices in the Kathmandu Valley. Consequently, it is one of the fastest growing metropolitan areas in

South Asia with a current population of about 2.5 million, and the population growth rate of 4% per year (World Bank, 2013) Likewise, approximately 50% of the total vehicle fleet (2.33 million) of the country is in Kathmandu Valley (DoTM, 2015). The consumption of fossil fuels such as liquefied petroleum gas (LPG), kerosene for cooking and heating dominates the residential consumption, while the rest use biofuel (fuel wood, agro-residue, and animal dung) for cooking and heating in the Kathmandu Valley. The commercial sector is also growing in the valley, and the latest data indicate the presence of 633 industries of various sizes. These are mainly associated with dyeing, brick kilns, and manufacturing industries. Fossil fuels such as coal and biofuels are the major fuels used in brick kilns. Brick kilns are reported as one of the major contributors of air pollution in the Kathmandu Valley (Chen et al., 2015; Kim et al., 2015; Sarkar et al., 2016). There are about 115 brick industries in the valley (personal communication with M. Chitrakar, President of the Federation of Nepalese Brick Industries). Acute power shortage in the Valley is common all around the year, especially in the dry season (winter/pre-monsoon) when the power cuts can last up to 12 hours a day (NEA, 2014). Energy demand during the power cut period is met with the use of small (67% of 776 generators surveyed for the World Bank study was with capacity less than 50kVA) but numerous captive power generators (diesel/petrol), which further contribute to valley's poor air quality. According to the World Bank's estimate, over 250,000 such generator sets are used in the Kathmandu Valley alone, producing nearly 200 MW of captive power, and providing about 28% of the total electricity consumption of the valley (World Bank, 2014). Apart from these sources, trash burning, which is a common practice (more prevalent in winter) throughout the valley, is one of the major sources of air pollutants and GHGs.

Climatologically, Kathmandu Valley has a sub-tropical climate with annual mean temperature of 18°C, and annual average rainfall of 1400 mm, of which 90% occurs in monsoon season (June-September). The rest of the year is dry with some sporadic rain events. The wind circulation at large scale in the region is governed by the Asian monsoon circulation and hence the seasons are also classified based on such large scale circulations and precipitation: Pre-Monsoon (March-May), Monsoon (June-September), Post-Monsoon (October-November) and Winter (December-February). Sharma et al. (2012) used the same classification of seasons while explaining the seasonal variation of BC concentrations observed in the Kathmandu Valley. Locally in the valley, the mountain-valley wind circulations play an important role in influencing air quality. The wind speed at the valley floor is calm ($\leq$ 1 m s^{-1}) in the morning and night, while a westerly wind develops after 11:00 AM in the morning till dusk, and

switches to a mild easterly at night (Panday and Prinn, 2009; Regmi et al., 2003). This is highly conducive to building up of air pollution in the valley, which gets worse during the dry season.

2.2.2. Study sites

Two sites, a semi-urban site within the Kathmandu Valley and a rural site outside the Kathmandu Valley, were selected for this study. The details of the measurements carried out in these sites is described Table 2.1 and in section 2.2.2.1 and 2.2.2.2.

2.2.2.1. Bode (SusKat-ABC supersite)

The SusKat-ABC supersite was set up at Bode, a semi-urban location (Figure 1) of the Madhyapur Thimi municipality in the Bhaktapur district in the eastern side of the Kathmandu Valley. The site is located at 27.68^0N latitude, 85.38^0E longitude, and 1344 masl. The local area around the site has a number of scattered houses and agricultural fields. The agriculture fields are used for growing rice paddies in the monsoon season. It also receives outflow of polluted air from three major cities in the valley: Kathmandu Metropolitan City and Lalitpur Sub-Metropolitan City, both mainly during daytime, and Bhaktapur Sub-Metropolitan City mainly during nighttime. Among other local sources around the site, about 10 brick kilns are located in the east and southeast direction, approximately within 1-4 km from the site which are operational only during dry season (January to April). There are close to 20 small and medium industries (pharmaceuticals, plastics, electronics, tin, wood, aluminum, iron, fabrics etc.) scattered in the same direction. The Tribhuvan International Airport (TIA) is located approximately 4 km to the west of Bode.

2.2.2.2. Chanban

Chanban is a rural/background site in Makwanpur district outside of the Kathmandu Valley (Figure 2.1). This site is located ~25 km aerial distance due southwest from Bode. The site is located on a small ridge (27.65^0N, 85.14^0E, 1896 masl) between two villages - Chitlang and Bajrabarahi - within the forested watershed area of Kulekhani Reservoir, which is located approximately 4.5 km southwest of the site. The instruments were set up on the roof of 1-storey building in an open space inside the Nepali Army barrack. There was a kitchen of the army barrack at about 100 m to the southeast of the measurement site. The kitchen uses LPG, electricity, kerosene, and firewood for cooking activities.

Table 2.1. Instruments and sampling at Bode (semi-urban site) and Chanban (rural site)

Site	Instrument	Species	Sampling interval	Measurement period	Inlet or sensor height above ground (m)
Bode	i. Cavity ring-down spectrometer (G2401; Picarro, USA)	CO_2, CH_4, CO, water vapor	5 s	6 Mar 2013–5 Mar 2014 14 Jul 2015–7 Aug 2015	20
	ii. CO monitor (AP-370; Horiba, USA)	CO	5 min	6 Mar 2013–7 Jun 2013	20
	iii. Ceilometer (CL31; Vaisala, Finland)		15–52 min	6 Mar 2013–5 Mar 2014	20
	iv. AWS (Campbell Scientific, USA)		1 min		23
	a. CS215	RH, *T*		6 Mar 2013–24 Apr 2013	
	b. CS300 pyranometer	SR		6 Mar 2013–5 Mar 2014 14 Jul 2015–7 Aug 2015	
	c. R.M. Young 05103-5	WD, WS		6 Mar 2013–5 Mar 2014 14 Jul 2015–7 Aug 2015	
	v. Airport AWS (Environdata, Australia)				
	a. TA10	*T*		18 Jun 2013–13 Jan 2013	
	b. RG series	RF		6 Mar 2013–15 Dec 2013	
Chanban	i. Cavity ring-down spectrometer (G2401; Picarro, USA)	CO_2, CH_4, CO, water vapor	5 s	15 Jul 2015–3 Oct 2015	3
	ii. AWS (Vantage Pro2; Davis Instruments, USA)	RH, *T*, SR, WD, WS, RF, *P*	10 min	14 Jul 2015–7 Aug 2015	2

AWS: automatic weather station, RH: ambient relative humidity, *T*: ambient temperature, SR: global solar radiation, WS: wind speed, WD: wind direction, RF: rainfall, *P*: ambient pressure.

2.2.3. Instrumentation

The measurements were carried out in two phases in 2013-2014 and 2015. In phase one, a cavity ring down spectrometer (Picarro G2401, USA) was deployed in Bode to measure ambient CO_2, CH_4, CO, and water vapor mixing ratios. Twelve months (6 March 2013 - 5 March 2014) of continuous measurements were made in Bode. The operational details of the instruments deployed in Bode are also provided in Table 2.1. In phase two, simultaneous measurements were made in Bode and Chanban for a little less than 3 months (15 July to 03 October 2015).

The Picarro G2401 analyzer quantifies spectral features of gas phase molecules by using a novel wavelength-scanned cavity ring down spectroscopic technique (CRDS). The instrument has a 30 km path length in a compact cavity that results in high sensitivity. Because of the high precision wavelength monitor, it uses absolute spectral position and maintains accurate peak quantification. Further, it only monitors the special features of interest to reduce drift. The instrument also has water correction to report dry gas fraction. The reported measurement precisions for CO_2, CH_4, CO and water vapor in dry gas is < 150 ppb, < 30 ppb, < 1ppb and < 200 ppm for 5 seconds with 1 standard deviation (Picarro, 2015).

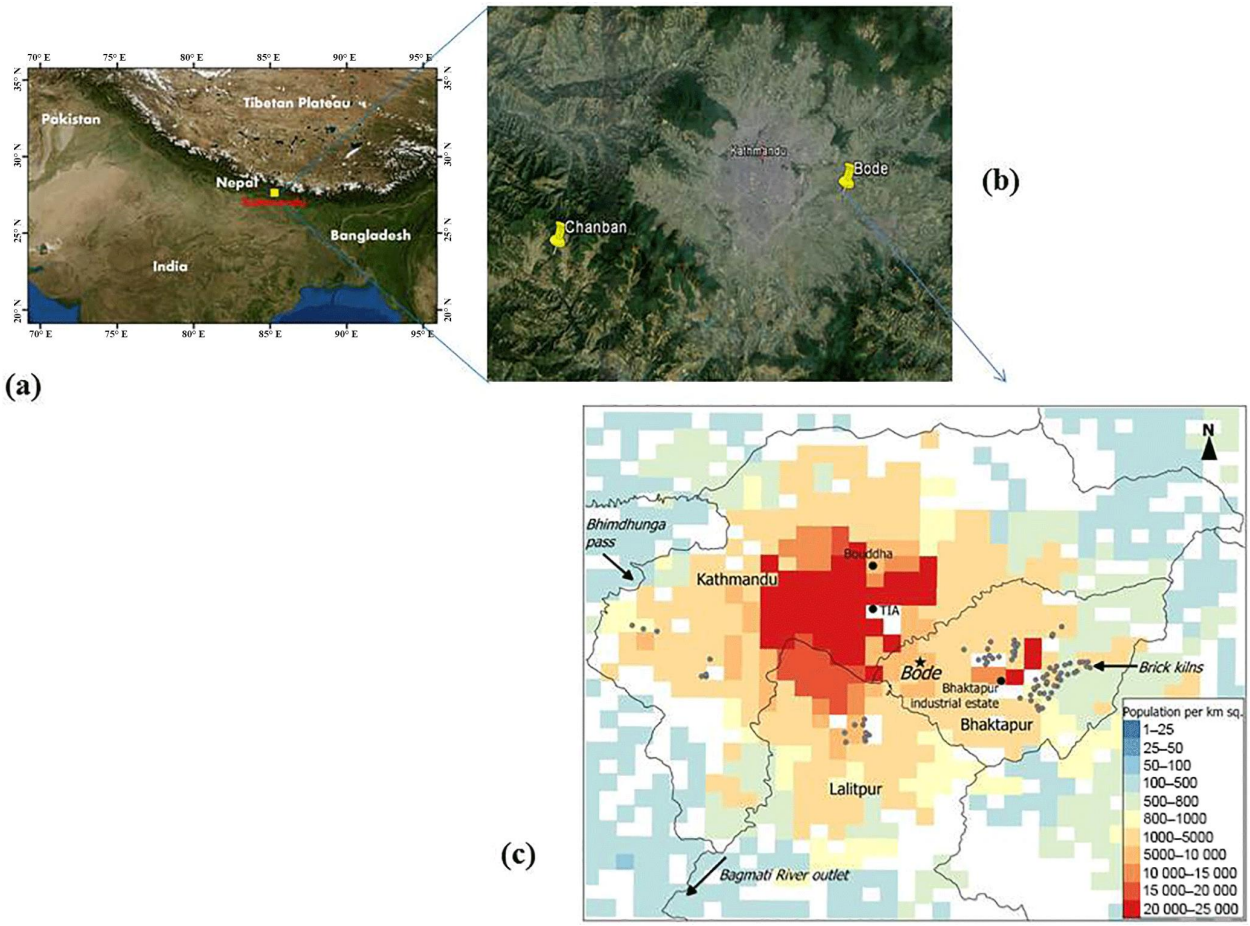

Figure 2.1. Location of measurement sites: (a) Kathmandu Valley (b) semi-urban measurement site at Bode in Kathmandu Valley, and a rural measurement site at Chanban in Makawanpur district Nepal, (c) general setting of Bode site. The colored grid and TIA represent population density and the Tribhuvan International Airport respectively.

In Bode, the Picarro analyzer was placed on the 4th floor of a 5-storey building with an inlet at 0.5 m above the roof of the building with a 360 degree view (total inlet height: 20 m above ground). The sample air was filtered at the inlet to keep dust and insects out and was drawn into the instrument through a 9 m Teflon tube (1/4 inches ID). The Picarro analyzer was set to record data every 5 second and recorded both directly sampled data and water corrected data for CO_2 and CH_4. In this paper, only water-corrected or dry mixing ratios of CH_4 and CO_2 were used to calculate the hourly averages for diurnal and seasonal analysis.

The instruments were factory calibrated before commencing the field measurements. Picarro G2401 model is designed for remote application and long term deployment with minimal drift and less requirement for intensive calibration (Crosson, 2008) and thus was chosen for the current study in places like Kathmandu where there is no or limited availability of high quality reference gases. Regular calibration of Picarro G2401 in field during 2013-2014 deployment

was not conducted due to challenges associated with the quality of the reference gas, especially for CO and CH_4. One time calibration was performed for CO_2 (at 395, and 895 ppmv) in July 2015 before commencing the simultaneous measurements in Bode and Chanban in 2015. The difference between CO_2 mixing ratio reported by the analyzer and the reference mixing ratio was within 5%. CO observations from Picarro G2401 were compared with observations from another CO analyzer (Horiba, model AP370) that was also operated in Bode for 3 months (March - May 2013). The Horiba CO monitor was a new unit, which was factory calibrated before its first deployment in Bode. Nevertheless, this instrument was inter-compared with another CO analyzer (same model) from the same manufacturer prior to the campaign and its correlation coefficient was 0.9 [slope of data from the new unit (y-axis) vs the old unit (x-axis) = 1.09]. Primary gas cylinders from Linde UK (1150 ppbv) and secondary gases from Ultra-Pure Gases and Chemotron Science Laboratories (1790 ppbv) were used for the calibration of CO instrument. Further details on CO measurements and calibration of Horiba AP370 can be found in Sarangi et al. (2014; 2016). A statistically significant correlation (r = 0.99, slope = 0.96) was found between Picarro and Horiba hourly average CO mixing ratio data (Supplementary Information Figure S1). Furthermore, the monthly mean difference between these two instruments (Horiba AP370 minus Picarro G2401) was calculated to be 0.02 ppm (3%), 0.04 ppm (5%) and 0.02 ppm (4%) in March, April and May, respectively. For the comparison period of 3 months, the mean difference was 0.02 ppm (4%). Overall differences were small to negligible during the comparison period and thus, adjustment in the data was deemed unnecessary.

Besides being highly selective to individual species, Picarro G2401 has a water correction function and thus accounts for the any likely drift in CO, CO_2 and CH_4 mixing ratios with the fluctuating water vapor concentration (Chen et al., 2013; Crosson, 2008). Crosson (2008) also estimated a peak to peak drift of 0.25 ppmv. Further, Crosson (2008) observed a 1.2 ppbv/day drift in CO_2 after 170 days from the initial calibration. For a duration of one year the drift will be less than 1 ppmv, which is less than 1% of the observed mixing ratio in (hourly ranges: 376-537 ppm) Bode even if the drift was in same magnitude as in case of Crosson (2008). Crosson (2008) reported 0.8 ppbv peak to peak drift in CH_4 measurements for 18 days after the initial calibration.

There were other instruments concurrently operated in Bode; a ceilometer for measuring mixing layer height (Vaisala Ceilometer CL31, Finland), and an Automatic Weather Station (AWS) (Campbell Scientific, USA). The ceilometer was installed on the rooftop (20 m above

ground) of the building (Mues et al., 2017). For measuring the meteorological parameters, a Campbell Scientific AWS (USA) was set up on the roof of the building with sensors mounted at 2.9 m above the surface of the roof (22.9 m from the ground). The Campbell Scientific AWS measured wind speed and direction, temperature, relative humidity and solar radiation every minute. Temperature and rainfall data were taken from an AWS operated by the Department of Hydrology and Meteorology (DHM), Nepal at the Tribhuvan International Airport (TIA, see Figure 1), ~4 km due west of Bode site.

At Chanban, the inlet for Picarro gas analyzer was kept on the rooftop ~3 m above the ground and the sample air was drawn through a 3 m long Teflon tube (1/4 inches ID). The sample was filtered at the inlet with a filter (5-6 µm pore size) to prevent aerosol particles from entering into the analyzer. An AWS (Davis Vantage Pro2, USA) was also set up in an open area, about 17 m away from the building and with the sensors mounted at 2 m above ground.

2.3. Results and discussion

The results and discussions are organized as follow: Sub-section 2.3.1 describes a year round variation in CH_4, CO_2, CO and water vapor at Bode; sub-sections 2.3.2, 2.3.3 present the analysis of the observed monthly and seasonal variations and diurnal variation. Sub-sections 2.3.4 and 2.3.5 discuss the interrelation of CO_2, CH_4 and CO and potential emission sources in the valley and sub-section 2.3.6 compares and contrasts CH_4, CO_2, CO at Bode and Chanban.

2.3.1. Time series of CH_4, CO_2, CO and water vapor mixing ratios

Figure 2.2 shows the time series of hourly mixing ratios of CH_4, CO_2, CO, and water vapor at Bode. Meteorological data from Bode and the Tribhuvan International Airport are also shown in Figure 2.2. Data gaps in Figure 2.2a and 2b were due to maintenance of the measurement station. In general, the changes observed in CO mixing ratio were higher in terms of % change than the variations observed in CH_4 and CO_2 mixing ratios during the sampling period. In contrast, CO mixing ratios decreased and water vapor mixing ratios increased significantly during the rainy season (June-September). For the entire sampling period, the annual average (± one standard deviation) of CH_4, CO_2, CO, and water vapor mixing ratios were 2.192 (±0.066) ppm, 419.3 (±6.0) ppm, 0.50 (±0.23) ppm, and 1.73 (±0.66) %, respectively. The relative standard deviation for the annual average of CH_4, CO_2 and CO were thus 3%, 1.4% and 46%, respectively. Their relative standard deviation at Mauna Loa were CH_4: 6% and CO_2: 0.5% and at Waliguan were CH_4: 0.48%, CO_2: 0.9%. The high variability in the annual mean, notably for CO in Bode could be indicative of the seasonality of emission sources and meteorology.

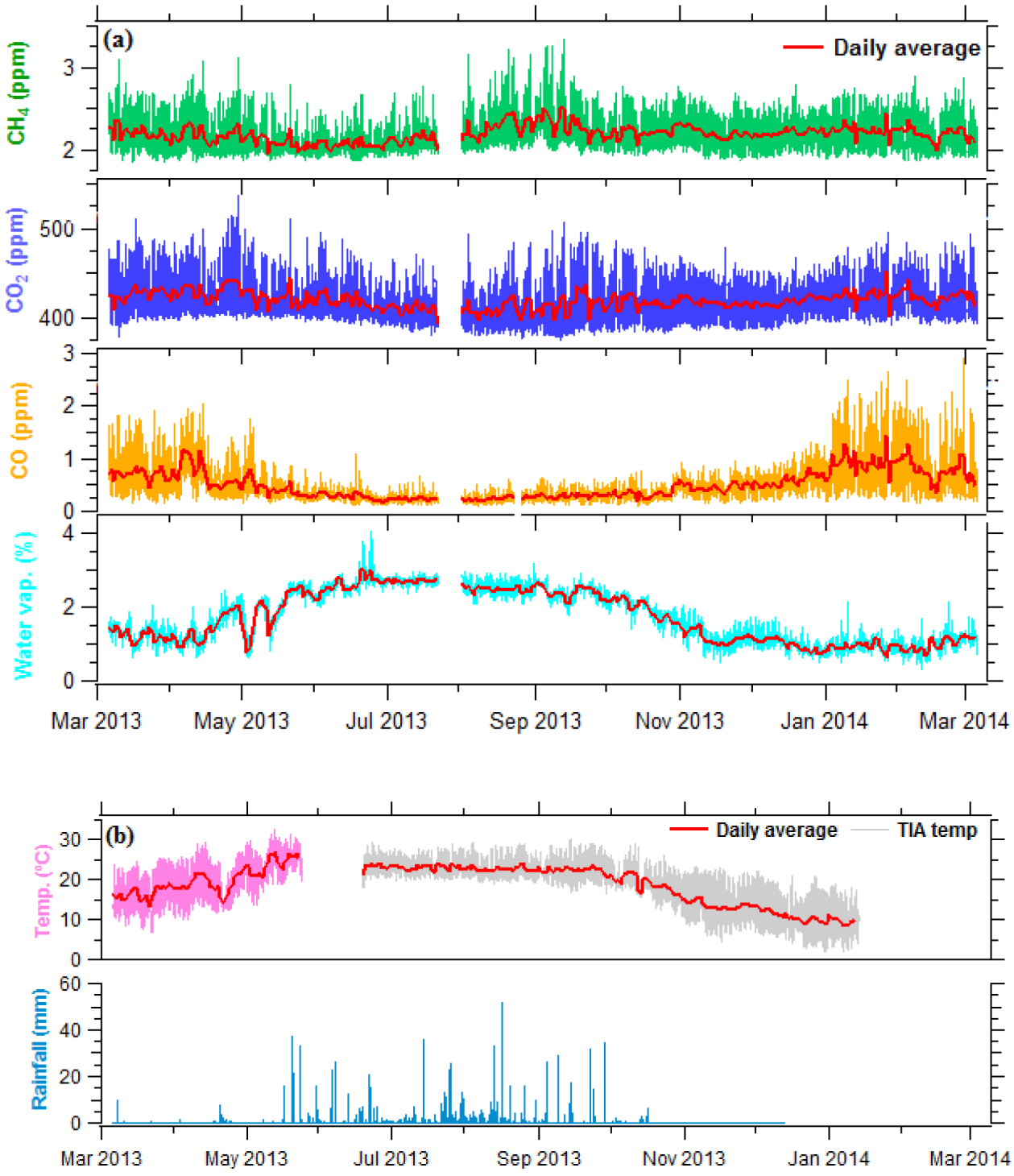

Figure 2.2. Time series of hourly average (a) mixing ratios of CH_4, CO_2, CO, and water vapor measured with a cavity ring down spectrometer (Picarro G2401) at Bode, and (b) temperature and rainfall monitored at the Tribhuvan International Airport (TIA), ~4 km to the west of Bode site in the Kathmandu Valley, Nepal. Temperature shown in pink color is observed at Bode site.

The annual CH_4 and CO_2 mixing ratios were compared to the historical background site (Mauna Loa Observatory, Hawaii, USA) and the background site (Waliguan, China) in Asia, which will provide insight on spatial differences. The selection of neighboring urban and semi-urban sites, where many emission sources are typical for the region, for comparison provides information on relative differences (higher/lower), which will help in investigating possible local emission sources in the valley. As expected, annual mean of CH_4 and CO_2 mixing ratios in the Kathmandu Valley were higher than the levels observed at background sites in the region and elsewhere (Table 2.4). We performed a significance test at 95% confidence level (t-test) of the annual mean values between the sites to evaluate whether the observed difference is statistically significant ($p < 0.05$), which was confirmed for the annual mean CH_4 and CO_2 between Bode and Mauna Loa, and between Bode and Waliguan. CH_4 was nearly 20% higher at Bode than at Mauna Loa observatory (1.831 ± 0.110 ppm) (Dlugokencky et al., 2017) and calculated 17% higher than at Mt. Waliguan (1.879 ± 0.009 ppm) for the same observation period (Dlugokencky et al., 2016). The slightly higher CH_4 mixing ratios between at Bode and Waliguan than at Mauna Loa Observatory could be due to rice farming as a key source of CH_4 in this part of Asia. Thus, it could be associated with such agricultural activities in this region.

Similarly, the annual average CH_4 at Bode during 2013-14 was found comparable to an urban site in Ahmedabad (1.880 ± 0.4 ppm, i.e., variability: 21.3%) in India for 2002 (Sahu and Lal, 2006) and 14% higher than in Shadnagar (1.92 ± 0.07 ppm, i.e., variability: 3.6%), a semi-urban site in Telangana state (~70 km north from Hyderabad city) during 2014 (Sreenivas et al., 2016). Likewise, the difference between annual mean mixing ratios at Bode (419.3 ±6.0 ppm, 1.4% variability) vs. Mauna Loa (396.8 ± 2.0 ppm, 0.5% variability) (NOAA, 2015) and Bode vs. Waliguan (397.7 ± 3.6 ppm, 0.9% variability) (Dlugokencky et al., 2016a) is statistically significant ($p < 0.05$).

The high CH_4 and CO_2 mixing ratios at Bode in comparison to Ahmedabad and Shadnagar could be due to more than 115 coal-biomass fired brick kiln, some of them are located near the site (less than 4 km) and confinement of pollutants within the Valley due to bowl shaped topography of the Kathmandu Valley. Although Ahmedabad is a big city with high population larger than Kathmandu Valley, the measurement site is far from the nearby heavy polluting industries and situated in plains, where ventilation of pollutants would be more efficient as opposed to the Kathmandu Valley. The major polluting sources were industries, residential cooking and transport sector in Ahmedabad (Chandra et al., 2016). Shadnagar is a small town

with a population of 0.16 million and major sources were industries (small-medium) and biomass burning in residential cooking (Sreenivas et al., 2016).

The monthly average of CO_2 mixing ratios in 2015 in Chanban (Aug: 403.4, Sep: 399.1 ppm) were slightly higher than the background sites at Mauna Loa Observatory (Aug: 398.89 ppm, Sep: 397.63 ppm) (NOAA, 2015) and Mt. Waliguan (Aug: 394.55 ppm, Sep: 397.68 ppm) (Dlugokencky et al., 2016a). For these two months in 2015, CH_4 mixing ratios were also higher in Bode (Aug: 2.281 ppm, Sep: 2.371 ppm) and Chanban (Aug: 2.050 ppm, Sep: 2.102 ppm) compared to Mauna Loa Observatory (Aug: 1.831 ppm, Sep: 1.846 ppm) (Dlugokencky et al., 2017) and Mt. Waliguan (Aug: 1.915 ppm, 1.911 ppm) (Dlugokencky et al., 2016). The small differences in CO_2 between Chanban and background sites mentioned above indicate the smaller number of and/or less intense CO_2 sources at Chanban during these months because of the lack of burning activities due to rainfall in the region. The garbage and agro-residue burning activities were also absent or reduced around Bode during the monsoon period. However, high CH_4 values in August and September in Bode, Chanban and Mt. Waliguan in comparison to Mauna Loa Observatory may indicate the influence of CH_4 emission from paddy fields in the Asian region.

Table 2.2. Summary of monthly average CH_4 and CO_2 mixing ratios observed at Bode, a semi-urban site in the Kathmandu Valley during March 2013 to Feb 2014 [mean, standard deviation (SD), median, minimum (Min.), maximum (Max.) and number of data points of hourly average values]

Month	CH_4 (ppm)					CO_2 (ppm)					Data points
	Mean	SD	Median	Min.	Max.	Mean	SD	Median	Min.	Max.	
Mar	2.207	0.245	2.152	1.851	3.094	426.6	26.4	418.3	378.8	510.8	596
Apr	2.183	0.252	2.094	1.848	3.121	430.3	27.4	421.0	397.0	536.9	713
May	2.093	0.174	2.040	1.863	2.788	421.7	22.1	413.4	395.9	511.2	725
Jun	2.061	0.142	2.017	1.869	2.675	417.9	21.3	410.4	390.5	495.7	711
Jul	2.129	0.168	2.074	1.893	2.770	410.3	18.2	406.3	381.0	471.0	500
Aug	2.274	0.260	2.181	1.953	3.219	409.9	22.8	405.3	376.1	493.1	737
Sep	2.301	0.261	2.242	1.941	3.331	414.9	30.2	404.0	375.9	506.2	710
Oct	2.210	0.195	2.156	1.927	2.762	417.0	25.1	411.8	381.9	486.7	743
Nov	2.207	0.203	2.178	1.879	2.705	417.2	20.7	415.7	385.7	478.9	717
Dec	2.206	0.184	2.193	1.891	2.788	417.7	17.3	418.0	386.7	467.6	744
Jan	2.233	0.219	2.198	1.889	2.744	424.8	20.9	422.3	392.7	494.5	696
Feb	2.199	0.223	2.152	1.877	2.895	423.2	22.0	417.9	392.2	484.6	658
Annual	2.192	0.066	2.140	1.848	3.331	419.3	6.0	413.7	375.9	536.9	

2.3.2. Monthly and seasonal variations

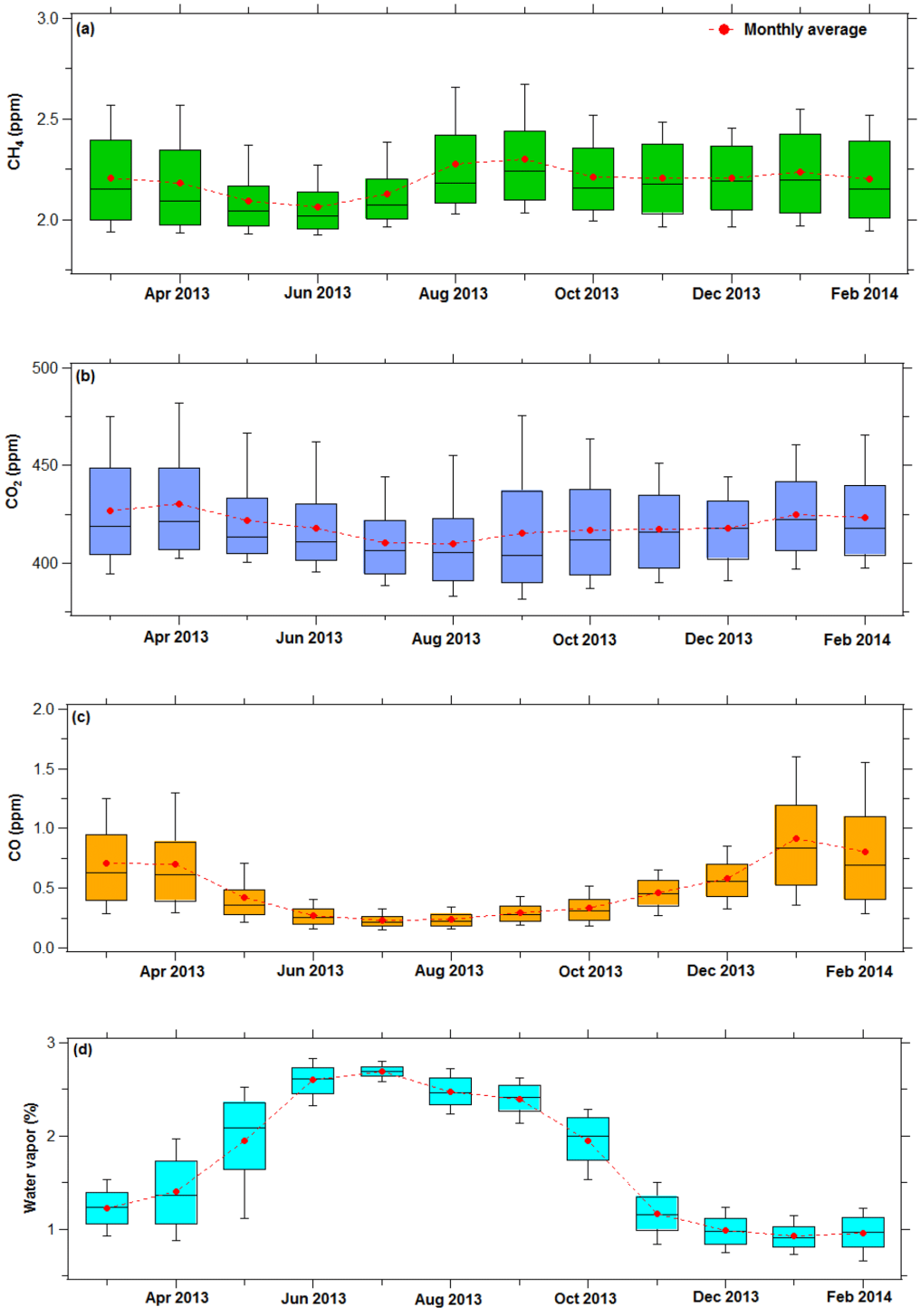

Figure 2.3. Monthly variations of the mixing ratios of hourly (a) CH_4, (b) CO_2, (c) CO, and (d) water vapor observed at a semi-urban site (Bode) in the Kathmandu Valley over a period of a year. The lower end and upper end of the whisker represents 10th and 90th percentile, respectively; the lower end and upper end of each box represents 25th and 75th percentile, respectively, and black horizontal line in the middle of each box is the median for each month while red dot represents mean for each month.

Figure 2.3 shows the monthly box plot of hourly CH_4, CO_2, CO and water vapor observed for a year in Bode. Monthly and seasonal averages of CH_4 and CO_2 mixing ratios at Bode are summarized in Table 2.2 and 2.3. CH_4 were lowest during May-July (ranges from 2.093-2.129 ppm) period and highest during August-September (2.274-2.301 ppm), followed by winter. In addition to the influence of active local sources, the shallow boundary layer in winter was linked to elevated concentrations (Panday and Prinn, 2009; Putero et al., 2015, Mues et al., 2017). The low CH_4 values from May to July may be associated with the absence of brick kiln and frequent rainfall in these months. Brick kiln were operational during January to April. Rainfall also leads to suppression of open burning activities in the valley (see Figure 2.2b).

Table 2.3. Summary of CH_4 and CO_2 mixing ratios at Bode across four seasons during March 2013 to Feb 2014 [seasonal mean, one standard deviation (SD), median, minimum (Min.) and maximum (Max.)]

Season	CH_4 (ppm)					CO_2 (ppm)				
	Mean	SD	Median	Min.	Max.	Mean	SD	Median	Min.	Max.
Pre-monsoon	2.157	0.230	2.082	1.848	3.121	426.2	25.5	417.0	378.8	536.9
Monsoon	2.199	0.241	2.126	1.869	3.331	413.5	24.2	407.1	375.9	506.2
Post-monsoon	2.210	0.200	2.167	1.879	2.762	417.3	23.1	414.1	381.9	486.7
Winter	2.214	0.209	2.177	1.877	2.895	421.9	20.3	419.3	386.7	494.5

The CH_4 was slightly higher (statistically significant, $p<0.05$) in monsoon season (July–September) than in the pre-monsoon season (unlike CO_2 which was higher in pre-monsoon), and could be associated with the addition of CH_4 flux from the water-logged rice paddies (Goroshi et al., 2011). There was a visible drop in CH_4 from September to October but remained consistently over 2.183 ppm from October to April with little variation between these months. Rice-growing activities are minimal or none in October and beyond, and thus may be related to the observed dip in CH_4 mixing ratio.

Comparison of seasonal average CH_4 mixing ratios at Bode and Shadnagar (a semi-urban site in India) indicated that CH_4 mixing ratios at Bode were higher in all seasons than at Shadnagar: pre-monsoon (1.89 ± 0.05 ppm), monsoon (1.85 ± 0.03 ppm), post-monsoon (2.02 ± 0.01 ppm), and winter (1.93 ± 0.05 ppm) (Sreenivas et al., 2016). The possible reason for lower CH_4 at Shadnagar in all seasons could be associated with geographical location and difference in local emission sources. The highest CH_4 mixing ratio in Shadnagar was reported in post-monsoon which was associated with harvesting in the Kharif season (July – October), while the minimum was in monsoon. Shadnagar is a relatively small city (population: ~0.16 million)

compared to Kathmandu Valley and the major local sources which may have influence on CH_4 emissions include bio-fuel, agro-residue burning and residential cooking.

Table 2.4. Comparison of monthly average CH_4 and CO_2 mixing ratios at a semi-urban and a rural site in Nepal (this study) with other urban and background sites in the region and elsewhere.

Site	Bode, Nepal (Urban)				Chanban, Nepal (Rural)		Mauna Loa, USA (Background)[c]		Waliguan, China (Background)[d]	
Setting										
Species	CO_2	CH_4	*CO_2	*CH_4	*CO_2	*CH_4	CO_2	CH_4	CO_2	CH_4
Unit	ppm	ppm	ppm	ppm	ppm	ppm	ppm	ppm	ppm	ppm
Mar 2013	426.6	2.207					397.3	1.840	399.5	1.868
Apr	430.3	2.183					398.4	1.837	402.8	1.874
May	421.7	2.093					399.8	1.834	402.5	1.878
Jun	417.9	2.061					398.6	1.818	397.4	1.887
Jul	410.3	2.129					397.2	1.808	393.3	1.888
Aug	409.9	2.274	411.3	2.281	403.4	2.050	395.2	1.819	392.0	1.893
Sep	414.9	2.301	419.9	2.371	399.1	2.102	393.5	1.836	393.1	1.894
Oct	417.0	2.210					393.7	1.836	395.6	1.876
Nov	417.2	2.207					395.1	1.835	397.1	1.875
Dec	417.7	2.206					396.8	1.845	398.6	1.880
Jan 2014	424.8	2.234					397.8	1.842	398.8	1.865
Feb	423.2	2.199					397.9	1.834	401.1	1.878
Annual										
Bode	419.3	2.192								
Mauna Loa							396.8	1.832		
Waliguan									397.7	1.880
Shadnagar (2014)[a]	394.0									
Ahmedabad (2013–2015)[b]	413.0	1.920								

* The monthly values for CO_2 and CH_4 in 2015 and in [a] Sreenivas et al. (2016), [b] Chandra et al. (2016), [c] Dlugokencky et al. (2017) and NOAA (2015), [d] Dlugokencky et al. (2016a) and Dlugokencky et al. (2016b).

The seasonal variation in CO_2 could be due to (i) the seasonality of major emission sources such as brick kilns (ii) seasonal growth of vegetation (CO_2 sink) (Patra et al., 2011) and (iii) atmospheric transport associated with regional synoptic atmospheric circulation (monsoon circulation and westerly disturbance in spring season) which could transport regional emission sources from vegetation fire and agriculture residue burning (Putero et al., 2015), and a local mountain-valley circulation effect (Kitada and Regmi, 2003; Panday et al., 2009). The concentrations of most pollutants in the region are lower during the monsoon period (Sharma et al., 2012, Marinoni, 2013; Putero et al., 2015) because frequent and heavy rainfall suppresses emissions sources. We saw a drop in the CO_2 mixing ratio during the rainfall period due to changes in various processes such as enhanced vertical mixing, uptake of CO_2 by vegetation and soils, and, where relevant, reduction in combustion sources. CO_2 can also dissolve into rainfall, forming carbonic acid, which may lead to a small decrease in the CO_2 mixing ratio as has been observed during high intensity rainfall (Chaudhari et al., 2007; Mahesh et al., 2014). Monsoon is also the growing season with higher CO_2 assimilation by plants than other seasons

(Sreenivas et al., 2016). In contrast, winter, pre-monsoon and post-monsoon season experiences an increase in emission activities in the Kathmandu Valley (Putero et al., 2015).

The CO_2 mixing ratios were in the range of 376 - 537 ppm for the entire observation period. Differences with CH_4 were observed in September and October where CO_2 was increasing (mean/median) in contrast to CH_4 which showed the opposite trend. The observed increase in CO_2 after October may be related to little or no rainfall, which results in the absence of rain-washout and/or no suppression of active emission sources such as open burning activities. However, the reduction in CH_4 after October could be due to reduced CH_4 emissions from paddy fields, which were high in August-September. CO_2 remains relatively low during July-August, but it is over 420 ppm from January to May. Seasonal variation of CO_2 in Bode was similar in seasonal variation but the values are higher than the values observed in Shadnagar, India (Sreenivas et al., 2016).

The variations in CO were more distinct than CH_4 and CO_2 during the observation period (Figure 3). The highest CO values were observed from January-April (0.71-0.91 ppm). The seasonal mean of CO mixing ratios at Bode were: pre-monsoon (0.60 ±0.36 ppm), monsoon (0.26±0.09 ppm), post-monsoon (0.40±0.15 ppm), and winter (0.76±0.43 ppm). The maximum CO was observed in winter, unlike CO_2 which was maximum in pre-monsoon. The high CO in winter was due to the presence of strong local pollution sources (Putero et al., 2015) and shallow mixing layer heights. The addition of regional forest-fire and agro-residue burning augmented CO_2 mixing ratios in pre-monsoon. The water vapor mixing ratio showed a seasonal pattern opposite of CO, with a maximum in monsoon (2.53 %) and minimum in winter (0.95 %), and intermediate values of 1.56 % in pre-monsoon and 1.55 % in post-monsoon season.

There were days in August-September when the CH_4 increased by more than 3 ppm (Figure 2). Enhancement in CO_2 was also observed during the same time period. In the absence of tracer model simulations, the directionality of the advected air masses is unclear. Figure 2.4 shows that during these two months, CO_2 mixing rations were particularly high (> 450 CO_2 and > 2.5 ppm CH_4) with the air masses coming from the East-Northeast (E-NE). CO during the same period was not enhanced and didn't show any particular directionality compared to CH_4 and CO_2 (Figure 4c). Areas E-NE to Bode are predominantly irrigated (rice paddies) during August-September, and sources such as brick kilns were not operational during this time period. Goroshi et al. (2011) reported that June to September is a growing season for rice paddies in South Asia with high CH_4 emissions during these months and observed a peak in

September in the atmospheric CH_4 column over India. Model analysis also points to high methane emissions in September which coincides with the growing period of rice paddies (Goroshi et al., 2011, Prasad et al., 2014). The CH_4 mixing ratios at Bode in January (2.233 ± 0.219 ppm) and July (2.129 ± 0.168 ppm) were slightly higher than the observation in Darjeeling (Jan: 1.929±0.056 ppm; Jul: 1.924±0.065 ppm), a hill station of eastern Himalaya (Ganesan et al., 2013). The higher CH_4 values in January and July at Bode compared to Darjeeling could be because of the influence of local sources, in addition to the shallow boundary layer in Kathmandu Valley. Trash burning and brick kilns are two major sources from December until April in the Kathmandu Valley while emission from paddy fields occurs during July-September in the Kathmandu Valley. In contrast, the measurement site in Darjeeling was located at higher altitude (2194 masl) and was less influenced by the local emission. The measurement in Darjeeling reflected a regional contribution. There are limited local sources in Darjeeling such as wood biomass burning, natural gas related emission and vehicular emission (Ganesan et al., 2013).

The period between January and April had generally higher or the highest values of CO_2, CH_4 and CO at Bode. The measurement site was impacted mainly by local Westerly-Southwesterly winds (W-SW) and East-Southeast (E-SE). The W-SW typically has a wind speed in the range ~1 - 6 m s^{-1} and was active during late morning to afternoon period (~11:00 to 17:00 NST, supplementary information Figure A.2 and A.3). Major cities in the valley such as Kathmandu Metropolitan City and Lalitpur Sub-Metropolitan City are W-SW of Bode (Figure 2.1c). Wind from E-SE were generally calm ($\leq$1m s^{-1}) and observed only during night and early morning hours (21:00 to 8:00 NST). The mixing ratio of all three species in air mass from the E-SE was significantly higher than in the air mass from W-SW (Figure 2.4). There are 10 biomass co-fired brick kilns and Bhaktapur Industrial Estate located within 1-4 km E-SE from Bode (Sarkar et al., 2016). The brick kilns were only operational during January-April. Moreover, there were over 100 brick kilns operational in the Kathmandu Valley (Putero et al., 2015) which use low-grade lignite coal imported from India and biomass fuel to fire bricks in inefficient kilns (Brun, 2013).

Fresh emissions from the main city center were transported to Bode during daytime by W-SW winds which mainly include vehicular emission. Compared to monsoon months (June-August), air mass from W-SW had higher values of all three species (Figure 2.4) during winter and pre-monsoon months. This may imply that in addition to vehicular emission, there are other potential sources which were exclusively active during these dry months.

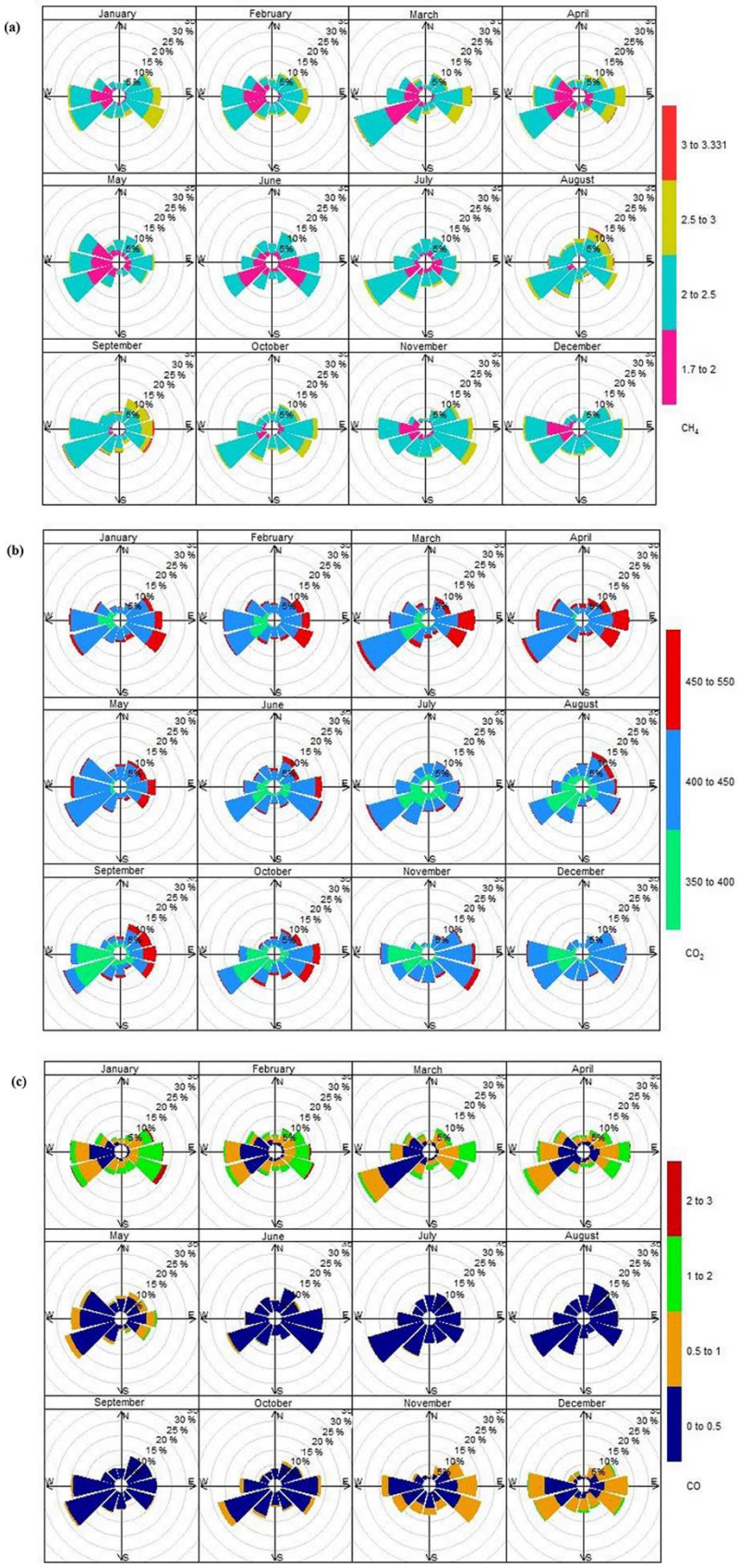

Figure 2.4. Relation between mixing ratios and wind direction observed at Bode in the Kathmandu Valley (a) CH_4, (b) CO_2 and (c) CO from March 2013 to February 2014. The figure shows variations of CH_4, CO_2 and CO mixing ratios based on frequency counts of wind direction (in %) as represented by circle. The color represents the different mixing ratios of the gaseous species. The units of CH_4, CO_2 and CO are in ppm.

Municipal trash burning is also common in the Kathmandu Valley, with a reported higher frequency from December to February (Putero et al., 2015). The frequency in the use of captive

power generator sets are highest during the same period, which is another potential source contributing to air coming from W-SW direction (World Bank, 2014; Putero et al., 2015).

Regional transport of pollutants into the Kathmandu Valley was reported by Putero et al. (2015). To relate the influence of synoptic circulation with the observed variability in BC and O_3 in the Kathmandu Valley, 5-day back trajectories (of air masses arriving in the Kathmandu Valley) were computed by Putero et al., (2015) using the HYSPLIT model. These individual trajectories which were initialized at 600 hPa, for the study period of one year and were clustered into nine clusters. Of the identified clusters, the most frequently observed clusters during the study period were the Regional and Westerly cluster or circulation (22% and 21%).

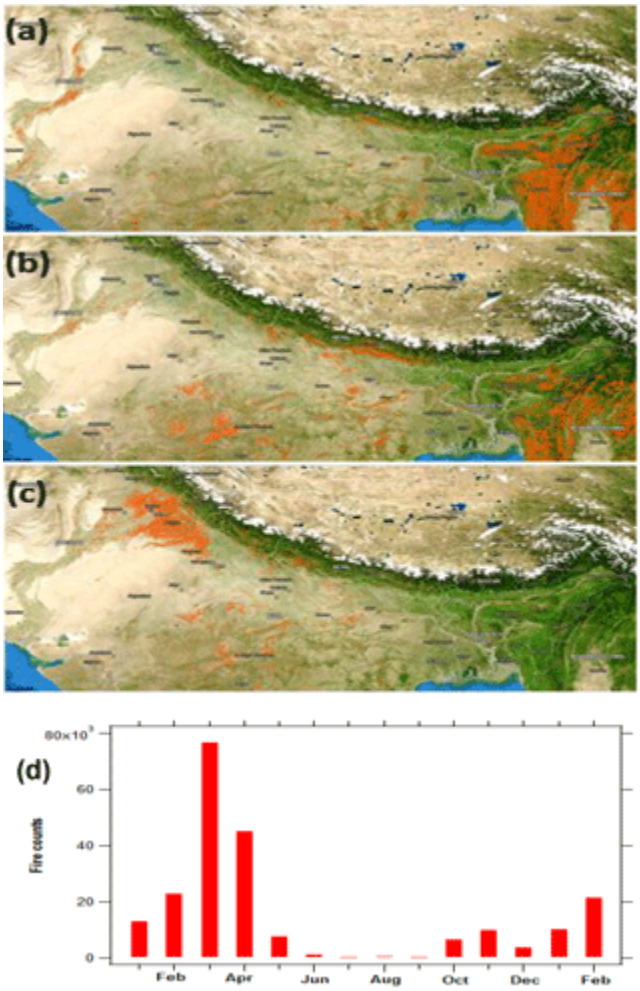

Figure 2.5. Satellite detected fire counts in (a) Mar, (b) Apr, (c) May 2013 in the broader region surrounding Nepal and (d) total number of fire counts detected by MODIS instrument onboard the Aqua satellite during Jan 2013-Feb 2014. Source: https://firms.modaps.eosdis.nasa.gov/firemap/

The trajectories in the regional cluster originate within 10^o x 10^o around the Kathmandu Valley, whereas the majority of trajectories in this westerly cluster originated broadly around 20-40^0 N, ~60^0 E. Putero et al (2015) found that the regional and westerly synoptic circulation were favorable for high values of BC and O_3 in the Kathamandu Valley. Other sources of CO_2 and CH_4 could be due to vegetation fires which were also reported in the region surrounding the

Kathmandu Valley during the pre-monsoon months (Putero et al., 2015). Similarly, high pollution events, peaking in the pre-monsoon, were observed at Nepal Climate Observatory-Pyramid (NCO-P) near Mt. Everest, which have been associated with open fires along with the Himalayan foothills, northern Indo-Gangetic Plain (IGP), and other regions in the Indian Subcontinent (Putero et al., 2014). MODIS derived forest counts (Figure 2.5), which also indicated high frequency of forest fire and farm fires from February to April and also during post-monsoon season. It is interesting that the monthly mean CO_2 mixing ratio was maximum in April (430 ± 27 ppm) which could be linked to the fire events. It is likely that the westerly winds (>2.5-4.5 m s^{-1}) during the daytime (supplementary information Figure A.2, A.3) bring additional CO_2 from vegetation fires and agro-residue burning in southern plains of Nepal including the IGP region (Figure 5). Low values of CO_2 and CH_4 during June-July (Figure 2.3) were coincident with the rainy season, and sources such as brick kiln emission, trash burning, captive power generators, and regional agriculture residue burning and forest fires are weak or absent during these months.

2.3.3. Diurnal variation

Figure 2.6 shows the average seasonal diurnal patterns of CH_4, CO_2, CO, and water vapor mixing ratios observed at Bode for four seasons. All the three-gas species had distinct diurnal patterns in all seasons, characterized by maximum values in the morning hours (peaked around 7:00-9:00), afternoon minima around 15:00-16:00, and a gradual increase through the evening until next morning. There was no clear evening peak in CH_4 and CO_2 mixing ratios whereas CO shows an evening peak around 20:00. The gradual increase of CO_2 and CH_4 in the evening in contrast to the increase until evening peak traffic hours and later decay of CO may be indicative of a few factors. As pointed out earlier, after the peak traffic hours, there are no particularly strong sources of CO, especially in the monsoon and post-monsoon season. It is also likely that some of the CO is decayed due to nighttime katabatic winds which replace polluted air masses with cold and fresh air from the nearby mountain (Panday and Prinn, 2009).

As for the CO_2, the biosphere respiration at night in the absence of photosynthesis can add additional CO_2 to the atmosphere which especially in the very shallow nocturnal boundary layer may explain part of the increase of the CO_2 mixing ratio. The well-defined morning and evening peaks observed in CO mixing ratios are associated with the peaks in traffic and residential activities. The CH_4 and CO_2 showed pronounced peaks in the morning hours (07:00-09:00) in all seasons with almost the same level of seasonal average mixing ratios.

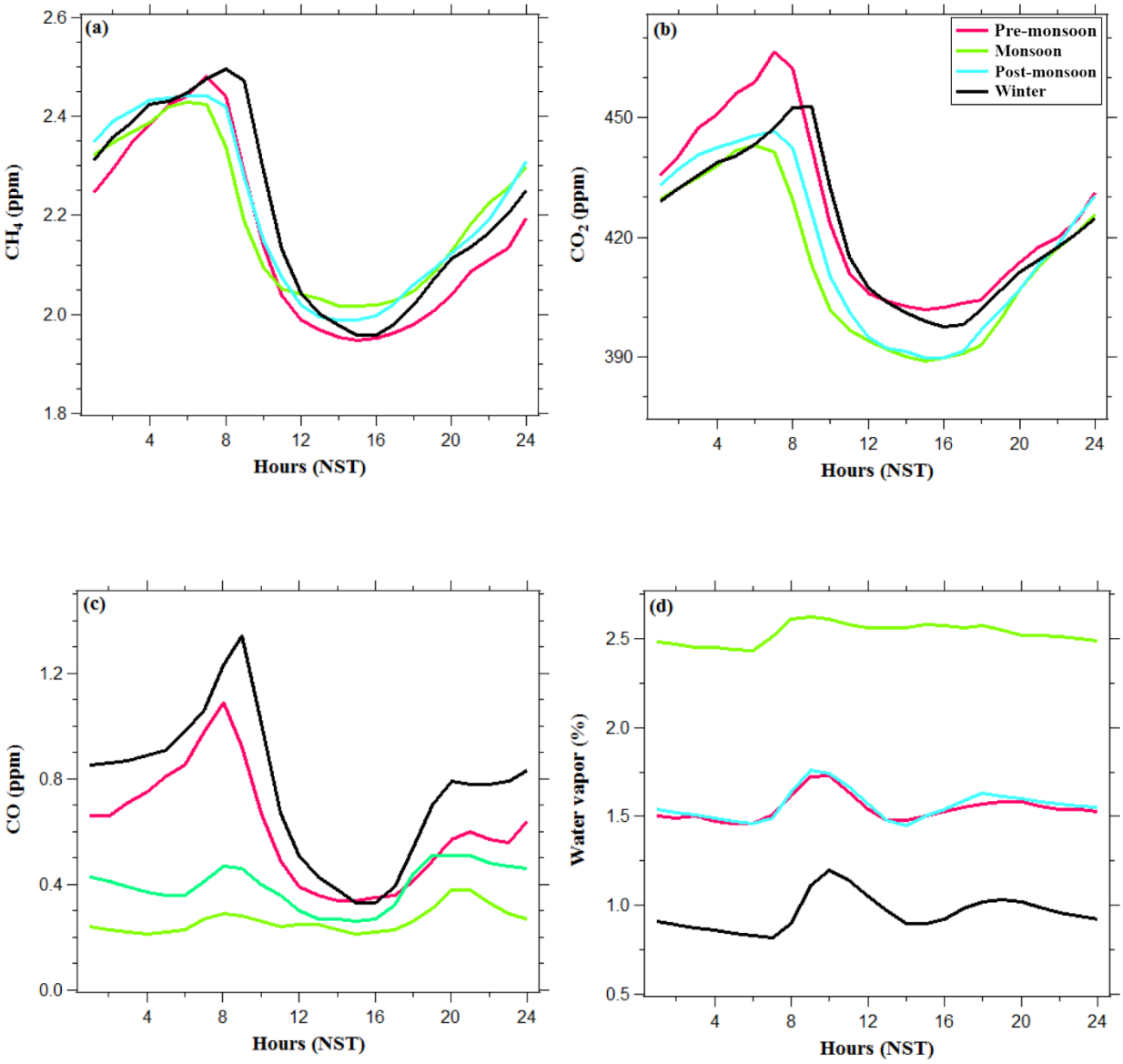

Figure 2.6. Diurnal variations of hourly mixing ratios in different seasons (a) CH_4, (b) CO_2, (c) CO, and (d) water vapor observed at Bode (semi-urban site) in the Kathmandu Valley during March 2013-February 2014. Seasons are defined as Pre-monsoon: Mar-May, Monsoon: Jun-Sep, Post-monsoon: Oct-Nov, Winter: Dec-Feb. The x axis is in Nepal Standard Time (NST).

CO had a prominent morning peak in winter and pre-monsoon season, but the peak was significantly lower in monsoon and post-monsoon. The CO (~1-1.4 ppm) around 08:00-09:00 am in winter and pre-monsoon were nearly 3-4 times higher than in monsoon and post-monsoon season. It appears that CH_4 and CO_2 mixing ratios were continuously building up at night until the following morning peak in all seasons.

The similar seasonal variations in CH_4 and CO_2 across all seasons could be due to their long-lived nature, as compared to CO, whose diurnal variations are strongly controlled by the

evolution of the boundary layer. Kumar et al. (2015) also reported morning and evening peaks and an afternoon low in CO_2 mixing ratios in industrial, commercial, and residential sites in Chennai in India. The authors also found high early morning CO_2 mixing ratios at all sites and attributed it to the temperature inversion and stable atmospheric condition.

The daytime low CH_4 and CO_2 mixing ratios were due to (i) elevated mixing layer height in the afternoon (Figure 2.7), (ii) development of upslope wind circulation in the valley, and (iii) development of westerly and southwesterly winds which blows through the valley during the daytime from around 11 am to 5 pm (supplementary information Figure A.2), all of which aid in dilution and ventilation of the pollutants out of the valley (Regmi et al., 2003; Kitada and Regmi, 2003; Panday and Prinn, 2009). In addition, the daytime CO_2 minimum in the summer monsoon is also associated with high photosynthetic activities in the valley as well as in the broader surrounding region. In the nighttime and early morning, the mixing layer height was low (only around 200-300 m in all seasons) and remains stable for almost 17 hours a day. In the daytime, it grows up to 800-1200 m for a short time (ca. from 11:00 to 6:00) (Mues et al., 2017). Therefore, the emissions from various activities in the evening after 18:00 (cooking and heating, vehicles, trash burning, and bricks factories in the night and morning) were trapped within the collapsing and shallow boundary layer, and hence mixing ratios were high during evening, night and morning hours. Furthermore, plant and soil respiration also increases CO_2 mixing ratio during the night (Chandra et al., 2016). However, Ganesan et al. (2013) found a distinct diurnal cycle of CH_4 mixing ratios with twin peaks in the morning (7:00-9:00), and afternoon (15:00-17:00) and a nighttime low in winter but no significant diurnal cycle in the summer of 2012 in Darjeeling, a hill station (2194 m asl.) in the eastern Himalaya. The authors described that the morning peaks could be due to the radiative heating of the ground in the morning, which breaks the inversion layer formed during night, and as a result, pollutants are ventilated from the foothills up to the site. The late afternoon peaks match wind direction and wind speed (upslope winds) that could bring pollution from the plains to the mountains.

The diurnal variation of CO is also presented along with CO_2 and CH_4 in Figure 6c. CO is an indicator of primary air pollution. Although the CO mixing ratio showed distinct diurnal pattern, it was different from the diurnal patterns of CO_2 and CH_4. CO diurnal variation showed distinct morning and evening peaks, afternoon minima, and a nighttime accumulation or decay. Nighttime accumulation in CO was observed only in winter and pre-monsoon and decay or decrease in monsoon season and post-monsoon season (Figure 2.7). The lifetime of CO (weeks to months) is very long compared to the ventilation timescales for the valley, so the different

diurnal cycles would be due to differences in nighttime emissions. While the biosphere respires at night which may cause a notable increase in CO_2 in the shallow boundary layer, most CO sources (transport sector, residential cooking) except brick kilns remain shut down or less active at night. This also explains why nighttime values of CO drop less in the winter and pre-monsoon than in other seasons. Furthermore, the prominent morning peaks of CO in pre-monsoon and winter compared to other seasons results from nighttime accumulation, additional fresh emissions in the morning and recirculation of the pollutants due to downslope katabatic winds (Pandey and Prinn, 2009; Panday et al., 2009). Pandey and Prinn (2009) observed nighttime accumulation and gradual decay during the winter (January 2005). The measurement site in Pandey and Prinn (2009) was near the urban core of the Kathmandu Valley and had significant influence from the vehicular sources all over the season including the winter season. Bode lies in close proximity to the brick kilns which operate 24 hours during the winter and pre-monsoon period. Calm southeasterly winds are observed during the nighttime and early morning (calculated 22:00 – 8:00) in pre-monsoon and winter, which transport emissions from brick kiln to the site (Sarkar et al., 2016). Thus, the gradual decay in CO was not observed in Bode.

The timing of the CO morning peak observed in this study matches with observations by Panday et al. (2009). They also found CO morning peak at 8:00 in October 2004 and at 9:00 in January 2005. The difference could be linked to the boundary layer stability. As the sun rises later in winter, the boundary layer stays stable for a longer time in winter keeping mixing ratios higher in morning hours than in other seasons with an earlier sunrise. The morning peaks of CO_2 and CH_4 mixing ratios occurred around 6:00-7:00 local time in the pre-monsoon, monsoon, and post monsoon season, whereas in winter their peaks are delayed by 1-2 hours in the morning; CH_4 at 8:00 and CO_2 at 9:00. The CO showed that its morning peak was delayed compared to CO_2 and CH_4 morning peaks by 1-2 hour in pre-monsoon, monsoon and post-monsoon (at 8:00) and in winter (at 9:00). The occurrence of morning peaks in CO_2 and CH_4 1-2 hours earlier than CO is interesting. This could be due to the long lifetimes and relatively smaller local sources of CH_4 and CO_2, as CO is mainly influenced by emissions from vehicles during rush hour, as well as from biomass and trash burning in the morning hours. Also, CO increases irrespective of change in the mixing layer (collapsing or/rising, Figure 2.7) but CO_2 and CH_4 start decreasing only after the mixing layer height starts to rise. Recently, Chandra et al. (2016) also reported that the CO_2 morning peak occurred earlier than CO in observations in

Ahmedabad City India. This was attributed to CO_2 uptake by photosynthetic activities after sunrise but CO kept increasing due to emissions from the rush hour activities.

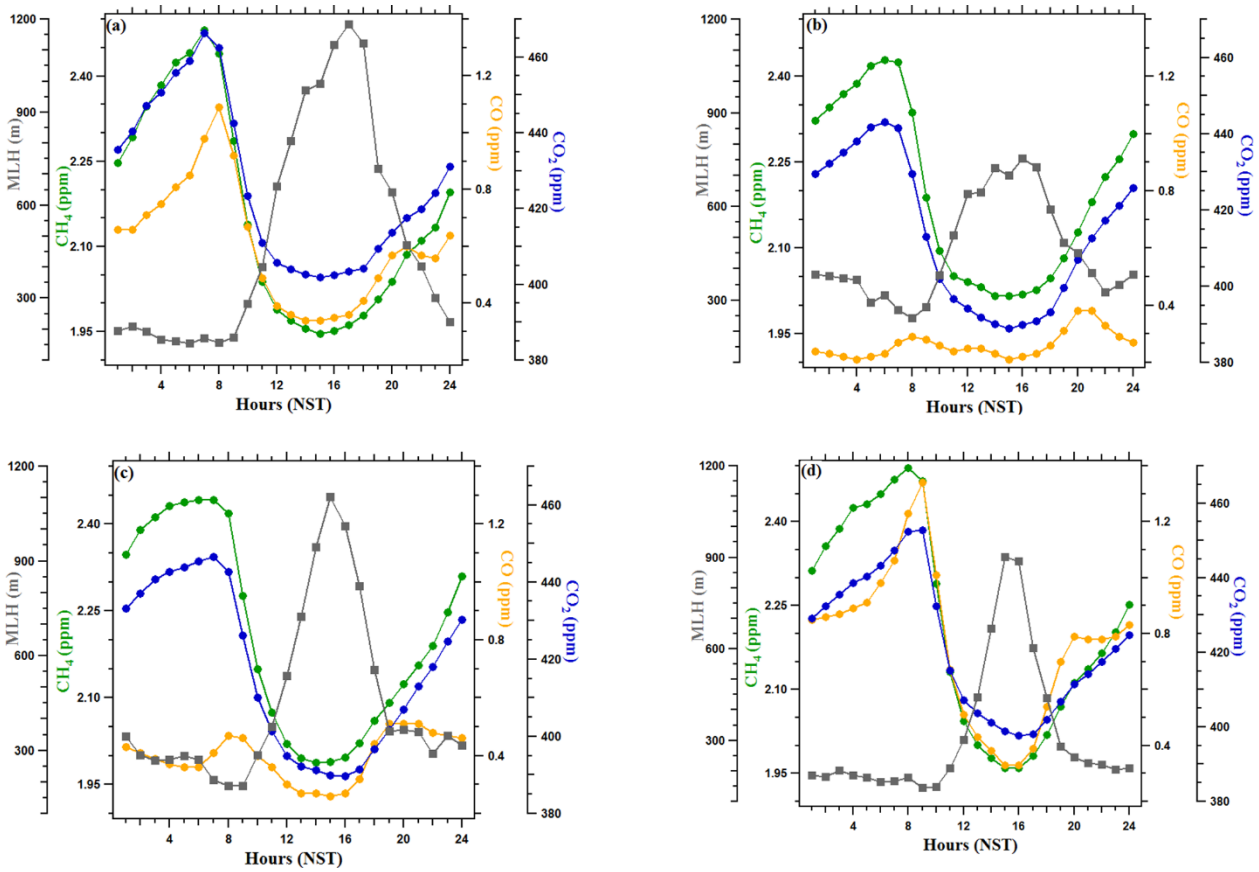

Figure 2.7. Diurnal variations of hourly mixing ratios of CH_4, CO_2, CO, and mixing layer height (MLH) at Bode (a semi-urban site in the Kathmandu Valley) in different seasons (a) pre-monsoon (Mar-May), (b) monsoon (Jun-Sep), (c) post-monsoon (Oct-Nov) and (d) winter (Dec-Feb) during March 2013- Feb 2014.

The highest daytime minimum of CO_2 was observed in the pre-monsoon followed by winter (Figure 2.6b). The higher daytime minimum of CO_2 mixing ratios in the pre-monsoon season than in other seasons, especially winter, is interesting. The local emission sources are similar in pre-monsoon and winter and the boundary layer is higher (in the afternoon) during the pre-monsoon (~1200 meters) than in winter (~900 meters) (Mues et al., 2017). Also, the biospheric activity in the region is reported to be higher in the pre-monsoon (due to high temperature and solar radiation) than winter (Rodda et al., 2016). Among various possible causes, transport of CO_2 rich air from outside the Kathmandu Valley has been hypothesized as a main contributing factor, due to regional vegetation fires combined with westerly mesoscale to synoptic transport Putero et al. (2015). In monsoon and post-monsoon seasons, the minimum CO_2 mixing ratios

in the afternoon drops down to 390 ppm, this was close to the values observed at the regional background sites Mauna Loa and Waliguan.

2.3.4. Seasonal interrelation of CO_2, CH_4 and CO

The Pearson's correlation coefficient (r) between CO_2 and CO was strong in winter (0.87), followed by monsoon (0.64), pre-monsoon (0.52) and post-monsoon (0.32). The higher coefficient in winter indicates that common or similar sources for CO_2 and CO and moderate values in pre-monsoon and monsoon indicates the likelihood of different sources. To avoid the influence of strong diurnal variations observed in the valley, daily averages, instead of hourly, were used to calculate the correlation coefficients. The correlation coefficients between daily CH_4 and CO_2 for four seasons are as follows: winter (0.80), post-monsoon (0.74), pre-monsoon (0.70) and monsoon (0.22). A semi-urban measurement study in India also found a strong positive correlation between CO_2 and CH_4 in the pre-monsoon (0.80), monsoon (0.61), post-monsoon (0.72) and winter (0.8) (Sreenivas et al., 2016). It should be noted here that Sreenivas et al., (2006) used hourly average CO_2 and CH_4 mixing ratios. The weak monsoon correlation at Bode, which is in contrast to Sreenivas et al. (2016), may point to the influence of dominant CH_4 emission from paddy field during the monsoon season (Goroshi et al., 2011). Daily CH_4 and CO was also weakly correlated in monsoon (0.34) and post-monsoon (0.45). Similar to CH_4 and CO_2, the correlation between CH_4 and CO were moderate to strong in pre-monsoon (0.76) and winter (0.75).

Overall, the positive and high correlations between CH_4 and CO mixing ratios and between CH_4 and CO_2 in the pre-monsoon and winter indicate common sources, most likely combustion related sources such as vehicular emission, brick kilns, agriculture fire etc., or the same source regions (i.e. their transport due to regional atmospheric transport mechanisms). Weak correlation, between CH_4-CO_2 and between CH_4-CO, during monsoon season indicates sources other than combustion-related may be active, such as agriculture as a key CH_4 source (Goroshi et al., 2013).

2.3.5. CO and CO_2 ratio: Potential emission sources

The ratio of the ambient mixing ratios of CO and CO_2 was used as an indicator to help discriminate emission sources in the Kathmandu Valley. The ratio was calculated from the excess (dCO and dCO_2) relative to the background values of ambient CO and CO_2 mixing ratios. The excess value was estimated by subtracting the base value which was calculated as the fifth percentile of the hourly data for a day (Chandra et al., 2016).

Table 2.5. Emission ratio of CO/CO_2 (ppb ppm-1) derived from emission factors (mass of gas emitted from per kilogram of fuel burned, "except for the transport sector" which is derived from gram of gases emitted per kilometer distance travelled)

Sectors	Details	CO/CO_2	Reference
1. Residential and commercial			
i. LPG		4.8	Smith et al. (2000)
ii. Kerosene		13.4	Smith et al. (2000)
iii. Biomass		52.9–98.5	*
iv. Diesel power generators	< 15 years old	5.8	The World Bank (2014)
	>15 years old	4.5	
2. Transport			**
a. Diesel			
i. HCV diesel bus	> 6000 cc, 1996–2000	4.9	
	post-2000 and 2005	5.4	
ii. HCV diesel truck	> 6000 cc, post-2000	7.9	
b. Petrol			
i. Four-stroke motorcycle	< 100 cc, 1996–2000	68	
	100–200 cc, post-2000	59.6	
ii. Passenger cars	< 1000 cc, 1996–2000	42.4	
iii. Passenger cars	< 1000 cc, post-2000	10.3	
3. Brick industries			
i. BTK fixed kiln		17.2	Weyant et al. (2014)
ii. Clamp brick kiln		33.7	Stockwell et al. (2016)
iii. Zigzag brick kiln		3.9	Stockwell et al. (2016)
4. Open burning			
i. Mixed garbage		46.9	Stockwell et al. (2016)
ii. Crop residue		51.6	Stockwell et al. (2016)

* Westerdahl et al. (2009)
** http://www.cpcb.nic.in/Emission_Factors_Vehicles.pdf

Average emission ratios from the literature are shown in Table 2.5, and average ratios of dCO/dCO_2 are shown in Table 2.6, disaggregated into morning hours, evening hours, and seasonal values. It must be stated that due to the large variance in the calculated ratio from this study (Table 2.6) as well as the likely variation in the estimated ratio presented in Table 2.5, the interpretation and conclusion about sources should be cautiously drawn and will be indicative. Higher ratios were found in pre-monsoon (12.4) and winter (15.1) season compared to post-monsoon (8.3) and monsoon (7.5). These seasonal differences in the dCO/dCO_2 ratio are depicted in Figure 8, which shows a clear relationship with the wind direction and associated emissions, with the highest values especially for stronger westerly winds. Compared to the other three seasons, the ratio in winter was also relatively high for air masses from the east, likely due to emissions from brick kilns combined with accumulation during more stagnant meteorological conditions (supplementary information Figure A.2, A.3). In other seasons, emission emanating from the north and east of Bode were characterized by a

dCO/dCO_2 ratio below 15. Air masses from the west and south generally have a ratio from 20 to 50 in all but post-monsoon season, where the ratio sometimes exceeds 50. A ratio of 50 or over is normally due to very inefficient combustion sources (Westerdahl et al., 2009; Stockwell et al., 2016), such as agro-residue burning, which is common during the post-monsoon season in the Kathmandu Valley.

For interpretability of emission ratio with sources, the ratio was classified into three categories: (i) 0 – 15, (ii) 15 – 45, and (iii) greater than 45. This classification was based on the observed distribution of emission ratio during the study period (Figure 2.8) and a compilation of observed emission ratios typical for different sources from Nepal and India (see Table 2.5). An emission ratio below 15 is likely to indicate residential cooking and diesel vehicles, and captive power generation with diesel-powered generator sets (Smith et al., 2000; ARAI, 2008; World Bank, 2014). The emission from brick kilns (FCBTK and Clamp kilns, both common in the Kathmandu Valley), and inefficient, older (built before 2000) gasoline cars fall in between 15 - 45 (ARAI, 2008; Weyant et al., 2014; Stockwell et al., 2016). Four-stroke motorbikes and biomass burning activities (mixed garbage, crop-residue and biomass) are one of the least efficient combustion sources, with emission ratios higher than 45 (ARAI, 2008; Westerdahl et al., 2009; Stockwell et al., 2016).

Although ratio of CO/CO_2 is a weak indicator of sources and the mean ratio has large variance (See Table 2.6), the conclusions drawn, from using Figure 2.8 and the above mentioned classification, are not conclusive. The estimated CO/CO_2 ratio tentatively indicates that the local plume impacting the measurement site (Bode) from the north and east could be residential and/or diesel combustion. The estimated CO/CO_2 ratio of the local plume from the south and west generally falls in the 15-45 range which could indicate emissions from brick kilns and inefficient gasoline vehicles. Very high ratios were also estimated from the south west during the post-monsoon season. Among other possible sources, this may indicate agro-residue open burning.

The emission inventory for CO identifies (aggregate for a year) residential, and gasoline related emission from transport sector (Sadavarte et al., 2019). The inventory is not yet temporally resolved, so no conclusion can be drawn about the sources with respect to different seasons. From the 1km x1km emission inventory of the Kathmandu Valley for 2011, the estimated sectoral source apportionment of CO is residential (37%), transport sector (40%) and industrial

(20%). The largest fraction from the residential sector is cooking (24 %) whereas the majority of transport sector related CO in the Kathmandu Valley is from gasoline vehicles.

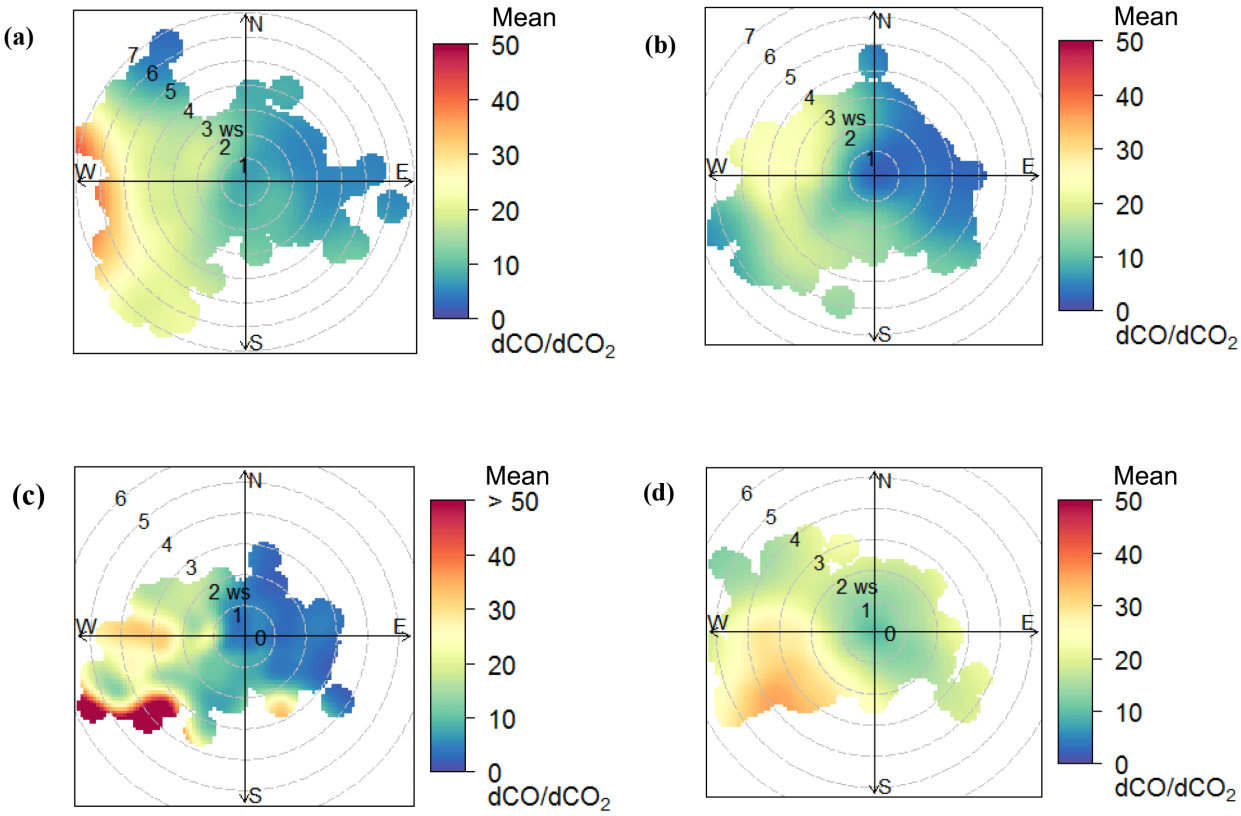

Figure 2.8. Seasonal polar plot of hourly dCO/dCO_2 ratio based upon wind direction and wind speed: (a) pre-monsoon, (b) monsoon, (c) post-monsoon and (d) winter seasons.

The dCO/dCO_2 ratio also changes markedly between the morning peak hours (7:00-9:00, except in winter season when the peak occurs during 8:00-9:00) and evening peak hours (19:00-21:00 pm) (Table 2.6). Morning and evening values were lowest (2.2, 8.0) during the monsoon and highest (11.2, 21.6) in the winter season, which points to the different emission characteristics in these two seasons. This feature is similar to Ahmedabad, India, another urban site in south Asia, where the morning/evening values were lowest (0.9/19.5) in monsoon and highest in winter (14.3/47.2) (Chandra et al., 2016). In the morning period, the ratio generally falls within a narrower range, from less than 1 to about 25, which indicates a few dominant sources, such as cooking, diesel vehicles, and diesel gen-sets (see Figure 2.9). In the evening period, the range of the ratio is much wider, from less than 1 to more than 100, especially in winter. This is partly due to the shallower boundary layer in winter, giving local CO emissions a chance to build up more rapidly compared to the longer-lived and well-mixed CO_2, and also indicating the prevalence of additional sources such as brick kilns and agro-residue burning.

Table 2.6 Average (SD) of the ratio of dCO to dCO_2, their Geometric mean (GeoSD) over a period of 3 hours during (a) morning peak (b) evening peak and (c) seasonal (all hours) of the ambient mixing ratios of CO and CO_2 and their lower and upper bound (LB and UB).

Period	Season	Mean (SD)	Median	*N*	Geomean (GeoSD)	LB	UB
a. Morning hours (07:00–09:00)	Pre-monsoon	7.6 (3.1)	7.8	249	11.3 (1.5)	5.2	24.8
	Monsoon	2.2 (1.6)	1.9	324	9.9 (1.9)	2.7	36.3
	Post-monsoon	3.1 (1.4)	2.8	183	11.1 (1.5)	4.7	26.3
	Winter*	11.2 (4.4)	11	255	11.4 (1.5)	5.3	24.2
b. Evening hours (19:00–21:00)	Pre-monsoon	15.1 (9.0)	12.7	248	10.5 (1.7)	3.5	31.6
	Monsoon	8.0 (5.2)	6.3	323	10.2 (1.8)	3.1	33.5
	Post-monsoon	11.5 (5.6)	10.6	182	11.0 (1.6)	4.4	27.6
	Winter	21.6 (14.1)	18.2	254	10.2 (1.8)	3.1	33.6
c. Seasonal (all hours)	Pre-monsoon	12.2 (13.3)	8.8	1740	8.2 (2.4)	1.4	48.4
	Monsoon	7.5 (13.5)	2.9	2176	5.9 (3.3)	0.5	65.6
	Post-monsoon	8.3 (12.4)	4.4	1289	6.8 (3.0)	0.8	59.2
	Winter	15.1 (13.3)	12.5	1932	9.2 (2.1)	2.0	41.7

* The morning peak was delayed by 1 h in winter, and thus the 08:00–10:00 period data were used in the analysis.

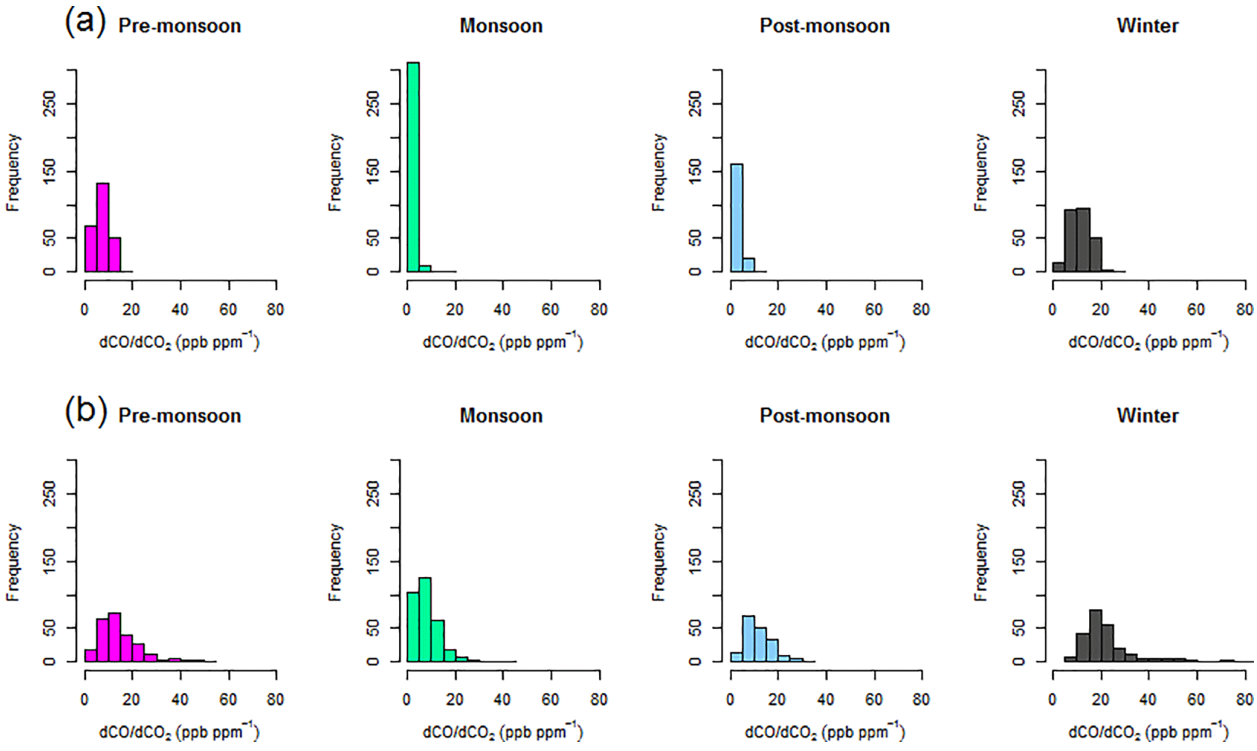

Figure 2.9. Seasonal frequency distribution of hourly dCO/dCO_2 ratio (a) morning hours (7:00-9:00) in all seasons except winter (8:00-10:00), (b) evening hours (19:00-21:00).

2.3.6. Comparison of CH_4 and CO_2 at semi-urban site (Bode) and rural site (Chanban)

Figure 2.10 shows time series of hourly average mixing ratios of CH_4, CO_2, CO and water vapor observed simultaneously at Bode and Chanban for the period of 15th July to 3rd October

2015. The hourly meteorological parameters observed at Chanban are shown in supplementary Figure A.4. The hourly temperature ranges from 14 to 28.5 °C during the observation period. The site experienced calm winds during the night and moderate southeasterly winds with hourly maximum speed of up to 7.5 m s^{-1} during the observation period. The CH_4 mixing ratios at Chanban varied from 1.880 ppm to 2.384 ppm, and generally increased from the last week of July until early September, peaking around 11th September and then falling off towards the end of the month. CO followed a generally similar pattern, with daily average values ranging from 0.10 ppm to 0.28 ppm. The hourly CO_2 mixing ratios ranged from 375 to 453 ppm, with day to day variations, but there was no clear pattern as observed in trend like CH_4 and CO mixing ratios.

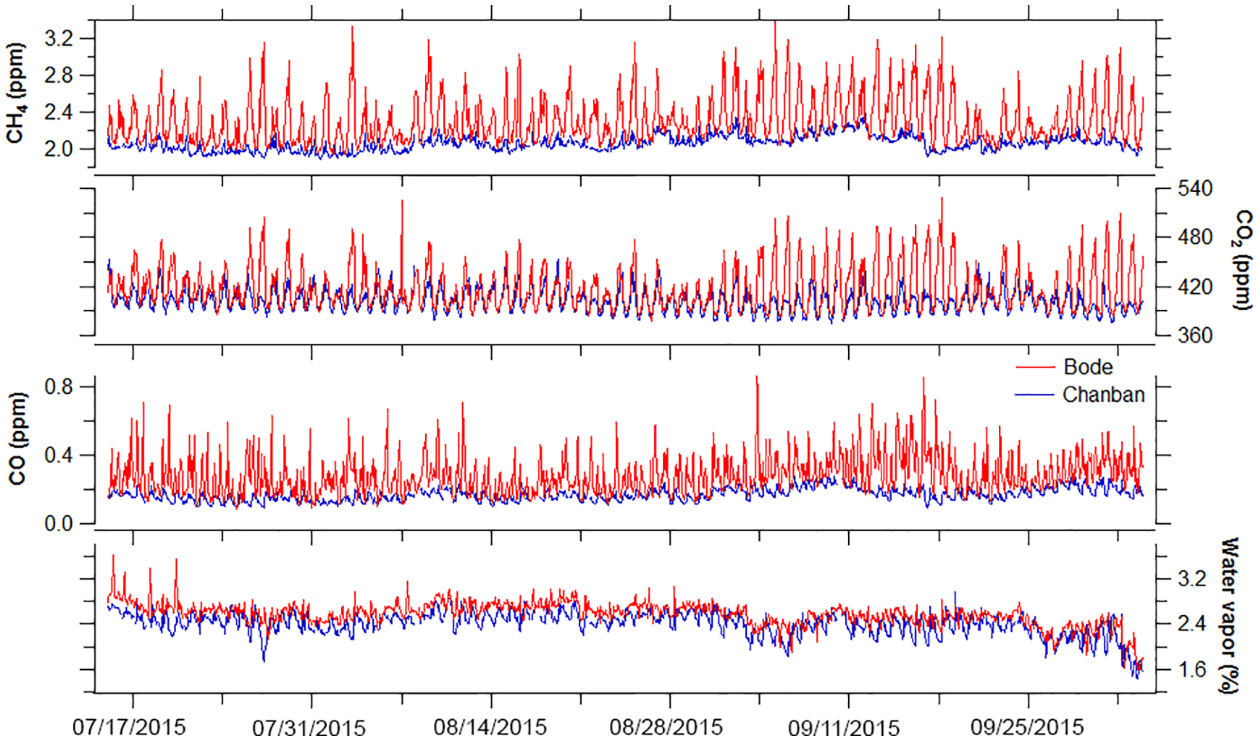

Figure 2.10. Comparison of hourly average mixing rations of CH_4, CO_2, CO, and water vapor observed at Bode (a semi-urban site) in the Kathmandu Valley and at Chanban (a rural/background site) in Makawanpur district, ~ 20 km from Kathmandu, on other side of a tall ridge.

The CH_4, CO_2, and CO mixing ratios were higher in Bode than in Chanban (Figure 2.10, Table 2.4), with Chanban approximately representing the baseline of the lower envelope of the Bode levels. The mean CO_2, CH_4 and CO mixing ratios over the entire sampling period of nearly three months at Bode are 3.8%, 12.1%, and 64% higher, respectively, than at Chanban. The difference in the CO_2 mixing ratio could be due to the large uptake of CO_2 in the forested area at Chanban and surrounding regions compared to Bode, where the local anthropogenic

emissions rate is higher and less vegetation for photosynthesis. The coincidence between the base values of CO and CH_4 mixing ratios at Bode and the levels observed at Chanban implies that Chanban CO and CH_4 mixing ratios are indicative of the regional background levels. A similar increase in CO and CH_4 mixing ratios at Chanban from July to September was also observed at Bode, which may imply that the regional/background levels in the broader Himalayan foothill region also influences the baseline of the daily variability of the pollutants in the Kathmandu Valley, consistent with Panday and Prinn (2009).

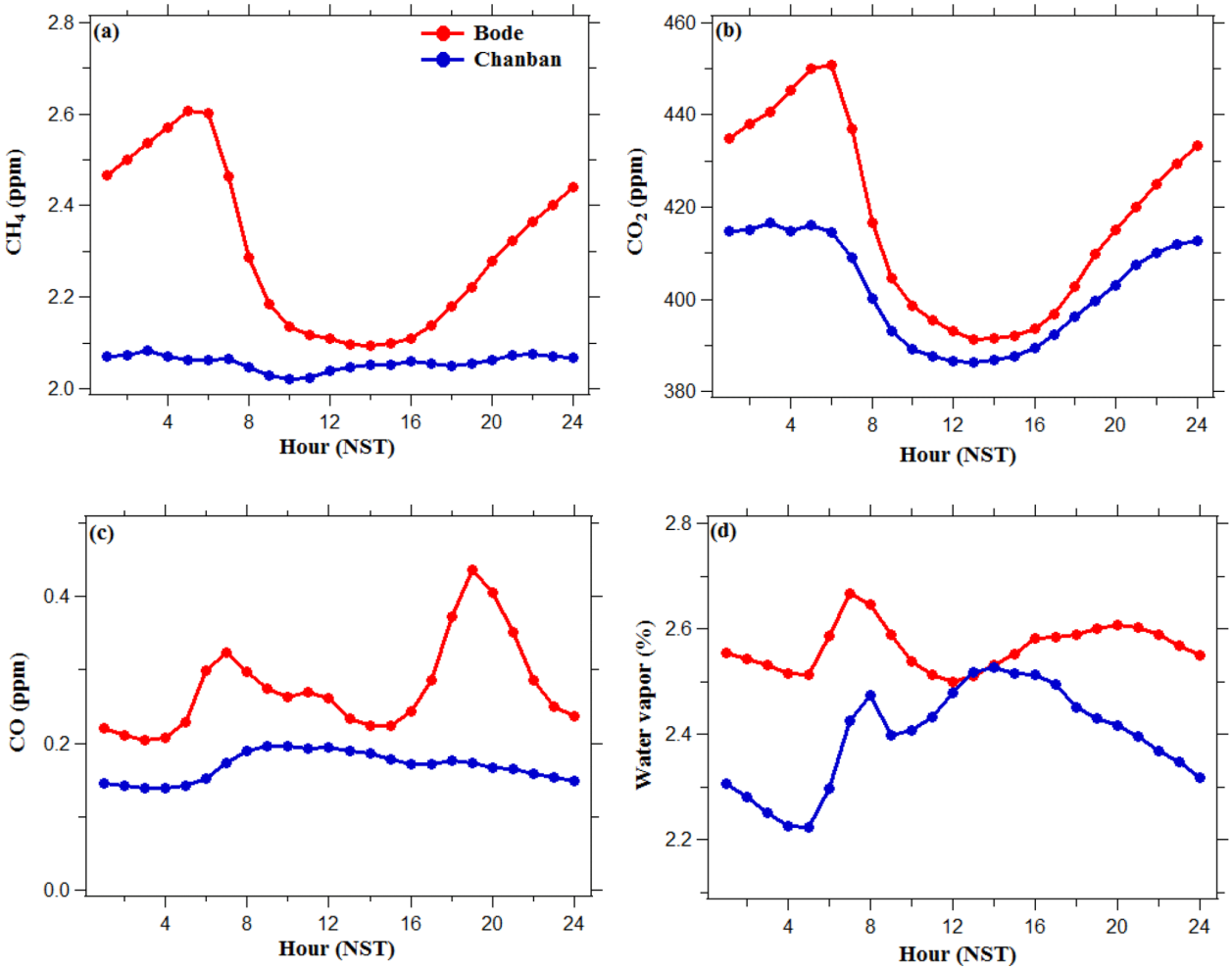

Figure 2.11. Diurnal variations of hourly average mixing ratios of (a) CH_4, (b) CO_2, (c) CO and (d) water vapor observed at Bode in the Kathmandu Valley and at Chanban in Makawanpur district during 15 July- 03 October 2015.

Figure 2.11 shows the comparison of average diurnal cycles of CO_2, CH_4, CO and water vapor mixing ratios observed at Bode and Chanban. The diurnal pattern of CO_2 mixing ratios at both sites is similar, but more pronounced at Bode, with a morning peak around 6:00-7:00, a daytime minimum, and a gradual increase in the evening until the next morning peak. A prominent

morning peak at Bode during the monsoon season indicates the influence of local emission sources. The daytime CO_2 mixing ratios are also higher at Bode than at Chanban because of local emissions less uptake of CO_2 for photosynthesis in the valley in comparison to the forested area around Chanban. Like the diurnal pattern of CO_2 depends on the evolution of the mixing layer at Bode, as discussed earlier, it is expected that the mixing layer evolution similarly influences the diurnal CO_2 mixing ratios at Chanban. CO, on the other hand, shows very different diurnal patterns at Bode and Chanban. Sharp morning and evening peaks of CO are seen at Bode, indicating the strong local polluting sources, especially cooking and traffic in the morning and evening peak hours. Chanban, in contrast, only has a subtle morning peak and no evening peak. After the morning peak, CO sharply decreases at Bode but not at Chanban. The growth of the boundary layer after sunrise and entrainment of air from the free troposphere, with lower CO mixing ratios, causes CO to decrease sharply during the day at Bode. At Chanban, on the other hand, since the mixing ratios are already more representative of the local and regional background levels which will also be prevalent in the lower free troposphere, CO does not decrease notably during the daytime growth of the boundary layer as observed at Bode.

Similarly, while there is very little diurnal variation in the CH_4 mixing ratios at Chanban, there is a strong diurnal cycle of CH_4 at Bode, similar to CO_2 there. At Chanban, the CH_4 mixing ratio only shows a weak minimum at around 11 am, a slow increase during the day until its peak around 22:00, followed by a slow decrease during the night and a more rapid decrease through the morning. The cause of this diurnal pattern at Chanban is presently unclear, but the levels could be representative of the regional background throughout the day and show only limited influences of local emissions.

2.4 Conclusions

A cavity ring down spectrometer (Picarro G2401, USA) was used to measure ambient CO_2, CH_4, CO, and water vapor mixing ratios at a semi-urban site (Bode) in the Kathmandu Valley for a year. This was the first 12-months of continuous measurements of these four species in the Kathmandu Valley in the foothills of the central Himalaya. Simultaneous measurement was carried out at a rural site (Chanban) for approximately 3 months to evaluate urban-rural differences.

The measurement also provided an opportunity to establish diurnal and seasonal variation of these species in one of the biggest metropolitan cities in the foothills of Himalayas. Annual

average of the mixing ratio of CH_4 and CO_2 in Bode revealed that they were higher than the mixing ratios at the background sites such as the Mauna Loa, USA and Mt. Waliguan, China, as well as higher than urban/semi-urban sites in nearby regions such as Ahmedabad and Shadnagar in India. These comparisons highlight potential sources of CH_4 and CO_2 in the Kathmandu Valley, such as brick kilns in the valley.

Polluted air masses were transported to the site mainly by two major local wind circulation patterns, East-South and North-East and West-Southwest throughout the observation period. Strong seasonality was observed with CO compared to CO_2 and CH_4. Winter and pre-monsoon high CO are linked to emission sources active in these seasons only and are from east-southeast and west-southwest. Emission from the east-southeast are most likely related to brick kilns (winter and pre-monsoon), which are in close proximity to Bode. Major city-centers are located in the west-southwest of Bode (vehicular emission) which impact the site all-round the year, although higher during winter season. Winter high was also observed with CO_2 and CH_4, which are mostly local influence of brick kilns, trash burning and emission from city-center. Nighttime and early morning accumulation of pollutants in winter due to a shallow stable mixing height (ca. 200 m) also contribute to elevated levels than other seasons. Diurnal variation across all seasons indicates the influence of rush-hour emissions related to vehicles and residential emissions. The evolution of the mixing layer height (200-1200 m) was a major factor which controls the morning-evening peak, afternoon low and night-early morning accumulation or decay. Thus, the geographical setting of the Kathmandu Valley and its associated meteorology play a key role in the dispersion and ventilation of pollutants in the Kathmandu Valley. The ratio of CO/CO_2 across different seasons and wind directions suggested that emissions from inefficient gasoline vehicles, brick kilns, residential cooking and diesel combustion are likely to impact Bode.

The differences in mean values for urban-rural measurements at Bode and Chanban is highest for CO (64 %) compared to CO_2 (3.8%) and CH_4 (12%). Low values of CH_4 and CO_2 mixing ratios at the Chanban site could represent regional background mixing ratios.

This study has provided valuable information on key greenhouse gases and air pollutants in the Kathmandu Valley and the surrounding regions. These observations can be useful as ground-truthing for evaluation of satellite measurements, as well as climate and regional air quality models. The overall analysis presented in the paper will contribute along with other recent

measurement and analysis to providing a sound scientific basis for reducing emissions of greenhouse gases and air pollutants in the Kathmandu Valley.

Chapter 3

Observation and Analysis of Spatio-temporal Characteristics of Surface Ozone and Carbon Monoxide at Multiple Sites in the Kathmandu Valley, Nepal

Abstract

Residents of the Kathmandu Valley experience severe particulate and gaseous air pollution throughout most of the year, even during much of the rainy season. The knowledge base for understanding the air pollution in the Kathmandu Valley was previously very limited, but is improving rapidly due to several field measurement studies conducted in the last few years. Thus far, most analyses of observations in the Kathmandu Valley have been limited to short periods of time at single locations. This study extends the past studies by examining the spatial and temporal characteristics of two important gaseous air pollutants (CO and O_3) based on simultaneous observations over a longer period at five locations within the valley and on its rim, including a supersite (at Bode in the valley center, 1345 m above sea level) and four satellite sites (at Paknajol, 1380 m asl in the Kathmandu city center, at Bhimdhunga (1522 m asl), a mountain pass on the valley's western rim, at Nagarkot (1901 m asl), another mountain pass on the eastern rim, and Naikhandi (1233 m asl), near the valley's only river outlet). CO and O_3 mixing ratios were monitored from January to July 2013, along with other gases and aerosol particles by instruments deployed at the Bode supersite during the international air pollution measurement campaign SusKat-ABC (Sustainable Atmosphere for the Kathmandu Valley – endorsed by the Atmospheric Brown Clouds program of UNEP). The monitoring of O_3 at Bode, Paknajol and Nagarkot as well as the CO monitoring at Bode were extended until March 2014 to investigate their variability over a complete annual cycle. Higher CO mixing ratios were found at Bode than at the outskirt sites (Bhimdhunga, Naikhandi and Nagarkot), and all sites except Nagarkot showed distinct diurnal cycles of CO mixing ratio with morning peaks and daytime lows. Seasonally, CO was higher during pre-monsoon (March-May) season and winter (December-February) season than during monsoon season (June-September) and post-monsoon (October-November) season. This is primarily due to the emissions from brick industries, which are only operational during this period (January-April), as well as increased

domestic heating during winter, and regional forest fires and agro-residue burning during the pre-monsoon season. It was lower during the monsoon due to rainfall, which reduces open burning activities within the valley and in the surrounding regions, and thus reduces sources of CO. The meteorology of the valley also played a key role in determining the CO mixing ratios. The wind is calm and easterly in the shallow mixing layer, with a mixing layer height (MLH) of about 250 m, during the night and early morning. The MLH slowly increases after the sunrises and decreases in the afternoon. As a result, the westerly wind becomes active and reduces the mixing ratio during the day time. Furthermore, there was evidence of an increase in the O_3 mixing ratios in the Kathmandu Valley as a result of emissions in the Indo-Gangetic Plains (IGP) region, particularly from biomass burning including agro-residue burning. A top-down estimate of the CO emission flux was made by using the CO mixing ratio and mixing layer height measured at Bode. The estimated annual CO flux at Bode was 4.9 $\mu g\ m^{-2}\ s^{-1}$, which is 2-14 times higher than that in widely used emission inventory databases (EDGAR HTAP, REAS and INTEX-B). This difference in CO flux between Bode and other emission databases likely arises from large uncertainties in both the top-down and bottom-up approaches to estimating the emission flux. The O_3 mixing ratio was found to be highest during the pre-monsoon season at all sites, while the timing of the seasonal minimum varied across the sites. The daily maximum 8-hour average O_3 exceeded the WHO recommended guideline of 50 ppb on more days at the hilltop station of Nagarkot (159/357 days) than at the urban valley bottom sites of Paknajol (132/354 days) and Bode (102/353 days), presumably due to the influence of free-tropospheric air at the high-altitude site, as also indicated by Putero et al., (2015) for the Paknajol site in the Kathmandu Valley as well as to titration of O_3 by fresh NOx emissions near the urban sites. More than 78% of the exceedance days were during the pre-monsoon period at all sites. The high O_3 mixing ratio observed during the pre-monsoon period is of a concern for human health and ecosystems, including agroecosystems in the Kathmandu Valley and surrounding regions.

3.1 Introduction

Air pollution is one of the major health risks globally. It was responsible for premature loss of about 7 million lives worldwide in 2012 (WHO, 2014), with about 1.7 million of these being in South Asian countries (India, Pakistan, Nepal and Bangladesh) in 2013 (Forouzanfar, 2015). The latest report shows that the indoor and outdoor air pollution are each responsible for 4 million premature deaths every year (http://www.who.int/airpollution/en/). South Asia is considered to be a major air pollution hotspot (Monks et al., 2009) and it is expected to be one

of the most polluted regions in the world for surface ozone (O_3) and other pollutants by 2030 (Dentener et al., 2006; IEA 2016; OECD 2016). Past studies have shown that the air pollution from this region affects not only the region itself, but is also transported to other parts of the world, including comparatively pristine regions such as the Himalayas and the Tibetan plateau (Bonasoni et al., 2010; Ming, et al., 2010; Lüthi et al., 2015), as well as to other distant locations such as northern Africa and the Mediterranean (Lawrence and Lelieveld, 2010).The pollutants are also uplifted to the tropopause by convective air masses and transported to the extratropical stratosphere during the monsoon season (Tissier and Legras., 2016; Lawrence and Lelieveld, 2010; Fueglistaler et al., 2009; Highwood and Hoskins, 1998). Air pollution is particularly alarming in many urban areas of South Asia, including in the city of Kathmandu and the broader Kathmandu Valley, Nepal (Chen et al., 2015; Putero et al., 2015; Kim et al., 2015; Sarkar et al., 2016; Shakya et al., 2017). This is due to their rapid urbanization, economic growth and the use of poor technologies in the transportation, energy and industrial sectors. In Kathmandu topography also plays a major role: the bowl-shaped Kathmandu Valley is surrounded by tall mountains and only a handful of passes. Topography is a key factor in governing local circulations, where low MLH (typically in the range 250 m to 1,500 m) and calm winds, have been observed particularly during nights and mornings. This in turn results in poor ventilation (Mues et al., 2017). Overall, this is conducive to trapping air pollutants and the deterioration of air quality in the valley. Effectively mitigating air pollutants in the regions like the Kathmandu Valley requires scientific knowledge about characteristics and sources of the pollutants. To contribute to this urgently-needed scientific knowledge base, in this study we focus on the analysis of measurements of two important gaseous species, carbon monoxide (CO and O_3, at multiple sites in and around the Kathmandu Valley. This study analyzes data from January 2013 to March 2014, which includes the intensive phase of an international air pollution measurement campaign – SusKat-ABC (Sustainable Atmosphere for the Kathmandu Valley – Atmospheric Brown Clouds) – conducted during December 2012 - June 2013 (Rupakheti et al., 2019, manuscript in preparation, submission anticipated in 1-2 months), with measurements of O_3 and CO at some sites continuing beyond the intensive campaign period (Bhardwaj et al., 2017; Mahata et al., 2017).

CO is a useful tracer of urban air pollution as it is primarily released during incomplete combustion processes that are common in urban areas. Forest fires and agro-residue burning in the IGP and foothills of the Himalaya are other important contributors of CO in the region (Bhardwaj et al., 2018; Mahata et al., 2017). CO is toxic at high concentrations indoors and

outdoors, but our focus here is on ambient levels. The main anthropogenic sources of CO in the Kathmandu Valley are vehicles, cooking activities (using liquefied petroleum gas, kerosene, and firewood), and industries, including brick kilns, especially biomass co-fired kilns with older technologies, and until recently diesel power generator sets (Panday and Prinn, 2009; Kim et al, 2015; Sarkar et al., 2016; Mahata et al., 2017; Sarkar et al., 2017). Tropospheric O_3, which is formed by photochemical reactions involving oxides of nitrogen (NO_x) and volatile organic compounds (VOCs), is a strong oxidizing agent in the troposphere. Because of its oxidizing nature, it is also deleterious to human health and plants already at typically polluted ambient levels (Lim et al., 2012; Burney and Ramanathan, 2014; Feng, 2015; Monks et al., 2015). Tropospheric O_3 is estimated to be responsible for about 5-20 % of premature deaths caused by air pollution globally (Brauer et al., 2012; Lim et al., 2012; Silva et al., 2013). It has also been estimated that high concentrations of O_3 are responsible for a global loss of crops equivalent to $ 11-18 billion annually (Avnery et al., 2011; UNEP and WMO, 2011), a substantial fraction of which is associated with the loss in wheat in India alone (equivalent to $ 5 billion in 2010) (Burney and Ramanathan, 2014). O_3 can also serve as a good indicator of the timing of the breakup of the nighttime stable boundary layer (when the ozone levels increase rapidly in the morning due to downward transport from the free troposphere (Panday and Prinn, 2009; Geiß et al., 2017).

Only a few past studies have reported measurements of ambient CO mixing ratios in the Kathmandu Valley. Davidson et al. (1986) measured CO in the city center and found mixing ratios between 1 and 2.5 ppm in the winter (December – February) of 1982-1983. Panday and Prinn (2009) measured similar levels of CO mixing ratios during September 2004 – June 2005, although the main sources of CO shifted from biofuel-dominated air pollutants from cooking activities in the 1980s to vehicle-dominated pollutants in the 2000s. The growth rate in the vehicle fleet has had a substantial influence on air pollution in the valley, including CO and O_3. Out of 2.33 million vehicles in Nepal, close to half of them are in the Kathmandu Valley (DoTM, 2015). Shrestha et al. (2013) estimated annual emission of CO of 31 kt in 2010 from a fraction of today's vehicle fleet in the Kathmandu Valley by using data from a field survey as input to the International Vehicle Emission (IVE) model. The model simulation considered motorcycles, buses, taxis, vans and three wheelers, but did not include personal cars, trucks and non-road vehicles. The studied fleets covered ~73% of the total fleet (570,145) registered in the valley in 2010, with motorcycles being the most common vehicle (69% of the total fleet).

Past studies have investigated the diurnal and seasonal variations of CO and O_3 mixing ratios in the Kathmandu Valley. Panday and Prinn (2009) observed distinct diurnal variations of CO mixing ratios and particulate matter concentrations observed during September 2004 – June 2005 at Bouddha (about 4 km northwest of the SusKat-ABC supersite at Bode), with morning and evening peaks. They found for the Kathmandu Valley that such peaks were created by the interplay between the ventilation, as determined by the local meteorology, and the timing of emissions, especially traffic and cooking emissions. The morning CO peak was also associated with the recirculation of the pollutants transported down from an elevated residual pollution layer (Panday and Prinn, 2009).

O_3 was observed to have lower nighttime levels in the city center than at the nearby hilltop site of Nagarkot (Panday and Prinn, 2009). Pudasainee et al. (2006) studied the seasonal variations of O_3 mixing ratios based on the observation for a whole year (2003-2004) in Pulchowk in the Lalitpur district, just south of central Kathmandu Metropolitan City (KMC) in the Kathmandu Valley. They reported seasonal O_3 mixing ratios to be highest during the pre-monsoon (March – May) and lowest in the winter (December – February). As a part of the SusKat-ABC Campaign, Putero et al. (2015) monitored O_3 mixing ratios at Paknajol, an urban site in the center of the KMC over a full-year period (February 2013-January 2014). They also observed similar seasonal variations in O_3 mixing ratios in the valley to those observed by Pudasainee et al. (2006), with highest O_3 during the pre-monsoon (1 February – 12 May) season, followed by the monsoon (13 May – 6 October), post-monsoon (7 October – 26 October) and winter (27 October – 31 January) seasons. They found that during the pre-monsoon season, westerly winds and regional synoptic circulation transport O_3 and its precursors from regional forest fires located outside the Kathmandu Valley. In another study conducted as part of the SusKat-ABC Campaign, 37 non-methane volatile organic compounds (NMVOCs) were measured at Bode, with data recording every second, during winter of 2012-2013; the measurements included isoprene, an important biogenic precursor of O_3 (Sarkar et al., 2016). They found concentrations to vary in two distinct periods. The first period was marked by no brick kiln operations and was associated with high biogenic emissions of isoprene. During the second period nearby brick kilns, which use coal mixed with biomass, were operational; they contributed to elevated concentrations of ambient acetonitrile, benzene and isocyanic acid. Furthermore, the authors found that oxygenated NMVOCs and isoprene combined accounted for 72% and 68% of the total O_3 production potential in the first period and second period, respectively.

Prior to the SusKat-ABC campaign there were no studies that simultaneously measured ambient CO and O_3 mixing ratios at multiple sites in the Kathmandu Valley over extended periods of time. Past studies either focused on one long-term site, or on short-term observation records at various sites (Panday and Prinn, 2009), or they investigated the seasonal characteristics of single pollutants such as O_3 at a single site in the valley (Pudasainee et al., 2006). The most comparable past study is by Putero et al. (2015), who described O_3 mixing ratios at one SusKat-ABC site (Paknajol) in the Kathmandu city center observed during the SusKat-ABC campaign, and discussed O_3 seasonal variations. There is also a companion study on regional CO and O_3 pollution by Bhardwaj et al. (2017) which is based on O_3 and CO mixing ratios monitored at the SusKat-ABC supersite at Bode in the Kathmandu Valley for a limited period (January-June 2013) and at two sites in India (Pantnagar in Indo-Gangetic Plain and Nainital in Himalayan foothill). They reported simultaneous enhancement in O_3 and CO levels at these three sites in spring, highlighting contribution of regional emissions, such as biomass burning in northwest Indo-Gangetic Plain (IGP), and regional transport to broader regional scale pollution, including in the Kathmandu Valley. In this study, we document the diurnal and seasonal (where applicable) characteristics and spatial distributions of CO and O_3 mixing ratios based on simultaneous observations at several locations within the valley and on the valley rim mountains over a full year, helping to characterize the pollution within the valley and the pollution plume entering and exiting the valley. We also compute the first top-down estimates of CO emission fluxes for the Kathmandu Valley and compare these to CO emissions fluxes in widely-used emission datasets such as EDGAR HTAP (Janssens-Maenhout et al., 2000), REAS (Kurokawa et al., 2013) and INTEX-B (Zhang et al., 2009).

3.2 Study sites and methods

The Kathmandu Valley, situated in the foothills of the Central Himalaya, is home to more than 3 million people. The valley floor has an area of about 340 km^2, with an average altitude of about 1300 m above sea level (m asl.). It is surrounded by peaks of about 1900-2800 m asl. The valley has five major mountains passes on its rim: the Nagdhunga, Bhimdhunga and Mudku Bhanjhyang passes in the west, and the Nala and Nagarkot passes in the east, as shown in Figure 3.1. The passes are situated at altitudes of 1480-1530 m asl. There is also one river outlet (the Bagmati River) towards the south, which constitutes a sixth pass for air circulation in and out of the valley (Regmi et al., 2003; Panday and Prinn, 2009). We selected five measurement sites, including two on the valley floor (Bode and Paknajol), two on mountain ridges (Bhimdhunga and Nagarkot) and one near the Bagmati River outlet (Naikhandi) to

characterize the spatial and temporal variabilities of CO and O_3 mixing ratios in the Kathmandu Valley. A short description of the measurement sites is presented here and in Table 1, while details on instruments deployed at those sites for this study are presented in Table 3.2. Further details of the measurement sites are described in the SusKat-ABC campaign overview paper (Rupakheti et al., 2019, manuscript in preparation).

Table 3.1 Information on the sampling sites (of the SusKat-ABC campaign) used in this study with sampling carried out during 2013-2014 in the Kathmandu Valley. The altitude is in meter above mean sea level (m asl.).

Site	General setting of site	Location, altitude (m a.s.l.)
Bode	Suburban, tallest building with scattered houses surrounded by agricultural fields	27.69° N, 85.40° E, 1345
Bhimdhunga	Rural, on the ridge, close to the pass separating the Kathmandu Valley from a valley of a tributary the Trishuli River to the west	27.73° N, 85.23° E, 1522
Paknajol	Urban, city center, the tallest building in the neighborhood	27.72° N, 85.30° E, 1380
Naikhandi	Rural, at outlet of Bagmati River in southwest corner of the valley	27.60° N, 85.29° E, 1233
Nagarkot	Rural, mountaintop site of the eastern valley rim, north-facing towards the Kathmandu Valley	27.72° N , 85.52° E, 1901

Bode (27.69°N and 85.40°E, 1344 m asl.): This was the supersite of the SusKat-ABC Campaign. Bode is located in the Madhyapur Thimi municipality in the just east of the geographic center of the valley. It is a semi-urban site surrounded by urban buildings and residential houses scattered across agricultural lands. Within 4 km there are 10 brick kilns and the Bhaktapur Industrial Estate towards the southeast (refer to Sarkar et al., 2016; Mahata et al., 2017 for details). The O_3 and CO instruments at Bode site were placed on the fifth floor of a 6-story building, the tallest in the area. The inlets of the CO and O_3 analyzers were mounted on the roof top of the temporary lab, 20 m above the ground level.

Bhimdhunga: This site (27.73°N, 85.23°E, 1522 m asl.) is located on the Bhimdhunga pass on the western rim of the valley. It is one of the lowest points on the north-south running mountain ridge between the Kathmandu Valley to the east and a valley of a tributary of the Trishuli River to the west. It is situated about 5.5 km from the western edge of the KMC (Kathmandu Metropolitan City), in a rural setting with very few scattered rural houses nearby. The CO instrument was placed on the ground floor of a small one-story building and its inlet was 2 m

above ground. An automatic weather station (AWS) (Hobo Onset, USA) was set up on the roof of another one-story building at a distance of ca. 15 m from the first building.

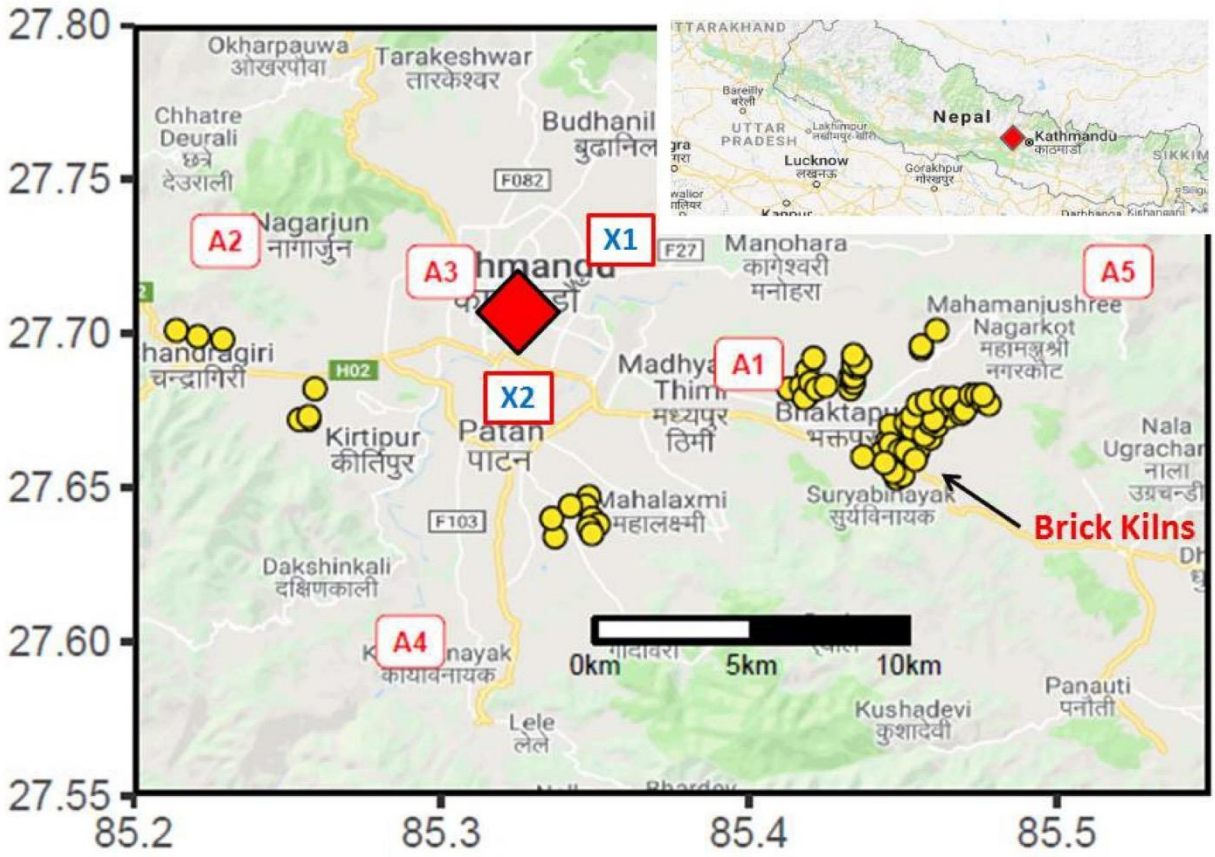

Figure 3.1. Observation sites in the SusKat-ABC international air pollution campaign during 2013-2014 in the Kathmandu Valley. A1 = Bode, A3 = Paknajol, and A4 = Naikhandi were selected within the valley floor and A2 = Bhimdhunga and A5 = Nagarkot on the mountain ridge. Naikhandi site is also near the Bagmati River outlet. Past study sites, Bouddha (X1) and Pulchowk (X2), which are referred in the manuscript, are also shown in the Figure. Source: Google Maps.

Paknajol: This site (27.72°N, 85.30°E, 1380 m asl.) is located at the city center in the KMC, near the popular touristic area of Thamel. It is in the western part of the valley and about 10 km distance from the Bode supersite. The O_3 and meteorological instruments relevant to this study were placed on the top floor and rooftop of a 6-story building, the tallest in the area (details in Putero et al., 2015; note that CO was not measured here). The inlet of the O_3 analyzer was placed 25 m above the ground.

Naikhandi: This site (27.60°N, 85.29°E, 1233 m asl) is located within the premises of a school (Kamdhenu Madhyamik Vidhyalaya) located at the southwestern part of the valley (~7 km south from the nearest point of the Ring Road). The school premise is open, surrounded by

sparsely scattered rural houses in agricultural lands. The nearest village (~75 houses) is about 500 m away in the southwest direction. There are 5 brick kilns within 2 km distance (2 to the north and 3 to the northeast) from the site. The instruments were kept in a one-story building of the school and its inlet was 5 m above the ground. The AWS (Hobo Onset, USA) was installed on the ground near the Bagmati River, ~100 m away from the main measurement site.

Nagarkot: This site is located on a mountain ridge (27.72°N, 85.52°E, 1901 m asl), ca. 13 km east of Bode, in the eastern part of the valley. The site faces the Kathmandu Valley to the west and small rural town, Nagarkot, to the east. The instruments were set up in a 2-story building of the Nagarkot Health Post and their inlets were 5 m above the ground. The AWS (Vaisala WXT520, Finland) was set up on the roof of the building.

Table 3.2. Details of the instruments deployed at different sites during the observation period during January 2013-March 2014 in the Kathmandu Valley.

Location	Instrument	Parameters	Inlet/sensor height (above ground)	Duration	Group
Bode	Horiba APMA-370	CO	20 m	1 Jan–7 Jun 2013	ARIES
	Teledyne 400E	O_3	20 m	1 Jan–7 Jun 2013	ARIES
	Thermo Scientific 49i	O_3	20 m	18 Jun–31 Dec 2013	IASS
	Picarro G2401	CO	20 m	6 Mar 2013–5 Mar 2014	ICIMOD
	Campbell AWS	T, RH, SR, WS, WD, RF	22 m	1 Jan–30 Mar 2013	IASS
	Davis AWS (Vantage Pro2)	T, RH, P, RF	21 m	30 May–Jul 2013	UVA
	Ceilometer (Vaisala CL31)	MLH	20 m	1 Mar 2013–28 Feb 2014	JGUM
Bhimdhunga	Thermo Scientific 48i TLE	CO	2 m	1 Jan–15 Jul 2013	UVA
	AWS Hobo Onset	T, RH, SR, WS, WD, P	5 m	1 Jan–30 Jun 2013	UVA
Naikhandi	Thermo Scientific 48i TLE	CO	5 m	3 Jan–6 Jun 2013	UVA
	2B Tech. Model 205	O_3	5 m	1 Feb–25 May 2013	UVA
	AWS Hobo Onset	T, RH, SR, WS, WD, P	2 m	3 Jan–25 Apr 2013	UVA
Nagarkot	Thermo Scientific 48i TLE	CO	5 m	13 Feb–Apr 3 2013; 8 Jun–15 Jul 2013	UVA
	Thermo Scientific 49i	O_3	5 m	9 Jan–30 Jun 2013	UVA
	Campbell AWS	T, RH, SR, WS, WD, RF	7 m		IASS
	AWS (Vaisala WXT 520)	T, RH, SR, WS, WD, RF, P	7 m	10 Feb–30 Jun 2013	RTS
Paknajol	Thermo Environmental (49i)	O_3	25 m	1 Feb 2013–30 Jan 2014	EV-K2-CNR
	AWS (Vaisala WXT 425)	T, RH, SR, WS, WD, RF, P	25 m	1 Feb 2013–30 Jan 2014	EV-K2-CNR

Note: T - temperature, RH - relative humidity, SR- solar radiation, WS - wind speed, WD - wind direction, RF- rainfall, P – pressure and MLH – Mixing layer height; ARIES - Aryabhatta Research Institute of Observational Sciences, India; ICIMOD - International Center for Integrated Mountain Development, Nepal; IASS – Institute for Advanced Sustainability Studies, Germany; UVA- University of Virginia, USA; JGUM – Johannes Gutenberg University Mainz, Germany; RTS - Real Time Solutions, Nepal; Ev-K2-CNR - Everest-Karakorum - Italian National Research Council, Italy.

Bhimdhunga Pass in the west and Naikhandi near the Bagmati River outlet in the southwest are the important places for interchange of valley air with outside air. The Bhimdhunga and Naikhandi sites are approximately 5.5 and 7 km away from the nearest edge of the city, respectively. Similarly, Bode is located downwind of the city centers and thus receives

pollution outflow from nearby city centers of Kathmandu and Lalitpur due to strong westerly and southwesterly winds (4-6 m s^{-1}) during the day time, and emissions from the Bhaktapur area to the east and southeast direction by calm easterly winds (< 1 m s^{-1}) during the night (Sarkar et al., 2016; Mahata et al., 2017).

A freshly calibrated new CO analyzer (Horiba APMA-370, Japan) was deployed for the first time at Bode. This instrument is based on the IR absorption method at 4.6 µm by CO molecules. Before field deployment at Bode, it was compared with the bench model of the Horiba (APMA-370), and the correlation (r) between them was 0.9 and slope was 1.09. The instrument was regularly maintained by running auto-zero checks (Bhardwaj et al., 2017). Similarly, another CO analyzer (Picarro G2401, USA) which is based on cavity ring-down spectroscopy technique (CRDS) was also a new factory calibrated unit, and was deployed in Bode along with the Horiba APMA-370. An IR-based Horiba CO monitor (APMA-370) was run simultaneously with a co-located cavity ring down spectrometry based Picarro CO analyzer for nearly 3 months. The correlation coefficient and slope between the two measurements were found to be 0.99 and 0.96, respectively (Mahata et al., 2017). This indicates that there was very little drift in the IR-based CO values due to room temperature change, within acceptable range (i.e., within the measurement uncertainties of the instruments). Therefore, we did not any apply correction in the IR-based CO data. All other CO analyzers (Thermo Scientific, 48i-TLE, USA), which are also based on IR absorption by CO molecules, deployed at Bhimdhunga, Naikhandi and Nagarkot, were set up for regular automatic zero checks on a daily basis. In addition, a span check was also performed during the observations by using span gas of 1.99 ppm (Gts-Welco, PA, USA) on March 8, 2013 at Naikhandi and Nagarkot, and on March 9 at Bhimdhunga. The IR-based CO instruments' span drifts were within a 5 % range.

For the O_3 monitor (Teledyne 400E, USA) at Bode, regular zero and span checks were carried out using the built-in O_3 generator and scrubber (Bhardwaj et al., 2017). This unit was used in Bode from 01 January 2013 to 09 June 2013. New factory-calibrated O_3 monitors (Thermo Scientific, 49i, USA) were used for the rest of the measurement period (18 June 2013 to 31 December 2013) at Bode, and for the full year of measurements at Nagarkot. A Thermo Environmental O_3 analyzer (Model 49i, USA) was used at the Paknajol site (Putero et al., 2015) with the same experimental set up as described in Cristofanelli et al. (2010). The working principle of all of the O_3 instruments is based on the attenuation of UV radiation by O_3 molecules at ~254 nm.

In order to characterize observations across the seasons, we considered the following seasons as defined in Shrestha et al. (1999) and used in other previous studies in the Kathmandu Valley (Sharma et al., 2012; Chen et al., 2016; Mahata et al, 2017): Pre-monsoon (March, April, May); Monsoon (June, July, August September); Post-monsoon (October, November); and Winter (December, January, February).

3.3 Results and discussion

3.3.1 CO mixing ratio at multiple sites

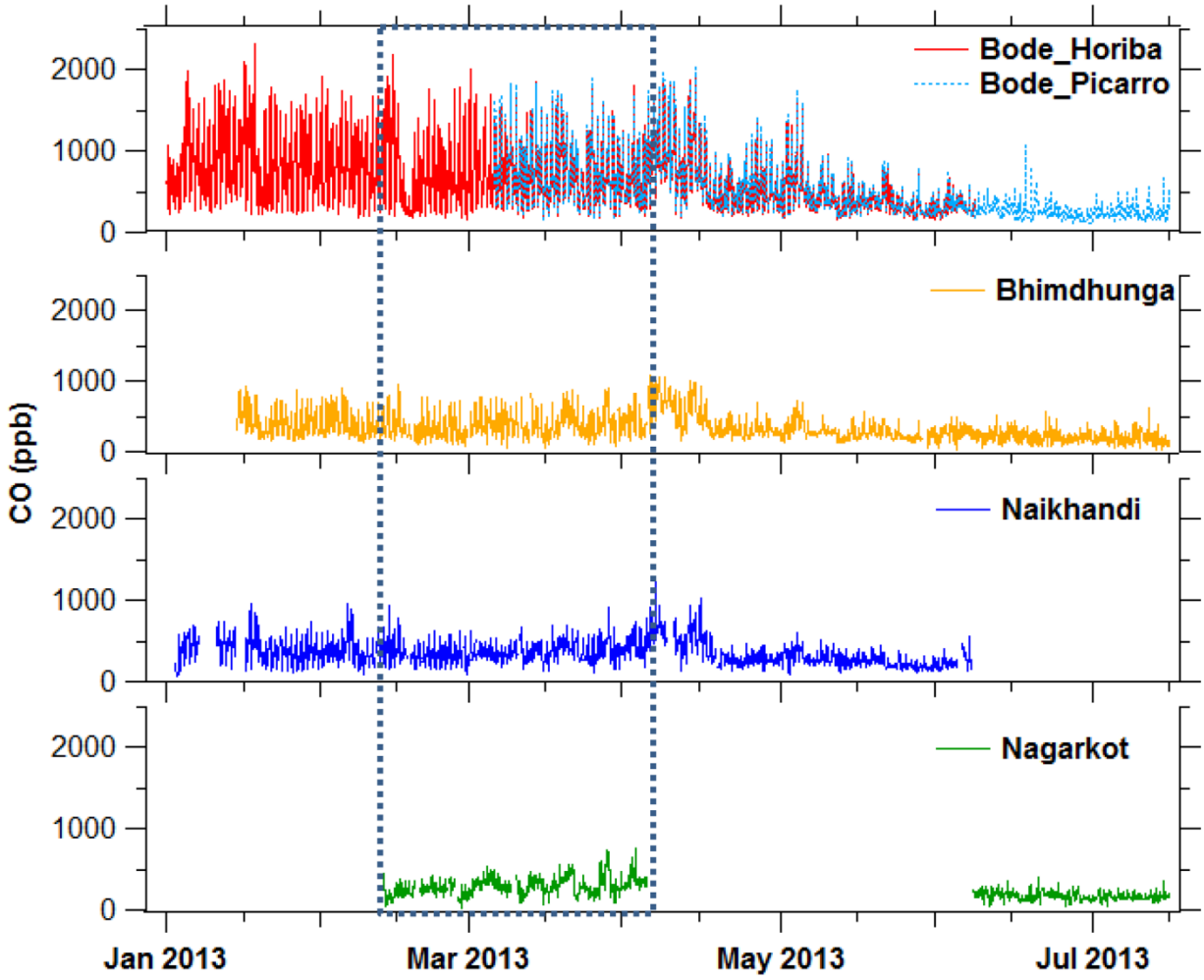

Figure 3.2. Hourly average CO mixing ratios observed at supersite (Bode) and three satellite sites (Bhimdhunga, Naikhandi and Nagarkot) of the SusKat-ABC international air pollution measurement campaign during January to July 2013 in the Kathmandu Valley. The dotted box represents a period (13 February - 03 April, 2013) during which data for all four sites were available.

Figure 3.2 shows the time series of the hourly average CO mixing ratios at the four sites (Bode, Bhimdhunga, Naikhandi and Nagarkot). Fluctuations in CO mixing ratios were higher during

the winter and pre-monsoon than during the monsoon season at all sites. The monsoon rain generally starts in Nepal around mid-June. In 2013, however, there were more frequent rain events in the month of May than in previous years.

The CO mixing ratios (measured in parts per billion by volume, hereafter the unit is denoted as ppb) of hourly averaged data over the total observation periods at four sites and their standard deviation were: Bode - 569.9 ± 383.5 ppb during 1 January - 15 July, Bhimdhunga - 321.5 ± 166.2 ppb during 14 Jan - 15 July, Naikhandi - 345.4 ± 147.9 ppb during 3 January - 6 June and Nagarkot - 235.5 ± 106.2 ppb during 13 February - 15 July (except 4 April to 7 June). Nagarkot had only about 3 months of CO data (due to a problem in zeroing of the instrument) during the observation period. For the measurement period, the CO mixing ratio at Nagarkot (~13 km far from Bode) showed small fluctuations compared with the other sites.

High CO values in the Kathmandu Valley during the dry season (November-May) were also reported by Panday and Prinn (2009) based on their measurements during September 2004-May 2005 at Bouddha (~ 4 km in northwest from Bode). The simultaneous episodes of high CO observed from April 1to15 in Bhimdhunga, Bode and Naikhandi indicate the influence of regional sources, in addition to local sources. This is discussed further in section 3.2.3.

3.3.2 Diurnal and seasonal variations of CO

3.3.2.1 Diurnal pattern of CO at multiple sites

Figure 3.3 shows the diurnal cycles of CO mixing ratios at four sites (plotted for the period of 13 February to 3 April 2013, when the data were available from all four sites). The variation in the mixing ratios during the day was characterized by a pronounced morning peak, a weaker evening peak, and a daytime low; except at Nagarkot where peaks are less visible. Multiple sources contribute to the morning and evening peaks, especially emission from vehicles, residential burning (fossil fuel and biomass), brick kilns and trash burning (Kim et al., 2015; Sarkar et al., 2016; Mahata et al., 2017). Other studies conducted during the SusKat-ABC campaign have identified garbage (household waste and yard waste) burning as a key source of various air pollutants, such as organic carbon (OC) and elemental carbon (EC) (Kim et al., 2015), poly-cyclic aromatic hydrocarbon (PAHs) (Chen et al., 2015), and NMVOCs (Sarkar et al., 2016; Sarkar et al., 2017). Garbage burning is often done in small fires and quite sporadic, normally taking place in the evenings and mornings (partly chosen to avoid attention from the responsible authorities). The rate of waste (and also biomass) burning in the morning is higher in winter due to the use of the fires for providing warmth on colder days.

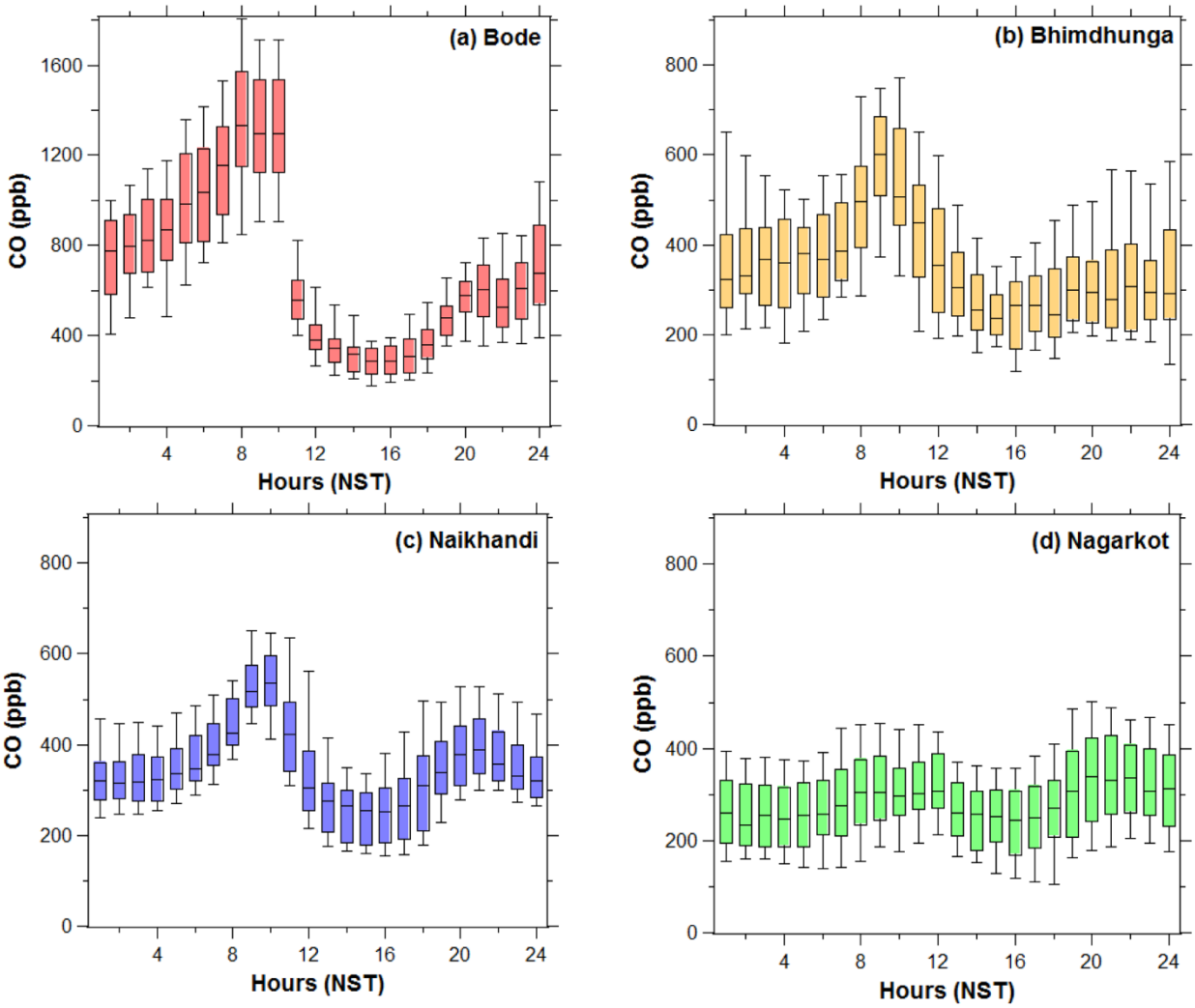

Figure 3.3. Diurnal variations of hourly average CO mixing ratios during the common observation period (13 February–03 April, 2013) at Bode, Bhimdhunga, Naikhandi and Nagarkot. The lower end and upper end of the whisker represents 10th and 90th percentile, respectively; the lower end and upper end of each box represents the 25th and 75th percentile, respectively, and the black horizontal line in the middle of each box is the median for each month. Note: the y-axis scale of Bode is twice that of the other three sites.

The observed diurnal cycle of CO is similar to that reported in a previous study (Panday and Prinn, 2009), and is also similar to the diurnal pattern of black carbon (BC) in the Kathmandu Valley (Sharma et al., 2012; Mues et al., 2017). The diurnal cycles of these primary pollutants are closely coupled with the valley's boundary layer height, which is about 1200 m during daytime, and falls to approximately 200 m at nighttime in Bode (Mues et al., 2017). Nagarkot and Bhimdhunga, both on mountain ridges, are generally above the valley's boundary layer, especially at night, and thus the diurnal profile especially at Nagarkot is distinct compared to other three sites, being relatively flat with small dip during 12:00-18:00 LT (local time).

Distinct morning peaks were observed in Bode, Bhimdhunga and Naikhandi at 08:00, 09:00, and 10:00, respectively, i.e., the morning peak lags by 1-2 hours in Bhimdhunga and Naikhandi compared to Bode. Bhimdhunga on the mountain ridge may receive the Kathmandu Valley's pollution due to upslope winds (~2 m s^{-1}) from the east direction in the morning hours after the dissolution of the valley's boundary layer due to radiative heating of the mountain slopes. However, Naikhandi is in close proximity to brick kilns and could be impacted by their plumes carried to the site by northerly winds in the early morning (ca. 07:00-10:00, not shown). The evening peak values at Bode and Bhimdhunga were less pronounced compared to the morning maxima. The morning peak at Bode was influenced by nighttime accumulation of CO along with other pollutants from nearby brick kilns (Sarkar et al., 2016; Mahata et al., 2017; Mues et al., 2017) and recirculation of air from above (Panday and Prinn, 2009). Similarly, the local pollution from the nearby village and city area due to upslope winds from the valley floor is expected to contribute to the morning peak at Bhimdhunga. The evening peak at Naikhandi was at 21:00 and was closer to the morning values in comparison to the large difference between morning and evening peaks at Bode and Bhimdhunga. A nighttime build-up (linear increase) of various pollutants compared to the afternoon minimum was typically observed in Bode during the SusKat-ABC measurement period, including the main campaign period (Sarkar et al., 2016; Mahata et al., 2017; Mues et al., 2017). This is mainly associated with the persistent emissions such as those from brick kilns, which are in close proximity to the Bode measurement site under the stable boundary layer. The isolated peak during the morning transition phase at Bhimdhunga could be due to an elevated polluted layer because of the slope wind (Panday et al., 2009). There appears to be less influence of nighttime polluting sources at Naikhandi and Bhimdhunga than at Bode.

The MLH starts increasing after radiative heating of the surface by incoming solar radiation. The heating of the ground causes thermals to rise from the surface layer resulting in the entrainment of cleaner air from above the boundary layer leading to the dissolution of nocturnal stable boundary layer. Increasing wind speeds (4-6 m s^{-1}) during daytime also support turbulent vertical diffusion, as well as flushing of the pollution by less polluted air masses from outside the valley, with stronger horizontal winds allowing significant transport of air masses into the valley. In addition, reduced traffic and household cooking activities during daytime compared to morning and evening rush hours contribute to the reduced CO mixing ratios.

3.3.2.2 CO diurnal variation across seasons

Due to the lack of availability of simultaneous CO data at all sites covering the entire sampling period, a one-month period was selected for each season to examine the diurnal variation across the seasons, and to get more insights into the mixing ratios at different times of the day, as reported in Table 3.4. Figure 3.4 shows the diurnal variation of CO mixing ratios in Bode, Bhimdhunga, and Naikhandi during the selected periods for the three seasons.

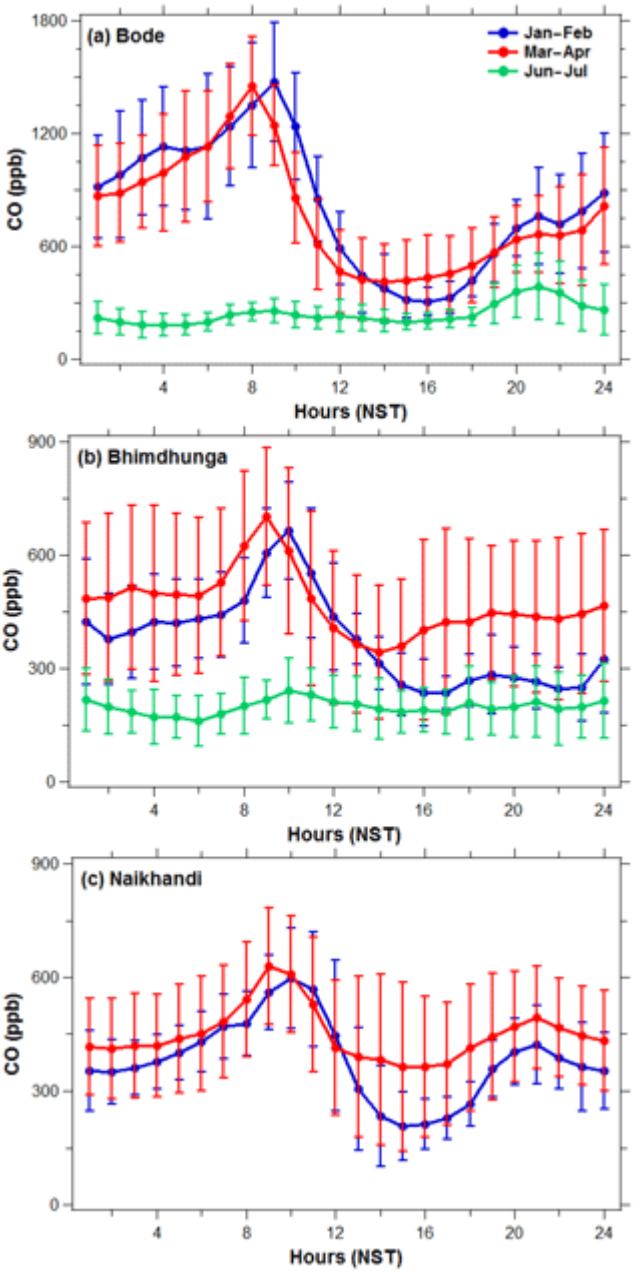

Figure 3.4. Comparison of diurnal variation of hourly average CO mixing ratios for four seasons at Bode, Bhimdhunga and Naikhandi. Due to the lack of continuous data at some sites, data of one month in each season were taken for comparison as representative of the winter (16 Jan – 15 Feb), pre-monsoon (16 Mar – 15 Apr) and monsoon (16 Jun – 15 Jul) season of 2013. Note: y-axis scale of the top panel (Bode) is double than lower two panels (Bhimdhunga and Naikhandi).

The diurnal cycles during each season had different characteristics. The most prominent distinction was that the CO mixing ratio was low during the monsoon period over all sites (Figure 3.4, Table 3.4) as a result of summer monsoon rainfall in the valley, which is 60 - 90%

of the 1400 mm rainfall for a typical year (Nayava, 1980; Giri et al., 2006). Because of the rainfall, the brick production activities are stopped in the valley (usually they are operational from January-April every year). Further, the rainfall also diminishes many burning activities (forest fires, agro-residue and trash burning) within the valley and surrounding region, and thus reduces CO emissions. Afternoon CO mixing ratios were higher in the pre-monsoon season than in the other two seasons in Bode, Bhimdhunga and Naikhandi (also see Table 3.4), with the most likely sources being emissions from forest fires and agro-residue burning arriving from outside the valley during this season (this will be discussed further in section 3.2.3). Nighttime accumulation was observed in Bode and Bhimdhunga, but not at Naikhandi, where the mixing ratio decreased slightly from about 20:00 until about 04:00, after which the mixing ratios increased until the morning peak. The nighttime accumulation of CO in Bode during pre-monsoon and winter is due to the influence of nearby brick kilns (Mahata et al., 2017) because of the calm easterly wind (refer supplementary Figure A.2 in Mahata et al., 2017). Previous studies carried out at the Bode site during the SusKat-ABC campaign have attributed over a dozen brick kilns located near Bode as strong sources of BC and EC (Kim et al., 2015; Mues et al., 2017), NMVOCs (Sarkar et al, 2016; Sarkar et al., 2017), SO2 (Kiros et al., 2016) and CO (Mahata et al., 2017), and the enhanced concentrations were observed during nighttime and mornings when winds blew from east and southeast bringing emissions from the location of the brick kilns to the observation site.

Bhimdhunga is not near any major polluting sources such as brick kilns, and it is unclear whether the nighttime CO accumulation in Bhimdhunga is primarily due to ongoing local residential pollution emissions, and/or to pollution transported from remote sources. The transition of the wind from westerlies during the day to easterlies during the night, with moderate wind speed (~2-4 m s^{-1}) at Bhimdhunga, may bring polluted air masses westwards which were initially transported to the eastern part from the Kathmandu Valley during the daytime (Regmi et al., 2003; Panday and Prinn, 2009; Panday et al., 2009).

The distinct shift in the morning peak was seen at all 3 sites by season. The one hour shift in the morning peak from the pre-monsoon to winter is due to an earlier onset of the morning transition. However, the one hour difference in the morning peak between Bode (pre-monsoon at 8:00; winter at 9:00) and Bhimdhunga/Naikhandi (pre-monsoon at 9:00 LT; winter at 10:00 LT) in the pre-monsoon and winter is associated with commencement of early local emissions

under the shallow boundary layer at Bode. The one hour lag in the morning peak at Bhimdhunga and Naikhandi may be due to transport of city pollutants to the site, respectively.

Across the seasons, the afternoon (12:00-16:00 LT) CO mixing ratio was higher during the pre-monsoon than in the winter at all three stations (p value for all sites < 0.5) (Table 3.4), although the mixing layer was higher in the pre–monsoon season than in the winter in Bode (and presumably at the other sites as well). This is not likely to be explained by local emissions in the valley, since these are similar in the winter and pre-monsoon periods. Putero et al. (2015) suggested instead that this reflects an influx of polluted air into the valley due to large synoptic circulation patterns during the pre-monsoon season. Such regional influences are explored further in the next section.

3.3.2.3 Regional influence on CO in the valley

Recent studies have indicated the likelihood of regional long-range transport contributing to air pollution in different parts of Nepal (Marinoni et al., 2013; Tripathee et al., 2014; Dhungel et al., 2016; Rupakheti et al., 2016; Lüthi et al., 2016; Wan et al., 2017), including the Kathmandu Valley, especially during the pre-monsoon period (Panday and Prinn, 2009; Putero et al., 2015; Bhardwaj et al., 2017). During the pre-monsoon season, frequent agro-residue burning and forest fires are reported in the IGP region including southern Nepal and the Himalayan foothills in India and Nepal (Ram and Sarin, 2010; Vadrevu et al., 2012), and in the Kathmandu Valley. This season is also characterized by the strongest daytime local wind speeds (averaging 4-6 m s^{-1}) in the Kathmandu Valley (Mahata et al., 2017). Our study also observed several episodes of days with both elevated CO mixing ratios (Figure 3.2) and O_3 mixing ratios (also measured in parts per billion by volume, hereafter the unit is denoted as ppb) (Figure 3.5) during April and May, especially during the late afternoon period. The influence of regional pollutants was investigated by comparing a 2-week period with normal CO levels (16–30 March (hereafter "period I") with an adjacent two week period (1-15 April) with episodically high CO mixing ratios (hereafter "period II"), which nicely fit with the "burst" in regional fire activity presented by Putero et al. (2015) in their Figure 3.9. The t-test of the two-hourly data means of CO in period I and period II at Bode, Bhimdhunga and Naikhandi (as in Figure 3.5) were performed at 95% confidence level and the differences were found to be statistically significant (p < 0.5).

Figure 3.5a shows the diurnal cycle of CO mixing ratios during period I (faint color) and period II (dark color) at Bode, Bhimdhunga and Naikhandi.

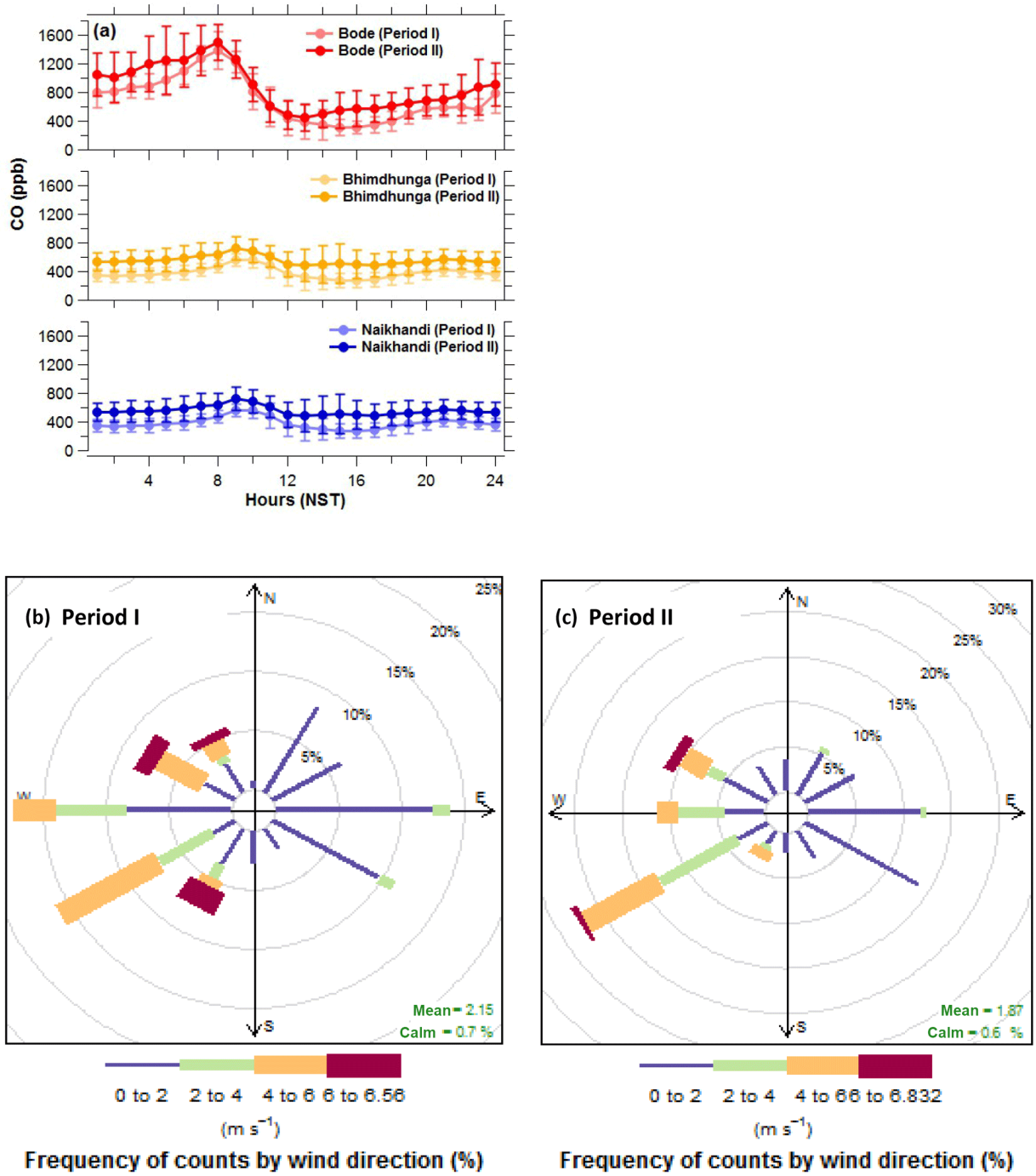

Figure 3.5. Comparison of hourly average CO mixing ratios during normal days (March 16-30), labelled as period I (faint color) and episode days (April 1-15), labelled as period II (dark color) in 2013 at (a) Bode, Bhimdhunga and Naikhandi in the Kathmandu Valley. The wind roses at Bode corresponding to two periods are also plotted (b) period I and (c) period II respectively.

The difference between two periods was calculated by subtracting the average of period I from average of period II. The average CO mixing ratios during period II were elevated with respect to period I by 157 ppb at Bode, 175 ppb at Bhimdhunga, and 176 ppb at Naikhandi.

The enhancements in mixing ratios at the three sites were fairly similar from hour to hour throughout the day, with the exception of the late afternoon when the enhancement was generally greatest. This consistency across the sites suggests that the episode was caused by a large-scale enhancement (regional contribution) being added onto the prevailing local pollution levels at all the sites. A large-scale source would also be consistent with the greater enhancements of CO at the outskirt sites, which would be most directly affected by regional pollution, compared to the central valley site of Bode, with strong local sources. The enhancement during the period II is substantial (statistically significant as mentioned above), representing an increase of approximately 45% at the outskirt sites of Bhimdhunga and Naikhandi (which start with lower CO levels), and 23% at Bode. During both periods I and II, local winds from west (the opposite direction from the brick kilns, which were mostly located to the southeast of Bode) were dominant during daytime at Bode (Figure 3.5b, c). This suggests that the elevation in CO levels was caused by additional emissions in period II in the regions to the west and southwest of the Kathmandu Valley, e.g., large scale agricultural burning and forest fires during this period, as also noted by Putero et al. (2015) (see their Figure 3.9). Far away, in Lumbini in the southern part of Nepal (Rupakheti et al., 2016), and Pantnagar in northern IGP in India (Bharwdwaj et al., 2017), about 220 km (aerial distance) to the southwest and 585 km to the west, respectively, of the Kathmandu Valley, CO episodes were also observed during the spring season of 2013, providing a strong indication that the episode in period II was indeed regional in nature.

3.3.3 O_3 in the Kathmandu Valley and surrounding areas

Figure 3.6 shows the hourly average and daily maximum 8-hour average of O_3 mixing ratios at Bode, Paknajol, and Nagarkot from measurements during the SusKat campaign and afterwards, along with O_3 mixing ratios from a previous study (November 2003 - October 2004; Pudasainee et al., 2006) at the Pulchowk site (4 km away from Paknajol) in the Latitpur district. The daily maximum 8-hour average O_3 was calculated by selecting the maximum O_3 mixing ratio from 8 hour running averages during each day. The nighttime mixing ratio of hourly O_3 drops close to zero in Bode, Paknajol and Pulchowk in the winter season. This is a typical characteristic of many urban areas where reaction with NO at night depletes O_3 from the boundary layer (e.g., Talbot et al., 2005). In the pre-monsoon and monsoon months, the titration is not as strong and the hourly O_3 falls, but generally remains above 10 ppb. Similar patterns of ozone mixing ratios were observed at other sites in northern South Asia.

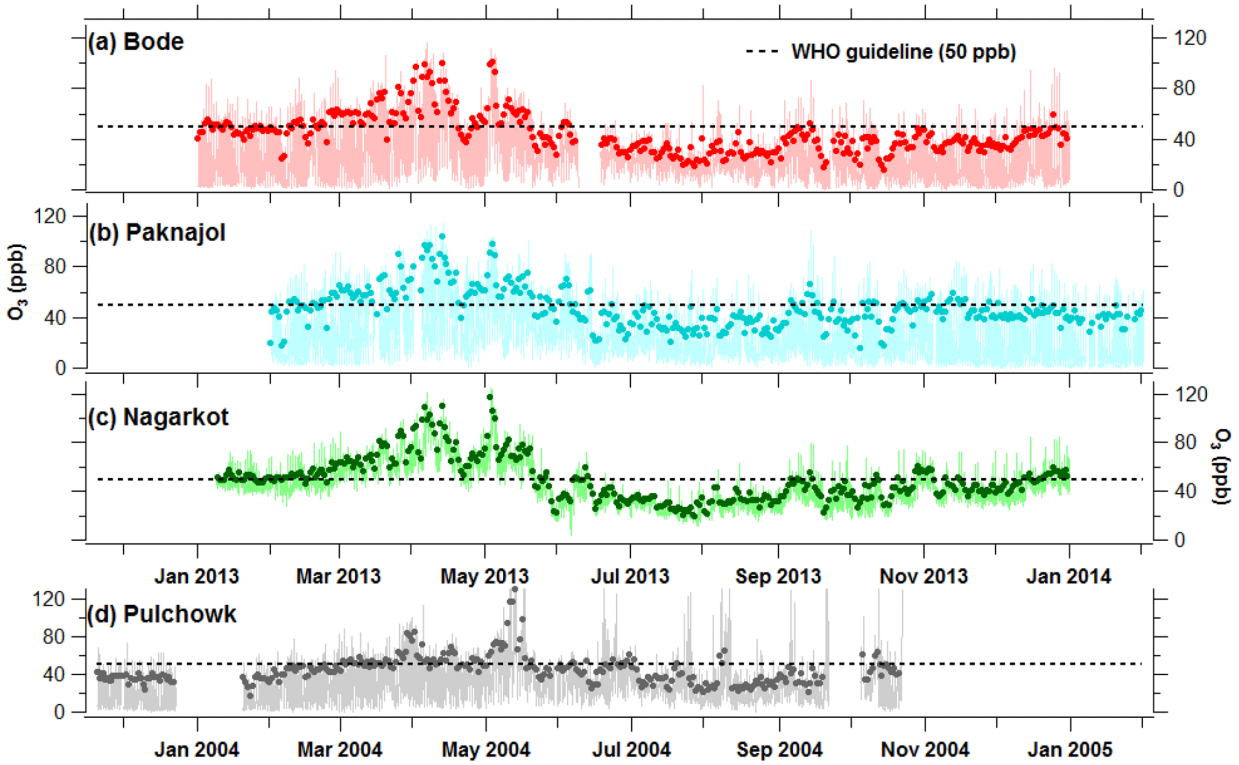

Figure 3. 6. Time series of hourly average (faint colored line) and daily maximum 8-hr average (solid colored circle) O_3 mixing ratio at (a) Bode (semi-urban), (b) Paknajol (urban) and (c) Nagarkot (hilltop) observed during 2013-2014, and (d) Pulchowk (urban) observed during November 2003-October 2004 in the Kathmandu Valley. Black dotted line represents WHO guideline (50 ppb) for daily maximum 8-hr average of O_3.

For example, higher O_3 mixing ratios were observed in the afternoon (84 ppb) and lower during the night and early morning hours (10 ppb) at Kullu Valley, a semi-urban site located at 1154 m asl, in the North-western Himalaya in India (Sharma et al. 2012). A similar dip in O_3 value in the dark hours was observed at Ahmedabad, India by Lal et al. (2000). Nagarkot, in contrast, is above the valley's boundary layer and has lesser NO for titration at night at this hill station as has been observed in another hill station in Himalayan foothills (Naja and Lal, 2002). Thus, the O_3 level remains above 25 ppb during the entire year at Nagarkot. As also shown in Table 3.3, at all sites, the O_3 mixing ratios were highest in the pre-monsoon, but the timing of the lowest seasonal values varied across the sites: post-monsoon in Bode, winter in Paknajol and monsoon in Nagarkot. Such differences in minimum O_3 across the sites can be anticipated due to the locations of the sites (e.g., urban, semi-urban, rural and hilltop sites, with differing availabilities of O_3 precursors from different emission sources). The seasonal variations of O_3 observed at Bode in this study are consistent with Putero et al. (2015) and Pudasainee et al. (2006), who also observed O_3 maxima during the pre-monsoon, but O_3 minima during the winter season.

The daily maximum 8-hour average O_3 mixing ratio (solid colored circles in Figure 3.6) exceeded the WHO recommended guideline of 50 ppb (WHO, 2006, black dotted line in Figure 3.6) most frequently during the pre-monsoon period and the winter. During the observation period, the daily maximum 8-hour average O_3 exceeded the WHO guideline on 102 out of 353 days of observation (29%) at Bode, 132/354 days (37%) at Paknajol and 159/357 days (45%) at Nagarkot. The higher exceedance rate at Nagarkot is because it is at higher altitude, which results in (i) greater exposure to large-scale regional pollution, especially from forest fire in the Himalayan foothills and agro-residue burning in the IGP region, outside the Kathmandu Valley (Sinha et al., 2014, Putero et al., 2015), (ii) less titration of O_3 by NO_x, being farther away from the main pollution sources, and (iii) exposure to O_3 rich free tropospheric air, including influences from stratospheric intrusions.

Table 3.3. Summary of the monthly average ozone mixing ratios (ppb) [average (Avg), standard deviation (SD), minimum (Min.) and maximum (Max.)] at four sites* in the Kathmandu Valley, Nepal during 2013-2014 and two sites (Manora Peak and Delhi) in India.

	Bode	Paknajol	Nagarkot	Manora Peak[a]	Delhi[b]
Month	Avg ± SD (Min., Max.)	Avg ± SD (Min., Max.)	Avg ± SD (Min., Max.)	Avg ± SD	Avg (Min., Max.)
January	23.5 ± 19.9 (1.4, 87.1)	16.9 ± 18.3 (0.1, 71.7)*	46.7 ± 5.7 (36.4, 73.7)	37.3 ± 14.8	19.3 (10, 14.7)
February	25.6 ± 20.4 (1.2, 94.5)	24.2 ± 20.1 (1.6, 91.7)	47.5 ± 7.5 (28.2, 83.6)	43.8 ± 16.8	25.3 (10.9, 55.7)
March	37.4 ± 24.3 (1.2, 105.9)	37.7 ± 23.8 (1.6, 95.8)	62.4 ± 9.5 (40.5, 98.9)	56.6 ± 11.4	29.7 (13.8, 58)
April	43.4 ± 26.6 (1.4, 116.2)	46.7 ± 26.8 (1.0, 115.5)	71.5 ± 15.5 (40.1, 121.0)	63.1 ± 11.7	33 (13.7, 64.3)
May	38.5 ± 21.2 (2.0, 111.1)	42.8 ± 20.6 (6.7, 103.3)	59.0 ± 20.6 (15, 0, 124.5)	67.2 ± 14.2	35.4 (19.8, 62)
June	27.8 ± 12.0 (1.7, 68.4)	27.5 ± 17.0 (0.6, 90.7)	34.2 ± 9.1 (4.6, 72.0)	44.0 ± 19.5	25.6 (12.8, 46.4)
July	21.1 ± 9.5 (1.7, 82.0)	20.5 ± 13.4 (2.0, 77.9)	25.9 ± 6.2 (11.1, 48.0)	30.3 ± 9.9	19.1 (9.4, 37.1)
August	20.3 ± 9.9 (2.0, 70.9)	20.1 ± 12.6 (0.8, 73.1)	28.3 ± 5.8 (15.5, 62.9)	24.9 ± 8.4	14.3 (9.7, 29.5)
September	23.3 ± 14.9 (0.5, 85.9)	24.9 ± 17.4 (0.4, 108.1)	34.8 ± 9.6 (16.1, 79.7)	32.0 ± 9.1	17.7 (7.7, 37.7)
October	19.4 ± 13.8 (0.1, 70.9)	22.6 ± 17.0 (0.6, 83.5)	35.2 ± 10.2 (18.0, 73.8)	42.4 ± 7.9	21.7 (9, 56.9)
November	18.6 ± 15.1 (0.3, 67.7)	22.4 ± 20.9 (0.1, 84.0)	40.1 ± 8.1 (25.6, 73.3)	43.9 ± 7.6	22.6 (9, 55.1)
December	21.7 ± 17.8 (1.0, 96.6)	19.5 ± 19.7 (0.1, 82.0)	43.8 ± 9.0 (24.8, 85.11)	41.6 ± 6.3	20.2 (9.1, 40.3)
Season:					
Winter	24.5 ± 20.1 (1.2, 94.5)	20.2 ± 19.6 (0.1, 91.7)	45.8 ± 7.8 (24.8, 85.1)	40.9	21.6 (9.1, 55.7)
Premonsoon	39.8 ± 24.2 (1.2, 116.2)	42.4 ± 24.0 (1.0, 115.5)	64.3 ± 16.7 (14, 9, 124.5)	62.3	32.7 (13.7, 64.3)
Monsoon	22.7 ± 12.0 (0.5, 85.9)	23.2 ± 15.5 (0.4, 108.1)	30.8 ± 8.7 (4.6, 79.7)	32.8	19.2 (7.7, 46.4)
Postmonsoon	19.0 ± 14.5 (0.1, 70.9)	22.5 ± 18.9 (0.1, 84.0)	37.6 ± 9.5 (18.0, 73.8)	39.4	22.2 (9, 56.9)

[a] Kumar et al. (2010), [b] Ghude et al. (2008). * O_3 data of Paknajol on January was of 2014.

Table 3.4. Averege CO mixing ratio (ppb) at different time of the day (daytime - 12:00 – 16:00 LT), and nighttime - 23:00 – 03:00 LT) and the monthly average (total) at four sites in the Kathmandu Valley

	Winter (16 Jan–15 Feb)			Premonsoon (16 Mar–15 Apr)			Monsoon (16 Jun–15Jul)			Postmonsoon (16 Oct–15 Nov)		
Sites	Daytime	Nighttime	Total	Daytime	Nighttime	Total	Daytime	Nighttime	Total	Daytime	Nighttime	Total
Bode	405.35	927.21	819.17	430.91	839.17	770.52	210.59	230.08	241.34	269.10	453.95	397.24
Bhimdhunga	324.62	354.23	374.27	374.64	479.37	471.33	196.61	202.85	198.40			
Naikhandi	280.97	356.14	380.40	382.71	425.17	449.83						
Nagarkot							141.68	158.78	160.41			

The diurnal profiles of O_3 mixing ratios (Figure 3.7) at three sites Bode and Pakanajol in the Valley and Nagarkot, a hilltop site normally above the Kathmandu Valley's boundary layer show, notably in the morning hours, that the residual layer above the Kathmandu Valley's mixing layer contains a significant amount of ozone. Based on the surface ozone data collected at Paknajol during 2013-14, Putero e al. (2015) concluded that downward mixing of ozone from the residual layer contributes to surface ozone in the Kathmandu Valley in the afternoon hours (11:00-17:00 LT). It is likely that the same source has also contributed to higher ozone mixing ratios at Nagarkot. Such mixing has been observed at other sites as well. Wang et al. (2012) reported the increase in downward mixing of O_3 from the stratosphere to the middle troposphere (56%) and the lower troposphere (13%) in spring and summer in Beijing. The downward flux was highest in the middle troposphere (75%) in winter. Similarly, Kumar et al. (2010) reported that more than 10 ppb of stratospheric contribution at a high-altitude site (in Nainital) during January to April. However, there were no significant stratospheric intrusions seen in spring and summer (seen only in winter) at Nepal Climate Observatory-Pyramid (Putero et al., 2016).

During the SusKat-ABC campaign in 2013 and later in 2014, passive sampling of gaseous pollutants (SO_2, NO_x, NH_3 and O_3) was carried out at fourteen sites including urban/semi-urban sites (Bode, Indrachowk, Maharajganj, Mangal Bazar, Suryabinayak, Bhaisepati, Budhanilkantha, Kirtipur, and Lubhu) and rural sites (Bhimdhunga, Naikhandi, Sankhu, Tinpiple, and Nagarkot) in the Kathmandu Valley (Kiros et al., 2016). Similar to this study, they also observed higher O_3 mixing ratios in rural areas than the urban/semi-urban sites in the Kathmandu Valley. Exceedances of the WHO standard is most common during the pre-monsoon season, occurring 78% (72/92 days), 88% (78/89 days) and 92% (85/92 days) of the time at Bode, Paknajol and Nagarkot, respectively. A study by Putero et al., (2015), based on O_3 mixing ratio measurements at Paknajol in the Kathmandu Valley, as a part of the SusKat-ABC campaign, has reported that the dynamics (both by horizontal and vertical winds) plays a key role in increased O_3 mixing ratios in the afternoon in the Kathmandu Valley. They estimated that the contribution of photochemistry varied as a function of the hour of the day, ranging from 6 to 34 %. Unfortunately, no viable NOx measurements were obtained at any site in the Kathmandu Valley and surrounding mountain ridges during the SusKat-ABC campaign. Speciated VOCs were measured at Bode only for about 2 months but NOx was not available for the same period. Therefore, we were not able to discern quantitatively proportional contributions of NOx, VOCs and intrusion (chemistry vs. dynamics) from the free troposphere

or lower stratosphere to observed O_3 concentrations at Nagarkot, Bode and other sites in the valley. In the context of protecting public health, crops and regional vegetation, the O_3 mixing ratios in the Kathmandu Valley and surrounding areas clearly indicate the urgent need for mitigation action aimed at reducing emissions of its precursor gases NOx and VOCs. However, air quality management plans need to consider carefully the reduction strategies of NMVOCs or NOx while aiming at mitigating the O_3 pollution in the Kathmandu Valley. If the correct strategy (NMVOCs vs. NOx) is not applied, then O_3 mixing ratios could increase, for example, as seen in Huszar et al. (2016) where they reported that reducing NMVOCs in urban areas in central Europe leads to O_3 reduction whereas the focus on NOx reduction results in O_3 increase.

The SusKat-ABC O_3 data can be compared to observations made about a decade ago by Pudasainee et al. (2006) at the urban site of Pulchowk, not far from Paknajol, as plotted in Figure 6d. The daily maximum 8-hour average O_3 had exceeded the WHO guideline at Pulchowk for 33% (95/292 days) of days during the observation from November 2003 to October 2004. The exceedance was 38% (133/354 days) of days at Paknajol during Feb 2013 - March 2014. Due to inter-annual variability and differences in the seasonal observation time periods at Pulchowk and Pakanajol, we cannot draw any conclusions about trends over the decade between the observations because of the difference in location and sampling height as well as a general difference in instrument calibration. However, a clear similarity between the observations is that most of the exceedance took place during pre-monsoon season, during which both studies have observations throughout the season (~90 days). The percentage of exceedance at Pulchowk during the pre-monsoon season in 2003-2004 was 70% (63/90 days) and at Pakanajol in 2013 it was 88% (78/89 days). However, just like for the annual fraction of exceedances, due to inter-annual variability we cannot say that the 18% (or ca. 15 days) difference in the exceedances is significant. A longer term O_3 record would be needed to really establish if there is a trend in the ozone concentrations.

3.3.4 O_3 seasonal and diurnal variation

The seasonal average O_3 mixing ratios at Bode, Nagarkot and Paknajol are shown in Table 3.3. For comparison, the O_3 mixing ratios measured at two sites in India, (i) Manora Peak (1958 m asl), ca. 9 km from Nainital city, a site in rural mountain setting and (ii) Delhi, a highly-polluted urban setting in northwest IGP are also listed in the Table, based on results from Kumar et al. (2010) and Ghude et al. (2008). There is a strong similarity between the urban and semi-urban

sites in Nepal (i.e., Bode, Pakanajol) and India (i.e., Delhi), as well as between the rural and mountain sites in Nepal (i.e., Nagarkot) and India (i.e., Manora Peak), with small differences.

The peak mixing ratios were in the pre-monsoon period: at the rural and mountain sites the peak ozone mixing ratio values were very similar (64 and 62 ppb for Nagarkot and Manora Peak, respectively) and are due to influences discussed earlier for Nagarkot; at the sub-urban and urban sites the pre-monsoon values are significantly lower (ca. 40, 42, 33 ppb for Bode, Paknajol, Delhi, respectively) due to fresh NOx emissions near the urban sites and the consequent titration of ozone with NO. The lowest O_3 seasonal values at rural and mountain sites typically occur in the monsoon months while for semi-urban and urban sites, the minimum was observed during post-monsoon (Bode) and winter (Paknajol).

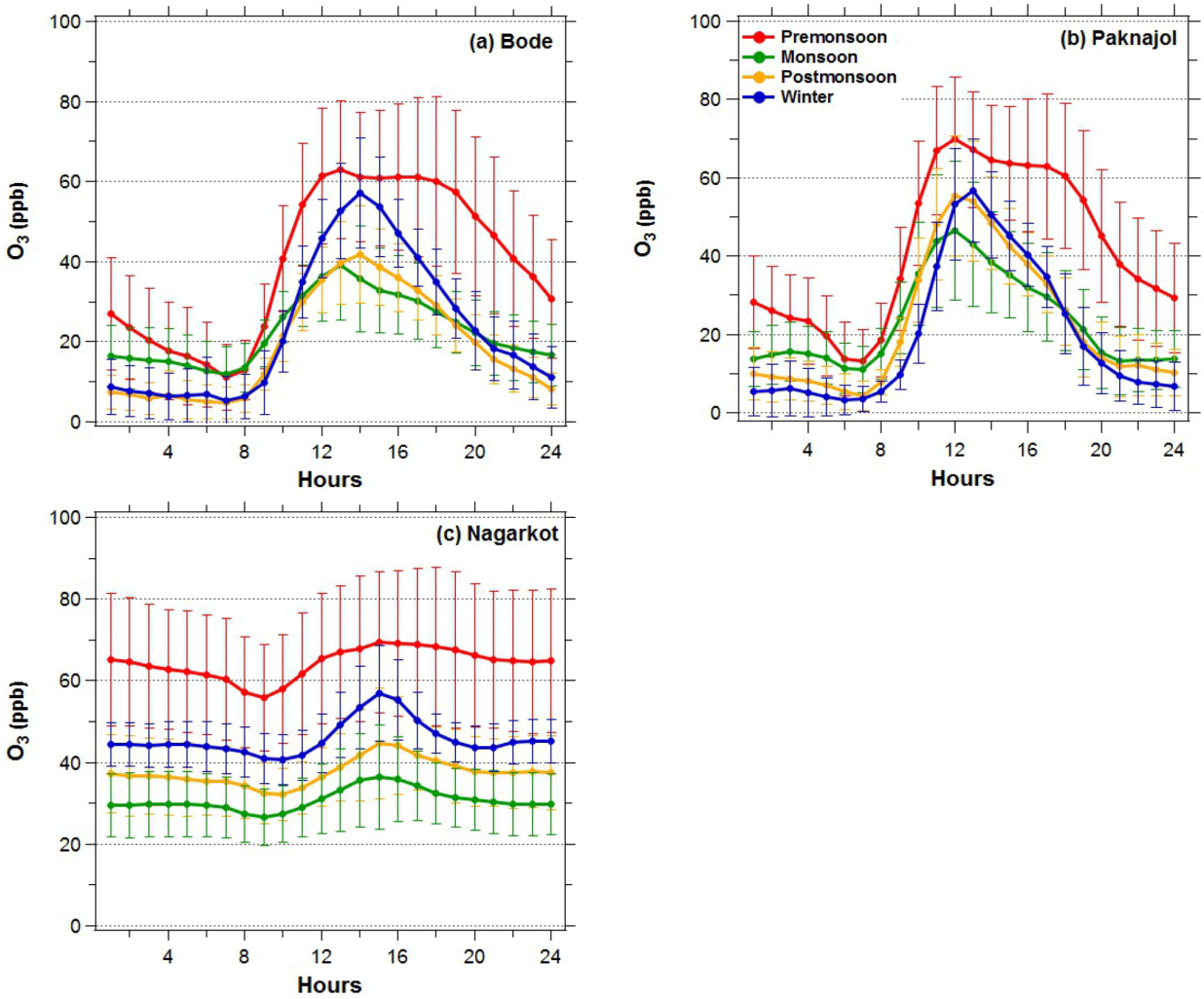

Figure 3.7. Diurnal pattern of hourly average O_3 mixing ratio for different seasons during January 2013-January 2014 at (a) Bode, (b) Paknajol, and (c) Nagarkot in the Kathmandu Valley. The four seasons (described in the text) are defined as: pre-monsoon (Mar-May), monsoon (Jun-Sep), post-monsoon (Oct-Nov), winter (Dec-Feb).

Figure 3.7 shows the diurnal variation of O_3 mixing ratios at Bode, Paknajol and Nagarkot in the different seasons. The typical O_3 maximum mixing ratio in the early afternoon at the urban and semi-urban sites is mainly due to daytime photochemical production as well as entrainment of ozone due to dynamics (both intrusion of ozone rich free tropospheric air into the boundary layer, and regional scale horizontal transport of ozone), as explained in case of Paknajol by Putero et al. (2015).

The ozone mixing ratios are relatively constant throughout the day at Nagarkot (~1901 m asl), which, being a hilltop site, is largely representative of the lower free tropospheric regional pollution values, however, it is also affected by ozone production from precursors transported from the Kathmandu Valley due to westerly winds during the afternoon hours. The dip in O_3 at Nagarkot (Figure 3.7) in the morning transition hours indicates the upward mixing of air from polluted (and Ozone-depleted) nocturnal boundary layer as it is breaking up.

3.3.5 CO emission flux estimate

It is possible to determine a top-down estimate of the average CO emission flux for the morning hours for the region around the Bode site by applying an approach that was developed and used in Mues et al. (2017) to estimate the emission fluxes of BC at Bode. The analysis of Mues et al. (2017) found BC fluxes for the Kathmandu Valley that were considerably higher than the widely-used EDGAR HTAP emission database (Version 2.2). Support for this top-down estimate was found by considering the BC concentrations and fluxes for the Kathmandu Valley in comparison to Delhi and Mumbai; although the observed BC concentrations were similar in all three locations, the EDGAR HTAP V2.2 emissions of BC for the Kathmandu Valley are much lower than those for Delhi and Mumbai, while the top-down emissions estimate for the Kathmandu Valley were similar to the emissions from EDGAR HTAP V2.2 for Delhi and Mumbai (Mues et al., 2017).

Here we apply the same method as developed in Mues et al. (2017) to estimate the CO fluxes based on the observed CO mixing ratio and ceilometer observations of the mixing layer height (*MLH*) in Bode for the period of 1 year (March 2013-February 2014). Using the approach used by Mues et al. (2017), the CO fluxes can be calculated from the increase in CO concentrations during the nighttime period when the *MLH* is nearly constant, using:

$$FCO(t_x, t_y) = \frac{\Delta CO \times ave(MLH(t_x), MLH\ (t_y))}{\Delta t \times 3600} \times \frac{MLH(t_y)}{MLH\ (t_x)} \quad (1)$$

where *FCO* (t_x, t_y) is the CO emission flux (in µg m^{-2} s^{-1}) between time t_x and t_y (in hours), ΔCO is the change in CO mixing ratio (in µg m^{-3}) between time t_x and t_y, *ave(MLH(*t_x*), MLH(*t_y*)* are average of the mixing layer heights (in m) between time t_x and t_y, Δt is the time interval between t_x and t_y, and *MLH(*t_y*)/MLH(*t_x*)* is mixing layer collapse factor, accounting for the small change in MLH between the night and the morning hours. The calculation of the emission flux is based on mean diurnal cycle per month of CO and MLH and tx and ty represent the time with the minimum (tx) and the maximum (ty) CO concentration in the night and morning (see Mues et al., 2017 for details).

This method of calculating the CO emission flux is based on five main assumptions:

i. CO is well-mixed horizontally and vertically within the mixing layer in the region immediately surrounding the Bode site.

ii. The *MLH* remains fairly constant during the night so that the product of the CO concentration (µg m^{-3}) and the *MLH* (m) represents CO mass per unit area within the column, and any change in mass per unit area represents the net flux into the column.

iii. The transport of air pollutants into and out of the stable nocturnal boundary layer of the valley is negligible, which is supported by the calm winds (<1 m s^{-1}) during the night and morning hours at the site (Mahata et al., 2017).

iv. The vertical mixing of pollutants between the mixing layer and the free atmosphere is assumed to be negligible at night, thus strictly seen is the estimated CO flux calculated with eq. 1 only valid for the morning hours. When applied to the whole day the implicit assumption is that the emissions are similar during the rest of the 24 h period. An assumption that is viable on average for some sources like brick kilns which operate day and night, but which does not apply to all sources, e.g., the technique will tend to underestimate emissions due to traffic, which are typically much stronger during the day than at night, while it will overestimate emissions due to waste burning, which is typically more prevalent during the night and early

morning (pre-sunrise) than during the daytime. This assumption is made because Eq. (1) only works well for calculating the CO flux from night to morning, when there is a relatively constant *MLH* and limited vertical and horizontal mixing.

v. CO emission is assumed to be uniform throughout the valley; this may not be correct, but cannot be verified until a high resolution emission inventory data is available, which is being developed for the Kathmandu Valley and rest of Nepal with a 1 km x 1km spatial resolution (Sadavarte et. al., 2019).

During nighttime assumption (i) might not be entirely correct since the degree of mixing in the nocturnal stable layer and thus the vertically mixing is drastically reduced compared to daytime (and thus the term "mixing layer" is not entirely accurate, but we nevertheless apply it here due to its common use with ceilometer measurements). This adds a degree of uncertainty to the application of ceilometer observations to compute top-down emissions estimates, which will only be resolved once nocturnal vertical profile measurements are also available in order to characterize the nocturnal boundary layer characteristics and the degree to which the surface observations are representative of the mixing ratios throughout the vertical column of the nocturnal stable layer.

It is not possible to directly compute the emission flux for a full 24-hour day using this top-down method, since the emissions during the day could be either greater or smaller than at night, and because the other assumptions do not hold (in particular there is considerable vertical mixing with the free troposphere and stronger horizontal transport during the daytime). Thus, the top-down computation only provides a useful indicative value. However, while it is also not possible to estimate how much different the daytime emissions are, it is possible to determine an absolute lower bound for the CO flux (FCO_{min}) by making the extreme assumption that the CO emissions are non-zero only during the hours which were used in the calculation, and that they were zero during the rest of the day (this provides a lower bound to the emissions since the daytime emissions physically cannot be negative). This lower bound of the flux (FCO_{min}) is thus calculated by scaling back the 24-hour flux to only applying over the calculation time interval (Δt), using:

$$FCO_{min.} = FCO \times \frac{\Delta t}{24} \qquad (2)$$

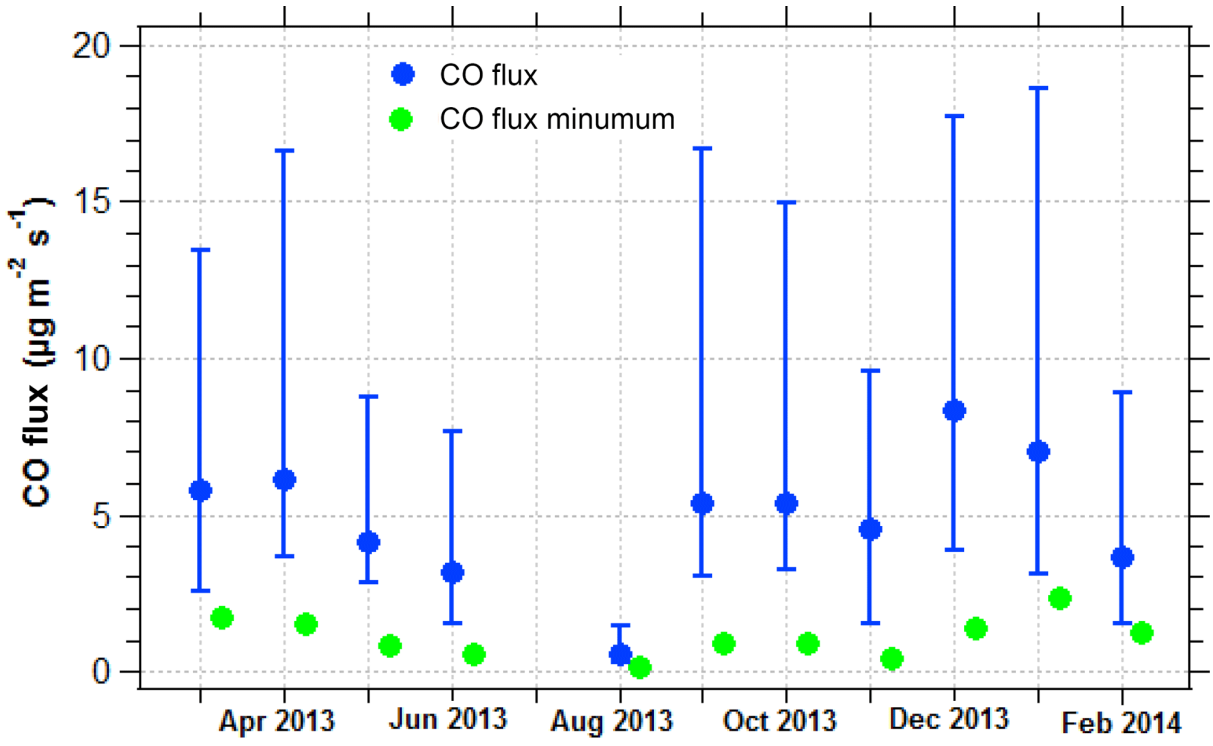

Figure 3. 8. The estimated monthly average CO emission flux, which is based on the mean diurnal cycle of CO mixing ratios of each month for two conditions: (i) with data of all days (CO Flux) (blue dot) with lower and upper ends of the bar representing 25th and 75th percentile respectively, and (ii) with data of morning hours (CO Flux minimum (green dot) in which zero emission is assumed for the other hours of the day. The fluxes for July were not estimated as there were insufficient (less than 15 days) of concurrent CO and mixing layer height data. It is expected that the FCO and $FCO_{min.}$ for July should fall between values for June and August 2013.

Figure 3.8 shows the estimated monthly CO emission flux, along with its 25th and 75th percentile values as an indication of the variability of the estimated flux in each month; the lower bound of the CO flux based on Equation 2 is also shown. The estimated annual mean CO flux at Bode is 4.9 µg m^{-2} s^{-1}. Seasonally, the emissions are computed to be highest during December to April (3.6-8.4 µg m^{-2} s^{-1}), coinciding with the brick kiln operation period, which resulted in elevated concentrations of most pollutants at Bode (Kim et al., 2015; Chen et al., 2016; Sarkar et al., 2016; Mahata et al., 2017; Mues et al., 2017), including CO (Bhardwaj et al., 2017; Mahata et al., 2017), while the emissions were generally lower during the remaining months (0.5-5.4 µg m^{-2} s^{-1}).

The uncertainty in the top-down CO emissions estimate will be largest during June to October, due to the greater diurnal and day-to-day variability with the minimum and maximum CO

mixing ratio values during the night and early morning used in Equation 1 often being less distinct than in the other months.

Comparing the annual mean top-down estimated CO emission flux at Bode (4.9 µg m^{-2} s^{-1}) with available global and regional emission inventories, the top-down estimated CO flux is twice the value, 2.4 µg m^{-2} s^{-1}, for the Kathmandu Valley in the EDGAR HTAP V2.2 emission inventory database for 2010 [note that the CO emission values for the location at Bode and the whole averaged for the valley (27.65-27.75°N, 85.25-85.40°E) were found to be the same up to two significant figures]. The estimated CO flux was 6.5-8 times as high as in the REAS database (0.63-0.76 µg m^{-2} s^{-1}, based on the 2008 values in Kurokawa et al., 2013), and between 3 and 14 times higher than the values in the INTEX-B database for 2006 (0.35-1.77 µg m^{-2} s^{-1}; Zhang et al., 2009). The large differences between our estimated CO emission flux and these emission databases is not likely to be due to the comparison of data for different years; rather, it indicates the substantial uncertainties in both the top-down and bottom-up approaches to estimating the emission flux. Although our approximation of the emission flux relies on several assumptions, the fact that the lower bound value that we calculate is still as high as or higher than the values in some of the published emission datasets likely indicates that the bottom-up emissions are missing or underestimating some important sources, which will be important to examine carefully and improve as a basis for interpreting future modelling studies of CO pollution in the Kathmandu Valley and surrounding regions, as well as for assessing possible mitigation options.

The emission estimates computed here are subject to several further uncertainties which are discussed in detail in Mues et al., (2017). In short, the uncertainties of CO flux estimates arise from (i) the assumptions that Bode site represents the whole atmospheric column and entire valley, which is not possible to verify without having many simultaneous monitoring stations in the valley (measurements at a few sites where CO was monitored for this study show some difference in CO mixing ratios), (ii) the higher variability (unclear minima and maxima during the morning and night hours) in the diurnal cycles of CO from June to October show a much higher variability than other months, that in turn makes it difficult to choose the exact hour of CO minimum and maximum needed for the flux estimation and (iii) the possible impact of wet deposition is not taken into account but would rather generally cause the emission rate to be underestimated.

3.4 Conclusions

Ambient CO and O_3 mixing ratios were measured in the framework of the SusKat-ABC international air pollution measurement campaign at five sites (Bode, Paknajol, Bhimdhunga, Naikhandi and Nagarkot) in the Kathmandu Valley (Table 3.1) and its fringes, initially during January to July 2013, and later extended to one year at three sites (Bode, Paknajol and Nagarkot) to better understand their seasonal characteristics. The observed CO and O_3 levels at all sites except Nagarkot were characteristic of highly-polluted urban settings, with the particular feature that the bowl-shaped valley and resulting meteorology had several effects on the pollution levels.

At all sites, the CO mixing ratios were higher during the early morning and late evening, an observation that is especially connected to the interplay between the ventilation of the boundary layer and the diurnal cycles of the emission sources. Under calm wind conditions that limited mixing within, into and out of the Kathmandu Valley, the morning CO peak tended to be more pronounced due to the buildup of pollution at night in the shallow planetary boundary layer. This nocturnal buildup was especially strong during January to April at Bode, with the mean CO mixing ratio increasing by about a factor of 4 in the 12 hours from 20:00 to 08:00 LT, especially due to operation of nearby brick kilns continuing through night. During the daytime, the wind becomes stronger and the horizontal and vertical circulation dilutes and transports pollution around and out of the valley.

Although normally the pollution levels are presumed to be higher in the heavily populated valley than in the immediate surrounding region, occasionally the synoptic circulation will transport in CO and O_3-rich air, especially that influenced by forest fires and agro-residue burning in the IGP region and Himalayan foothills, as was observed during a few episodes in the pre-monsoon season.

The observed O_3 mixing ratio was highest in the pre-monsoon season at all sites, and the daily maximum 8-hour average O_3 exceeded the WHO guideline of 50 ppb on about 80% of the days during this season at the semi-urban/urban sites of Bode and Paknajol, while at Nagarkot (which is in the free troposphere, i.e., above valley's boundary layer most of the time, especially during nighttime) it exceeded the WHO guideline on 92% of the days in pre-monsoon season. During the whole observation period, the 8 hour maximum average O_3 exceeded the WHO recommended value on 29%, 37% and 45% of the days at Bode, Paknajol and Nagarkot, respectively. The diurnal cycle showed evidence of photochemical production,

larger scale advection of polluted air masses as well as possible down-mixing of O_3 during the daytime, as also observed by Putero et al., (2015) at Paknajol, with the hourly mixing ratio at the polluted site increasing from typically 5-20 ppb in the morning to an early afternoon peak of 60-120 ppb (Putero et al., 2015; Bhardwaj et al., 2018).

These high O_3 levels have deleterious effects on human health and ecosystems, including agro-ecosystems in the Kathmandu Valley and surrounding regions, thus justifying mitigation measures to help reduce the levels of O_3 (its precursors VOCs and NOx), CO and other pollutants. Determining the most effective mitigation measures will be challenging due to the complicated interplay of pollution and meteorology as well as local and regional pollution sources. This study has provided information on current ambient levels and the diurnal/seasonal variations. This will be helpful in the design of future policies, both as a baseline for evaluating the effectiveness of mitigation measures, as well as giving insight into the connections between various pollutant sources (e.g., brick kilns) and their impacts on seasonally elevated CO levels, especially at nighttime. One particular contribution has been the development of a top-down estimate of the total emission flux of CO at Bode, which was found to be 4.9 µg m^{-2} s^{-1}. This is several times higher (by a factor of 2-14 times) than the CO emission fluxes for the Kathmandu Valley in state-of-the-art inventories such as EDGAR-HTAP, REAS, and INTEX-B. This points out the need for the development of updated comprehensive emission inventory databases for this region. The improved emission inventory is necessary to provide more accurate input to model simulations to assess air pollution processes and mitigation options for the Kathmandu Valley and the broader surrounding region.

While the high levels of particulate pollution in the Kathmandu Valley have caught the main attention of the public and policymakers, due to their immediately visible nature, our paper points out that ozone is also a serious problem here. In fact, its higher levels on the nearby mountaintop location of Nagarkot, which is much more representative of regional air pollution, point to an ozone problem in the wider foothills of the Himalayas. In fact, the extent of ozone pollution in the large surrounding Himalayan foothills has been insufficiently recognized until our study. This needs monitoring and research to identify feasible mitigation options.

Chapter 4

An Overview on the Airborne Measurement in Nepal, - Part 1: Vertical Profile of Aerosol Size-Number, Spectral Absorption, and Meteorology

Abstract

The paper provides an overview of an airborne measurement campaign with a microlight aircraft, over the Pokhara Valley region, Nepal, a metropolitan region in the central Himalayan foothills. This is the first aerial measurements in the central Himalayan foothill region, one of the polluted but relatively poorly sampled regions of the world. Conducted in two phases (in May 2016 and December 2016-January 2017), the goal of the overall campaign was to quantify the vertical distribution of aerosols over a polluted mountain valley in the Himalayan foothills, as well as to investigate the extent of regional transport of emissions into the Himalayas. This paper summarizes results from first phase where test flights were conducted in May 2016 (pre-monsoon), with the objective of demonstrating the potential of airborne measurements in the region using a portable instrument package (size with housing case: 0.45 m x 0.25 m x 0.25 m, 15 kgs) onboard an ultralight aircraft (IKARUS-C42). A total of five sampling test flights were conducted (each lasting for 1-1.5 h) in the Pokhara Valley to characterize vertical profiles of aerosol properties such as aerosol number and size distribution (0.3-2 µm), total particle concentration (>14 nm), aerosol absorption (370-950 nm), black carbon (BC), and meteorological variables. Although some interesting observations were made during the test flight, the study is limited to a few days (and only a few hours of flight in total) and thus, the analysis presented may not represent the entire pollution-meteorology interaction found in the Pokhara Valley

The vertical profiles of aerosol species showed decreasing concentrations with altitude (815 to 4500 m asl.); steep concentration gradient below 2000 m (asl.) in the morning and mixed profiles (up to ca. 4000 m asl.) in the afternoon. The near-surface (<1000 m asl.) BC concentrations observed in the Pokhara Valley were much lower than pre-monsoon BC concentrations in the Kathmandu Valley, and similar in range to Indo-Gangetic Plain (IGP) sites such as Kanpur in India. The sampling test flight also detected an elevated polluted

aerosol layer (around 3000 m asl.) over the Pokhara Valley, which could be associated with the regional transport. The total aerosol and black carbon concentration in the polluted layer was comparable with the near-surface values (<1000 m asl.). The elevated polluted layer was also characterized by high aerosol extinction coefficient (at 550 nm) and was identified as smoke and a polluted dust layer. The observed shift in the westerlies (at 20-30° N) entering Nepal during the test flight period could be an important factor for the presence of elevated polluted layers in the Pokhara Valley.

4.1 Introduction

The Himalayas and surrounding regions are one of the unique ecosystems in the world, with a great variety in the geography and socio-economics, and a notable significance in the context of regional and global environmental change. Areas in the foothills of the Himalayas still constitute large regions of rural populations along with pockets of rapidly growing cities. Consequently, there is a complex interaction among changing emission sources and their interaction with regional and global climate change. Among emitted air pollutants, the chemical and physical properties of aerosols have been linked to significant burdens of disease, to melting of glaciers, to crop loses, to hydrological changes and to cloud properties (Bollasina et al., 2011; Vinoj et al., 2014; Lau, 2014; Burney and Ramanathan, 2014; Brauer et al., 2012; Cong et al., 2015; Li et al., 2016).

Sources of aerosols in the Himalayas and the nearby Indo-Gangetic Plain (IGP) typically vary between urban, peri-urban and rural locations; fossil fuel and industrial emissions such as vehicles, brick kilns, waste burning, cement factories etc., are typically urban and peri-urban; biomass cookstove, agriculture and waste burning and forest fires are often linked to emissions from rural areas (Guttikunda et al., 2014; Venkataraman et al., 2006; Stone et al., 2010). Secondary chemical pathways also contribute to the aerosols in the ultrafine and accumulation-mode range via particle formation events (Venzac et al., 2008; Neitola et al., 2011).

Aerosol properties in the Himalayas have large spatial and temporal variations, especially in the pre-monsoon and monsoon season. These observed variations are influenced by emission sources, regional meteorology, and geography (Dey and Di Girolamo, 2010). The influence of aerosol particles on local and regional weather during these adjacent seasons has significant implications for timing, intensity and spatial distribution of the summer monsoon in the region (Bollasina et al., 2011; Ramanathan et al., 2001). Studies describing the aerosol-meteorology interaction are often missing in the Himalayan region partly due to lack of surface and airborne

measurements of aerosol properties along with meteorology. Most past campaign-mode measurements in the Himalayan regions, to our knowledge, have been ground measurements, which have aided in evaluating aerosol properties, and their transformation and transport mechanisms (Shrestha et al., 2013; Shrestha et al., 2010; Ramana et al., 2004; Marcq et al., 2010; Panday and Prinn, 2009; Cho et al., 2017). Long-term continuous measurements of aerosols and meteorology are limited to a few stations in the High Himalayas, such as the recently discontinued Nepal Climate Observatory at Pyramid (NCO-P, 27.95° N, 86.81° E, 5050 m asl.), a high-altitude observatory located near basecamp of Mt. Everest. Columnar and satellite measurements such as AERONET and CALIPSO have provided a regional overview of aerosol type and vertical distribution, as well as estimation of the aerosol heating rate in the atmospheric column (Kuhlmann and Quaas, 2010; Gautam et al., 2011; Pandey et al., 2017). However, these measurement techniques often suffer from large uncertainty and biases while retrieving the complex nature of the aerosols observed in the region (Jai Devi et al., 2011).

Regional meteorology in the 850-500 mb range plays an important role in the transformation and transport of aerosols from Western Asia to the IGP, the Himalayan foothills, the Himalayan and Tibetan Plateau region (Decesari et al., 2010; Marinoni et al., 2013; Lüthi et al., 2015). At these altitudes, synoptic- scale air masses are mostly westerly/northwesterly during the pre-monsoon and southwesterly/easterly during the monsoon. These air masses are often linked to dust aerosol transport during the pre-monsoon season from Western Asia into the Himalayas, including populated mountain valley such as Kathmandu and Pokhara Valley in Nepal. The transported dust aerosol also mixes with the primary emission (or anthropogenic aerosols) in the IGP and accumulates from northern to eastern IGP along the Himalayan foothills (Gautam et al., 2009b; Gautam et al., 2011). The total aerosol loading is often the highest during the pre-monsoon season in the IGP (Gautam et al., 2009a; Raatikainen et al., 2014), intensified further by weak surface/zonal winds and numerous open biomass burning and forest fires events (Kaskaoutis et al., 2012). The polluted aerosol layer in the IGP is advected into the Himalayas by synoptic-scale westerlies (~500 mb) and also by the valley wind circulation within or along the planetary boundary layer (PBL) (Lüthi et al., 2015). The advection is also facilitated by the strong updraft and PBL expansion (the highest in the pre-monsoon in the IGP) often mixing with the synoptic-scale westerlies (Raatikainen et al., 2014). Because of strong convective activity in the IGP, the polluted air masses near the surface are often lifted up to 5-7 km or higher (Kuhlmann and Quaas, 2010). In addition to the synoptic-scale transport, thermally-driven valley winds also enable the transport of humid and polluted air mass (with enhanced

absorbing fraction) from IGP into the Himalayan foothills, and further up into the mountain valleys and elevated locations (Raatikainen et al., 2014; Lüthi et al., 2015; Gogoi et al., 2014; Putero et al., 2014; Decesari et al., 2010; Marcq et al., 2010). Strongly coupled with the expansion of the PBL in the IGP, the upslope movement of polluted air masses into the foothills and further east is characterized by late afternoon peaks in aerosol optical depth (AOD) in many measurement sites along the Himalayan range such as Hanle Valley (Ladakh, India), Mukteswar and Manora site (Nainital, India), Hetauda (Nepal), Langtang Valley (Nepal), Dhulikhel (Nepal), Kathmandu Valley (Nepal) and NCO-P (Nepal). The temporal and spatial extent of this observed "ventilation" at multiple locations could be indicative of a regional-scale transport than mesoscale (Gogoi et al., 2014; Raatikainen et al., 2014; Gautam et al., 2011; Putero et al., 2015; Marcq et al., 2010).

To date, there have been no observations of vertical distributions of aerosol and gaseous species carried out in the Himalayan region. Therefore, the airborne measurement campaign was designed to address two major questions: (i) what is the variation in the aerosol properties, notably the vertical distributions, over a polluted mountain valley, and (ii) what is the quantitative extent of regional transport of aerosols in the higher Himalayas? The campaign was carried out in two phases in the Pokhara Valley and surrounding areas in Nepal. In the first phase, test flights were conducted in May 2016 and in the second phase, intensive sampling flights were carried out in December 2016-January 2017. This paper provides an overview of the measurement campaign and results from the test flights in May 2016 which include snapshots of vertical profiles of aerosol size, number, and composition, along with meteorological parameters. The airborne measurements presented in this paper are supplemented with observations of local and regional meteorology, as well as satellite and ground-based column-integrated aerosol microphysics and radiative properties (see section 4.3.1.1 and 4.3.1.2, also Supplementary B.7). A companion paper will follow with more detailed observations and results based on the intensive measurements carried out during December 2016-January 2017.

4.2 Ultralight measurements in Nepal

4.2.1 Details of the airborne measurement unit

A single-engine two-seater microlight aircraft (IKARUS C-42, COMCO IKARUS, Germany) was used as the aerial platform. The technical specification of the aircraft includes approximately 4 h of flying time, a short take-off run, an additional payload of up to 50 kg, and

it is suitable for small spiral movement in the air. The aircraft has a cruising speed of 165 kmh^{-1}, and a 5-6 ms^{-1} rate of climb which makes it an appropriate aerial vehicle to perform measurements at altitudes within the PBL and as close as 50 m above ground level. More detail about the aircraft is available here (http://www.comco-ikarus.de/Pages/c42a-technik.php?lang=en Last access: 8 September 2017). Its size, speed, and maneuverability offered a decent climb to the free troposphere to capture vertical profiles in the rough terrains of Nepal. The aircraft used for the study is operated by the Pokhara Ultralight Company for recreational flights around the Pokhara Valley.

Table 4.1. Instrument package deployed in the microlight aircraft

Parameters	Instruments	Method	Sampling time resolution
Aerosol particle number size distribution (0.3–20 µm)	GRIMM OPS 1.108	Light scattering	6 s
Total particle number concentration (> 14 nm)	TSI CPC 3760	Condensation/light scattering	1 s
Aerosol spectral absorption	Magee AE42	Seven wavelengths, light attenuation	2 min
Dew point sensor	METEOLABOR, TPS3	Chilled mirror	1 Hz
Temperature	Thermocouple	–	1 Hz
Data acquisition system	PC 104 + GPS	–	–
Power supply	Aircraft battery pack, $LiFEPO_4$ battery	12 V, > 15 AH	

The instrument package was specifically designed and tested for aerial measurements (Junkermann, 2001). Table 4.1 describes each instrument and the integration performed to prepare the package for the aerial deployment. The instrument package consists of a GRIMM OPS (optical particle spectrometer) model 1.108 for particle size distributions (0.3 to 20 µm, 16 size bins) with sampling frequency of 6 s, and a TSI condensation particle counter (CPC) 3760 for total particle concentration (>14 nm) at 1 s resolution (See Figure B.1 in the supplement). The package also included a Magee Scientific aethalometer (AE42) for aerosol absorption at seven different wavelengths (370 -950 nm). The instruments were reduced in weight for use on the aircraft. The CPC was operated with a constant mass flow and an internal direct current (DC) pump instead of the original flow regulation by a critical orifice. Meteorological parameters including temperature and dew point were sampled at a rate of 1 s using METEOLABOR (TPS3). All the sensors were connected to a modular computer (PC104) for data acquisition. The PC104 is also equipped with a Global Positioning System (GPS), and multiple serial and analog connectors. For inflight instrument checks and quick online overview of the atmospheric conditions, a small liquid crystal display (LCD) was also

connected to the PC104 and placed in the cockpit areas for the flight crew. This display showed real-time aerosol number concentrations and meteorological parameters.

The instrument package weighs approximately 15 kg and consumes <60 W, well within the power supply range of the aircraft battery. It is housed in an aluminum box (0.45 m x0.25 mx0.25 m) and can be easily integrated with a mobile platform such as the IKARUS (See Figure B.1). In IKARUS, the instrument was placed in the rear section behind the seats which is otherwise almost empty or used for cargo, and only contains the fuel tank and supporting aluminum bars. The sample inlet line (internal diameter of 0.004 m or ~4.0 mm ID brass tubing) ran along the wingspan and was approximately 1.8 m (in length, sampling tube) from the cockpit. Once the sample line is inside the aircraft, it is distributed to all the aerosol instruments using a simple metal flow splitter (0.006 m ID). No external pump was used to pull the aerosol into the sampling line, the total flow (~ 3.0 L min^{-1}) in the sampling line (before the split) was due to the internal pump of all the instruments. The sample inlet positioning at the end of the wingspan also minimizes the influence of the aircraft propeller, located in the front of the cockpit.

4.2.2 Site description

Pokhara Valley is Nepal's second largest populated valley (pop. >250,000) after the Kathmandu Valley (CBS, 2011). The valley is approximately at 815 m asl. ~150 km west of the Kathmandu Valley, and ~90 km northeast of the southern plains (~100 m asl.) bordering IGP. The valley is surrounded by mountains which are approximately 1000-2000 m asl. Further north of the Pokhara Valley, within 30 km the elevation gradient increases rapidly to over 7000 m asl. or higher (see Figure 4.1). This steep elevation gradient is conducive for the orographic lift of humid air masses, and thus the valley also receives one of the highest rates of precipitation in Nepal and occasional strong convective updrafts leading to hailstorms and thunderstorms (Aryal et al., 2015). The mixing of dry westerly air masses with heated moist air masses from the Bay of Bengal produces strong convection over the Pokhara Valley, and thus results in strong updrafts. These strong convective activities are frequent in the pre-monsoon and monsoon season but do not occur during the winter season.

4.2.3 Test flight patterns over the Pokhara Valley

Five test flights were conducted in the morning and evening period around Pokhara Valley (83.97° E, 28.19° N, 815 m asl.) with each flight lasting for about 1 to 1.5 h from 5-7 May

2016. The flight pattern was consistently flown over the northwest part of the valley (Figure 1). A typical flight commenced from the Pokhara Regional Airport (818 m asl.) and steadily flew 5-10 km northwest along the Pokhara Valley leaving the direct airport vicinity toward the Himalayas. This was followed by spirals up and down sampling from approximately 1000 to 4000 m, often reaching close to the lower base of the clouds in the free troposphere. Further climbs into the cloud layer were avoided during the test flights.

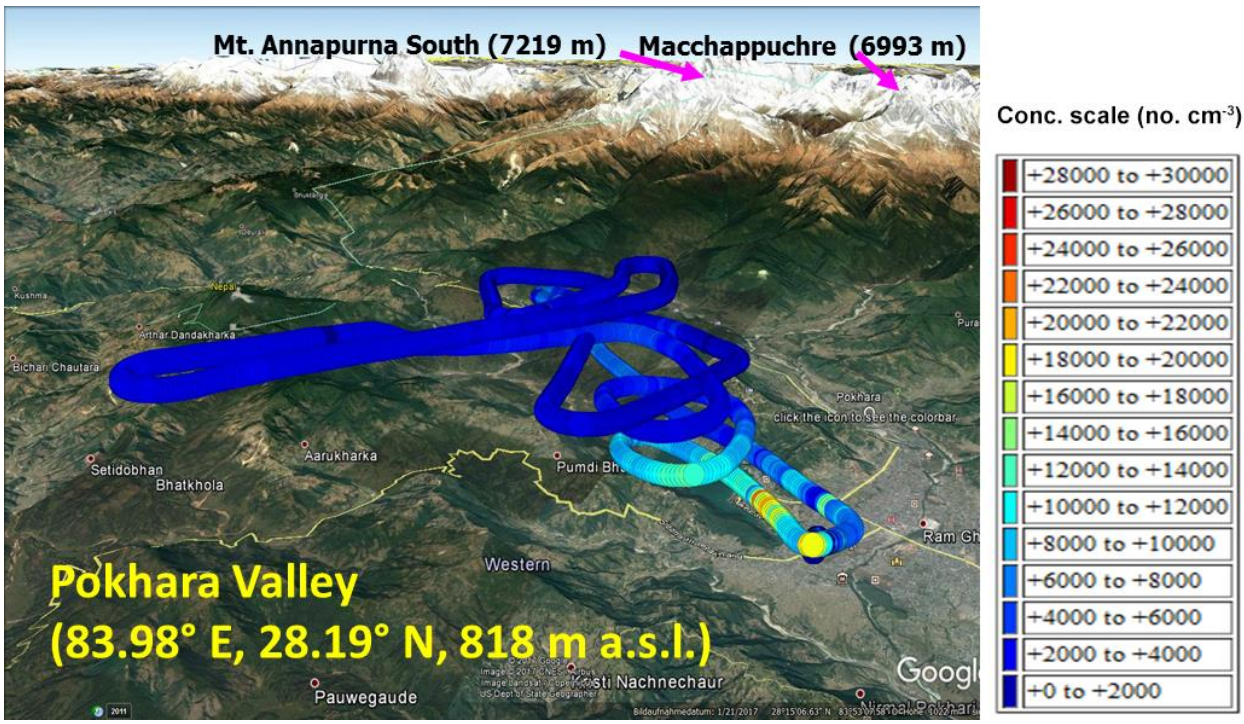

Figure 4.1. A typical test flight within the Pokhara Valley on 5 May 2016. The plot is generated using a Matlab-Google Earth toolbox (https://www.mathworks.com/matlabcentral/fileexchange/12954-google-earth-toolbox, last access: 3 March 2017, ©Scott L. Davis). Each dot is a single sample point (sampling frequency of 1Hz); the color of the dot indicates the total aerosol number concentration and the value of each color is shown as a color bar.

4.2.4 Data processing and quality

The data from all the instruments were synced with the GPS clock, and the PC104 received all the data simultaneously and created a common time-stamped data file. Prior to each test flight, a zero test was conducted to identify any possible leaks in the sample line.

The collected data from the five test flights went through multiple steps of quality control and quality assurance. Occasionally during the radio communication by the pilot with the ground station or air traffic controller, the CPC and the temperature sensor would record exceedingly

high values. This noise is an interference picked up by the sensors from the 5 W radio transmission. The CPC and aethalometer is also sensitive to vibration in the aircraft, especially during upward and downward spiral motion, which may result in flow imbalance in these analyzers. This resulted in random noise segments for a few seconds in the data, which were flagged and not included in the analysis.

4.3 Results

4.3.1 General meteorology and air quality, aerosol properties in the Pokhara Valley

4.3.1.1 Local and synoptic meteorology in the Pokhara Valley

Climatologically, Pokhara Valley has a humid subtropical climate, characterized by a summer monsoon season from late June to September, preceded by a dry pre-monsoon (March-May, see Figure B.2 in the supplement). Dominant winds in the valley are from the southeast and southwest with a strong diurnal variability in the wind speed (Aryal et al., 2015). On a local/regional scale, the winds in May 2016 were predominantly from the southeast with only occasional strong winds from the southwest (see Figure B.3 in the supplement, using data available at the regional meteorological station at the Pokhara Airport). During the test flight period (5-7 May 2016), the wind was similar in directionality, with an hourly mean wind speed of 1.8 to 3.0 ms^{-1}, with low wind speed (<2.0 ms^{-1}) before noon, usually from the southeast, followed by stronger winds from the southwest and northwest (>2.4 ms^{-1}) which can continue until late night. The increased wind speed in the afternoon could be katabatic in nature as a result of differential heating of the mountain valley slopes and could be linked to pollution transport from surrounding regions (Gautam et al., 2011).

Three dominant synoptic meteorology regimes characterize the seasonality of South Asia (Lawrence and Lelieveld, 2010). They are summer (June-September), the winter monsoon (mid-November to February) and monsoon-transition periods, which include the pre-monsoon season (March-May) and post-monsoon season (mid-September to mid-November). These synoptic regimes are also active in the Himalayas, including the Pokhara Valley. The monsoon transition period, during which the test flights were conducted, is characterized by westerlies over 20-30° N at 850 mb and above (see Figure 4.2). Figure 4.2 shows the daily wind vector over South Asia for 3, 5, 6 and 7 May 2016 generated using the NCEP NCAR Reanalysis data at 2.5°x 2.5° horizontal resolution. While the reanalysis data can be expected to represent the synoptic-scale phenomena in this region reasonably well, the rough terrain in the Himalayas

presents a significant challenge for modeling and the data is thus likely to suffer from biases and other deviations from the observed meteorology (Xie et al., 2007).

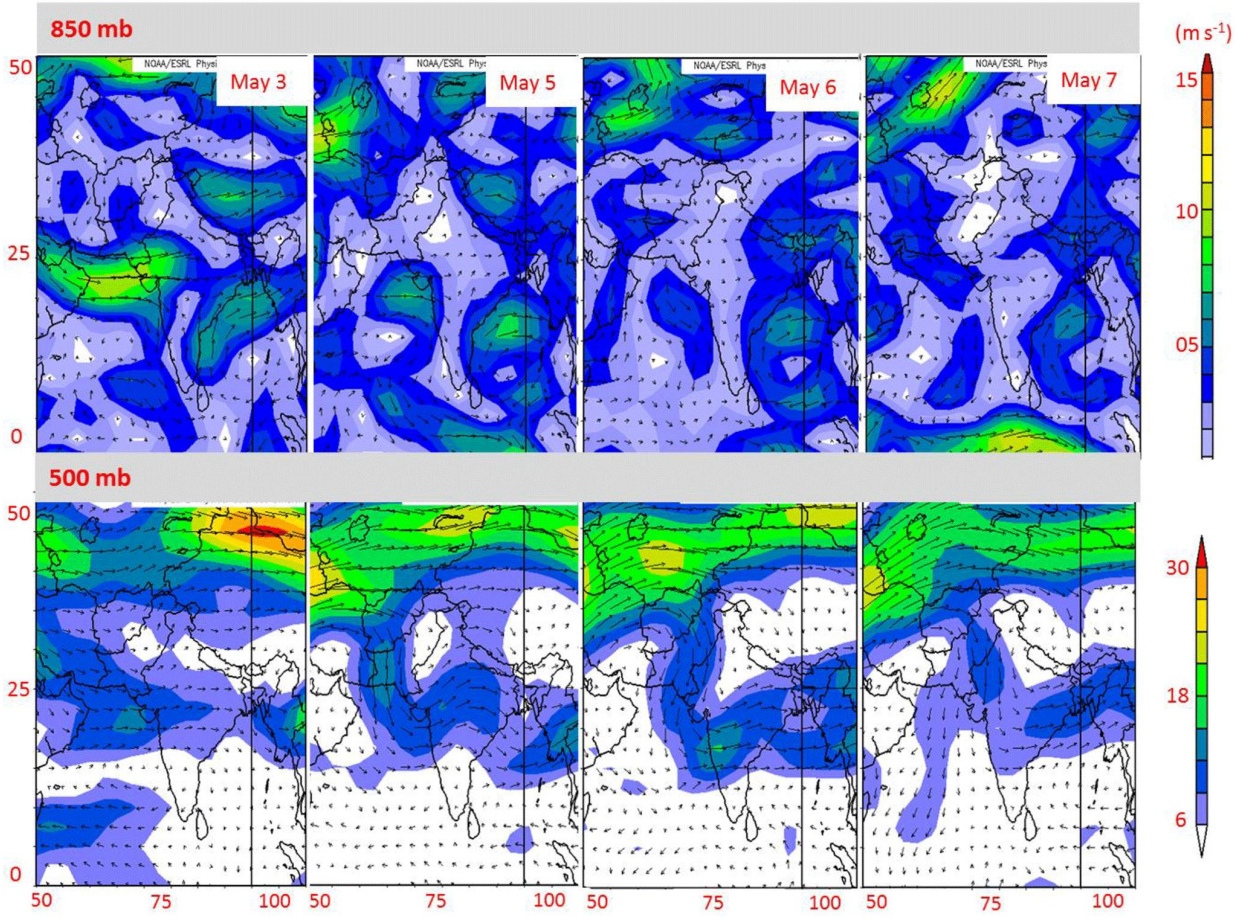

Figure 4.2. Daily wind vector data at 850 and 500 mb, plotted using the NCEP NCAR reanalysis (2.5° x 2.5°) data over South Asia from 1-7 May 2016. The colors indicate the wind speed in ms^{-1}. The plots were generated using the default setup at www.esrl.noaa.gov/psd/data/composites/day/, last access: 4 May 2017).

The wind vector at 850 mb in the 20-30° N latitude band was westerly with variable wind speeds in the IGP region near the Himalayan foothills. The wind direction varies diurnally at the 850 mb level, with the wind direction shifting to southwesterly near the Himalayan foothills. Westerlies were also generally prevalent at the 500 mb; however, in the mid-latitudes between 40-50° N (Central Asia), a trough and crest-like feature of the westerlies moving from west to east Asia is visible (also observed by Lüthi et al., 2015), which was also present prior to the study period. This wind feature was colder and more humid (see Figure B.4 in the supplementary material) than the westerlies observed between 20-30° N. The meandering features (i.e., trough and crest) observed between 40-50° N affects the direction and magnitude of air masses (at 20-30° N) entering Nepal. For instance, the crest feature of the westerly was

prevalent over the IGP and Nepal prior to 3 May, transitions into the trough feature after the 3rd and continues during the study period. The prevalence of the trough was characterized by the intrusion of wind into lower latitudes as well as into the IGP, also indicated by the change in the temperature and humidity (Figure B.4). The intrusions of mid-latitude air masses also influence the westerlies entering Nepal in the 20-30° N sector (Lüthi et al., 2015). As discussed later, variations in the vertical profiles of aerosols above 3000 m a.s.l. could be associated with variations observed in these upper layer winds.

4.3.1.2 Overview of the aerosol properties in the Pokhara Valley during the test flight period

The variation in aerosol loading (as reflected by AOD) reveals a strong seasonality in the Pokhara Valley (see supplementary figure B.7 for a detailed description of aerosol properties in the Pokhara Valley during 2010-2016). The pre-monsoon season (also the time of the test flight) has the highest AOD values (AOD_{500nm}>0.6: Figs. B.7a, b, and B.5) followed by the monsoon low (AOD_{500nm} ~0.2-0.3), most likely due to the wet removal of aerosols.

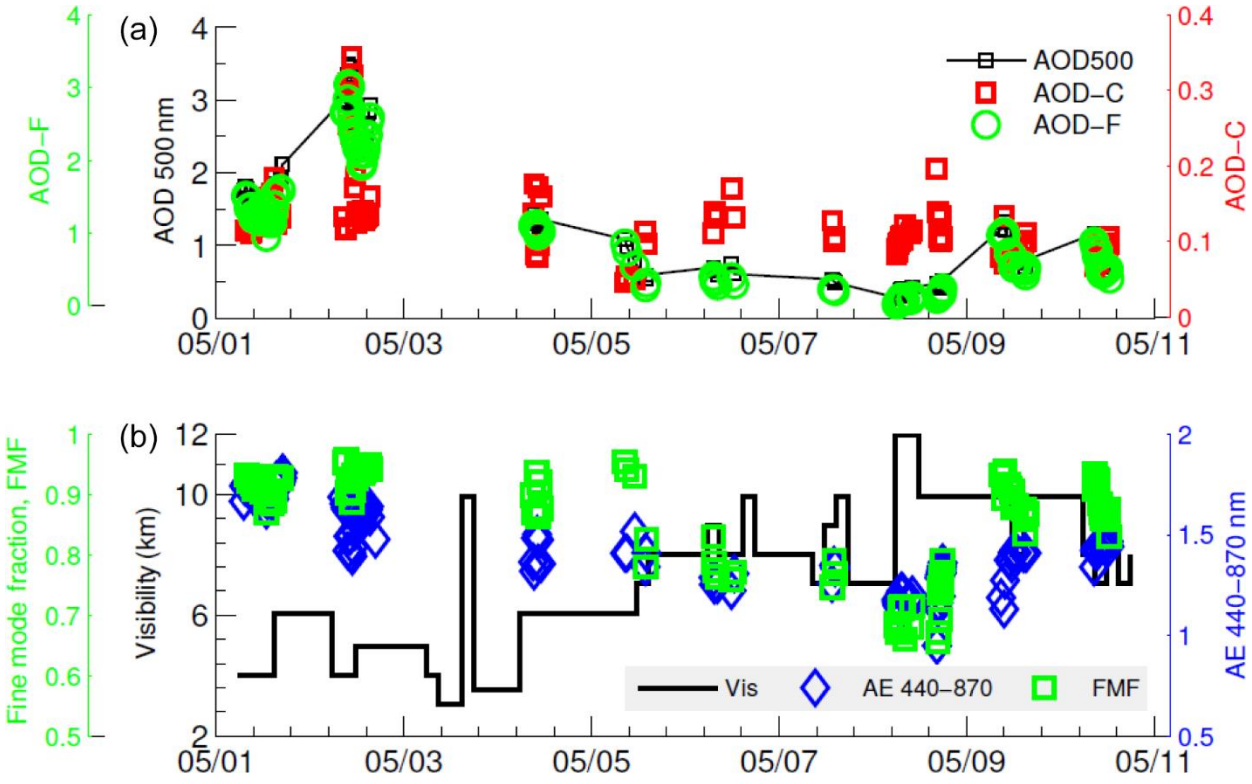

Figure 4.3. AOD and other data products from the Level1.5 AERONET direct product in the Pokhara Valley from 1-10 May 2016. The top panel includes AOD at 500nm and the AOD for coarse and fine modes (as shown in figure above as AOD-C, AOD-F). The bottom panel includes the Ångström Exponent (AE) for 440-870nm, the fine mode fraction and the visibility

(km). The visibility data was available from the synoptic meteorology data available at http://www7.ncdc.noaa.gov/CDO/cdo, last access: 3 July 2018).

AOD gradually increased (to ~0.4-0.5) during the post-monsoon through winter to the pre-monsoon season. Generally, the increase of total AOD (sum of fine and coarse) over the Pokhara Valley is dominated by fine-mode aerosol particles, except during the pre-monsoon and monsoon season, when a substantial fraction of coarse-mode particles was also present. The dominant aerosol in the Pokhara Valley is mostly *BC–like* (Giles et al., 2012), based on the values of absorption and extinction Ångstrom exponent (AAE and EAE at 440-870 nm); however, a substantial seasonal variation was observed from more mixed or dust-like in the pre-monsoon months, to more BC-like in the post-monsoon and winter months.

The aerosol optical properties (columnar) and synoptic meteorology are shown in Figure 4.3 and Figure B.6 (in the supplementary). Prior to the flights days (1-4 May), higher AOD values were recorded in the Pokhara Valley (AOD>1) and dominated by a fine-mode fraction (~0.95). Hazy condition and low visibility (≤5 km) was recorded during the period in the valley (see Figure B.6). Moving into the flight days, the AOD values decreased below 1, markedly by the drop in the fine-mode fraction and the improvement in haze condition and visibility.

The flight day periods were also characterized by the presence of scattered clouds and thunderstorms (with no precipitation) in the afternoon, which also imply conditions for the strong vertical mixing of pollutants. It is indicative from Figure 4.3 and Figure B.7 that the presence of high levels of pollution over the region from 1-4 May is followed by a short period of (relatively) cleaner conditions, which also coincides with the changes in the synoptic situation observed in the winds at 500 mb (described in section 4.3.1.1.)

4.3.2 Vertical profiles of absorbing aerosols, particle number and size distribution, temperature, and dew point

The five test flights are labeled as F1-5 in Figure 4.4, except F3 which is shown in the supplement (Fig. B.10). F1 and F2 were conducted on 5 May, F3 and F4 on 6 May and F5 on 7 May 2016. Due to limitations of the flight permit, the test flights were conducted remaining within the Pokhara Valley as indicated by Figure 4.1. Among the five sampling flights, F1, F3, and F5 were morning flights, and F2 and F4 were afternoon flights (for details on sampling flights, see Table T.1 in the supplement).

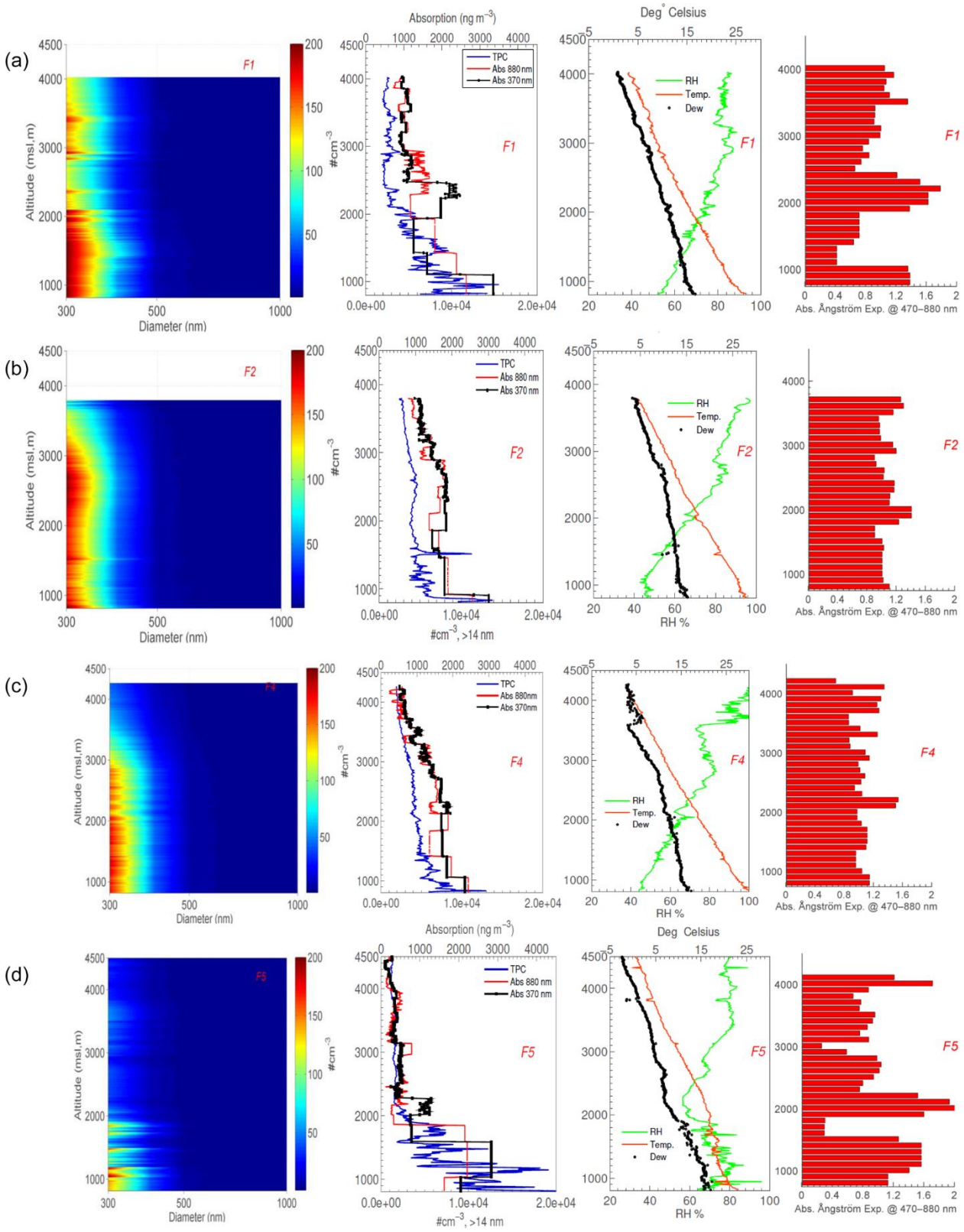

Figure 4.4. Vertical profiles of aerosol species and meteorological parameters during the 5-7 May 2016 test flights in the Pokhara Valley using the IKARUS microlight aircraft. The subplot in each row is arranged by (i) size distribution measured by the GRIMM OPS 1.108 (0.3-20 µm), limited to 1 µm in the figure, (ii) Total particle number concentration (also indicated as TPC, Dp > 14 nm) measured by the CPC 3760, along with absorbing aerosol mass density at

370 nm and 880 nm (iii) temperature (red line, in °C) and dew point (black dots, in °C) and relative humidity (or RH %), (iv) calculated absorption Ångstrom exponent averaged for every 500 meters elevation band. For the size distribution plot, the x-axis represents the optical diameter of the aerosol (nm), and the color bar represents the concentration (10^x in #cm^{-3}). Of the five test flights, only F1-2, F4-5 is shown here (**a-d**), F3 is in the supplementary. Number size distribution data from Flight F3 is not available due to the failure of the Grimm's pump during flight initiation. In each subplot, the y-axis is the altitude above the mean sea level (in m). The origin of the y-axis is at 815 m asl.

4.3.3 Diurnal variation in the vertical profiles

All the vertical aerosol profiles (Figure 4.3) showed a strong gradient below 2000 m (asl.). Because of the valley geography, with surrounding mountains of about ~2000 m (asl.) or higher, it is likely that the gradient observed below 2000 m (asl.) could be related to emissions from the Pokhara Valley. The development (or dissolution) of the boundary layer during the day clearly influenced the evolution of the aerosol vertical profiles in the Pokhara Valley. The shallow boundary layer in the night, which continued till the morning, led to the accumulation of aerosols below 2000 m (asl.) in the morning (see the morning flights (F1, F3, and F5) and a strong decrease with altitude was observed. For instance, in the morning profiles, the concentrations near the surface (<1000 m asl.) for total particle number concentrations (also indicated as TPC in Figure 4) were mostly $>10^3$ cm^{-3}, but could reach ~ $3x10^4$ cm^{-3} or higher (see F5 in Figure 4.4), which is attributed to the coupling of the shallow boundary layer and the emissions in the contained valley topography (Mues et al., 2017). Also, all the measured aerosol parameters (number size distribution for particles with diameters between 0.3 and 0.5 µm), the total particle concentration (>14 nm), and the absorption) vary similarly as a function of the altitude irrespective of the timing of the profiles. The similarity in the vertical concentration gradients of the absorbing aerosol mass concentrations and the aerosol number concentration above 2000 m asl. provides evidence of similar emission sources or origins.

Within the morning profiles, substantial variations were observed; in F1 (5 May), in addition to the strong gradient below 2000 m asl., there is a polluted layer above 3000 m asl. which is not evident in F5. The BC concentration was close to 1 $µgm^{-3}$ up to 4000 m asl. for F1 and stayed in that range until F5, where it dropped to about ~0.4 $µgm^{-3}$. The temperature and humidity profile also showed changes between the morning flights; the conditions during F1 are warmer (throughout the profile) and dryer (near the surface), compared to F5. This observed variation in the aerosol vertical profile (including the meteorology) may be indicative of cleaner atmospheric conditions (in terms of aerosol number and absorption) from 5 May to 7 May and could be associated with the arrival of colder airmasses in the Pokhara Valley. The

near-surface BC concentrations measured in this study were much lower than surface BC concentrations measured in the pre-monsoon season (2013) in the Kathmandu Valley in the Himalayan foothills (hourly average: ~5-40 μgm^{-3}, Mues et al. (2017)), but comparable to winter measurements (2004) in Kanpur in the IGP (1-3 min average: ~1-7 μgm^{-3}, Tripathi et al. (2005)). In Kanpur, Tripathi et al. (2005) observed BC concentrations close to 1 μgm^{-3} up to 2000 m asl. and a sharp gradient below 400 m asl., most likely due to a shallow boundary layer in winter.

The elevated polluted air mass in F1 could be an indication of transport related to the mountain valley winds and/or synoptic transport related to the westerlies, common during this season (Gautam et al., 2011; Raatikainen et al., 2014; Marcq et al., 2010). Pre-monsoon airborne measurements over the IGP and near the Himalayan foothills during CALIPEX-2009 found a polluted aerosol layer (2-4x10^3 cm^{-3} with a mean size of 0.13 µm diameter) below 4 km asl., attributed to biomass burning observed during this particular season (Padmakumari et al., 2013).

The afternoon profiles (F2: 5 May 2016 and F4: 6 May 2016) in contrast to the corresponding morning profile (F1 and F3) showed a more relatively mixed profile up to about 2500-3000 m, decreased then up to the maximum sampled altitude of just above 4000 m asl. For instance, the concentrations of measured aerosol parameters up to 3000 m asl. were comparable to the concentrations observed at ~1000 m asl. Slight differences exist within the afternoon profiles, which may be related to local meteorology (boundary layer evolution) and mountain valley wind circulation in the afternoon. Cloud layers were present during the afternoon flights at and above 4000 m asl. in F4 (also indicated by the sharp rise in RH from ca. 3600 m asl.), which may have led to the scavenging of the aerosol by cloud droplets and thus explaining the observed decrease in the measured aerosol parameters.

4.3.4 Nature of absorbing aerosols in the Pokhara Valley

The absorption at multiple wavelengths was used to calculate the absorption Ångstrom exponent (AAE), shown in the right-most subplot in each row of Figure 4.4. The AAE characterizes the wavelength (λ) dependence of absorption coefficient (absorption coefficient or abs. coeff = $K\lambda^{-AAE}$, Russell et al. (2010); Giles et al. (2012)). On a logarithmic scale, the above power relation between (Absorption coefficient and wavelength) is approximately a straight line (see supplementary S11 for an example case where both power and logarithmic form are plotted). The slope of the straight line is AAE. In our case, all the absorption

coefficient measured between the 470 and 880 nm wavelength was used for the calculation of AAE. The mass absorption coefficients (MAC) of 14.5 and 7.77 $m^2 g^{-1}$, as prescribed by the manufacturer of the aethalometer (Hansen et al., 1984) for wavelength 470 nm and 880 nm, respectively were used to calculate the absorption coefficient (the unit for the absorption coefficient is m^{-1}).

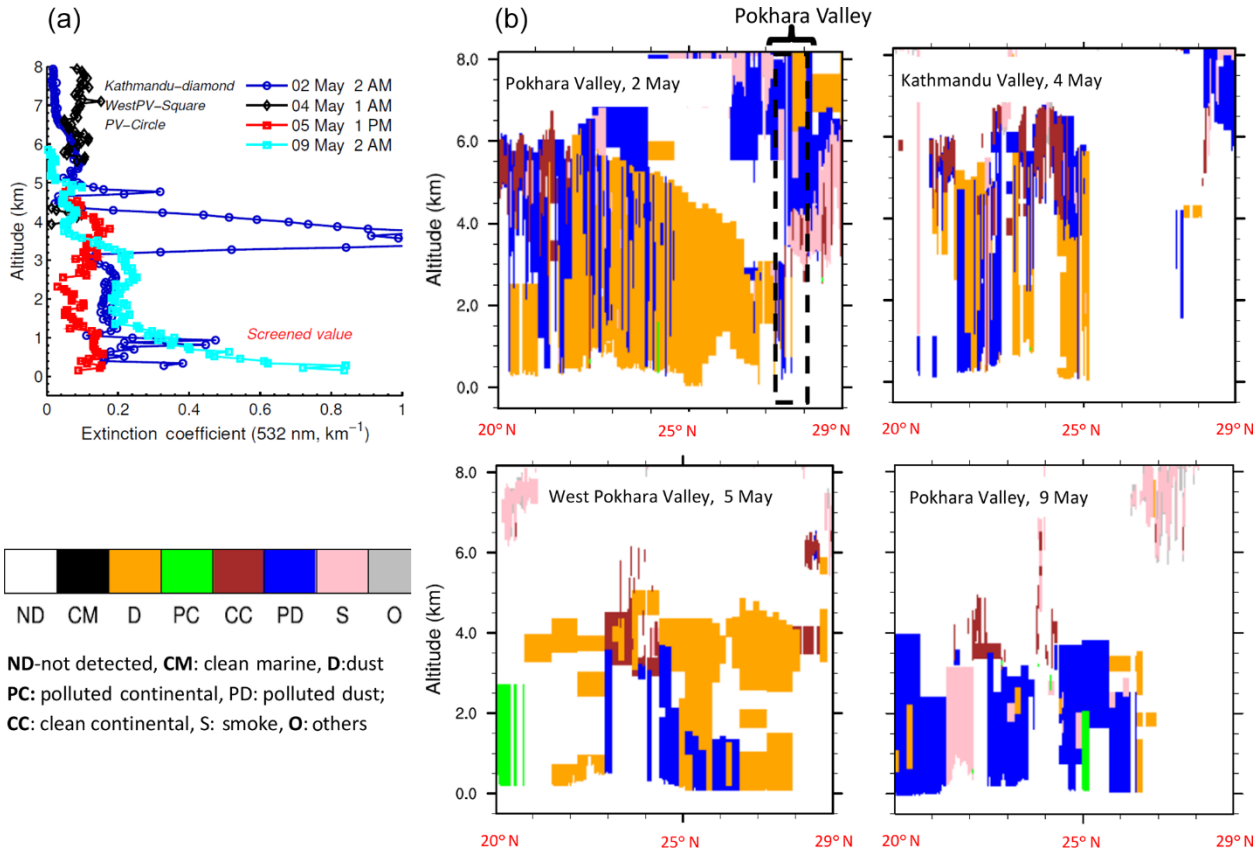

Figure 4.5. Aerosol extinction coefficient (at 532 nm) vertical profile (left) and aerosol type classification based on the CALIPSO level 2 retrieval (right). Only the CALIPSO overpass over the Pokhara Valley or nearby locations (such as Kathmandu Valley region, and the region to the west of Pokhara Valley) is included. The extinction profile is averaged for the region 27-28.5° N latitude, which also includes the Pokhara Valley.

The calculated AAE was averaged for each 100 m (a.s.l.), as shown in the figure. The sampling resolution for the aethalometer is 2 min (see Table 1), which resulted in no (in a few cases) or few data (after flagging) if smaller height bins were chosen. The AAE profile differed markedly between the morning (F1, F3, and F5) and afternoon (F2 and F4) profiles, with morning profiles showed large variations along the height. Surface AAE (~1000 m a.s.l.) was close to 0.8 to 1.2 for all the flights which indicate the presence of BC from a mix of sources (biomass burning and fossil fuel combustion. A source-diagnostic analysis of C-isotopes of elemental carbon

(EC) in TSP (total suspended particulates) collected in Pokhara during April 2013-March 2014 showed that the biomass burning and fossil fuel combustion contributes nearly 50 % each to the (annual average) EC concentration (Li et al., 2016). The AAE values above surface (>1000 m a.s.l.) varied from 0.5 to 2, but mostly fell into the range of 0.9- 1.2, which is typically reported for mixed to *BC like* aerosols from urban and industrial emissions (Russell et al., 2010; Yang et al., 2009; Dumka et al., 2014). AAE<1 could also be indicative of a composite aerosol, where a BC aerosol (or "core") is coated with absorbing or non-absorbing aerosols (Gyawali et al., 2009).

4.3.5 Comparison of the satellite-derived vertical profiles with measurements

The measured vertical profiles were also complemented with CALIPSO retrievals over the Pokhara Valley (Figure 4.5). Level 2 (version 4), cloud and quality screened data were used to generate the vertically resolved extinction (at 532 nm) and aerosol classification. The CALIPSO satellite had only three overpasses over the Pokhara Valley between 1 and 10 May 2016 (the extinction profile lines with circle markers are for the Pokhara Valley). Therefore, the satellite overpasses through nearby regions such as the Kathmandu Valley region to the east and the region to the west of the Pokhara Valley (denoted by *WestPV* in Figure 4.5) were also considered.

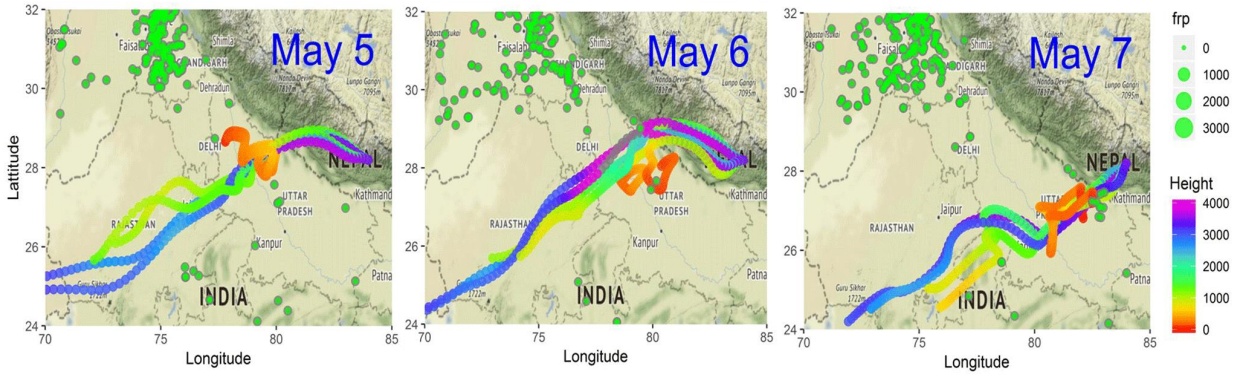

Figure 4.6. HYSPLIT (Hybrid Single Particle Lagrangian Integrated Trajectory, Draxler and Hess (1998)) 3 day back trajectories of air masses arriving at 3 different heights (800 m, 1500 m and 2500 m) from above the ground level (AGL~ 815 m asl.) in the Pokhara Valley (28.19° N, 83.98° E) during 5-7 May 2016. NCEP GDAS (Global Data Assimilation System) Reanalysis data with 1°x1° horizontal resolution were used as the input meteorology. The trajectory data is overlayed with the active fire data (extracted from the MODIS collection 6 databases, available at https://firms2.modaps.eosdis.nasa.gov/active_fire, last access: 10 October 2018). Each green dot with a gray edge is an active fire, and the strength of the active fire is indicated by the "frp" value, which is the fire radiative power in megawatts.

The range of extinction values for the Pokhara Valley (0.15-0.25 km^{-1} especially around 2000-4000 m asl.) were similar to pre-monsoon values (0.15-3 km^{-1}) reported in Nainital (a hilly station located ~2000 m (asl.) in India, and 400 km west of the Pokhara Valley) and slightly less than Kanpur, a site in the IGP, about 400 km to the southwest of Pokhara (Dumka et al., 2014). A large extinction (>0.5 km^{-1}) was observed on 1 May 2016 over the Pokhara Valley at an altitude of 3-4 km (asl.) which can be attributed to smoke (biomass- related) and polluted dust (a mixture of dust and biomass smoke or urban pollution) as evident by the aerosol type classification. Aerosols over the IGP and in the proximity of the Himalayan foothills were mainly "Dust" on 1 May 2016. Although not conclusive, the 9 May aerosol type classification is markedly different from 1 May with the absence of dust in the IGP, and absence of polluted dust or smoke over the Pokhara Valley.

4.3.6 Role of synoptic circulation in modulating aerosol properties over the Pokhara Valley

The measured vertical profiles and available satellite data from MODIS (See Figure B.8) and CALIPSO suggest that the synoptic-scale circulations were changing during the study period. The changing synoptic circulation also influenced the transport of polluted air into the Pokhara Valley. The regional meteorology station in the Pokhara Valley reported hazy conditions till 5 May 2016(see Figure B.6) which disappeared from 6 May 2016 onwards followed by clear days with scattered clouds during the daytime and thunderstorms in the afternoon. The variation in the AOD, AOD-F and Fine Mode Fraction (FMF) from AERONET (only level 1.5 data were available, see Figure B.7) also showed that high turbidity in the atmospheric column, dominated by fine-mode aerosols before 5 May 2016 (AOD_{500nm}>2.0, FMF >0.9), which declined sharply after 5 May 2016. The variation in the horizontal visibility (or visual range) measured at the meteorology station in the Pokhara Valley further indicates that the intensity of pollution declined during the study period, especially starting on 5 May 2016.

Three day back trajectories (72 h) were generated using HYSPLIT (Hybrid Single Particle Lagrangian Integrated Trajectory) for air masses arriving in the Pokhara Valley at 800 m, 1,500 m and 2,500 m from above ground level (agl.) for the test flight period (see Figure 6). The NCEP GDAS reanalysis data with a 1°x1° horizontal resolution were used as the input meteorology for the trajectories. The majority of air masses (especially at 1500 and 2000 m agl.) were westerly. A high resolution (0.0625° horizontal) simulation of air mass trajectories during the pre-monsoon period over the Himalayas and Tibetan Plateau region by Lüthi et al.

(2015) also identified synoptic-scale transport (as westerly advection around 500 mb) and a convection-enabled polluted airmass from the IGP as a major mechanism of transport of air pollution in the Himalayas. Transport of air pollution by both mechanisms was coupled with the diurnal expansion of PBL height in the IGP where the trajectory height was similar to planetary boundary layer (PBL) height thus allowing mixing up of the polluted layer, also observed by Raatikainen et al. (2014) over Gual Pahari (IGP site) and Mukteswor (Himalayan foothill site).

During the study period, the direction of the trajectories varied as the air masses entered Nepal and eventually into the Pokhara Valley. On 5 and 6 May 2016, the air masses (at 1500 and 2000 m a gl.) were mostly northwesterly traversing through northern India and western Nepal before entering the Pokhara Valley. A shift in the trajectory direction from north westerly to south westerly was observed on 7 May 2016, where the trajectories were moving through central India and the southern foothills into the Pokhara Valley. The observed shift in the trajectories at 1500 and 2500 m AGL was modulated by the synoptic-scale changes in the mid-latitude (over Central Asia) air masses (40-50° N) (Lüthi et al., 2015). The intrusion (in the form of a trough) of the cold and humid air masses from 40-50° N (see Figure 2) into 20-30° N occurred during the study period. As the trough moves eastward, it shifts the synoptic air mass at 20-30° N from northwesterly to southwesterly on 7 May 2016. The elevated polluted layer on 5 and 6 May 2016 (Figure 4.4) could be the result of this modulation of the westerly. The northwesterly airmass entered Nepal via Northern India, where MODIS retrievals showed a high aerosol loading (See Figure B.8), which could be mainly attributed to the numerous biomass fire events (See Figure B.9) observed in North India. In addition, numerous forest fires were also reported in western Nepal during the same period. However, the absorption signal from the flight measurement does not clearly show higher absorption at shorter wavelengths compared to absorption at 880 nm or longer wavelengths. This also implies that the observed elevated polluted layer in the Pokhara Valley is not entirely due to the biomass burning plume intercepted by the westerlies or north-westerlies. As the airmass origin shifts to southwesterly on 7 May 2016 (detected during flight F5), the synoptic air mass bypassed the high AOD loading over north India and contained the cold and relatively clean air from Central Asia. This resulted in the disappearance of the polluted layer over 2000 m asl. during flight F5.

4.4 Conclusion

This paper provides an overview of the pre-monsoon airborne measurement carried out with a microlight aircraft platform in the Pokhara Valley in Nepal, the first-of-their-kind airborne aerosol measurements in the Himalayan foothill region. The objective of the overall airborne campaign in the Himalayan region was to quantify the vertical distribution of aerosols over a polluted mountain valley region, as well as to measure the extent of regional transport into the Himalayas. In this paper, measurements from the test flights during May 2016 are summarized. These mainly include vertical profiles of aerosol number and size distribution, multi-wavelength aerosol absorption, black carbon, total particle concentration, and meteorological variables. The instrument package, designed for a microlight sampling was fitted to an IKARUS-C42 microlight aircraft. A total of five test flights were conducted between 5 and 7 May 2016, including morning and evening flights for about 1-1.5 h each, as well as vertical spirals to characterize vertical profiles of aerosols and meteorological parameters

The results presented in this paper should be considered as a pilot study mapping out the aerosol concentrations and their interactions with meteorological processes in the Pokhara Valley due to the limited flight time. In all the measured flights, the vertical profiles of aerosol parameters showed strong gradients along the atmospheric column. The observed total number concentration gradient was strongly influenced by the mountain valley boundary layer, which resulted in a sharp gradient below about 1500-2000 m (asl.). The increase of boundary layer height contributed to the differences in the morning and afternoon profiles. Similar vertical profiles of BC concentrations and aerosol total particle number concentrations provided evidence of common emission sources or co-located origins. The observed BC concentration near the surface (~ 1000 m asl.) was much lower than pre-monsoon BC concentrations measured in the Kathmandu Valley but comparable to values reported during the winter season in Kanpur in the IGP. The AAE estimates near the surface, based on the absorption value, fell in the range of 0.9-1.2, which indicates the presence of BC like and mixed (dust, urban, biomass) aerosols. An elevated polluted layer was observed at around 3 km (asl.) over the Pokhara Valley during this study. Characterized by a strong presence of dust in the IGP and polluted continental airmasses over the Pokhara Valley, the polluted layer could be linked with the westerly synoptic circulations and regional transport from the IGP and surrounding regions. The direction of the synoptic transport entering the Himalayan foothills and into Pokhara Valley, however, was influenced by the Westerlies at mid-latitudes (40-50° N). The extent of transport can be better quantified with regional airborne measurements along the south-north

transect through the region between the IGP and the Himalayan foothills at high altitudes in the Himalayas, including the Pokhara Valley. We will explore the extent of such regional transport in a subsequent publication that will be primarily based on the airborne measurements in phase II (December 2016- January 2017) in the Pokhara Valley and in the surrounding region. The subsequent paper will also characterize the extent of vertical transport from three different mountain valleys located at different elevations along the south-north transect.

Chapter 5

Discussion and Conclusions

5.1 Overview and key messages

As reported and analyzed using the data in this thesis, and in many past studies noted herein, the atmosphere of the Kathmandu Valley is highly polluted (Mahata et al., 2018; Shakya et al., 2017; Chen et al., 2015; Putero et al., 2015; Sarkar et al., 2015; Gurung et al., 2013), which is characteristic of much of the Himalayan region, as well as most of southern Asia. This air pollution has many impacts, on health, climate, agriculture, tourism and other sectors (Wester et al., 2019; WHO, 2016), which could potentially be mitigated to a large extent through various measures, many of which are readily available (e.g., better combustion technologies). In order to suggest appropriate measures to focus on for mitigating the local and/or regional impacts of air pollutants, of course, a greater knowledge base is needed, especially about the key pollutants and their distributions, seasonality and sources. This is where this thesis contributes. We achieve this by addressing three important issues: (i) temporal characteristics (daily, monthly, and seasonal) of two important GHGs in air, CO_2 and CH_4, and two key gaseous air pollutants, CO and O_3, (ii) spatial distributions of CO and O_3, and (iii) vertical distribution of particles (particulate matter, PM, and especially black carbon, BC) in the foothills of the central Himalaya. The first study (paper 1 as presented in Chapter 2) based on research questions (RQ) 1 and 2 (mentioned in the Introduction chapter) focused on CH_4 and CO_2 observations in the Kathmandu Valley and surrounding region, which were made as part of this thesis, which is the first of its kind reporting on the seasonal and temporal behavior of CH_4 and CO_2 in the central Himalayan region. The study further explored their possible emission sources in the Kathmandu Valley and surrounding regions. The second study (paper 2 in Chapter 3), which is also based on RQs 1 and 2, reported, for the first time, temporal distributions of CO and tropospheric O_3 based on simultaneous measurements of these two gases at multiple sites on the valley floor, on the mountain ridges in the east and west, and at the only river outlet, in the southwest corner of the valley. It also investigated prevalent local sources and interactions of emissions with meteorology and the influence of regional sources associated with mixing ratio increases in recent years in the Kathmandu Valley. Estimating the CO emission flux using the mixing layer height (MLH) and CO mixing ratios and its

comparison with currently available regional and global emission inventory datasets is a unique contribution of this study for the southern Asian region. The third study (paper 3 in Chapter 4) based on RQs 2 and 3 sheds light on the measurements of aerosol particles (PM, BC and particle number concentrations) and their vertical distributions in the Pokhara Valley in the foothills of the central Himalaya. The paper also describes the general meteorology of the Pokhara Valley during the pre-monsoon season. This study reports the first aerial sampling of air pollutants in the central Himalayan region.

While comparing the diurnal pattern of major GHGs with CO at the Bode site in the central Kathmandu Valley, it is observed that the diurnal behaviors of the CH_4 and CO_2 mixing ratios are found to be different from that of CO, which shows pronounced peaks in the morning and evening hours and a dip in the afternoon period (Figure 7, Mahata et al., 2017), similar to Panday et al. (2009). However, CH_4 and CO_2 show morning peaks, low afternoon values and again a general rise in the evening until the morning peak on the following day. Another important observation is a 1-2 hour delay in the morning peaks of CO at Bhimdhunga (mountain ridge on the west) and Naikhandi (river outlet in the southwestern corner of the Valley) compared to Bode in the central Kathmandu Valley. This indicates that the city pollution is influencing the morning peak of the outskirt sites Bhimdhunga and Naikhandi due to upslope winds and the wind channeled through the Bagmati River outlet, respectively, after the radiative heating of the surface in the morning (Mahata et. al., 2018, Mues et al., 2017). The mixing ratios of CH_4, CO_2 and CO are minimum in the afternoon (from 12:00 to 15:00 local time) due to the active circulation after the dissolution of the nocturnal stable layer and the increase in daytime MLH (Mues et al., 2017).

The main local emission sources which play important roles for pollutants and GHGs in the Kathmandu Valley are the transport sector, the residential sector, industries (mainly the brick industry) and waste burning. Furthermore, the bowl-shaped topography of the valley is also responsible for high mixing ratios during peak hours due to the low MLH. The recirculation of emitted species, which have spent one night in the elevated layer, partly enhances the mixing ratios of air pollutants and GHGs during the morning peak (Panday and Prinn, 2009; Panday et al., 2009). Furthermore, the mixing ratios of CH_4, CO_2 and CO are significantly influenced by several different sources in different seasons, such as the brick industries from January to April (Mahata et al., 2018; Mahata et al., 2017; Mues et al., 2017; Kim et al., 2016; Chen et al., 2015; Sarkar et al., 2015). The CO/CO_2 ratio analysis also indicated that the brick industries

are major polluting sources in winter in the valley (Mahata et al., 2017). This result is similar to Kim et al. (2016) who looked into PM2.5, OC and EC and Sarkar et al. (2015) who studied NMVOCs. Another important emission source is open trash burning that is quite common during the winter season. Moreover, the forest fires and agricultural residue burning in the region (including IGP) play important roles, increasing the mixing ratio of these species during the pre-monsoon season (Bhardwaj et al., 2018; Mahata et al., 2018; Putero et al., 2015). The ultralight flight measurement and long-term AERONET observations in the Pokhara Valley have also reported similar results of high AOD values in the pre-monsoon season when the wind direction is from the polluted region of the Indo-Gangetic Plain (Singh et al., 2019). Similarly, there are large changes in CO mixing ratios during episode days compared to normal days at Bhimdhunga and Naikhandi (outskirt sites), especially relative to the changes observed at Bode (Mahata et al., 2018). This indicated the contribution of regional emissions to the pollutants in the Kathmandu Valley. The higher O_3 mixing ratios at Nagarkot (hill site) (Mahata et al., 2018) also indicated regional-scale O_3 pollution.

Long-term (greater than a year) CH_4 and CO_2 observations at Bode and 3 months of simultaneous observations of these gases at Chanban, outside the Valley, are first of their kind in the central Himalayan region. The analyzed seasonality and diurnal variation of CH_4 and CO_2 at the two sites will be useful for evaluation of model simulations of the region. The comparison of CH_4 and CO_2 at Bode and Chanban shows the influence of urbanization at Bode, which provides useful information about the impacts of urban development. In contrast, the mixing ratios of CH_4, CO_2 and CO at Chanban are consistent with the baseline mixing ratios of these species in the Kathmandu Valley (Figure 2.10, Mahata et al., 2017), and thus can be considered as representative of the broader regional values.

Our study is not only focused on the spatial and temporal behavior of GHGs and air pollutants; we have also estimated CO emission flux in the Kathmandu Valley. The calculation of the CO emission flux was based on the observed CO mixing ratios and the MLH while it is near-constant at night, similar to what was done for BC in Mues et al. (2017). This is one of the unique contributions of this study (as also highlighted in the open access review of the paper by referee 2), providing insights into CO emissions in source regions like the Kathmandu Valley in the southern Asian region (Mahata et al., 2018). Although there are some limitations in calculating the CO emission flux by using MLH and CO mixing ratios, the estimated flux values in this study are 2-14 times higher than the values in widely-used global and regional

emission databases (EDGAR HTAP, REAS and INTEX-B) (Mahata et al., 2018). Mues et al. (2017), using the same method, also found a similar underestimation of BC emission fluxes. This indicates that there is a need for a more detailed emission inventory for CO and BC (and perhaps for other species as well) for the region.

Furthermore, this thesis also analyzed tropospheric O_3, an important gaseous air pollutant and GHG. The simultaneous O_3 observations at Bode, Paknajol and Nagarkot for a one year period provided quantitative information on O_3, and its spatial, temporal and seasonal distributions in the Kathmandu Valley. Daily 8-hour maximum O_3 exceeded the WHO guideline (50 ppb) about 80% of the days at all sites during the pre-monsoon season, which is of significant concern for impacts on health and agriculture in the Kathmandu Valley and surrounding regions. The high level of O_3 in this season is due to extensive photochemical production, the influence of regional forest fires, and agro-residue burning, along with possible stratospheric intrusion (Bhardwaj et al., 2018; Mahata et al., 2018; Putero et al., 2015; Cristofanelli et al., 2010; Pudasainee et al., 2006). Furthermore, daily 8 hour maximum O_3 exceeded the WHO limit for 92 % of the days during the pre-monsoon at the mountain site (Nagarkot), which is indicative of regional-scale high O_3 pollution. Hence, if appropriate mitigation options are not taken, the 8-hour maximum O_3 may end up exceeding the WHO recommended O_3 level even in the post-monsoon and winter season at all sites in the near future, which will have further adverse impacts on human health and ecosystems.

After publication of the scientific results of the SusKat-ABC campaign (which included the three papers in this thesis, along with numerous other studies, with several including the data collected in this thesis), the local and regional science, policy and regulatory communities (along with other stakeholders) have taken up discussion of these results, and the Government of Nepal has taken important first steps to address the serious air pollution issue in the country:

- National air quality monitoring with an aim of setting up 56 stations across the country. As of July 2021, there are 26 air quality monitoring stations functional in the country, including 7 in the Kathmandu Valley.
- After the 2015 April earthquake, most of the traditional brick kilns have been re-constructed using considerably less polluting designs and technologies.
- All public vehicles in the country more than 20 years old have been phased out since 18 March 2018 to reduce emission sources.

- The Government of Nepal introduced the Kathmandu Valley air pollution management action plan in 24 February 2020.

5.2 Conclusions and future priorities

This thesis has made an important contribution to understanding air pollution in the Kathmandu Valley and Nepal, and by providing a framework for analyzing air pollutants and the effects of circulation in similar other regions of southern Asia. Related studies, including several which have made use of the data collected in this thesis, have further helped to fill the gaps in this area. However much remains to be done in order to be able to really understand the local vs. the regional air pollution and its impacts and sources.

The conclusions of this thesis, which are based on the three research questions discussed above are as follows:

Research Question (RQ) 1: CO_2 and CH_4 (GHGs) and CO (an air pollutant) show distinct diurnal variations: morning and evening peaks with a dip in the afternoon in the Kathmandu Valley. The difference observed between two GHGs and CO is in their nighttime characteristics: CO decreases after an evening peak, while the GHG mixing ratios keep increasing until the next morning peak in the valley. This behavior of the GHGs is not observed at the Chanban site. The spatial study of CO and O_3 at multiple sites in the Kathmandu Valley shows the tight connection between meteorology (especially wind speed, wind direction and temperature) and the pollutants, as evident in the delayed morning peak of CO at the outskirt sites (Naikhandi and Bhimdhunga) in comparison to Bode. The greater exceedance of daily 8-hour maximum O_3 observed at the hilltop site (Nagarkot) than at the urban/semi-urban sites corroborates the role of meteorology, topography and regional contributions, with high levels of ozone partly coming from long-range transport, including from the Indo-Gangetic Plain.

RQ 2: The main local sources of GHGs and air pollutants in the valley are transport, residential activities, industries and trash burning. The CO/CO_2 ratio analysis shows that during the winter season, brick kilns and vehicles are the dominant sources. Similarly, regional forest fires and agro-residue burning within Nepal, as well as outside Nepal, especially in the IGP region affect the mixing ratios of CO and O_3 in the Kathmandu Valley during the pre-monsoon season.

RQ 3: The concentration of aerosol particles (PM, BC) decreases with the increasing height up to 4500 m asl. (The observational limit for the micro-light aircraft used in the study). However,

an elevated aerosol layer was regularly detected around 3000 m asl. during the flight measurements. The concentrations of PM and BC in the elevated layer are similar to their concentrations near the surface (ca. 800 m asl.) over the Pokhara Valley. The elevated aerosol layer, which contributes to the maximum AOD observed at Pokhara Valley during the pre-monsoon season, is primarily due to the transport of dust and other aerosol particles including forest fire emissions in the foothill region) by westerly advection from the IGP to the foothills of the Himalaya and the mountain valleys.

In order for the Government of Nepal to be able to develop effective, concrete plans and policies to mitigate GHGs and air pollution within Nepal, several steps will be needed. A more detailed knowledge of the regional O_3 chemistry is lacking; in particular, detailed knowledge of the O_3 precursors (NO_X and VOCs), especially distinguishing into either NOx or VOC dominated regimes, along with the regional meteorology in the valley is required. Achieving this would require long-term simultaneous monitoring of O_3 and key precursors at several places within the valley.

Thus, a final aspect to consider is the regional contribution to the air pollutants and GHGs in the Kathmandu Valley, as well as in other parts of the central Himalayan region, and how these could be more effectively mitigated. In particular, dedicated studies of source apportionment of regional emission sources will be helpful for policy makers to make better plan for improving air quality in the valley. Among the various pollutants, I would place the greatest emphasis on mitigation of O_3, since there is less awareness of it as a pollutant than PM, which already receives enhanced attention because it reduces visibility. Thus, we need to study O_3 chemistry and its precursors within the valley and surroundings, as well as regional contributions to O_3 in the valley, in order to develop effective science-informed mitigation options.

Appendix A

Supporting Information:

Seasonal and Diurnal Variations of Methane and Carbon Dioxide in the Kathmandu Valley in the Foothills of the Central Himalaya

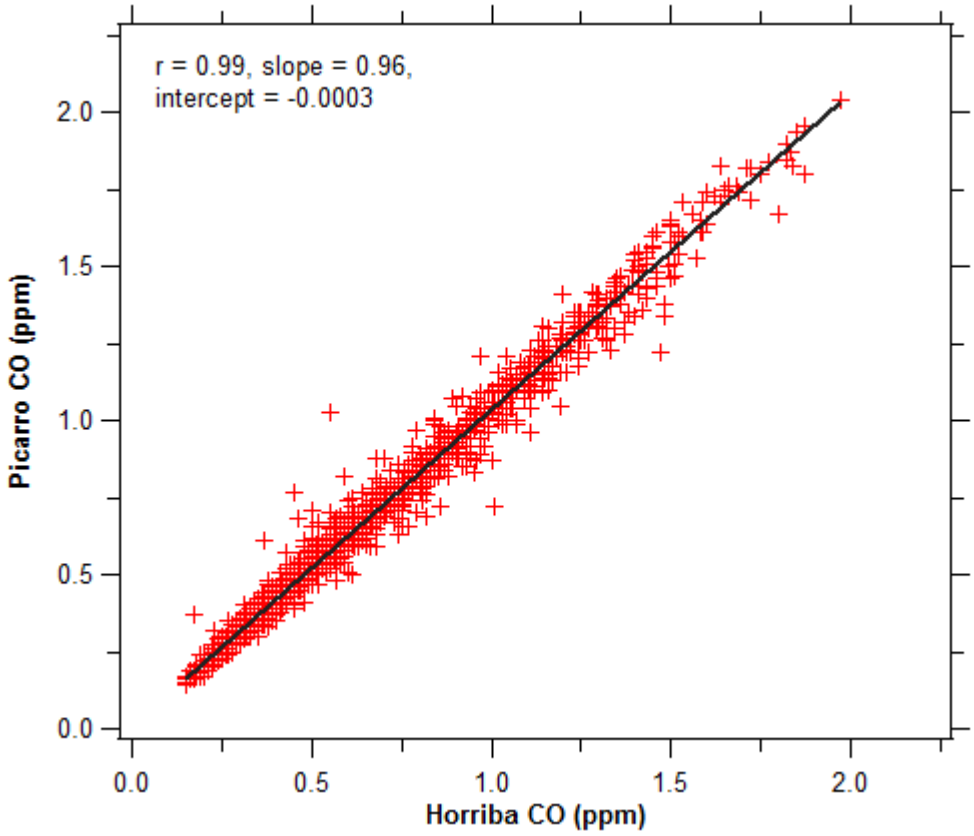

Figure A.1. Correlation between hourly CO mixing ratios measured simultaneously with a cavity ring down spectrometer (Picarro G2401, USA) and a CO analyzer (Horriba AP370, USA) at Bode, a semi-urban site in the Kathmandu Valley during 6 March to 7 June 2013.

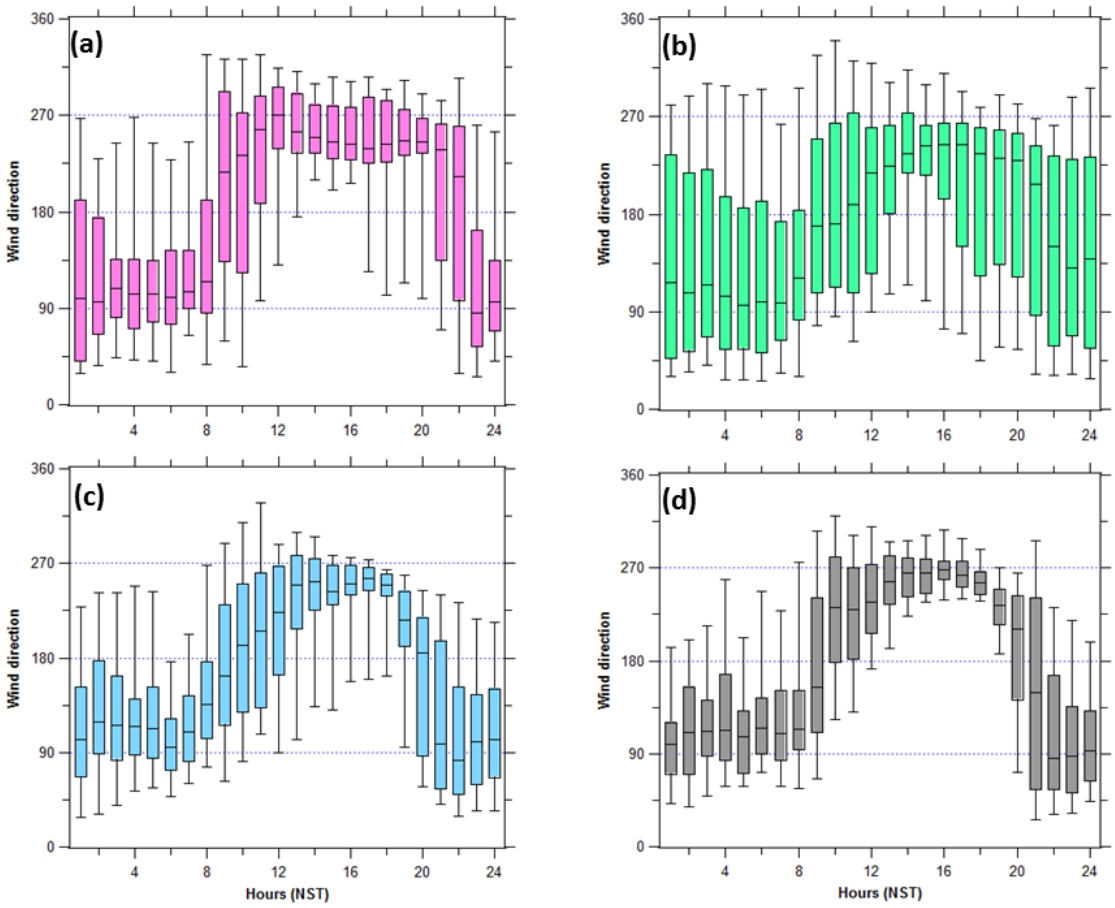

Figure A.2. Diurnal variation of hourly average wind directions in different seasons; (a) pre-monsoon, (b) monsoon, (c) post-monsoon, and (d) winter season observed at Bode for a year (06 Mar 2013- 04 Mar 2014). Seasons are defined as Pre-monsoon: Mar-May, Monsoon: Jun-Sep, Post-monsoon: Oct-Nov, Winter: Dec-Feb. The lower and upper end of the whisker represents 10^{th} and 90^{th} percentile, respectively; the lower end and upper end of each box represents 25^{th} and 75^{th} percentile, respectively, and black horizontal line in the middle of each box is the median for each month. The information on the box and whisker is same for Figure A3.

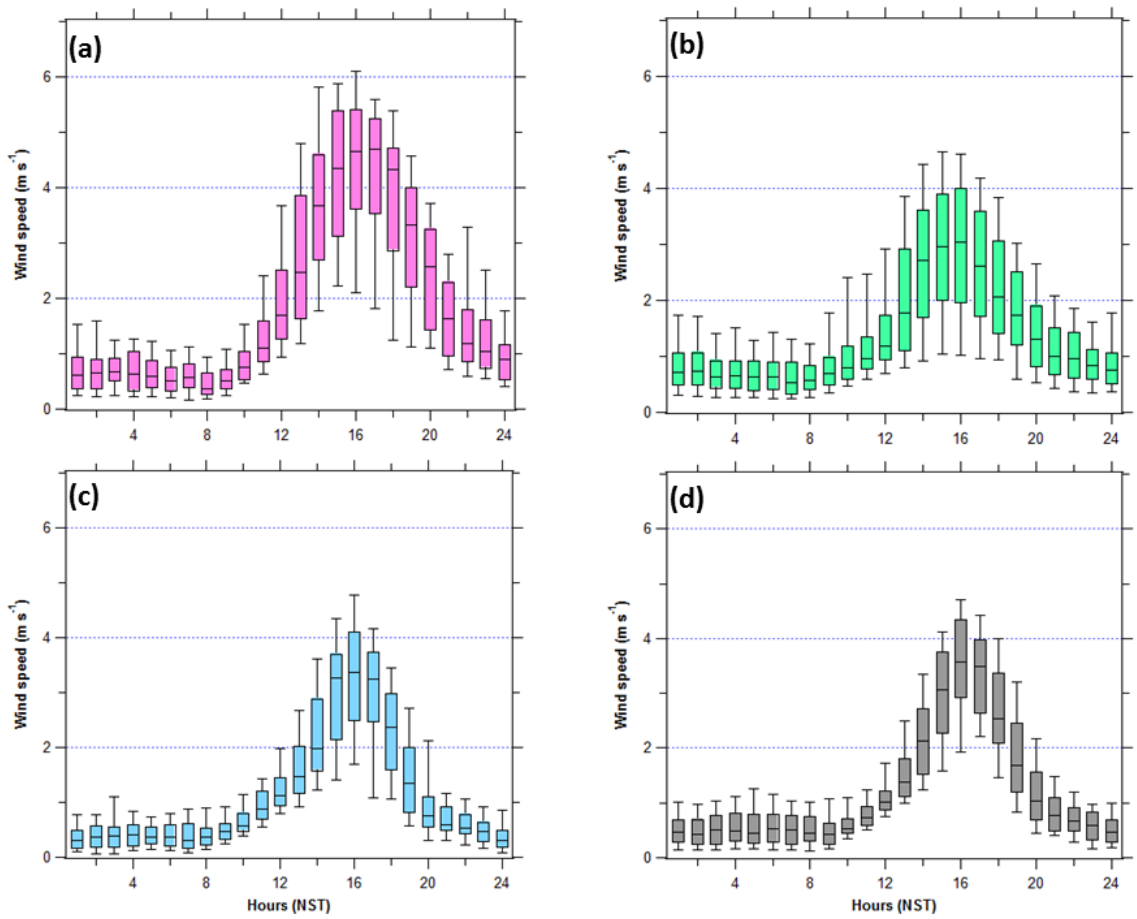

Figure A.3. Diurnal variation of hourly average wind speeds in different seaasons; (a) pre-monsoon, (b) monsoon, (c) post-monsoon and (d) winter season observed for a year (06 Mar 2013- 05 Mar 2014) at Bode.

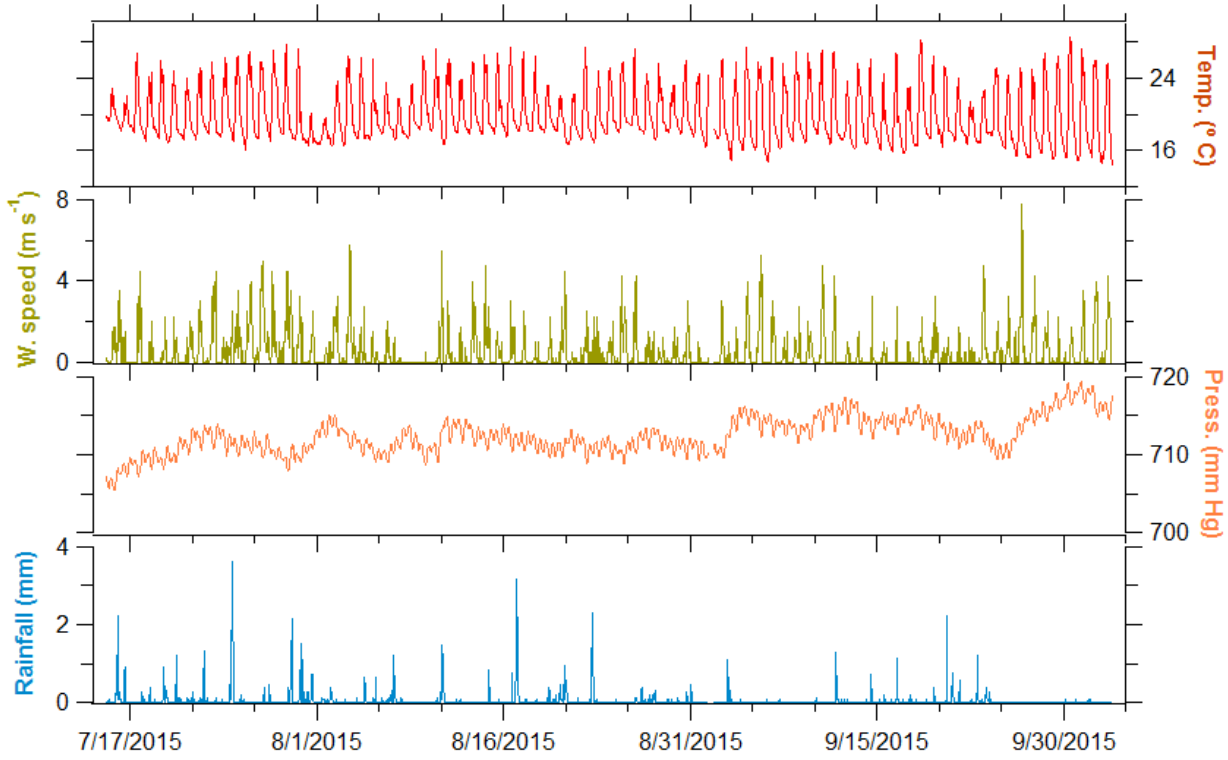

Figure A.4. Time series of hourly average ambient temperature, wind speed, pressure, and rainfall observed at Chanban, a rural site outside the Kathmandu Valley from 15 July to 03 October 2015.

Appendix B

Supplementary Information:

An Overview on the Airborne Measurement in Nepal, - Part 1: Vertical Profile of Aerosol Size - Number, Spectral Absorption and Meteorology

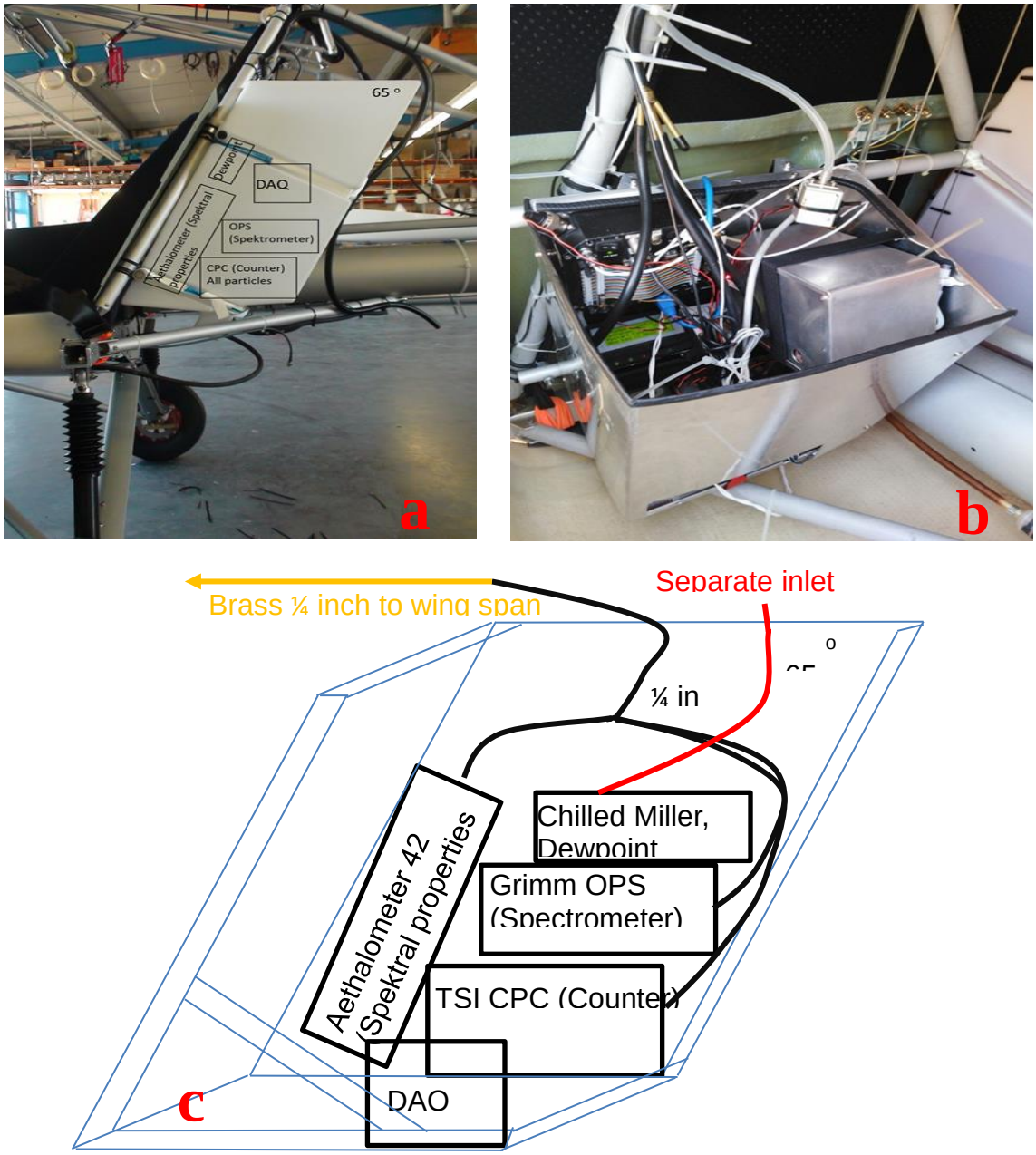

Figure B.1. Testing and assembly of the instrument package inside IKARUS-C42 in the COMCO IKARUS station in Germany (a) field station in Pokhara Valley (b) sketch of the Instrument package (c).

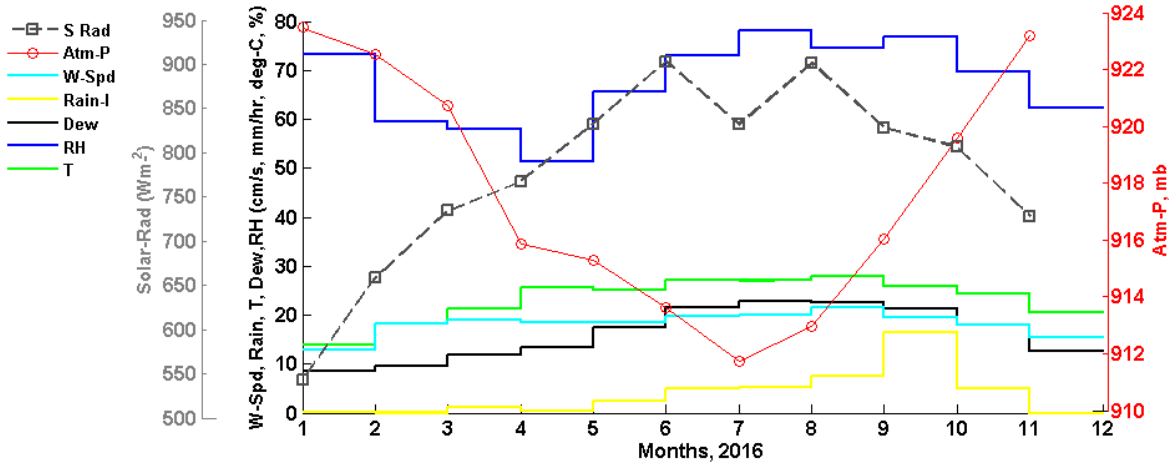

Figure B.2. Monthly mean values of key meteorological parameters measured at the Pokhara regional airport (station ID: 804, 28.1993528, 83.9784028, 820-meter altitude) using an ENVIRODATA weather station. December 2016 is missing due to data availability. The monthly value of solar radiation shown here is 95 percentiles of the daily values to reflect the peak insolation values. Wind speed and rainfall intensity are 10x for graphical clarity. Note that rainfall values presented here are not cumulative over a month, rather average of the month. (December data is not available).

The annual mean temperature in the valley was 22° C, with the lowest monthly mean in January (~15° C) and the highest in July (~ 25° C). Rainfall was also highest in the months of August and September (summer monsoon season), followed by relatively dry post-monsoon (October-November) and winter period (December-February). The late pre-monsoon to summer monsoon were also the periods of maximum monthly solar insolation (~900 Wm^{-2}) and the insolation is approximately half (~550 Wm^{-2}) during the winter.

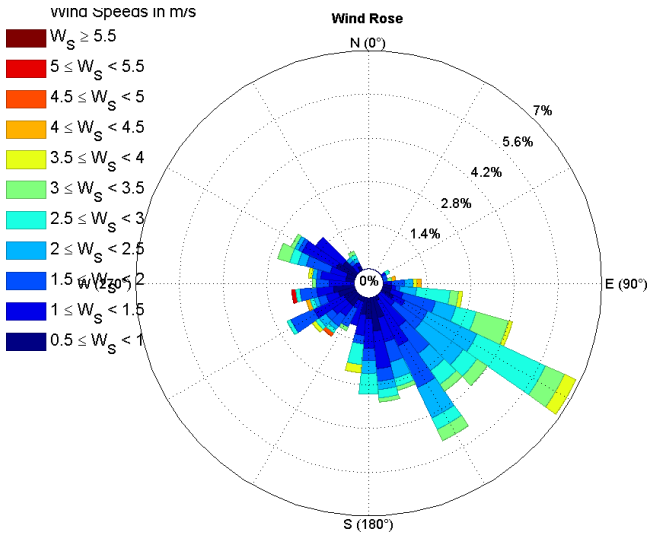

Figure B.3. Frequency of wind speed and direction observed in the Pokhara Valley during May 2016.

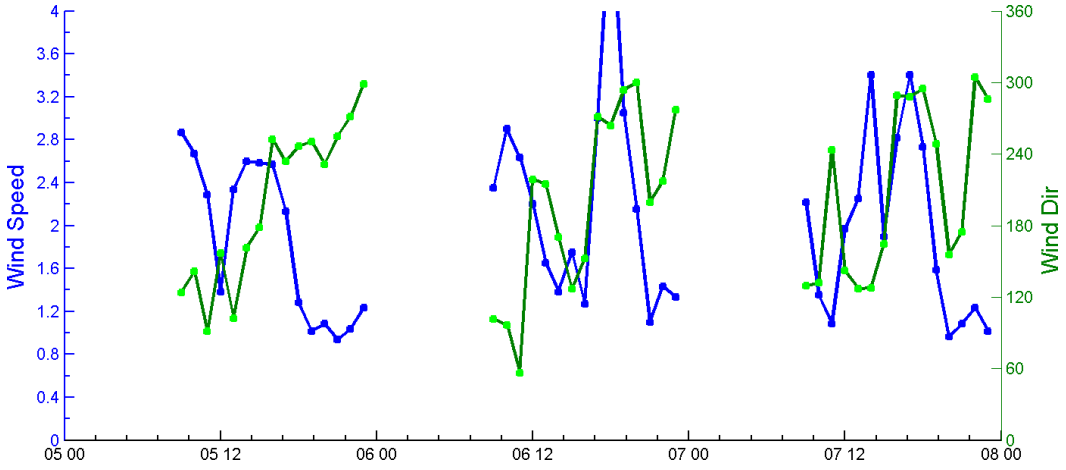

Figure B3.1: Wind speed (ms-1) and direction from 5-7 May 2016 measured at the Pokhara Regional Airport meteorological station.

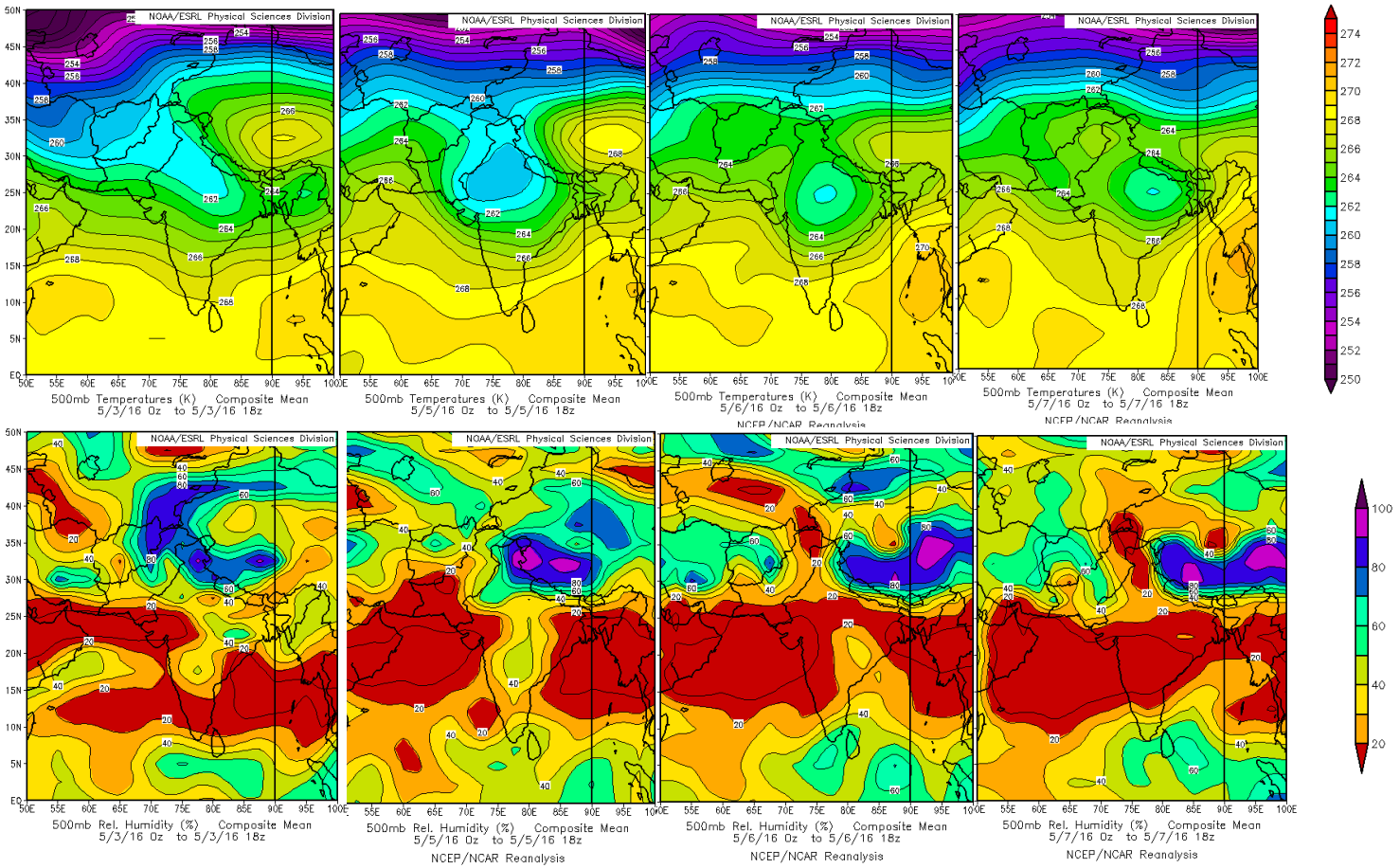

Figure B.4. Daily temperature and relative humidity at 500mb using the NCEP NCAR reanalysis (2.5x 2.5^{o}) data over South Asia from May 1 to 7 2016.

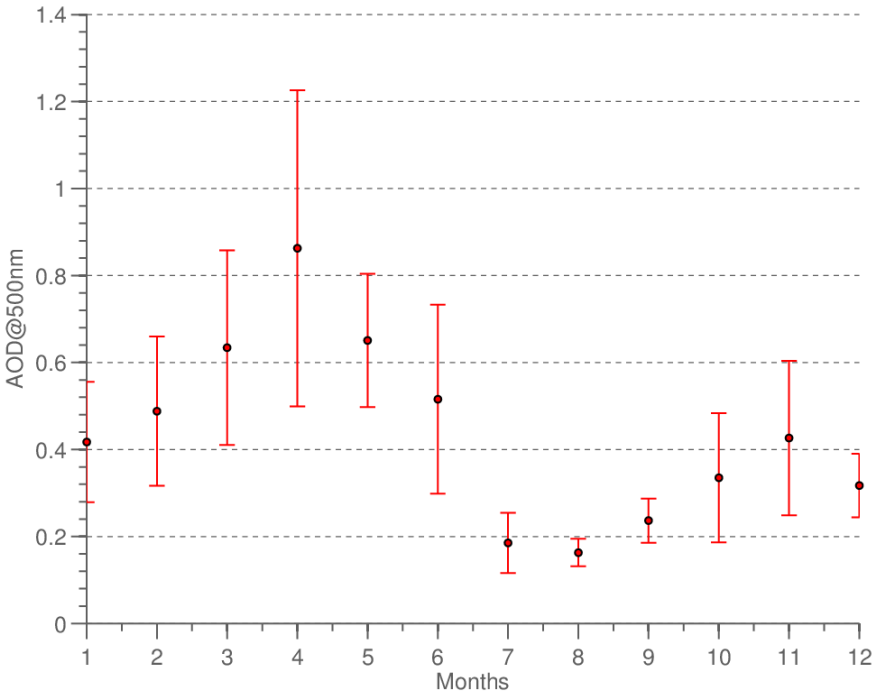

Figure B.5. Monthly mean value of AOD 500 nm in Pokhara Valley for 2010-2016 (Note: Level 2 and 1.5 were used).

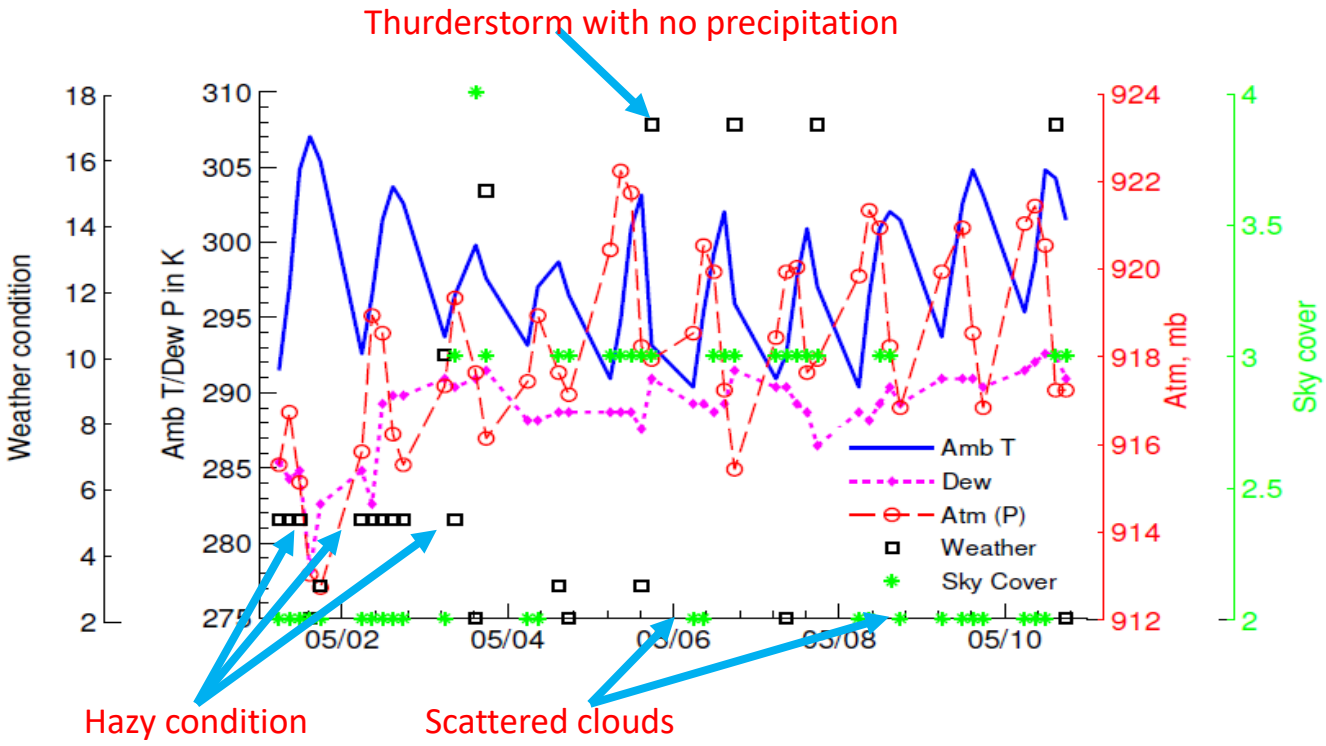

Figure B.6. Local Meteorology in the Pokhara Valley from 1-10 May 2016.

Weather condition is coded by individual number (see NOAA https://www7.ncdc.noaa.gov/CDO/dataproduct for details). Weather condition in the figure is shown as a black square box. Weather condition of 5 indicate Hazy conditions;17-thurderstorm but no precipitation; 3-cloud generally forming; 2-sky unchanged

The sky cover is numerically coded as follows:

CLEAR =1, SCATTERED (1/8 TO 4/8) =2, BROKEN-5/8 TO 7/8 =3, OVERCAST=4, OBSCURED=5, PARTIAL OBSCURATION=6

(Also see NOAA https://www7.ncdc.noaa.gov/CDO/dataproduct for details).

S7. Summary of aerosol properties using AERONET measurement from 2010-2016

AERONET measurements (Holben et al., 1998) have been made in the Pokhara Valley since January 2010. The AERONET station (83.97° N, 28.18° E, 807 m a.s.l.) is approximately 1.1 km southeast from the Pokhara Regional Airport, located in the semi-urban area of Pokhara City. Cloud-screened and quality assured (level 2) data were used in the study. Gaps in the level 2 data were supplemented with level 1.5 data. The AERONET retrieval suffers in the monsoon months (June to September) due to interference by monsoon clouds in the Pokhara Valley, as indicated by the gap in Figure 4.2.

A combination of direct products such as aerosol optical depth (AOD) and inversion products such as fine AOD, absorption Ångstrom exponent (AAE) and volume size distribution were used for the analysis presented in this study. The typical reported uncertainty in the AERONET data products for AOD (> 0.04) is approximately ±0.01 to ±0.02, and is higher for shorter wavelengths (Eck et al., 1999;Holben et al., 1998). The observed uncertainty in AOD also influences other AERONET products such as the Ångstrom exponent (AE) and the inversion products. Thus these derived products will have a higher uncertainty than the AOD (Schuster et al., 2006;Dubovik and King, 2000). Further details about the AERONET direct and inverted data products can be found in Holben et al. (2006).

In the Pokhara Valley, AOD values showed a strong seasonality in the wavelength bands between 340 and 1020 nm. The inter-annual variation in the AOD during 2010-2016 was closely associated with the enhancement in the fine-mode fraction, and to a lesser extent in the coarse mode for dust (Xu et al., 2014). The observed inter-annual variation in the AOD could be influenced by the interaction between aerosols and the mesoscale to synoptic-scale meteorology (Vinoj et al., 2014;Ram et al., 2010;Kaskaoutis et al., 2012a), as well as influences of the ENSO (El Niño southern oscillation) on West Asia and the IGP (Kim et al., 2016). AOD values were enhanced or elevated during the winter, with the aerosol load building up throughout the pre-monsoon months (AOD_{500nm}>0.6, Figure 3a, 3b, and S5) and then falling to their lowest values in the monsoon months (AOD_{500nm} ~0.2-0.3), most likely due to wet removal of aerosols. After the low AOD during the monsoon, AOD gradually increases (to ~0.4-0.5) during the post-monsoon through winter to the pre-monsoon season. AOD was usually highest in April (AOD_{500nm}:0.86±0.36), followed by March, May, and June. The increase in aerosols load (as reflected by the AOD) during the pre-monsoon months can also be seen at high altitude sites such as the NCO-P site in the Khumbu Valley near Mt. Everest,

located at 5057 m (a.s.l.) and about 300 km to the east of Pokhara (see Figure 3c), as well as at IGP sites in Kanpur (130 m a.s.l., 400 km southwest of the Pokhara Valley) and Gandi Nagar (60 m a.s.l., 250 km south of the Pokhara Valley). A similar AOD build-up was also observed by Ram et al. (2010) in Darjeeling (2194 m a.s.l., hill station ~450 km east of Pokhara Valley), and by Chatterjee et al. (2012) in Manora Peak (1950 m a.s.l., 460 km west of Pokhara Valley). This regional increase in aerosol load in the IGP and the Himalayan region is partly due to active transport during the pre-monsoon season, often linked with westerly advection bringing dust from West Asia and nearby arid regions (Gautam et al., 2011). The relatively dryness with little precipitation during this period also contributes to the total aerosol load, since washout will be limited. The AOD peaks occur in different months in these different sites in the IGP and Himalayas, reflecting the varying influence of local meteorology and increase in the emission sources such as agriculture residue burning dominated by dominated by fine-mode particles (Putero et al., 2014).

Fine-mode aerosol particles scatter more at shorter wavelengths (such as 340-500 nm) compared to 1020 nm (Schuster et al., 2006). The variation in the Ångstrom exponent was not as definitive as in the AOD values; the Ångstrom exponent was generally below 1 during pre-monsoon months and above 1 in the post-monsoon and winter months. Ångstrom exponent values of >1 are generally reported for sources such as biomass burning, fossil fuel combustion and other primary sources which have a dominant fine-mode fraction. Dust and other coarse-mode aerosols have Ångstrom exponents less than 1 (Eck et al., 1999). The highest values of the Ångstrom exponent (at least >1.2) were observed for the post-monsoon observation period, presumably due to emissions of primary fine-mode aerosol from sources such as open burning of agriculture, often reported in tshis season especially to the south and southeast of Pokhara Valley and in the IGP. In addition to the Ångstrom exponent, the temporal variation of AOD fine and coarse modes (at 500 nm) in Figure 3b and 3c also indicates that fine-mode aerosols nearly exclusively dominate the atmospheric column during the post-monsoon and winter seasons. In the pre-monsoon season, in addition to the fine-mode, a substantial fraction of coarse-mode also exists, which is also observed in the monsoon season. On the nature of aerosols or bulk composition, Figure 3e shows a simple scatter-plot based on the absorption and extinction Ångstrom exponents (AAE and EAE at 440-870 nm) which can be used to indicate the aerosol types (Giles et al., 2011; Giles et al., 2012; Dubovik et al., 2002). These two parameters describe the spectral dependence or “slope” of aerosols absorption and extinction at the measured wavelength (Seinfeld and Pandis, 2006). Extinction exponent is a

proxy for aerosol size, while the absorption exponent is a proxy for absorbing aerosols including a mixed aerosol. The classification employed by Giles et al. (2011) based on observations from the IGP AERONET sites defines *"Dust"* or "*Mostly Dust*" aerosols within the range of EAE <0.5 and AAE >2.0 and "*Mostly BC like"* aerosols with EAE EAE <0.8 and AAE ~1.0-2.0. Urban/industrial and biomass burning aerosols fall under the "Mostly BC" category (Dubovik et al., 2002; Giles et al., 2011). The mixed aerosol ("Dust+BC") centers around a value of EAE ~0.5 and AAE~1.5. Based on this approximate classification from a monthly data, the dominant aerosol in the Pokhara Valley is mostly *BC like*; however, the daily aerosol characteristics can vary from more mixed to dust-like in the pre-monsoon months, to more BC-like in the post-monsoon and winter months.

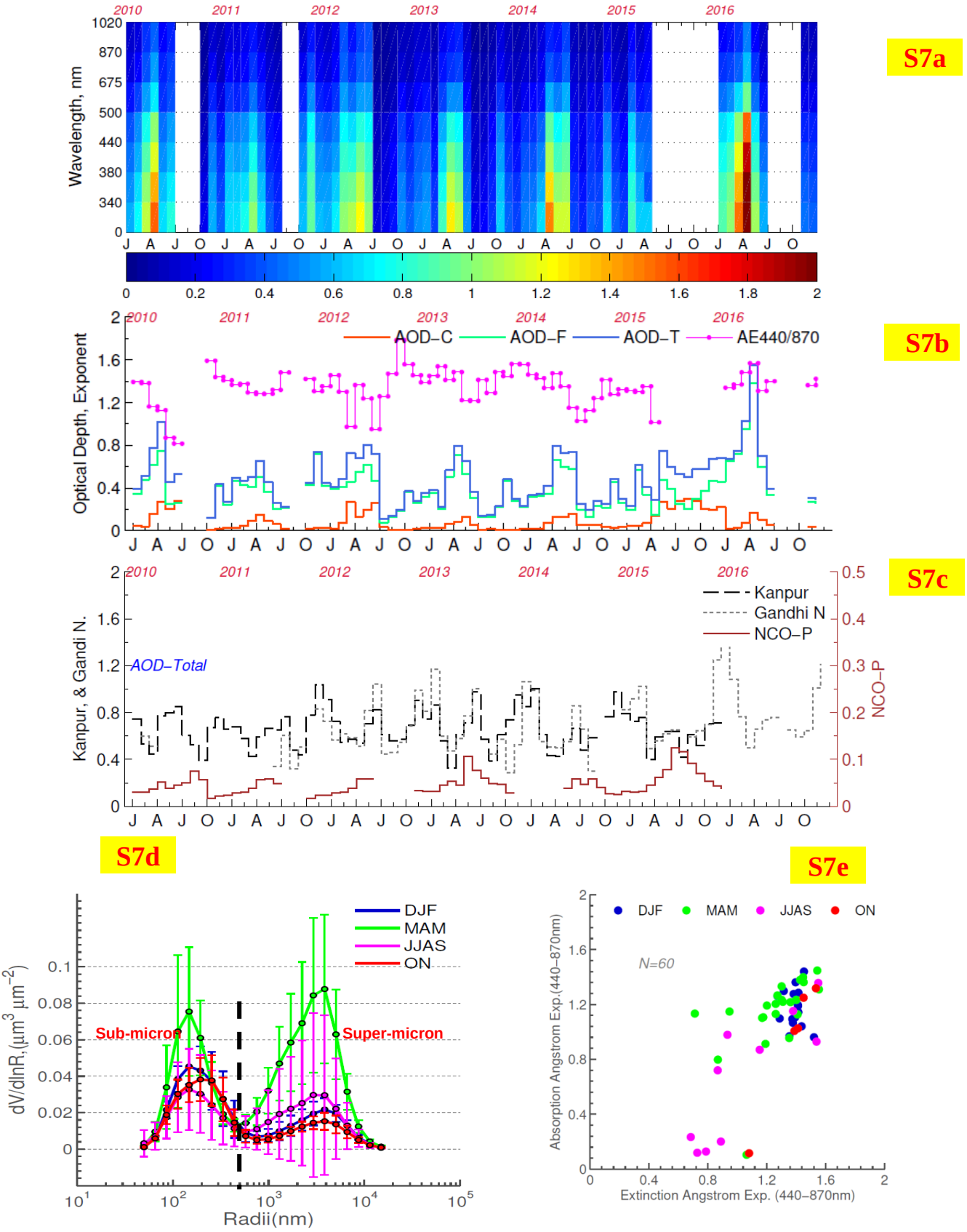

Figure B.7. The AERONET-based aerosol optical depth and radiative properties in the Pokhara Valley from 2010 to 2016. Monthly summaries are presented using level 2 collections and supplemented with level 1.5 for missing data points; **(S7a)** AOD at seven wavelengths; **(S7b)** Inversion products such as fine AOD (AOD-F), coarse AOD (AOD-C), and total AOD

(AOD-T), along with Ångstrom exponent (440-870 nm, magenta line); **(S7c)** AOD-T for Kanpur, Gandi Nagar (both IGP sites in India) and the NCO-P site (labeled EVK2-CNR, a high altitude site in the Khumbu Valley at the base of Mt. Everest); **(S7d)** Seasonal average of volume particle size distribution grouped by four seasons (the error bar indicates the standard deviation, and the uncertainty in the calculated size distribution is close to 20 % in the range 0.2 µm $<D_p<$ 14 µm). The four seasons are classified as winter (DJF: December, January and February), monsoon (JJAS: June, July, August and September), pre-monsoon (MAM: March, April and May) and post-monsoon (ON: October and November); **(S7e)** absorption Ångstrom exponent (440-870) and extinction Ångstrom exponent (440-870 nm), color-coded for the four seasons.

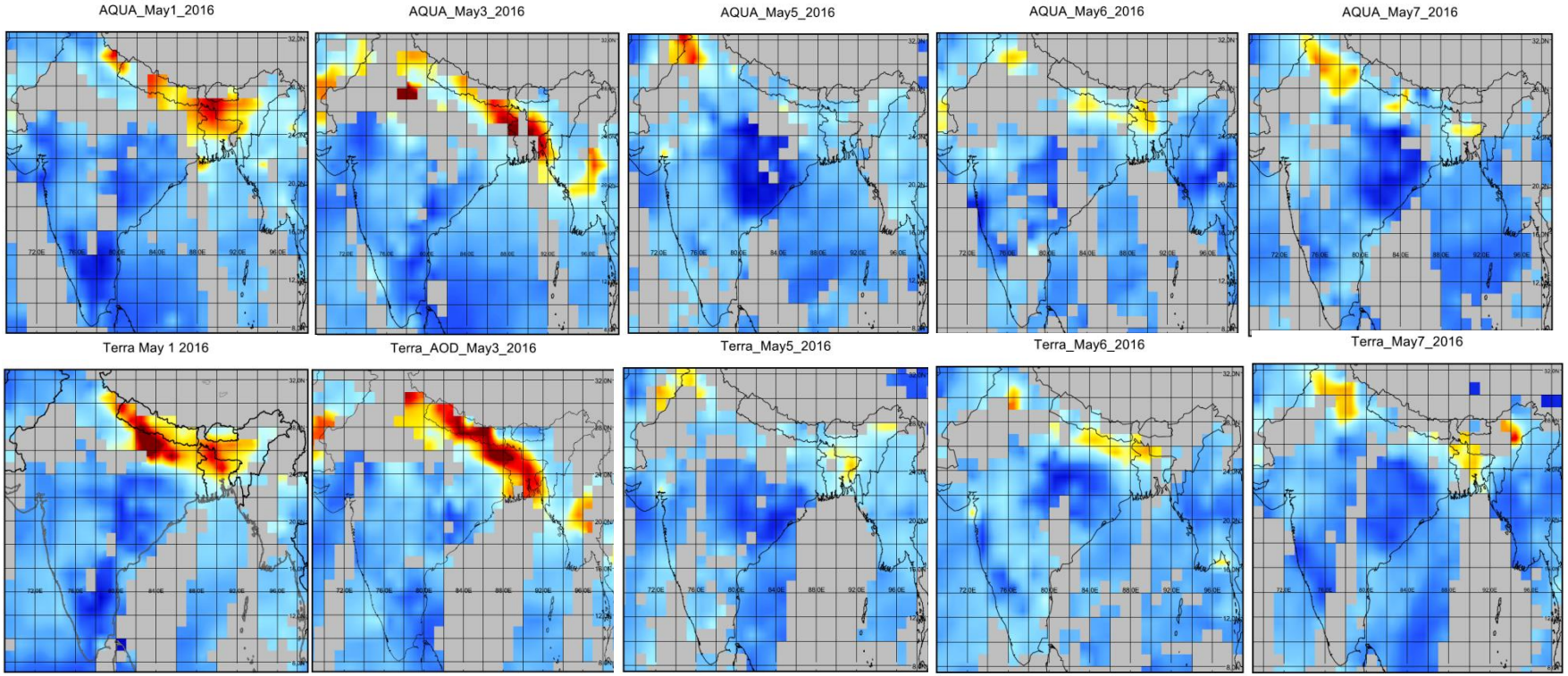

Figure B.8. MODIA AQUA AND TERRA AOD at 550 nm over the IGP and Himalayan region from 1 – 7 May. The plots were generated using the Level-3 MODIS Atmosphere Daily products, **MOD08_D3** at (1^o x 1^o) resolution. Top panel (AQUA) and bottom panel (TERRA).

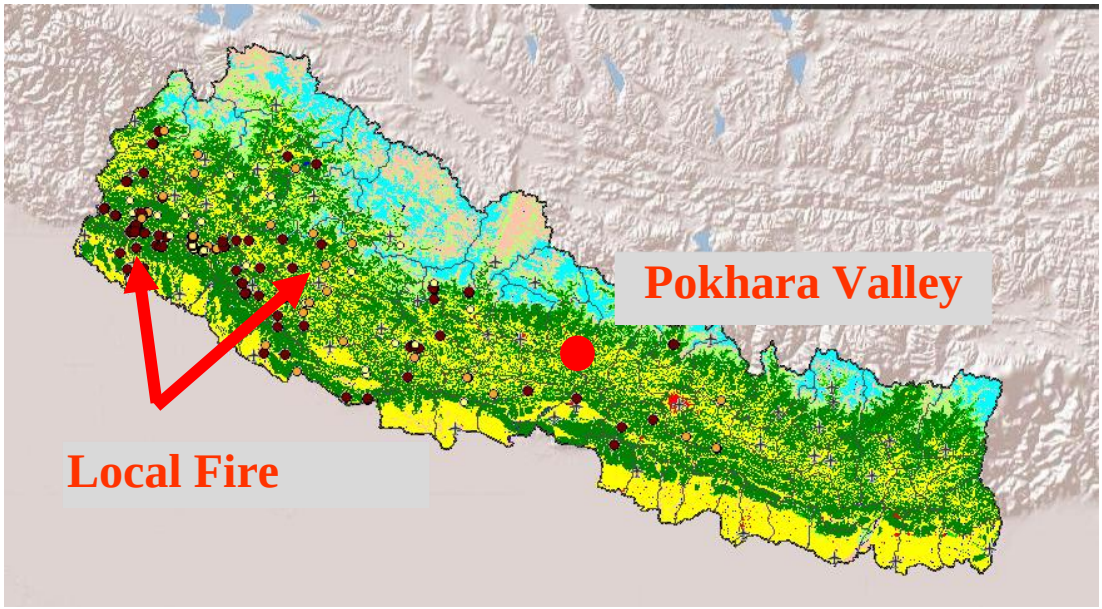

Figure B.9. Locally or nationally recorded active fire for the same period by the National Emergency Operation Centre (http://neoc.gov.np/en/) via the ICIMOD portal (http://118.91.160.238/NepalForestFire/index.html).

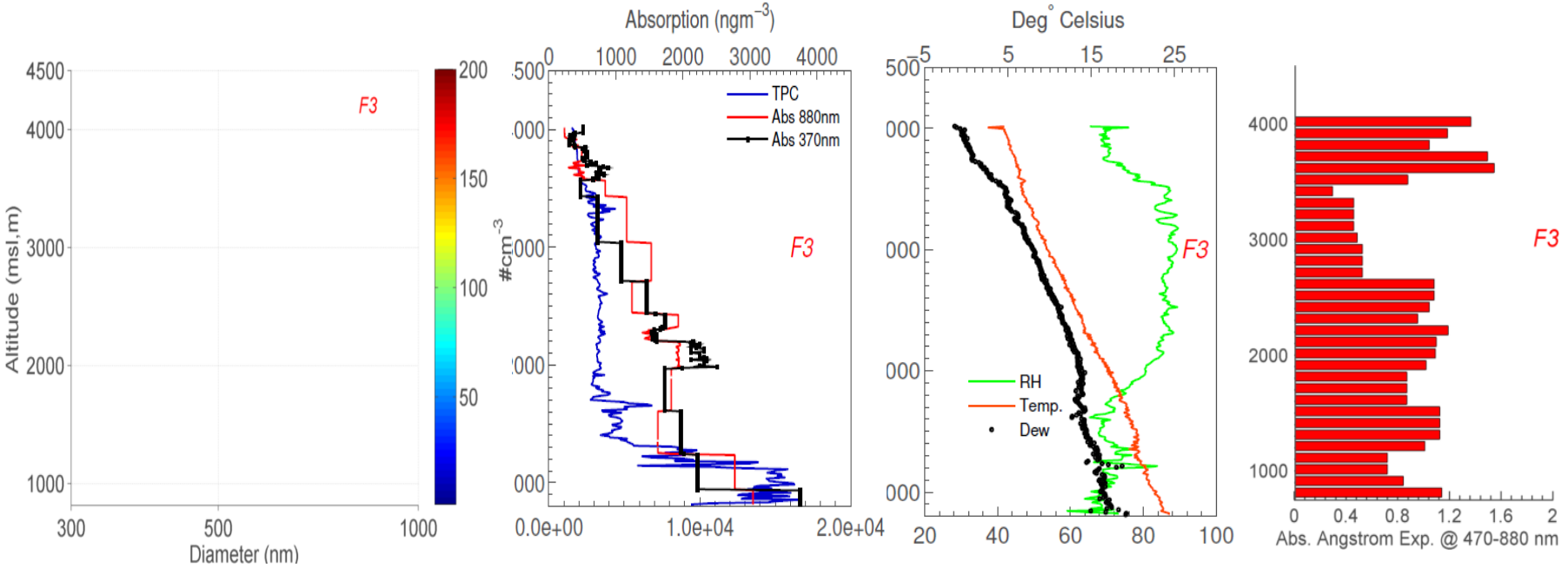

Figure B.10. Morning test flight (Flight F3) on 6 May 2016 is shown here, the rest of the results are already shown in in Figure. Each subplot is arranged by (i) Aerosol number size distribution measured by the Grimm OPC model 1.108 (0.3-20 µm), limited to 1 µm in the figure, (ii) Total particle number concentration (also indicated as TPC, Dp >11 nm) measured by the TSI CPC 3760 and absorption aerosol at 370 nm and 880 nm (iii) temperature (°C) and dew point (black dot, in °C) and relative humidity (or RH %), (iv) calculated absorption Ångstrom exponent averaged for every 100 meters elevation band.

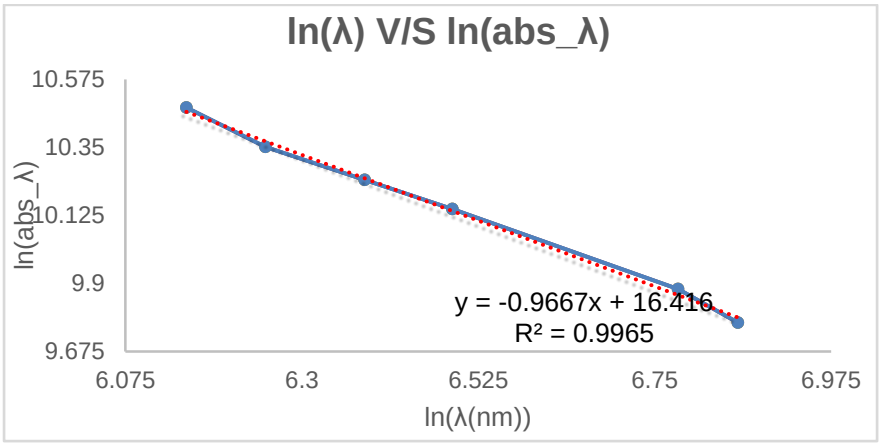

815m Linear Fit 815m Linear Fit 815m Linear Fit

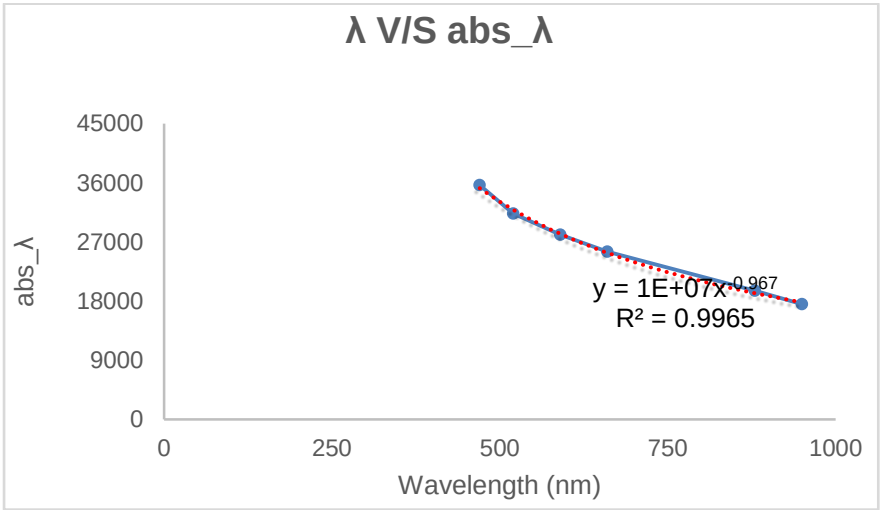

815m *Power Fit*

Figure B.11. Estimating the AAE value using the power fit and linear fit (left: power fit, right: linear fit).

Table T.1

Flight #	**Flight date**	**Flight time window**		**Measured parameter**
F1	5 May 2016	7:00-9:00	Morning flight	T, R, H, total particle count, number-size distribution, BC
F2	5 May 2016	14:00-17 :00	Afternoon flight	"
F3	6 May 2016	7:00-9:00	Morning flight	"
F4	6 May 2016	14:00-17 :00	Afternoon flight	"
F5	7 May 2016	7:00-9:00	Morning flight	"

Bibliography

Aryal, R. K., Lee, B.-K., Karki, R., Gurung, A., Baral, B., and Byeon, S.-H.: Dynamics of PM 2.5 concentrations in Kathmandu Valley, Nepal, J. Hazard. Mat., 168, 732-738, 2009.

Aryal, D., Rosoff, Y. N., and Devkota, L. P.: A Severe Hailstorm at Pokhara: CAPE Stability Index Calculations, Journal of Geosciences and Geomatics, 3, 142-153,

Automotive Research Association of India (ARAI).: Emission factor development for Indian vehicles (http://www.cpcb.nic.in/Emission_Factors_Vehicles.pdf), 2008.

Avnery, S., Mauzerall, D. L., Liu, J., and Horowitz, L. W.: Global crop yield reductions due to surface ozone exposure: 1. Year 2000 crop production losses and economic damage, Amos. Environ., 45, 2284–2296, doi:10.1016/j.atmosenv.2010.11.045, 2011.

Bhardwaj, P., Naja, M., Rupakheti, M., Panday, A. K., Kumar, R., Mahata, K., Lal, S., Lawrence, M. G., Chandola, H. C.: Variations in surface ozone and CO in the Kathmandu Valley during SusKat-ABC international field campaign, Atmos. Chem. Phys., 18, 11949–11971, 2018, https://doi.org/10.5194/acp-18-11949-2018.

Bollasina, M. A., Ming, Y., and Ramaswamy, V.: Anthropogenic Aerosols and the Weakening of the South Asian Summer Monsoon, Science, 334, 502-505, 10.1126/science.1204994, 2011.

Bonasoni P., P. Laj, A. Marinoni, M. Sprenger, F. Angelini, J. Arduini, U. Bonafè, F. Calzolari, T. Colombo, S. Decesari, C. Di Biagio, A. G. di Sarra, et al.: Atmospheric brown clouds in the Himalayas: first two years of continuous observations at the Nepal Climate Observatory-Pyramid (5079 m). Atmos. Chem. Phys., 10, 7515-7531, 2010.

Brauer, M., Amman, M., Burnett, R. T., Cohen, A., Dentener, F., Zenati, M., Henderson, S. B., Krzyzanowski, M., Martin, R. V., Van Dingenen, R., van Donkelaar, A., and Thurston, G. D.: Exposure assessment for estimation of the global burden of disease attributable to outdoor air pollution, Environ. Sci. Technol., 46, 652–660, doi:10.1021/es2025752, 2012.

Brun, V. (Eds. 1): Fried earth bricks, kilns and workers in Kathmandu Valley. Himal Books, Lazimpat-Kathmandu, Nepal, 2013.

Burney, J., and Ramanathan, V.: Recent climate and air pollution impacts on Indian agriculture, Proceedings of the National Academy of Sciences of the United States of America, 111, 16319-16324, doi:10.1073/pnas.1317275111, 2014.

Central Bureau of Statistics (CBS): Nepal Living Standards Survey 2010/11, Statistical Report Volume 1, Central Bureau of Statistics, Government of Nepal, 2011.

Chandra, N., Lal, S., Venkataramani, S., Patra, P. K., and Sheel, V.: Temporal variations of atmospheric CO 2 and CO at Ahmedabad in western India, Atmos. Chem. Phys., 16, 6153-6173, 2016.

Chang K-L, Petropavlovskikh I, Cooper OR, Schultz MG, Wang T.: Regional trend analysis of surface ozone observations from monitoring networks in eastern North America, Europe and East Asia. Elem Sci Anth., DOI:http://doi.org/10.1525/elementa.243, 2017.

Chen, H., Karion, A., Rella, C., Winderlich, J., Gerbig, C., Filges, A., Newberger, T., Sweeney, C., and Tans, P.: Accurate measurements of carbon monoxide in humid air using the cavity ring-down spectroscopy (CRDS) technique, Atmos. Meas. Tech., 6, 1031-1040, 2013.

Chen, P., Kang, S., Li, C., Rupakheti, M., Yan, F., Li, Q., Ji, Z., Zhang, Q., Luo, W., and Sillanpää, M.: Characteristics and sources of polycyclic aromatic hydrocarbons in atmospheric aerosols in the Kathmandu Valley, Nepal, Sci. Total Environ., 538, 86-92, 2015.

Chen, Y. H., and Prinn, R. G.: Estimation of atmospheric methane emissions between 1996 and 2001 using a three-dimensional global chemical transport model, J. Geophys. Res. Atmos., 111, 2006.

Cho, C., Kim, S. W., Rupakheti, M., Park, J. S., Panday, A., Yoon, S. C., Kim, J. H., Kim, H., Jeon, H., Sung, M., Kim, B. M., Hong, S. K., Park, R. J., Rupakheti, D., Mahata, K. S., Praveen, P. S., Lawrence, M. G., and Holben, B.: Wintertime aerosol optical and radiative properties in the Kathmandu Valley during the SusKat-ABC field campaign, Atmos. Chem. Phys., 17, 12617-12632, 10.5194/acp-17-12617-2017, 2017.

Cong, Z., Kawamura, K., Kang, S., and Fu, P.: Penetration of biomass-burning emissions from South Asia through the Himalayas: new insights from atmospheric organic acids, 5, 9580, 10.1038/srep09580 http://dharmasastra.live.cf.private.springer.com/articles/srep09580#supplementary-information, 2015.

Conrad, R.: Soil microorganisms as controllers of atmospheric trace gases (H2, CO, CH4, OCS, N2O, and NO), Microbiol.Rev., 60, 609-640, 1996.

Cristofanelli, P., Bracci, A., Sprenger, M., Marinoni, A., Bonafè, U., Calzolari, F., Duchi, R., Laj, P., Pichon, J. M., Roccato, F., Venzac, H., Vuillermoz, E., and Bonasoni, P.: Tropospheric ozone variations at the Nepal Climate Observatory- Pyramid (Himalayas,

5079ma.s.l.) and influence of deep stratospheric intrusion events, Atmos. Chem. Phys., 10, 6537–6549, doi:10.5194/acp-10-6537-2010, 2010.

Crosson, E.: A cavity ring-down analyzer for measuring atmospheric levels of methane, carbon dioxide, and water vapor, Appl. Phys. B: Lasers and Optics, 92, 403-408, 2008.

Davidson, C. I., Lin, S.-F., and Osborn, J. F.: Indoor and outdoor air pollution in the Himalayas, Environ. Sci. Technol., 20(6), 561 – 566, doi:10.1021/es00148a003, 1986.

Department of Transport Management (DoTM).: Annual report of Ministry of Labor and transport management, Nepal Government, 2015.

Decesari, S., Facchini, M. C., Carbone, C., Giulianelli, L., Rinaldi, M., Finessi, E., Fuzzi, S., Marinoni, A., Cristofanelli, P., Duchi, R., Bonasoni, P., Vuillermoz, E., Cozic, J., Jaffrezo, J. L., and Laj, P.: Chemical composition of PM₁₀ and PM₁ at the high-altitude Himalayan station Nepal Climate Observatory-Pyramid (NCO-P) (5079 m a.s.l.), Atmos. Chem. Phys., 10, 4583-4596, 10.5194/acp-10-4583-2010, 2010.

Deb Roy, S., Beig, G., Ghude, S.D.: Exposure-plant response of Ambient ozone over the tropical India region. Atmos. Chem. Phys. 9, 5253e5260, 2009.

Dentener, F., Stevenson, D., Ellingsen, K., Van Noije, T., Schultz, M., Amann, M., Atherton, C., Bell, N., Bergmann, D., and Bey, I.: The global atmospheric environment for the next generation, Environ. Sci. Technol., 40, 3586-3594, 2006.

Dey, S., and Di Girolamo, L.: A climatology of aerosol optical and microphysical properties over the Indian subcontinent from 9 years (2000–2008) of Multiangle Imaging Spectroradiometer (MISR) data, Journal of Geophysical Research: Atmospheres, 115, n/a-n/a, 10.1029/2009JD013395, 2010.

Dhungel, S., Kathayat, B., Mahata, K., and Panday, A.: Transport of regional pollutants through a remote trans-Himalayan valley in Nepal, Atmos. Chem. Phys., 18, 1203-1216, https://doi.org/10.5194/acp-18-1203-2018, 2018.

Dlugokencky, E.J., A.M. Crotwell, P.M. Lang, J.W. Mund, Atmospheric Methane Dry Air Mole Fractions from quasi-continuous measurements at Mauna Loa, Hawaii, 1986-2016, Version: 2017-01-20, path: ftp://aftp.cmdl.noaa.gov/data/trace_gases/ch4/in-situ/surface/, 2017.

Dlugokencky, E.J., Lang, P.M., Crotwell, A. M., Mund, J. W., Crotwell, M. J., and Thoning, K. W.: Atmospheric Methane Dry Air Mole Fractions from the NOAA ESRL Carbon Cycle Cooperative Global Air Sampling Network, 1983-2015, Version: 2016-07-07, Path: ftp://aftp.cmdl.noaa.gov/data/trace_gases/ch4/flask/surface/, 2016.

Dlugokencky, E.J., Lang, P.M., Mund, J.W., Crotwell, A. M., Crotwell, M. J., and Thoning, K. W.: Atmospheric Carbon Dioxide Dry Air Mole Fractions from the NOAA ESRL Carbon Cycle Cooperative Global Air Sampling Network, 1968-2015, Version: 2016-08-30, Path: ftp://aftp.cmdl.noaa.gov/data/trace_gases/co2/flask/surface/, 2016a.

Draxler, R. R., and Hess, G. D.: An overview of the HYSPLIT_4 modeling system for trajectories, dispersion, and deposition, Aust. Meteor. Mag, 47, 295–230, 1998.

Dumka, U. C., N. Tripathi, S., Misra, A., Giles, D. M., Eck, T. F., Sagar, R., and Holben, B. N.: Latitudinal variation of aerosol properties from Indo-Gangetic Plain to central Himalayan foothills during TIGERZ campaign, Journal of Geophysical Research: Atmospheres, 119, 4750-4769, 10.1002/2013jd021040, 2014.

EDGAR42FT: Global emissions EDGAR v4.2FT2010, available at http://edgar.jrc.ec.europa.eu/overview.php?v=42FT2010, last access: October 2013.

Feng, Z., Hu, E., Wang, X., Jiang, L., Liu, X.: Ground-level O_3 pollution and its impacts on food crops in China: A review, Environ. Pollut., 199, 42-24, https://doi.org/10.1016/j.envpol.2015.01.016, 2015.

Forouzanfar, M. H., Alexander, L., Anderson, H. R., Bachman, V. F., Biryukov, S., Brauer, M., Burnett, R., Casey, D., Coates, M. M., and Cohen, A.: Global, regional, and national comparative risk assessment of 79 behavioural, environmental and occupational, and metabolic risks or clusters of risks in 188 countries, 1990–2013: a systematic analysis for the global burden of disease study 2013, Lancet, 386, 2287-2323, doi: 10.1016/S0140-6736(15)00128-2, 2015.

Fowler, D., Flechard, C., Cape, J. N., Storeton-West, R. L., and Coyle, M.: Measurements of ozone deposition to vegetation quantifying the flux, the stomatal and nonstomatal components, Water Air Soil Pollut., 130, 63–74, doi:10.1023/a:1012243317471, 2001.

Fragkias, M., Lobo, J., Strumsky, D., and Seto, K. C.: Does size matter? Scaling of CO2 emissions and US urban areas, PLoS One, 8, e64727, 2013.

Fueglistaler, S., Dessler, A. E., Dunkerton, T. J., Folkins, I., Fu, Q., and Mote, P. W.: Tropical tropopause layer, Rev. Geophys., 47, RG1004, doi:10.1029/2008RG000267, 2009.

Ganesan, A., Chatterjee, A., Prinn, R., Harth, C., Salameh, P., Manning, A., Hall, B., Mühle, J., Meredith, L., and Weiss, R.: The variability of methane, nitrous oxide and sulfur hexafluoride in Northeast India, Atmos. Chem. Phys., 13, 10633-10644, 2013.

Gautam, R., Hsu, N. C., Lau, K. M., and Kafatos, M.: Aerosol and rainfall variability over the Indian monsoon region: distributions, trends and coupling, Ann. Geophys., 27, 3691-3703, 10.5194/angeo-27-3691-2009, 2009a.

Gautam, R., Hsu, N. C., Lau, K. M., Tsay, S. C., and Kafatos, M.: Enhanced pre-monsoon warming over the Himalayan-Gangetic region from 1979 to 2007, Geophysical Research Letters, 36, n/a-n/a, 10.1029/2009GL037641, 2009b.

Gautam, R., Hsu, N. C., Tsay, S. C., Lau, K. M., Holben, B., Bell, S., Smirnov, A., Li, C., Hansell, R., Ji, Q., Payra, S., Aryal, D., Kayastha, R., and Kim, K. M.: Accumulation of aerosols over the Indo-Gangetic plains and southern slopes of the Himalayas: distribution, properties and radiative effects during the 2009 pre-monsoon season, Atmospheric Chemistry and Physics, 11, 12841-12863, 10.5194/acp-11-12841-2011, 2011.

Geiß, A., Wiegner, M., Bonn, B., Schäfer, K., Forkel, R., von Schneidemesser, E., Münkel, C., Chan, K. L., and Nothard, R.: Mixing layer height as an indicator for urban air quality?, Atmos. Meas. Tech. Discuss., 2017, 1-32, doi:10.5194/amt-2017-53, 2017.

Ghude, S.D., Jain, S.L., Arya, B.C., Beig, G., Ahammed, Y.N., Kumar, A., Tyagi, B.: Ozone in ambient air at a tropical megacity, Delhi: characteristics, trends and cumulative ozone exposure indices, J. Atmos. Chem., 60: 237, https://doi.org/10.1007/s10874-009-9119-4, 2008.

Ghude, S. D., Jena, C., Chate, D. M., Beig, G., Pfister, G. G., Kumar, R., and Ramanathan, V.: Reductions in India's crop yield due to ozone, Geophys. Res. Lett., 41, 5685–5691, doi:10.1002/2014GL060930, 2014.

Giles, D. M., Holben, B. N., Eck, T. F., Sinyuk, A., Smirnov, A., Slutsker, I., Dickerson, R. R., Thompson, A. M., and Schafer, J. S.: An analysis of AERONET aerosol absorption properties and classifications representative of aerosol source regions, Journal of Geophysical Research: Atmospheres, 117, n/a-n/a, 10.1029/2012jd018127, 2012.

Giri, D., Murthy, K., Adhikary, P., Khanal, S.: Ambient air quality of Kathmandu Valley as reflected by atmospheric particulate matter concentrations (PM10), Int. J. Environ. Sci. Technol. 3, 403–410, 2006.

Gogoi, M. M., Moorthy, K. K., Kompalli, S. K., Chaubey, J. P., Babu, S. S., Manoj, M. R., Nair, V. S., and Prabhu, T. P.: Physical and optical properties of aerosols in a free tropospheric environment: Results from long-term observations over western trans-Himalayas, Atmospheric Environment, 84, 262-274, https://doi.org/10.1016/j.atmosenv.2013.11.029, 2014.

Goroshi, S. K., Singh, R., Panigrahy, S., and Parihar, J.: Analysis of seasonal variability of vegetation and methane concentration over India using SPOT-VEGETATION and ENVISAT-SCIAMACHY data, J. Indian Soc. Remote, 39, 315-321, 2011.

Guttikunda, S. K., Goel, R., and Pant, P.: Nature of air pollution, emission sources, and management in the Indian cities, Atmospheric Environment, 95, 501-510, http://dx.doi.org/10.1016/j.atmosenv.2014.07.006, 2014.

Gyawali, M., Arnott, W. P., Lewis, K., and Moosmüller, H.: In situ aerosol optics in Reno, NV, USA during and after the summer 2008 California wildfires and the influence of absorbing and non-absorbing organic coatings on spectral light absorption, Atmos. Chem. Phys., 9, 8007-8015, 10.5194/acp-9-8007-2009, 2009.

Hansen, A. D. A., Rosen, H., and Novakov, T.: The aethalometer — An instrument for the real-time measurement of optical absorption by aerosol particles, Science of The Total Environment, 36, 191-196, https://doi.org/10.1016/0048-9697(84)90265-1, 1984.

Highwood, E. J. and Hoskins, B. J.: The tropical tropopause, Q. J. Roy. Meteorol. Soc., 124, 1579–1604, doi:10.1002/qj.49712454911, 1998.

Huszar, P., Belda, M., and Halenka, T.: On the long-term impact of emissions from central European cities on regional air quality, Atmos. Chem. Phys., 16, 1331–1352, doi:10.5194/acp-16-1331-2016, 2016.

International Energy Agency (IEA).: Energy and air pollution, World Energy Outlook Special Report 2016, International Energy Agency, 2016.

International Centre for Integrated Mountain Development (ICIMOD).: Himalayas – Water for 1.3 Billion People. ICIMOD, Lalitpur, 2009.

Intergovernmental Panel for Climate Change (IPCC).: Climate Change 2013: The Physical Science Basis. Contribution of Working Group I to the Fifth Assessment Report of the Intergovernmental Panel on Climate Change, Cambridge University Press, Cambridge, United Kingdom and New York, NY, USA, 2013.

IPCC: Climate Change 2007: The Physical Science Basis. Contribution of Working Group I to the Fourth Assessment Report of the Intergovernmental Panel on Climate Change. Chapter 1, Historical Overview of Climate change, in: Intergovernmental Panel on Climate Change Climate change: The Physical Science Basis, Contribution of Working Group I to the Fourth Assessment Report of the IPCC, Cambridge University Press, Cambridge, 79–131, 2007.

Jai Devi, J., Tripathi, S. N., Gupta, T., Singh, B. N., Gopalakrishnan, V., and Dey, S.: Observation-based 3-D view of aerosol radiative properties over Indian Continental

Tropical Convergence Zone: implications to regional climate, Tellus B, 63, 971-989, 10.1111/j.1600-0889.2011. 00580.x, 2011.

Janssens-Maenhout, G., Dentener, F., van Aardenne, J., Monni, S., Pagliari, V., Orlandini, L., Klimont, Z., Kurokawa, J., Akimoto, H., Ohara, T., Wankmüller, R., Battye, B., Grano, D., Zuber, A., and Keating, T.: EDGAR-HTAP: a harmonized gridded air pollution emission dataset based on national inventories, Tech. Rep. JRC68434, Publications Office of the European Union, doi:10.2788/14102 (online), http://publications.jrc.ec.europa.eu/repository/handle/JRC68434, 2000.

Junkermann, W.: An Ultralight Aircraft as Platform for Research in the Lower Troposphere: System Performance and First Results from Radiation Transfer Studies in Stratiform Aerosol Layers and Broken Cloud Conditions, Journal of Atmospheric and Oceanic Technology, 18, 934-946, 10.1175/1520-0426(2001)018<0934:auaapf>2.0.co;2, 2001.

Kaskaoutis, D. G., Singh, R. P., Gautam, R., Sharma, M., Kosmopoulos, P. G., and Tripathi, S. N.: Variability and trends of aerosol properties over Kanpur, northern India using AERONET data (2001–10), Environmental Research Letters, 7, 024003, 10.1088/1748-9326/7/2/024003, 2012.

Kim, B. M., Park, J.-S., Kim, S.-W., Kim, H., Jeon, H., Cho, C., Kim, J.-H., Hong, S., Rupakheti, M., and Panday, A. K.: Source apportionment of PM 10 mass and particulate carbon in the Kathmandu Valley, Nepal, Atmos. Environ., 123, 190-199, 2015.

Kiros, F., Shakya, K. M., Rupakheti, M., Regmi, R. P., Maharjan, R., Byanju, R. M., Naja, M., Mahata, K., Kathayat, B., and Peltier, R. E.: Variability of Anthropogenic Gases: Nitrogen oxides, sulfur dioxide, ozone and ammonia in Kathmandu Valley, Nepal, Aerosol Air Qual. Res., 16: 3088–3101, 2016.

Kitada, T., and Regmi, R. P.: Dynamics of air pollution transport in late wintertime over Kathmandu Valley, Nepal: As revealed with numerical simulation, J. Appl. Meteorol., 42, 1770-1798, 2003.

Kuhlmann, J., and Quaas, J.: How can aerosols affect the Asian summer monsoon? Assessment during three consecutive pre-monsoon seasons from CALIPSO satellite data, Atmos. Chem. Phys., 10, 4673-4688, 10.5194/acp-10-4673-2010, 2010.

Kumar, M. K., and Nagendra, S. S.: Characteristics of ground level CO_2 concentrations over contrasting land uses in a tropical urban environment, Atmos. Environ., 115, 286-294, 2015.

Kumar, R., Naja, M., Satheesh, S.K., Ojha, N., Joshi, H., Sarangi, T., Pant, P., Dumka, U.C., Hegde, P., Venkataramani, S.: Influences of the springtime northern Indian biomass

burning over the central Himalayas. J. Geophys. Res., 116, D19302. http://dx.doi.org/10.1029/2010JD015509, 2011.

Kumar, R., Naja, M., Venkataramani, S., and Wild, O.: Variation in surface ozone at Nainital: A high-altitude site in the central Himalayas, J. Geophys. Res., 115 (D16), doi:10.1029/2009JD013715, 2010.

Kurokawa, J., Ohara, T., Morikawa, T., Hanayama, S., Janssens-Maenhout, G., Fukui, T., Kawashima, K., and Akimoto, H.: Emissions of air pollutants and greenhouse gases over Asian regions during 2000-2008: Regional emission inventory in Asia (REAS) version 2, Atmos. Chem. Phys., 13, 11 019–11 058, doi:10.5194/acp-13-11019-2013, 2013.

Lal, S., Naja, M., and Subbaraya B. H.: Seasonal variations in surface ozone and its precursors over an urban site in India, Atmos. Environ., 34, 2713-2724, doi: 10.1016/S1352-2310(99)00510-5, 2000.

Lau, W.: Atmospheric science: Desert dust and monsoon rain, Nature Geosci, 7, 255-256, 10.1038/ngeo2115, 2014.

Lawrence, M., and Lelieveld, J.: Atmospheric pollutant outflow from southern Asia: a review, Atmos. Chem. Phys., 10, 11017-11096, 2010.

Li, C., Bosch, C., Kang, S., Andersson, A., Chen, P., Zhang, Q., Cong, Z., Chen, B., Qin, D., and Gustafsson, O.: Sources of black carbon to the Himalayan-Tibetan Plateau glaciers, Nat Commun, 7, 12574, 10.1038/ncomms12574, 2016.

Li, C., Yan, F., Kang, S., Chen, P., Han, X., Hu, Z., Zhang, G., Hong, Y., Gao, S., Qu, B., Zhu, Z., Li, J., Chen, B., and Sillanpää, M.: Re-evaluating black carbon in the Himalayas and the Tibetan Plateau: concentrations and deposition, Atmos. Chem. Phys., 17, 11899-11912, https://doi.org/10.5194/acp-17-11899-2017, 2017.

Lim, S. S., Vos, T., Flaxman, A. D., Danaei, G., Shibuya, K., Adair-Rohani, H., Amann, M., Anderson, H. R., Andrews, K. G., Aryee, M., Atkinson, C., Bacchus, L. J., Bahalim, A. N., Balakrishnan, K., Balmes, J., Barker-Collo, S., Baxter, A., Bell, M. L., Blore, J. D., Blyth, F., Bonner, C., Borges, G., Bourne, R…and Ezzati, M.: A comparative risk assessment of burden of disease and injury attributable to 67 risk factors and risk factor clusters in 21 regions, 1990-2010: a systematic analysis for the global burden of disease study 2010, Lancet, 380, 2224–2260, 2012.

Lüthi, Z. L., Škerlak, B., Kim, S. W., Lauer, A., Mues, A., Rupakheti, M., and Kang, S.: Atmospheric brown clouds reach the Tibetan Plateau by crossing the Himalayas, Atmos. Chem. Phys. 15, 6007-6021., doi:10.5194/acp-15-6007-2015, 2015.

Mahata, K. S., Panday, A. K., Rupakheti, M., Singh, A., Naja, M., and Lawrence, M. G.: Seasonal and diurnal variations of methane and carbon dioxide in the Kathmandu Valley in the foothills of the central Himalaya, Atmos. Chem. Phys., 17, 12573-12596, https://doi.org/10.5194/acp-17-12573-2017, 2017.

Mahata, K. S., Rupakheti, M., Panday, A. K., Bhardwaj, P., Naja, M., Singh, A., Mues, A., Cristofanelli, P., Pudasainee, D., Bonsai, P., and Lawrence, M. G.: Observation and analysis of spatio-temporal characteristics of surface ozone and carbon monoxide at multiple sites in the Kathmandu Valley, Nepal, Atmos. Chem. Phys., 18, 1-20, 2018, https://doi.org/10.5194/acp-18-1-2018.

Marcq, S., Laj, P., Roger, J. C., Villani, P., Sellegri, K., Bonasoni, P., Marinoni, A., Cristofanelli, P., Verza, G. P., and Bergin, M.: Aerosol optical properties and radiative forcing in the high Himalaya based on measurements at the Nepal Climate Observatory-Pyramid site (5079 m a.s.l.), Atmos. Chem. Phys., 10, 5859-5872, 10.5194/acp-10-5859-2010, 2010.

Marinoni, A., Cristofanelli, P., Laj, P., Duchi., R., Putero, D., Calzolari, F., Landi., T. C., Vuillermoz, E., Maione, M., and Bonasoni, P.: High black carbon and ozone concentrations during pollution transport in the Himalayas: Five years of continuous observations at NCO-P global GAW station, J. Environ. Sci., 25(8) 1618–1625, http://dx.doi.org/10.1016/S1001-0742(12)60242-3, 2013.

Ming, J., Xiao, C., Sun, J., Kang, S.-C, and Bonasoni, P.: Carbonaceous particles in the atmosphere and precipitation of the Nam Co region, central Tibet, J. Environ. Sci.-CHINA, 22(11), 1748-1756, 2010.

Ministry of Environment (MoE).: Status of climate change in Nepal, Kathmandu Nepal. Kathmandu, Ministry of Environment, 2011.

Ministry of Environment and Forest (MoEF).: Indian Network for Climate Change Assessment: India: Greenhouse Gas Emissions 2007, Tech. rep., 2007.

Monks, P. S., Archibald, A. T., Colette, A., Cooper, O., Coyle, M., Derwent, R., Fowler, D., Granier, C., Law, K. S., Mills, G. E., Stevenson, D. S., Tarasova, O., Thouret, V., von Schneidemesser, E., Sommariva, R., Wild, O., and Williams, M. L.: Tropospheric ozone and its precursors from the urban to the global scale from air quality to short-lived climate forcer, Atmos. Chem. Phys., 15, 8889-8973, https://doi.org/10.5194/acp-15-8889-2015, 2015.

Monks, P. S., Granier, C., Fuzzi, S., Stohl, A., Williams, M. L., Akimoto, H., Amann, M., Baklanov, A., Baltensperger, U., Bey, I., Blake, N., Blake, R. S., Carslaw, K., Cooper, O.

R., Dentener, F., Fowler, D., Fragkou, E., Frost, G. J., Generoso, S., Ginoux, P., Grewe, V., Guenther, A., Hansson, H. C., Henne, S., Hjorth, J., Hofzumahaus, A., Huntrieser, H., Isaksen, I. S. A., Jenkin, M. E., Kaiser, J., Kanakidou, M., Klimont, Z., Kulmala, M., Laj, P., Lawrence, M. G., Lee, J. D., Liousse, C., Maione, M., McFiggans, G., Metzger, A., Mieville, A., Moussiopoulos, N., Orlando, J. J., O'Dowd, C. D., Palmer, P. I., Parrish, D. D., Petzold, A., Platt, U., Poeschl, U., Prevot, A. S. H., Reeves, C. E., Reimann, S., Rudich, Y., Sellegri, K., Steinbrecher, R., Simpson, D., ten Brink, H., Theloke, J., van derWerf, G. R., Vautard, R., Vestreng, V., Vlachokostas, C., and von Glasow, R.: Atmospheric composition change – global and regional air quality, Atmos. Environ., 43, 5268–5350, doi:10.1016/j.atmosenv.2009.08.021, 2009.

Mues, A., Rupakheti, M., Münkel, C., Lauer, A., Bozem, H., Hoor, P., Butler, T., and Lawrence, M.: Investigation of the mixing layer height derived from ceilometer measurements in the Kathmandu Valley and implications for local air quality. Atmos. Chem. Phys., doi:10.5194/acp-2016-1002, in press, 2017.

Naja, M., and Lal, S.: Surface ozone and precursor gases at Gadanki (13.5°N, 79.2°E), a tropical rural site in India, J. Geophys. Res. 107 (D14), ACH 8-1-ACH 8–13, doi:10.1029/2001jd000357, 2002.

Nayava, J. L.: Rainfall in Nepal, the Himalayan Rev. Nepal, Geographical Society, 12:1– 18, 1980.

Neitola, K., Asmi, E., Komppula, M., Hyvärinen, A. P., Raatikainen, T., Panwar, T. S., Sharma, V. P., and Lihavainen, H.: New particle formation infrequently observed in Himalayan foothills – why?, Atmos. Chem. Phys., 11, 8447-8458, 10.5194/acp-11-8447-2011, 2011.

Nepal Electricity Authority (NEA).: A year in review - fiscal year - 2013/2014 (http://www.nea.org.np/images/supportive_docs/Annual%20Report-2014.pdf), 2014.

NOAA ESRL Global Monitoring Division. updated annually.: Atmospheric Carbon Dioxide Dry Air Mole Fractions from quasi-continuous measurements at Mauna Loa, Hawaii. Compiled by K.W. Thoning, D.R. Kitzis, and A. Crotwell. National Oceanic and Atmospheric Administration (NOAA), Earth System Research Laboratory (ESRL), Global Monitoring Division (GMD): Boulder, Colorado, USA. Version 2016-8 at http://dx.doi.org/10.7289/V54X55RG, 2015.

Organisation for Economic Co-operation and Development (OECD): The economic consequences of outdoor air pollution, OECD Publishing, doi: http://dx.doi.org/10.1787/9789264257474-en, 2016.

Organisation for Economic Co-operation and Development (OECD): The economic consequences of outdoor air pollution, OECD Publishing, doi: http://dx.doi.org/10.1787/9789264257474-en, 2016.

Padmakumari, B., Maheskumar, R. S., Morwal, S. B., Harikishan, G., Konwar, M., Kulkarni, J. R., and Goswami, B. N.: Aircraft observations of elevated pollution layers near the foothills of the Himalayas during CAIPEEX-2009, Quarterly Journal of the Royal Meteorological Society, 139, 625-638, 10.1002/qj.1989, 2013.

Panday, A. K., and Prinn, R. G..: Diurnal cycle of air pollution in the Kathmandu Valley, Nepal: Observations, J. Geophys. Res., 114 (D9), doi:10.1029/2008JD009777, 2009.

Panday, A. K. Prinn, R. G., and Schär, C.: Diurnal cycle of air pollution in the Kathmandu Valley, Nepal: 2. Modeling results, J. Geophys. Res., 114 (D21), doi:10.1029/2008JD009808, 2009.

Pandey, A., Sadavarte, P., Rao, A. B., Venkataraman C.: Trends in multipollutant emissions from a technology-linked inventory for India: II. Residential, agricultural and informal industry sectors, Atmos. Environ., 99, 341-352, doi: 10.1016/j.atmosenv.2014.09.080, 2014.

Pandey, S. K., Vinoj, V., Landu, K., and Babu, S. S.: Declining pre-monsoon dust loading over South Asia: Signature of a changing regional climate, Scientific Reports, 7, 16062, 10.1038/s41598-017-16338-w, 2017.

Patra, P. K., Canadell, J. G., Houghton, R. A., Piao, S. L., Oh, N.- H., Ciais, P., Manjunath, K. R., Chhabra, A., Wang, T., Bhattacharya, T., Bousquet, P., Hartman, J., Ito, A., Mayorga, E., Niwa, Y., Raymond, P. A., Sarma, V. V. S. S., and Lasco, R.: The carbon budget of South Asia, Biogeoscience, 10, 513–527 (2013).

Patra, P., Niwa, Y., Schuck, T., Brenninkmeijer, C., Machida, T., Matsueda, H., and Sawa, Y.: Carbon balance of South Asia constrained by passenger aircraft CO2 measurements, Atmos. Chem. Phys., 11, 4163-4175, 2011.

Picarro.: Picarro G2401 CO2, CH4, CO, Water vapor CRDS analyzer (http://hpst.cz/sites/default/files/attachments/datasheet-g2401-crds-analyzer-co2-co-ch4-h2o-air-oct15-1.pdf), 2015.

Prasad, P., Rastogi, S., and Singh, R.: Study of satellite retrieved CO2 and CH4 concentration over India, Adv. Space Res., 54, 1933-1940, 2014.

Pudasainee, D., Sapkota, B., Shrestha, M. L., Kaga, A., Kondo, A., and Inoue, Y.: Ground level ozone concentrations and its association with NOx and meteorological parameters in

Kathmandu Valley, Nepal, Atmos. Environ., 40(40), 8081–8087, doi:10.1016/j.atmosenv.2006.07.011, 2006.

Putero, D., Landi, T., Cristofanelli, P., Marinoni, A., Laj, P., Duchi, R., Calzolari, F., Verza, G., and Bonasoni, P.: Influence of open vegetation fires on black carbon and ozone variability in the southern Himalayas (NCO-P, 5079 m asl), Environ. Pollut., 184, 597-604, 2014.

Putero, D., Cristofanelli, P., Marinoni, A., Adhikary, B., Duchi, R., Shrestha, S., Verza, G., Landi, T., Calzolari, F., and Busetto, M.: Seasonal variation of ozone and black carbon observed at Paknajol, an urban site in the Kathmandu Valley, Nepal, Atmos. Chem. Phys., 15, 13957-13971, 2015.

Pommier, M.; McLinden, C. A.; Deeter, M.: Relative changes in CO emissions over megacities based on observations from space, Geophys. Res. Let. 40 (14): 3766. Bibcode:2013GeoRL.40.3766P. doi:10.1002/grl.50704, 2013.

Raatikainen, T., Hyvärinen, A. P., Hatakka, J., Panwar, T. S., Hooda, R. K., Sharma, V. P., and Lihavainen, H.: The effect of boundary layer dynamics on aerosol properties at the Indo-Gangetic plains and at the foothills of the Himalayas, Atmospheric Environment, 89, 548-555, 10.1016/j.atmosenv.2014.02.058, 2014.

Ram, K., and Sarin, M.: Spatio-temporal variability in atmospheric abundances of EC, OC and WSOC over Northern India, J. Aerosol Sci., 41, 88–98, 2010.

Ramana, M. V., Ramanathan, V., Podgorny, I. A., Pradhan, B. B., and Shrestha, B.: The direct observations of large aerosol radiative forcing in the Himalayan region, Geophysical Research Letters, 31, n/a-n/a, 10.1029/2003GL018824, 2004.

Ramanathan, V., Chung, C., Kim, D., Bettge, T., Buja, L., Kiehl, J. T., Washington, W. M., Fu, Q., Sikka, D. R., Wild, M.: Atmospheric brown clouds: Impacts on South Asian climate and hydrological cycle, PNAS., 102 (15) 5326-5333; DOI:10.1073/pnas.0500656102, 2005.

Ramanathan, V. and Carmichael, G.: Global and regional climate changes due to black carbon, Nat. Geosci., 1, 221–227, 2008.

Ramanathan, V., Crutzen, P. J., Kiehl, J. T., and Rosenfeld, D.: Aerosols, Climate, and the Hydrological Cycle, Science, 294, 2119-2124, 10.1126/science.1064034, 2001.

Russell, P. B., Bergstrom, R. W., Shinozuka, Y., Clarke, A. D., DeCarlo, P. F., Jimenez, J. L., Livingston, J. M., Redemann, J., Dubovik, O., and Strawa, A.: Absorption Angstrom Exponent in AERONET and related data as an indicator of aerosol composition, Atmos. Chem. Phys., 10, 1155-1169, 10.5194/acp-10-1155-2010, 2010.

Raub, J.A., Mathieu-Nolf, M., Hampson, N.B., Thom, S.R.: Carbon monoxide poisoning a public health perspective. Toxicology 145 (1), 1e14. http://dx.doi.org/10.1016/S0300-483X(99)00217-6, 2000.

Regmi, R. P., Kitada, T., and Kurata, G.: Numerical simulation of late wintertime local flows in Kathmandu Valley, Nepal: Implication for air pollution transport, J. Appl. Meteorol., 42, 389-403, 2003.

Rodda, S.R., Thumaty, K. C., Jha, C. S. and Dadhwal, V. K.: Seasonal Variations of Carbon Dioxide, Water Vapor and Energy Fluxes in Tropical Indian Mangroves. Forests, 7, 35; doi:10.3390/f7020035, 2016.

Rupakheti, D., Adhikary, B., Praveen, P. S., Rupakheti, M., Kang, S.-C., Mahata, K. S., Naja, M., Zhang, Q., Panday, A. K., and Lawrence, M. G.: Pre-monsoon air quality over Lumbini, a world heritage site along the Himalayan foothills, Atmos. Chem. Phys., 17, 11041-111063, https://doi.org/10.5194/acp-17-11041-2017, 2017.

Rupakheti, M., Panday, A. K., Lawrence, M. G., Kim, S. W., Sinha, V., Kang, S. C., Naja, M., Park, J. S., Hoor, P., Holben, B., Sharma, R. K., Mues, A., Mahata, K. S., Bhardwaj, P., Sarkar, C., Rupakheti, D., Regmi, R. P., and Gustafsson, Ö.: Air pollution in the Himalayan foothills: overview of the SusKat-ABC international air pollution measurement campaign in Nepal, Atmos. Chem. Phys., in preparation, 2019.

Sadavarte, P., Rupakheti, M., Shakya, K., Bhave, P.V., and Lawrence, M.G.: Nepal emission (NEEM): A high resolution technology - based bottom-up emissions inventory for Nepal 2001-2016, Atmos. Chem. Phys. Discuss., https://doi.org/10.5194/acp-2019-113, 2019.

Sahu, L. K., and Lal, S.: Distributions of C 2–C 5 NMHCs and related trace gases at a tropical urban site in India. Atmos. Environ., 40(5), 880-891, 2006.

Sarangi, T., Naja, M., S. Lal, Venkataramani, S., Bhardwaj, P., Ojha, N., Kumar, R., Chandola, H. C.: First observations of light non-methane hydrocarbons (C2–C5) over a high altitude site in the central Himalayas, Atmos. Environ., 125, 450–460, 2016.

Sarangi T., Naja, M., Ojha, N., Kumar, R., Lal, S., Venkataramani, S., Kumar, A., Sagar, R., and Chandola, H. C.: First simultaneous measurements of ozone, CO and NOy at a high altitude regional representative site in the central Himalayas, J. Geophys. Res., 119, doi:10.1002/2013JD020631, 2014.

Sarkar, C., Sinha, V., Kumar, V., Rupakheti, M., Panday, A., Mahata, K. S., Rupakheti, D., Kathayat, B., and Lawrence, M. G.: Overview of VOC emissions and chemistry from PTR-TOF-MS measurements during the SusKat-ABC campaign: high acetaldehyde, isoprene

and isocyanic acid in wintertime air of the Kathmandu Valley, Atmos. Chem. Phys., 16, 3979-4003, 2016.

Sarkar, C., Sinha, V., Sinha, B., Panday, A. K., Rupakheti, M., and Lawrence, M. G.: Source apportionment of NMVOCs in the Kathmandu Valley during the SusKat-ABC international field campaign using positive matrix factorization, Atmos. Chem. Phys., 17, 8129-8156, 2017.

Schneising, O., Buchwitz, M., Burrows, J., Bovensmann, H., Bergamaschi, P., and Peters, W.: Three years of greenhouse gas column-averaged dry air mole fractions retrieved from satellite–Part 2: Methane, Atmos. Chem. Phys., 9, 443-465, 2009.

Shakya, K. M., Rupakheti, M., Shahi, A., Maskey, R., Pradhan, B., Panday, A., Puppala, S. P., Lawrence, M., and Peltier, R. E.: Near-road sampling of PM2. 5, BC, and fine-particle chemical components in Kathmandu Valley, Nepal, Atmos. Chem. Phys., 17, 6503-6516, https://doi.org/10.5194/acp-17-6503-2017, 2017.

Sharma, R.K., Bhattarai, B.K., Sapkota, B.K., Gewali, M.B., Kjeldstad, B.: Black carbon aerosols variation in Kathmandu valley, Nepal, Atmos. Environ., 63:282-288, https://doi.org/10.1016/j.atmosenv.2012.09.023, 2012.

Shrestha, A. B., Wake, C. P., Mayewski, P. A., and Dibb, J.E.: Maximum Temperature Trends in the Himalaya and Its Vicinity: An Analysis Based on Temperature Records from Nepal for the Period 1971–94, J. Climate, 12, 2775-2786, 1999.

Sharma, P., Kuniyal, J. C., Chand, K., Guleria, R. P., Dhyani, P. P. and Chauhan, C.: Surface ozone concentration and its behavior with aerosols in the northwestern Himalaya, India. Atmos. Environ. 71, 44-53, doi:10.1016/12.042, 2013.

Shrestha, P., Barros, A. P., and Khlystov, A.: Chemical composition and aerosol size distribution of the middle mountain range in the Nepal Himalayas during the 2009 pre-monsoon season, Atmospheric Chemistry and Physics, 10, 11605-11621, 2010.

Shrestha, P., Barros, A. P., and Khlystov, A.: CCN estimates from bulk hygroscopic growth factors of ambient aerosols during the pre-monsoon season over Central Nepal, Atmospheric Environment, 67, 120-129, http://dx.doi.org/10.1016/j.atmosenv.2012.10.042, 2013.

Shrestha, R. M., and Rajbhandari, S.: Energy and environmental implications of carbon emission reduction targets: Case of Kathmandu Valley, Nepal, Energ. Policy, 38, 4818-4827, 2010.

Shrestha, S. R., Oanh, N. T. K., Xu, Q., Rupakheti, M., and Lawrence, M. G.: Analysis of the vehicle fleet in the Kathmandu Valley for estimation of environment and climate co-benefits of technology intrusions, Atmos. Environ., 81, 579-590, 2013.

Sinha, V., Kumar, V., and Sarkar, C.: Chemical composition of pre-monsoon air in the Indo-Gangetic Plain measured using a new air quality facility and PTR-MS: high surface ozone and strong influence of biomass burning, Atmos. Chem. Phys., 14, 5921-5941, 10.5194/acp-14-5921-2014, 2014.

Smith, K. R., Uma, R., Kishore, V., Zhang, J., Joshi, V., and Khalil, M.: Greenhouse implications of household stoves: an analysis for India, Ann. Rev. Energ. Environ., 25, 741-763, 2000.

Sreenivas, G., Mahesh, P., Subin, J., Kanchana, A. L., Rao, P. V. N., and Dadhwal, V. K.: Influence of Meteorology and interrelationship with greenhouse gases (CO_2 and CH_4) at a suburban site of India, Atmos. Chem. Phys., 16, 3953-3967, 2016.

Stevenson, D. S., Young, P. J., Naik, V., Lamarque, J.-F., Shindell, D. T., Voulgarakis, A., Skeie, R. B., Dalsoren, S. B., Myhre, G., Berntsen, T. K., Folberth, G. A., Rumbold, S. T., Collins, W. J., MacKenzie, I. A., Doherty, R. M., Zeng, G., van Noije, T. P. C., Strunk, A., Bergmann, D., Cameron-Smith, P., Plummer, D. A., Strode, S. A., Horowitz, L., Lee, Y. H., Szopa, S., Sudo, K., Nagashima, T., Josse, B., Cionni, I., Righi, M., Eyring, V., Conley, A., Bowman, K. W., Wild, O., and Archibald, A.: Tropospheric ozone changes, radiative forcing and attribution to emissions in the Atmospheric Chemistry and Climate Model Intercomparison Project (ACCMIP), Atmos. Chem. Phys., 13, 3063–3085, doi:10.5194/acp-13-3063-2013, 2013.

Stockwell, C. E., Christian, T. J., Goetz, J. D., Jayarathne, T., Bhave, P. V., Praveen, P. S., Adhikari, S., Maharjan, R., DeCarlo, P. F., and Stone, E. A.: Nepal ambient monitoring and source testing experiment (NAMaSTE): emissions of trace gases and light-absorbing carbon from wood and dung cooking fires, garbage and crop residue burning, brick kilns, and other sources, Atmos.pheric Chem. Phys., 16, 11043-11081, 2016.

Stone, E. A., Schauer, J. J., Pradhan, B. B., Dangol, P. M., Habib, G., Venkataraman, C., and Ramanathan, V.: Characterization of emissions from South Asian biofuels and application to source apportionment of carbonaceous aerosol in the Himalayas, Journal of Geophysical Research: Atmospheres, 115, n/a-n/a, 10.1029/2009JD011881, 2010.

Tan, G. and Shibasaki, R.: Global estimation of crop productivity and the impacts of global warming by GIS and EPIC integration, Ecolog. Mod., 168, https://doi.org/10.1016/S0304-3800(03)00146-7, 2003.

Talbot, R., Mao, H., and Sive, B.: Diurnal characteristics of surface level O_3 and other important trace gases in New England, J. Geophys. Res., 110 (D9), doi:10.1029/2004JD005449, 2005.

Tripathee, L., Kang, S.-C., Huang, J., Sharma, C., Sillanpaa, M., Guo, J., and Paudyal, R.: Concentrations of trace elements in wet deposition over the central Himalayas, Nepal, Atmos. Environ., 95, 231–238, 2014.

Tripathi, S. N., Dey, S., Tare, V., Satheesh, S. K., Lal, S., and Venkataramani, S.: Enhanced layer of black carbon in a north Indian industrial city, Geophysical Research Letters, 32, n/a-n/a, 10.1029/2005gl022564, 2005.

Tissier, A.-S. and Legras, B.: Convective sources of trajectories traversing the tropical tropopause layer, Atmos. Chem. Phys., 16, 3383–3398, doi:10.5194/acp-16-3383-2016, 2016.

United Nations Environment Programme and World Meteorological Organization (UNEP and WMO), Integrated Assessment of Black Carbon and Tropospheric Ozone, United Nations Environment Programme (UNEP), Nairobi, 2011.

Vadrevu, K., Ellicott, E., Giglio, L., Badarinath, K., Vermote, E., Justice, C., Lau, W.: Vegetation fires in the Himalayan region - aerosol load, black carbon emissions and smoke plume heights, Atmos. Environ., 47, 241–251, 2012.

Venkataraman, C., Habib, G., Kadamba, D., Shrivastava, M., Leon, J. F., Crouzille, B., Boucher, O., and Streets, D. G.: Emissions from open biomass burning in India: Integrating the inventory approach with high-resolution Moderate Resolution Imaging Spectroradiometer (MODIS) active-fire and land cover data, Global Biogeochemical Cycles, 20, n/a-n/a, 10.1029/2005GB002547, 2006.

Venzac, H., Sellegri, K., Laj, P., Villani, P., Bonasoni, P., Marinoni, A., Cristofanelli, P., Calzolari, F., Fuzzi, S., Decesari, S., Facchini, M. C., Vuillermoz, E., and Verza, G. P.: High frequency new particle formation in the Himalayas, Proc Natl Acad Sci U S A, 105, 15666-15671, 10.1073/pnas.0801355105, 2008.

Vinoj, V., Rasch, P. J., Wang, H., Yoon, J.-H., Ma, P.-L., Landu, K., and Singh, B.: Short-term modulation of Indian summer monsoon rainfall by West Asian dust, Nature Geosci, 7, 308-313, 10.1038/ngeo2107, http://www.nature.com/ngeo/journal/v7/n4/abs/ngeo2107.html#supplementary-information, 2014.

Wan, X., Kang, S.C., Li, Q.L., Rupakheti, D., Zhang, Q.G., Guo, J.M., Chen, P.F., Tripathee, L., Rupakheti, M., Panday, A.K., Wang, W., Kawamura, K., Gao, S.P., Wu, G.M., and

Cong, Z.Y.: Organic molecular tracers in the atmospheric aerosols from Lumbini (Nepal) in Indo-Gangetic Plains: the influence of biomass burning. Atmos. Chem. Phys., 17, 8867-8885,https://doi.org/ 10.5194/acp-17-8867-2017, 2017.

Wang, Y., Konopka, P., Liu, Y., Chen, H., Müller, R., Plöger, F., Riese, M., Cai, Z., and Lü, D.: Tropospheric ozone trend over Beijing from 2002–2010: Ozonesonde measurements and modeling analysis, Atmos. Chem. Phys., 12, 8389–8399, doi:10.5194/acp-12-8389-2012, 2012.

World Health Organization (WHO): WHO Air quality guidelines for particulate matter, ozone, nitrogen dioxide and sulfur dioxide, Global update 2005, Summary of risk assessment, WHO Press, Geneva, Switzerland, 2006.

World Health Organization (WHO).: 7 million premature deaths annually linked to air pollution, (http://www.who.int/mediacentre/news/releases/2014/air-pollution/en/, last access: 12 December 2017), 2014.

World Health Organization (WHO).: Giving care to air, (http://www.searo.who.int/nepal/documents/environment/AIR_UHI/en/, last access: 20 April 2019), 2019.

Xie, A., Ren, J., Qin, X., and Kang, S.: Reliability of NCEP/NCAR reanalysis data in the Himalayas/Tibetan Plateau, Journal of Geographical Sciences, 17, 421-430, 10.1007/s11442-007-0421-2, 2007.

Yang, M., Howell, S. G., Zhuang, J., and Huebert, B. J.: Attribution of aerosol light absorption to black carbon, brown carbon, and dust in China – interpretations of atmospheric measurements during EAST-AIRE, Atmos. Chem. Phys., 9, 2035-2050, 10.5194/acp-9-2035-2009, 2009.

Zhang, Q., Streets, D., Carmichael, G., He, K., Huo, H., Kannari, A., Klimont, Z., Park, I., Reddy, S., Fu, J., Chen, D., Duan, L., Lei, Y., Wang, L., and Yao, Z.: Asian emissions in 2006 for the NASA INTEX-B mission, Atmos. Chem. Phys., 9, 5131–5153, 2009.

Declaration of Authorship

I, Khadak Singh Mahata, would like to declare that this dissertation entitled “Spatiotemporal Variations of Key Air Pollutants and Greenhouse Gases in the Himalayan Foothills” and the entire work presented in the thesis are my own. I prepared this dissertation without any illegal assistance. I confirm that the work is original except where it is mentioned by the reference in the text and no part of the dissertation has been submitted for any other degree.

This dissertation has not been submitted to any other University for examination, neither in Germany nor in any other countries.